

RIKAGAKU KENKYUSHO

*the Institute of Physical and Chemical Research*

Wako-shi, Saitama Pref., JAPAN

'77

***IPCR cyclotron***  
**Progress Report 1977**

**Vol. 11**

**IPCR** Cyclotron Progress Report

**Vol. 11**

The Institute of Physical and Chemical Research  
"RIKAGAKU KENKYUSHO" Wako-shi, Saitama, 351 JAPAN  
December, 1977

## Editors

A. Hashizume	Y. Hattori
T. Inamura	H. Kamitsubo
A. Matsuyama	T. Nomura
T. Nozaki	M. Odera
N. Shiotani	

This volume contains recent information of the IPCR Cyclotron, informal reports and abstracts of papers which will be published at scientific meetings or in publications by staff members, guests, and visitors.

All rights reserved. This report or any part thereof may not be reproduced in any form (including photostatic or microfilm form) without written permission from the publisher.

# CONTENTS

		Page
1.	INTRODUCTION .....	1
2.	MACHINE OPERATION .....	2
3.	MACHINE DEVELOPMENT AND ACCELERATOR PHYSICS	
3-1.	Improvement of the Beam Probe System of the Cyclotron .....	4
3-2.	The Pulsed Ion Source .....	6
3-3.	Acceleration of Polarized Protons with S. F. Cyclotron at INS .....	8
3-4.	Design Study of a Linac-Injected Separated Sector Cyclotron (1) Four Sector SSC .....	10
3-5.	Design Study of a Linac-Injected Separated Sector Cyclotron (2) Six-sector SSC .....	13
3-6.	Beam Study on the Baby Cyclotron .....	15
4.	NUCLEAR PHYSICS	
	Scattering and Reactions	
4-1.	Spin Flip in the Inelastic Scattering of Polarized Protons on $^{12}\text{C}$ .....	18
4-2.	Two-Step Process in Proton Inelastic Scattering .....	20
4-3.	DWBA Analysis of Proton Inelastic Scattering from $^{28,29,30}\text{Si}$ and Blocking Effects in the Core-Excitation of $^{29}\text{Si}$ .....	22
4-4.	Analysis of (p, t) Reaction Induced by Polarized Protons .....	25
4-5.	Analyses of the $^{54}\text{Fe}(d, p)^{55}\text{Fe}$ Reaction Data at $E_d = 24 \text{ MeV}$ .....	28
4-6.	Coupled Channel Effects on (d, p) Reactions .....	31
4-7.	Quasimolecular Resonance by the $^{24}\text{Mg}(\alpha, ^{12}\text{C})^{16}\text{O}$ Reaction .....	34
4-8.	Quasimolecular Resonances Formed by the System $^{12}\text{C} + ^{13}\text{C}$ .....	36
4-9.	Fusion Reaction in $^{12}\text{C} + ^{14}\text{N}$ and $^{16}\text{O} + ^{10}\text{B}$ Systems .....	39
4-10.	$\alpha$ -Transfer Reactions between 1p or 2s-1d Shell Nuclei (2) .....	40
4-11.	Spin Polarization of $^{12}\text{B}$ in ( $^{10}\text{B}$ , $^{12}\text{B}$ ) and ( $^{12}\text{C}$ , $^{12}\text{B}$ ) Reactions on $^{100}\text{Mo}$ .....	43

	Page
4-12. On the Mechanism of Two-Nucleon Transfer Reactions Induced by Heavy Ions .....	45
4-13. Calculation of Friction Force in the Collision $^{28}\text{Si} + ^{20}\text{Ne}$ on the Basis of the Linear Response Theory .....	48
4-14. Canonical Quantization from the Time-Dependent Hartree-Fock Theory in the Lipkin Model .....	51
4-15. $\alpha$ -Particle and Light Product Correlation in the $^{14}\text{N} + ^{93}\text{Nb}$ Reaction .....	54
4-16. Light Fragment Excitation in the $^{14}\text{N} + ^{93}\text{Nb}$ Reaction .....	56
4-17. Angular Distribution and Energy Spectrum of "Direct" $\alpha$ -Particles Emitted from the $^{159}\text{Tb} + 95\text{MeV } ^{14}\text{N}$ Reaction .....	58
4-18. Energy Relaxation of a Composite System Deduced from Preequilibrium $\alpha$ -Particle Spectra in $^{209}\text{Bi} + ^{14}\text{N}$ Reactions .....	60
4-19. Preequilibrium $\alpha$ -Particle Emission from $^{209}\text{Bi} + ^{14}\text{N}$ Reactions .....	63
 5. NUCLEAR PHYSICS	
Nuclear Spectroscopy	
5-1. Cross Section for the $^{40}\text{Ca}(^{16}\text{O}, p)^{55}\text{Co}$ Reaction .....	66
5-2. $\gamma$ -Rays Following Fast $\alpha$ -Particles Emitted in the $^{159}\text{Tb} + 95\text{ MeV } ^{14}\text{N}$ Reactions .....	67
5-3. High Spin States of $^{162}\text{Yb}$ .....	69
5-4. High Spin States of $^{164}\text{Yb}$ .....	72
5-5. High Spin States of $^{166}\text{Yb}$ .....	74
5-6. Populations of the Particle-Hole K Isomer and the Ground State Rotational Level .....	77
5-7. Half-life of $^{207}\text{Bi}$ .....	79
 6. NUCLEAR INSTRUMENTATION	
6-1. A Particle Identification Program for the On-Line Use .....	81
6-2. Determination of the Etching Rate Versus Restricted Energy Loss Curves in CN Films and CTA Films by Using N-Ion Beams .....	82

	Page
6-3. Target Chamber for Recoil-distance Lifetime Measurements . . . . .	85
6-4. Gas $\Delta E$ -E Telescope for the Particle Identification of Heavy Ions . . . . .	87
7. ATOMIC AND SOLID-STATE PHYSICS	
7-1. Energy Loss and Straggling of C and He Ions in Metal Foils . . . . .	89
7-2. X-Rays Following Multiple Inner-Shell Ionization (1) . . . . .	91
7-3. X-Rays Following Multiple Inner-Shell Ionization (2) . . . . .	93
7-4. Gas Target System for Study of X-Rays Induced by Heavy Ions . . . . .	96
7-5. Chemical Effect in X-Ray Spectra Produced by Fast Ions . . . . .	99
7-6. Lattice Location of Ni Atoms Implanted into Al . . . . .	102
7-7. Damage Production Rate in TiO <sub>2</sub> as Measured by Channeling Method . . . . .	104
7-8. Perturbed Angular Correlation of $\gamma$ -Rays Emitted from <sup>111</sup> Cd in NiFe <sub>2</sub> O <sub>4</sub> . . . . .	106
7-9. On the Use of <sup>48</sup> V Source for the Study of Positron Annihilation . . . . .	109
7-10. Thermal Equilibrium Measurements of Positron Annihilation Line Shapes in KCl, KBr, and Ge . . . . .	111
7-11. Effects of Irradiation Temperature, Prestrain, and Helium Concentration on the Helium Embrittlement of Type 316 Stainless Steel . . . . .	114
8. RADIOCHEMISTRY AND NUCLEAR CHEMISTRY	
8-1. Charged Particle Activation Analysis for Surface Oxygen . . . . .	116
8-2. Charge Spectra of <sup>198</sup> Hg <sup>n+</sup> Ions from the <sup>198</sup> Au Decay . . . . .	119
9. RADIATION CHEMISTRY AND RADIATION BIOLOGY	
9-1. Emission Spectra of a KBr Single Crystal Irradiated with Heavy Ions at 4.2 K Time-Dependent Spectra . . . . .	122
9-2. Yields of Trapped Electron Produced by Heavy-Ion Irradiation in Ethanol Glass at 77 K . . . . .	124
9-3. Further Study of High LET Effect on Template/Primer Activity of DNA <u>in situ</u> . . . . .	126

	Page
9-4. Induction of Mutations in Bacteriophage $\phi$ X 174 by $\alpha$ -Particles and N-Ions .....	128
9-5. Inactivation of Ribonuclease A in Aqueous Solution by Cyclotron Beams .....	130
9-6. The Effects of High LET Radiations on Mammalian Cells .....	132
10. PREPARATION OF RADIOISOTOPES AND LABELED COMPOUNDS	
10-1. Production of Radioisotopes and Preparation of Labelled Compounds for Medical and Agricultural Use .....	134
10-2. Biosynthesis of Selenomethionine- $^{73}\text{Se}$ .....	137
10-3. Separation of Carrier-free Radioactive Krypton .....	139
11. RADIATION MONITORING	
11-1. Routine Monitoring .....	141
11-2. Leakage Radiation Measurement at the Underground Passage .....	143
12. HEAVY ION LINEAR ACCELERATOR PROJECT	
12-1. Status of the Constructional Work .....	144
12-2. The Proto-type Buncher .....	145
12-3. A Lay-out Plan of the Beam Diagnostic Elements .....	146
12-4. Orbit Analysis of the Beam after Charge Stripping .....	147
12-5. Test Facility for Heavy Ion Source .....	149
13. LIST OF PUBLICATIONS .....	151
14. LIST OF PERSONNEL .....	159
15. LIST OF OUTSIDE USERS AND THEIR THEMES .....	163
AUTHOR INDEX .....	165

## 1. INTRODUCTION

During the year the IPCR cyclotron was operated smoothly as before. Several improvements have been made in the machine itself and its accessory facilities which resulted in more stable and efficient operation.

In all fields of research using the machine a majority of research works have been carried out with heavy ions. Extensive studies of particle-gamma and particle-particle correlations and spin polarization of emitted particles were performed on the nuclear reactions induced by heavy ions. Heavy-ion induced X-rays were studied to get the information on the excitation mechanism as well as the effects of chemical environment on the X-ray spectra. Channeling experiments were continued to study location of impurity atoms and radiation damage. Positron annihilation studies were made on ionic crystals. Activation analysis by charged particles were applied to study the surface of the semi-conductor materials. Studies of the radiation chemistry and radiation biology were continued by using heavy ions as well as  $\alpha$ -particles.

The first resonator and the injector of the new heavy-ion linac were installed. Model study of the separated sector cyclotron was started.

*Hiromichi Kamitsubo*

---

Hiromichi Kamitsubo

Editor

## 2. MACHINE OPERATION

H. Takebe, S. Kohara, T. Kageyama, K. Ikegami,  
H. Nakajima, K. Ogiwara, S. Fujita, and I. Kohno

During the period from Oct. 23, 1976 to Oct. 22, 1977, the cyclotron was operated on 24 h a day basis.

Table 1 shows a statistics of machine operation. The beam time was 4346.9 h, decreased by 5.4% compared with that of the last year. This is due to the increase in the time spent for overhaul.

Following troubles occurred in this period. The water-cooling pipe on the moving earth-plate was damaged as a result of rather large number of discharges between the dee and the cooling pipe, experienced during these several years. The driving shafts for the moving earth-plate were also damaged by discharges. Because of the operation extending over 60000 h, the motor-generator for power supply to the main magnet (M. G) were damaged. Mainly for the repair of this M. G. system, the overhaul time was increased.

We constructed one more heavy ion source and at present we have three heavy ion sources. A pulsed arc power supply was also completed and pulsed operation of heavy ion source was frequently carried out to get much intensities of  $O^{5+}$  and  $Ne^{6+}$  ions.<sup>1)</sup> The automatic control system for evacuating pumps was equipped to the cyclotron in this summer.

Table 2 shows the machine time allotted to various activities in this period. Due to the request of research workers, beam time for heavy ions was increased in percentage compared with that of the last year.

Table 1. Machine operation.

	Oscillator	Ion source	Beam
Reading of time meter on Oct. 23, 1976	47050.3(h)	50354.3(h)	19474.9(h)
Reading of time meter on Oct. 23, 1977	51750.8	55308.8	23821.8
Difference	4700.5	4954.6	4346.9
Percentage of 365 days	53.7 %	56.6 %	49.6 %
-----			
Schedule in this period			
Beam time		231 (days)	
Overhaul and installation work		65	
Periodical inspection and repair		23	
Vacation and holidays		46	

Table 2. Scheduled beam time and subjects of activity in the period X.

Subject		Heavy ion	Light particles	Total
Nucl. Phys.	{ Nuclear reaction	2198(h)	812(h)	3010(h)
	{ In-beam spectroscopy	224	72	296
	{ RI production	0	4	4
Fields others than Nucl. Phys.	{ Nuclear chemistry	13	133	146
	{ Radiation chemistry	156	44	200
	{ Radiation biology	99	99	198
	{ Solid state physics	15	535	550
	{ Inner atomic shell excitation study	234	39	273
	{ Stopping power study	15	44	59
Outside users	{ Nuclear medicin	0	5	5
	{ Nuclear fuel study	0	192	192
	{ RI production	0	18	18
Development of instruments		17	0	17
Total		2971	1997	4968
Percent in total		59.8 %	40.2 %	100 %
Maintenance: operation and engineering				
Exchange of ion sources			76(h)	
Reserved for beam time adjustment and cooling of radioactivity			37	
Machine inspection and repair			552	
Total			665	

## Reference

- (1) H. Nakajima, S. Kohara, T. Kageyama, and I. Kohno: Report I. P. C. R., (in Japanese), 53, 132 (1977).

### 3. MACHINE DEVELOPMENT AND ACCELERATOR PHYSICS

#### 3-1. Improvement of the Beam Probe System of the Cyclotron

K. Ogiwara and H. Takebe

##### (1) Three- and four-finger beam probe

In order to measure the vertical distribution of the beam in the cyclotron, a three-finger beam probe was equipped and tested. Figure 1 shows three electrodes of the three-finger probe, length of which are 4 cm in the radial direction of the beam orbit.

The beam intensity distributions along the radial direction measured by the three-finger probe are shown in Fig. 2. Three curves in the upper figure are measured by upper, medium and lower fingers respectively. In this figure, it is seen that the beam passed above the median plane at some points of radius. The distribution of the total current measured by three fingers shows no smooth curve, as is seen in Fig. 2 (the lower part). This kind of total current distribution is not convenient for diagnosis of usual operation of the cyclotron. So we have made a four-finger probe which has three differential electrodes and an integrating electrode. Figure 3 shows the electrodes of the four-finger probe.

To sum up currents of the electrodes, the beam probe amplifier (Fig. 4, lower) has a sum circuit with four current amplifiers which can measure from 1 nA to 1 mA. This amplifier is

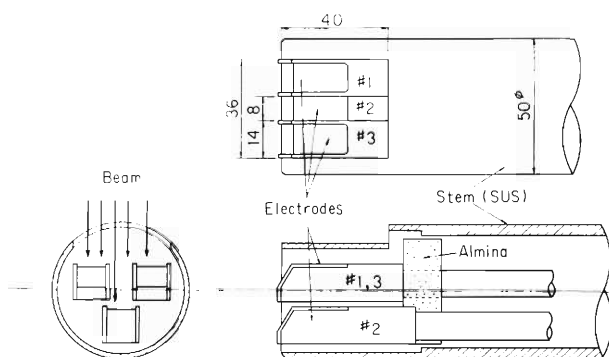


Fig. 1. Three-finger beam probe.

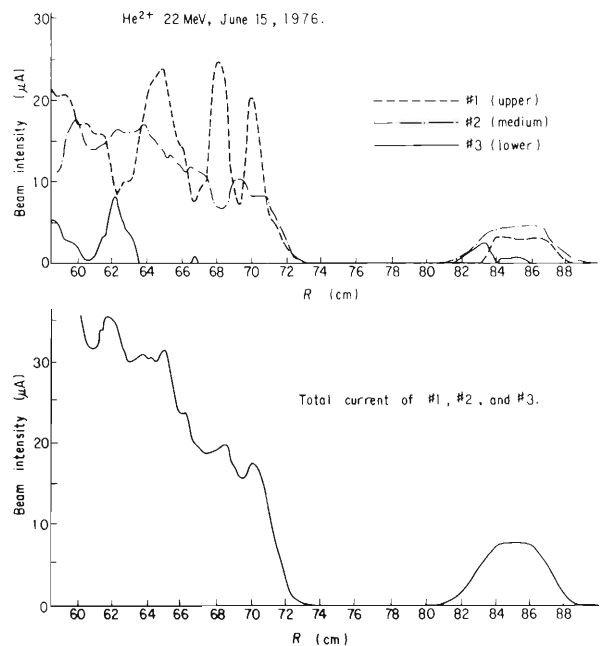


Fig. 2. The beam intensity distribution measured by the three-finger beam probe (upper) and the total current of them (lower) along the radial direction.

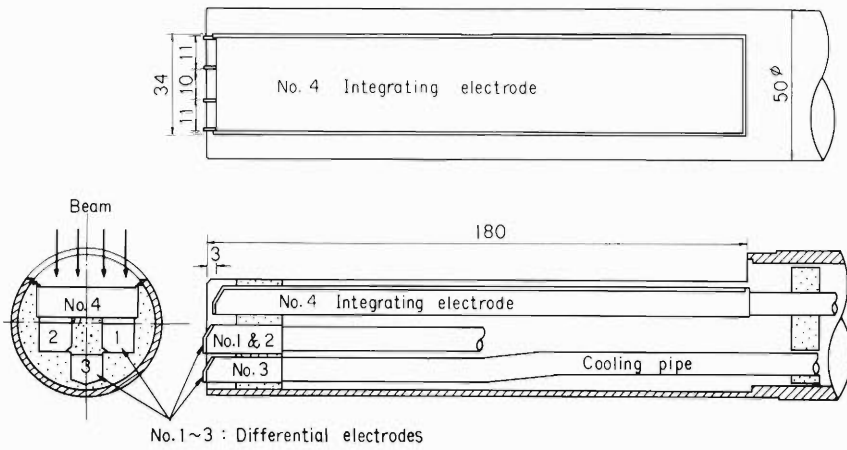


Fig. 3. Four-finger beam probe.

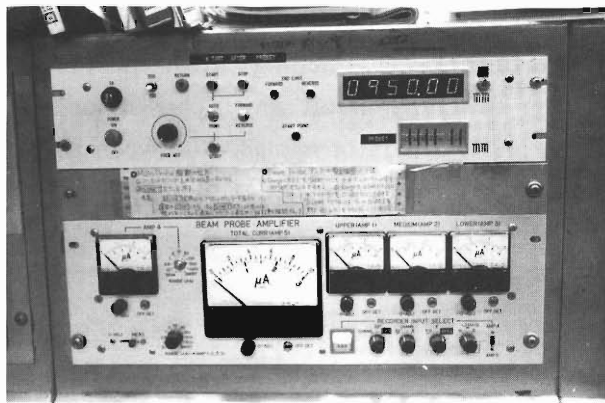


Fig. 4. A view of the control panel for driving system of the beam probe (upper) and the beam probe amplifier (lower).

connected with a four-pen recorder. The recorder can be switched to other operational parameters, for instance, vacuum pressures, frequency of the RF system, current of the main magnet and so on. It is very useful for the maintenance of the cyclotron to monitor those parameters for hours.

## (2) Improvement of the driving system for the beam probe

To simplify the cyclotron operation, the driving system for the beam probe was improved. The driving motor was changed from an induction motor to a pulse motor, and an indication of the beam probe from an analog meter to a digital meter. Figure 5 shows the schematic block diagram of the driving system using a pulse motor. The driving speed of the beam probe is 2 mm/sec which is almost as fast as before. The control panel for the driving system, shown in Fig. 4 (upper), assembles all of the operation keys and indicators. The beam probe is now easily handled by only pushing a start switch after presetting a digital switch to define the distance to move.

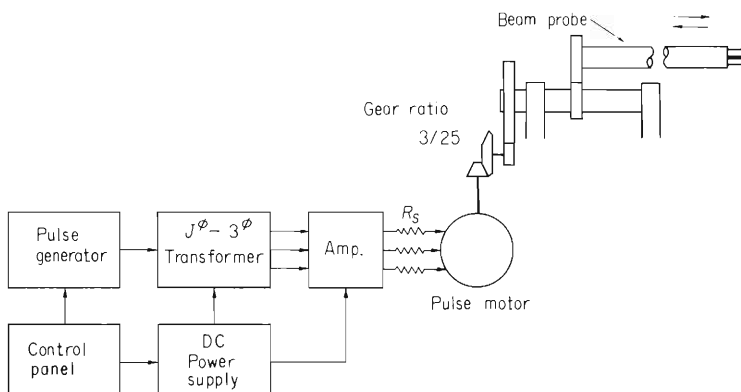


Fig. 5. The block diagram of the driving system for the beam probe.

H. Nakajima, S. Kohara, and T. Kageyama

In the cyclotron, the heavy ion source of electron bombarded hot cathode type is usually operated by applying direct current for arc discharge and has an available arc power dissipation of about 2.5 kW, which is inadequate to create highly charged light ions such as  $\text{Ne}^{6+}$  and  $\text{O}^{6+}$ . In order to produce a powerful arc discharge beyond the power dissipation limit of the source, pulsed operation of the source was proposed. A pulsed arc power supply which allows to furnish an ion source with an instantaneous arc power of about 10 kW was fabricated and operated successfully. The pulsed arc power supply is composed of a power switching circuit and the DC power supply used so far for CW operation. The power switching circuit which consists of a switching power tube, a transistorized driver stage and a pulse generator is placed between the source and the DC power supply, and produces periodically an arc potential at the source (Fig. 1).

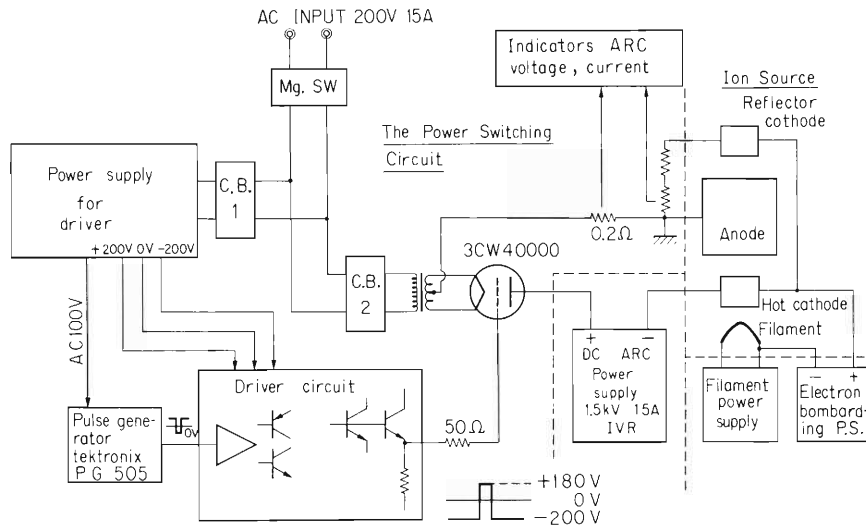


Fig. 1. Circuit of the pulsed arc power supply.

The power switching circuit as it is installed is shown in Fig. 2 and a typical wave form of arc discharge is presented in Fig. 3. The pulsed arc power supply has realized large power enhancements for arc discharge and a remarkable displacement of the mean charge state toward a larger value was observed in the charge state distribution of ion beams.<sup>1)</sup> Typically, the source was operated with an arc potential drop of about 500 V and an arc current of 8 to 12 A at peak. A duty cycle of about 30% and a pulse duration of about 1 ms were chosen.

$\text{Ne}^{6+}$  and  $\text{O}^{6+}$  ions were accelerated successfully up to 160 MeV and more than  $0.1 \mu\text{A}$  of those ions were extracted from the cyclotron.  $\text{C}^{5+}$ ,  $\text{Ne}^{7+}$ , and  $^{22}\text{Ne}^{6+}$  ions were also extracted with a modest intensity. The intensities of  $\text{C}^{4+}$ ,  $\text{N}^{4+}$ ,  $\text{N}^{5+}$ , and  $\text{O}^{5+}$  ions were increased by a factor of 5 or more, compared with those in DC operation.

Particles, energy ranges and particle yields obtained by using pulsed operation are shown in Table 1. A source life of about 5 h was obtained with a mean arc power of about 2 KW (7 KW

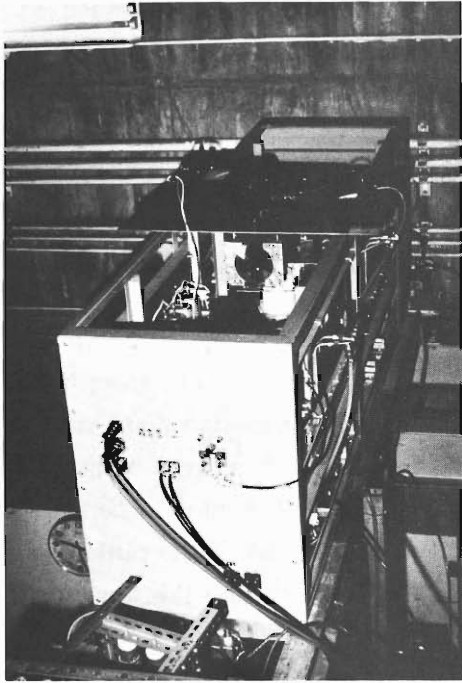


Fig. 2. The power switching circuit.

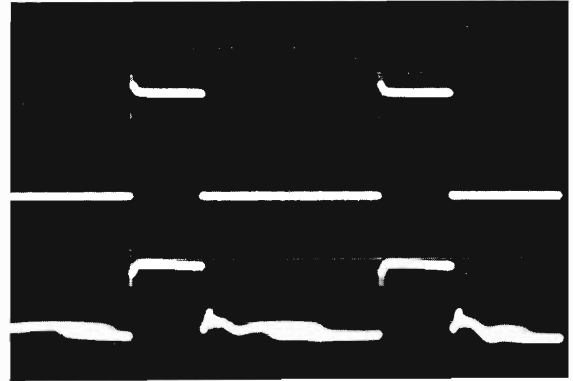


Fig. 3. Typical wave form of arc discharge. An arc current is shown by upper wave form. Vertical sensitivity: 5 A/div. Horizontal time: 1 ms/div., Lower wave form present an arc potential, Vertical sensitivity: 500 V/div.

at peak). This life is very short in comparison with a life estimated from an erosion of the upper cathode of about 20 h. The main problem remaining is to increase the source life time.

Table 1. Particles, energy ranges and particle yields.

Particle	Energy (MeV)	Extracted beam current
$C^{5+}$ *	49 – 130	0.1 $\mu A$
$O^{6+}$ *	65 – 160	0.2 $\mu A$
$^{20}Ne^{6+}$ *	82 – 160	0.2 $\mu A$
$^{20}Ne^{7+}$ *	82 – 185	< 10 nA
$^{22}Ne^{6+}$ *	90 – 155	< 10 nA**
$C^{4+}$	49 – 100	10 $\mu A$
$N^{4+}$	57 – 100	10 $\mu A$
$N^{5+}$	57 – 125	3 $\mu A$
$O^{5+}$	65 – 125	3 $\mu A$

Mean arc power: 2 kW, Pulse duration: 1.2 ms, Duty cycle: 30%.

\* Newly accelerated ions.

\*\* Natural Ne gas was fed.

## Reference

- 1) H. Nakajima, S. Kohara, T. Kageyama, and I. Kohno: Reports I. P. C. R., (in Japanese), 53, 132 (1977).

## 3-3. Acceleration of Polarized Protons with S.F. Cyclotron at INS

T. Fujisawa, S. Motonaga, N. Ueda,\* S. Yamada,\*  
T. Hasegawa,\* T. Wada, Y. Toba, and H. Kamitsubo

A polarized ion source for the proton and deuteron was installed on the S.F. Cyclotron at Institute for Nuclear Study (INS) in Tanashi.<sup>1)-3)</sup> The polarized proton beams from the ion source are vertically injected to the cyclotron at 10 keV and inflected to the median plane on the mirror at the centre of the cyclotron. The mirror voltage is about 7 kV. The energy of the extracted beams is 28 MeV. The size of the beam spot on a target was 2 mm  $\times$  4 mm. The intensities of the polarized proton beams were 5  $\mu$ A, 1.4  $\mu$ A, 50 nA, 10 nA, and 3 nA at the outlet of the source, the mirror, the inlet of the deflector, the outlet of the deflector and the target respectively. The carbon target for a polarimeter was a 5 mg/cm<sup>2</sup> self-supporting foil.<sup>4)</sup> The scattered protons were detected by 5 cm $\phi$   $\times$  2 cm NaI (T $\ell$ ) crystals mounted on photomultipliers with defining slits of 3 cm $\phi$  and placed symmetrically to the beam direction at positions 45 cm from the target. The energy resolution is enough to separate the ground state and the first 2<sup>+</sup> state of <sup>12</sup>C. The angles where the beam polarization was measured were corrected by measuring the angular distribution of the elastic scattering cross section of the unpolarized proton on <sup>12</sup>C and differences of detector efficiencies and solid angles were corrected by measuring the asymmetries of the unpolarized and polarized beams alternately.

Figure 1 shows the variation of the polarization of the proton beams against the RF field and the static magnetic field of the RF transition. Figure 2 shows the drift of the polarization degree of protons measured over a long time.

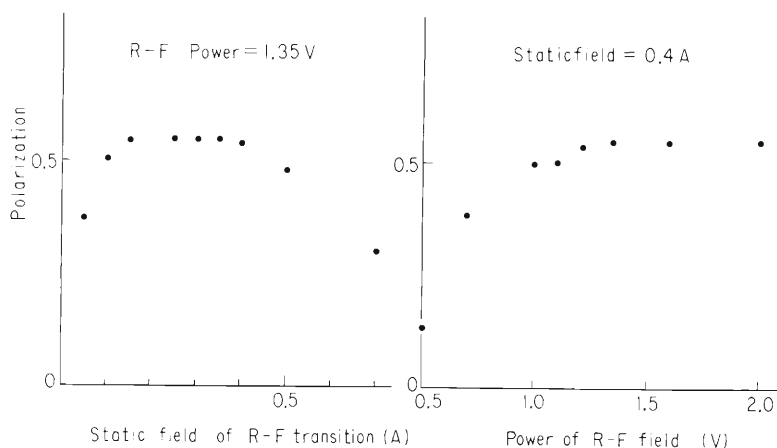


Fig. 1. Polarization of proton beams for static field and R. F. power of the R. F. transition.

\* Institute for Nuclear Study, University of Tokyo.

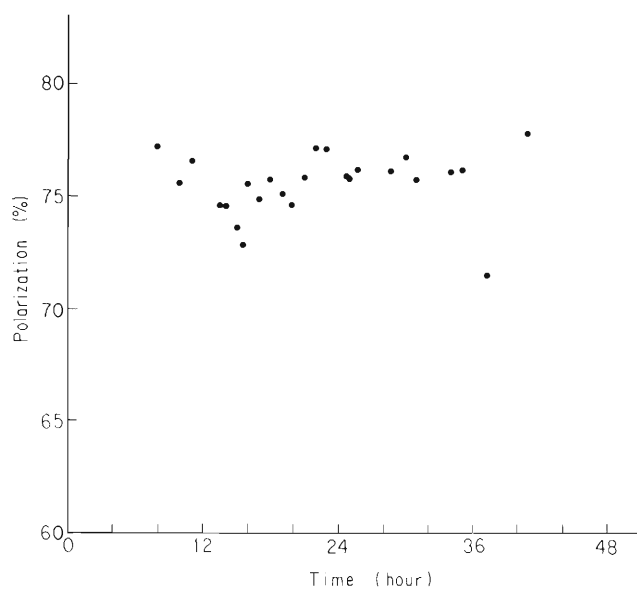


Fig. 2. The drift of the polarization degree of protons.

#### References

- 1) S. Motonaga, T. Fujisawa, I. Takeshita, K. Nishi, and H. Kamitsubo: *Genshikaku-Kenkyu*, (in Japanese), 21, 766 (1977).
- 2) S. Yamada, N. Ueda, Y. Sakurada, M. Sekiguchi, T. Tanabe, Y. Honma, and T. Hasegawa: *ibid.*, p.772.
- 3) S. Motonaga, T. Fujisawa, F. G. Resmini, Y. Toba, S. Yamada, N. Ueda, T. Hasegawa, and H. Kamitsubo: *IPCR Cyclotron Progr. Rep.*, 10, 16 (1976).
- 4) R. M. Craig, J. C. Dore, G. W. Greenlees, J. Lowe, and D. L. Watson: *Nucl. Phys.*, 83, 493 (1966).

## 3-4 Design Study of a Linac-Injected Separated Sector Cyclotron (1)

Four Sector SSC

S. Motonaga, H. Kamitsubo, N. Nakanishi, K. Ogiwara,  
F. Yoshida, and I. Yokoyama

A design study of a linac-injected separated sector cyclotron has been carried out in order to obtain particles of energy over 80 MeV/n for light heavy-ions and over 12 MeV/n for very heavy-ions using as an injector the variable frequency heavy-ion linac which is under construction in IPCR.<sup>1)</sup> Injection energy is in the range of 4 MeV/n for light heavy-ions to 1 MeV/n for very heavy-ions. The basic parameters of this cyclotron are given in Table 1. The magnet system of the cyclotron consists of 4 sector non-spiral magnets. The maximum field-radius product ( $B\rho$ ) is 3400 kG·cm. The effective sector angle of  $50^\circ$  was chosen to provide suitable axial and radial focusing property of the ion beam. Figure 1 shows the resonance diagram which is calculated by assuming an appropriate soft edge field.<sup>2)</sup> The locus of each particle does not cross any major resonance line. If the injection energy of light heavy-ions, such as  $C^{6+}$  and  $Ne^{9+}$ , are increased up to 4.8 MeV/n, these ions can be accelerated up to energy of 100 MeV/n. In the case of proton acceleration to energy of about 200 MeV, the proton beam must cross the  $\nu_r - 2\nu_z = 0$  and  $\nu_r = N/3$  resonance lines as shown in Fig. 2. It may not be impossible to pass through these resonance lines without any loss or deterioration of the beam, because of large energy gain per turn and good beam quality in this cyclotron as compared with an ordinary cyclotron. But extensive studies are needed to overcome this difficulty.

Table 1. Basic design parameters of the linac-injected separate sector cyclotron.

Maximum energy	
Proton $H^+$	( $\sim 200$ MeV, $E_{inj} \simeq 10$ MeV)
Carbon $C^{6+}$	80 MeV/n
Uranium $U^{40+}$	15 MeV/n
Number of sectors	4
Sector angle	$50^\circ$
Magnet fraction	0.555
Orbital fraction	0.558
Gap between poles	8 cm
Maximum Magnetic field	17.3 kG
Maximum field-radius product	3400 kG·cm
Number of trimming coils	$>20$ set
Injection radius	77 cm
Extraction radius	327 cm
Weight total	1900 ~ 2000 ton
Energy gain per turn	$\sim 1$ MeV
Number of dees	2
Angle of dee	$22.5^\circ$
Orbit frequency	2.5 - 5.55 (8.7) MHz
Accel. RF frequency	17 - 45 MHz
Harmonic number	8.6, (5)

Numbers in ( ) are values in case of proton acceleration.

Ion acceleration is done by  $22.5^\circ$  delta-shaped two dees located at opposite valley spaces between sector magnets. The frequency range of the system is 17-45 MHz and its acceleration harmonics is 8 to synchronize with the accelerating frequency of the linac.

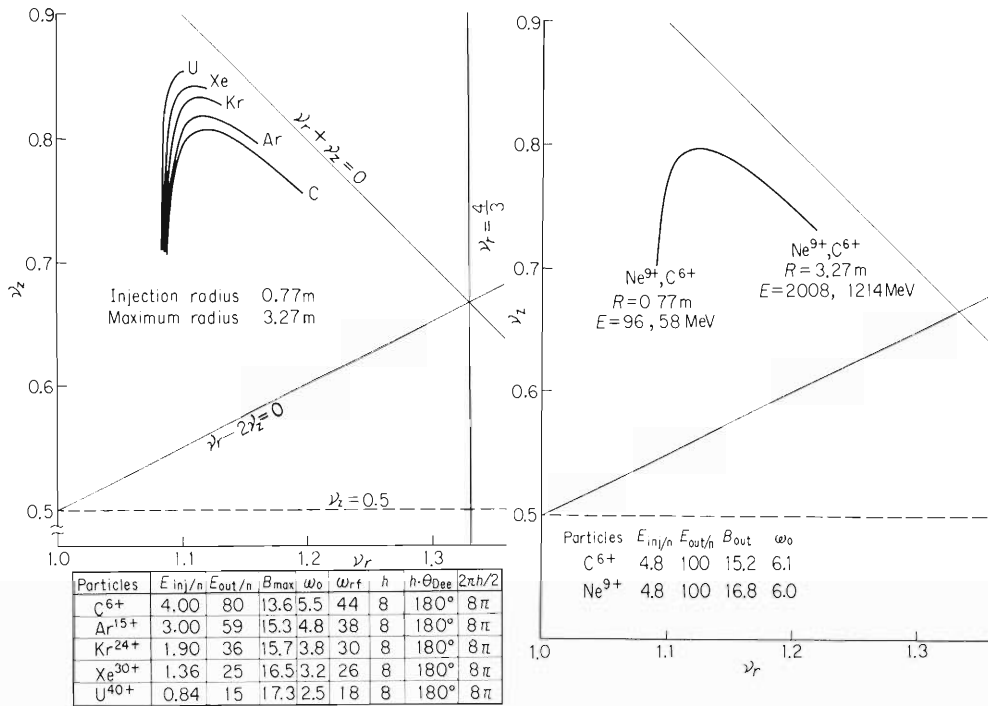


Fig. 1. Focusing properties calculated with soft edge approximation. (A) Injection energy ranges between 4 MeV/n and 1 MeV/n, for light heavy ion ( $C^{6+}$ ) and very heavy ion ( $U^{40+}$ ). (B) Injection energy is assumed to be 4.8 MeV/n for  $C^{6+}$  and  $Ne^{9+}$ .

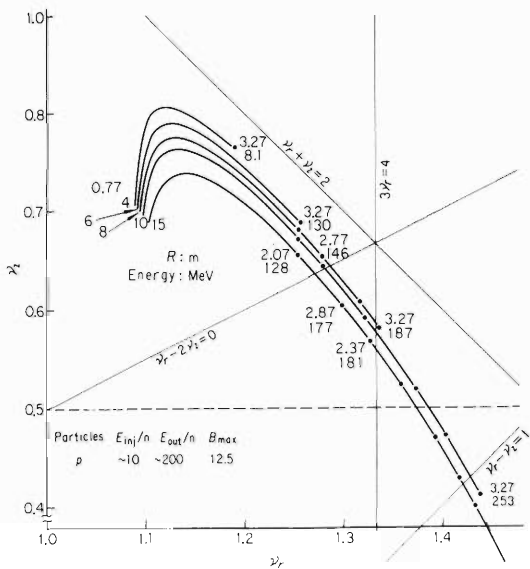


Fig. 2. Focusing properties for various injection energies of proton beam.

In order to specify the most favourite parameters, two 1/4-scale model magnets were constructed to obtain detailed information on properties of sector magnets: their excitation characteristics, field distribution which includes the interference by adjacent magnet, and field formation for accelerating the beam.

Excitation characteristics and relative field distribution inside and outside of the gap were measured preliminarily using an NMR calibrated Hall plate (SBV-595) without a temperature stabilizer. These measurements of the magnetic field were done to get rough information on properties of the sector magnets. The excitation curve obtained is shown in Fig. 3, being in good agreement with the calculated one. It may be seen that assumed magnetic induction at various points along the magnetic circuit is quite reasonable. The radial distributions along the center line of the sector magnet are shown in Fig. 4 at magnetic field of 1.2, 1.5, and 1.75 Wb/m<sup>2</sup>. The decrease of magnetic flux near the center is supposed to be due to slight local saturation effect. The correction for obtaining the isochronous field can be made by trimming coils.

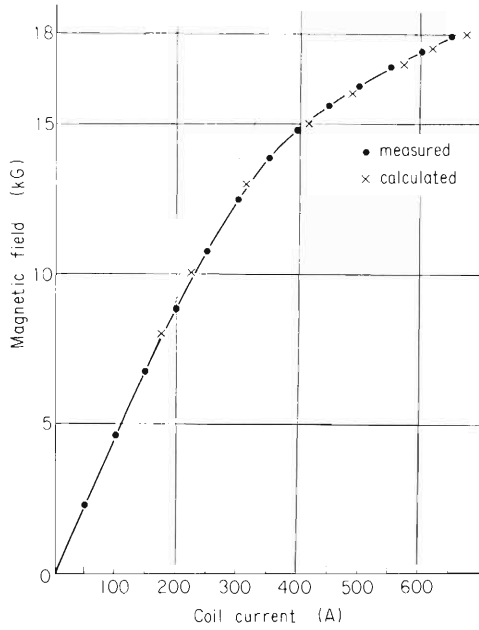


Fig. 3. Excitation characteristics of the model sector magnet.

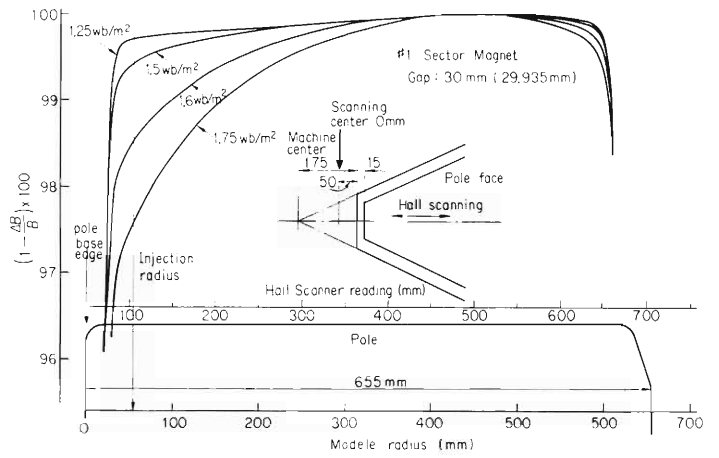


Fig. 4. Radial field distribution along the center line of the model sector magnet. Relative values are normalized to the maximum field at radius of 45 cm.

Azimuthal field distributions are measured at 4 radii in two regions: one where there exists the interference by the adjacent magnet and the other where there is no such interference. Results are shown in Fig. 5(a) and 5(b). Effect of interference is observed in the field distribution near the center. Accurate and extensive measurements of the magnetic field and computations of the beam dynamics are in progress.

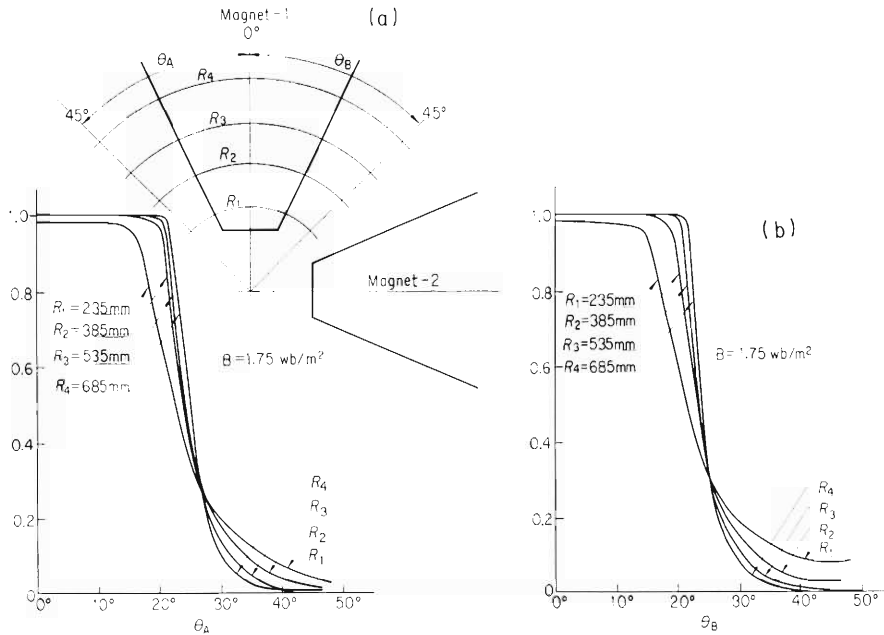


Fig. 5. Azimuthal field profiles of the magnetic field normalized to the maximum value at radius of 53.5 cm ( $Q_B$ ) and ( $Q_A$ ) indicate the region with and without the effect of interference by adjacent magnets.

References

- 1) M. Odera: Proc. Proton Linear Accelerator Conference., Chalk River, p. 62 (1976).
- 2) I. Miura: SPYRING CODE, private communication.

## 3-5. Design Study of a Linac-Injected Separated Sector Cyclotron (2)

Six-sector SSC

N. Nakanishi, F. Yoshida, S. Motonaga, and H. Kamitsubo

A separated sector cyclotron (SSC) is adopted as a booster accelerator for a variable frequency heavy ion linac. Possibility of a 6-sector SSC is investigated and a typical example is presented herein.

It is well known that beam stability depends on the property of its betatron oscillation around the equilibrium orbit. The behavior of focusing frequencies  $\nu_r$  and  $\nu_z$  shows the beam stability in the process of acceleration, in which these parameters  $\nu_r$ ,  $\nu_z$  are respectively the radial and axial oscillation frequencies expressed in units of the revolution frequency of the particle. Actually, the space of focusing frequency  $\nu_r - \nu_z$  is divided into several regions by resonance lines which make oscillation amplitude large. Thus it is required that the beam path in the  $\nu_r - \nu_z$  space should not cross the resonance lines, or that some measures should be taken technically if the path intersects the lines.

Investigations have been carried out to find out magnet configurations which satisfy kinematic conditions for beam focusing and isochronism. Calculations have been made modifying the code developed by Gordon.<sup>1)</sup>

The SSC composed of six sectors is assumed to have straight edges and an appropriate fringing field. Main parameters of the SSC are summarized in Table 1, and final energies expected for various particles are given in Table 2. Figure 1 shows the behaviors of focusing frequencies in the  $\nu_r - \nu_z$  space. Since curves for proton cross the resonance lines, further investigation has to be

Table 1. The parameters of the present separated-sector cyclotron.

Orbit	Energy constant K	260(C <sup>6+</sup> )~340(15 MeVp <sup>+</sup> )~445(U <sup>40+</sup> )
	Injection radius R <sub>i</sub>	0.88 m
	Extraction radius R <sub>e</sub>	3.40 m
	Burst numbers per turn	9
	Energy ratio E <sub>e</sub> /E <sub>i</sub>	14.5~22.5
	Betatron frequency	$\nu_r$ 1.0~1.5 $\nu_z < 0.95$
Magnet	Number of sectors	6
	Sector angle	29.4°
	Magnet gap	10 cm
	Field strength B	10~18 kG
	Number of trim coils	~20
	Iron weight	1500 t
RF	Number of dees	3
	Dee angle	20°
	Frequency range	18~45 MHz
	Harmonic number	≤ 9

Table 2. Final energies of some particles .

Particle	Initial energy (MeV)	Final energy (MeV)	Maximum field (kG)
$^1\text{p}^+$	10	189	12.2
$^1\text{p}^+$	15	336	16.8
$^4\text{He}^{2+}$	16	258	13.7
$^{12}\text{C}^{6+}$	48	773	13.8
$^{20}\text{Ne}^{9+}$	90	1468	16.4
$^{40}\text{Ar}^{15+}$	120	1887	15.6
$^{84}\text{Kr}^{24+}$	160	2452	16.1
$^{132}\text{Xe}^{30+}$	180	2724	17.0
$^{238}\text{U}^{37+}$	200	2991	19.3

made concerning beam dynamics.

As to the number of sectors it is considered that a SSC with 6 sectors is superior to one with 4 sectors because of the following reasons: (1) Resonance lines are less in the used region of the  $\nu_r - \nu_z$  space. (2) The total weight of the magnet is lighter. (3) There exists a possibility of larger turn-separation owing to three dee structure.

Investigation is also in progress for the magnet with spiral edges.

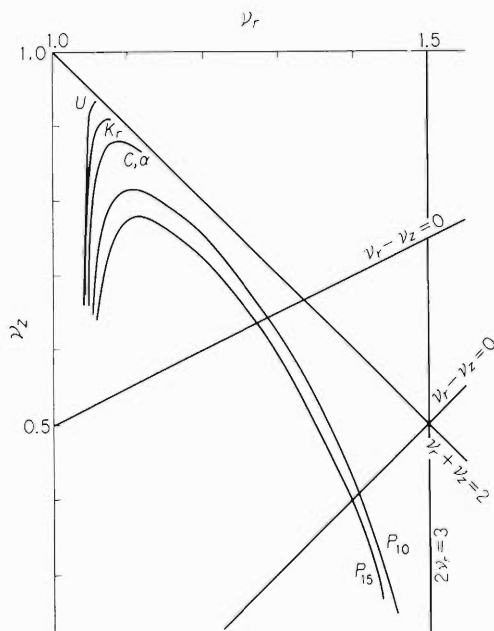


Fig. 1. Behaviors of focusing frequency in the  $\nu_r - \nu_z$  space. Straight lines are resonance lines. Symbols  $P_{10}$  and  $P_{15}$  represent curves corresponding to 10 MeV and 15 MeV protons, respectively.

#### Reference

- 1) M. M. Gordon: Nucl. Instr. and Meth., 83, 267 (1970).

## 3-6. Beam Study on the Baby Cyclotron

T. Karasawa

## (1) Phase history of an ion

The phase,  $\theta_1$ , of an ion crossing the acceleration gap at the radius,  $r_1$ , is given by the following equation for the 2nd harmonic acceleration with two 45-degree dees in push-push excitation,

$$\sin(\theta_1 - 45^\circ) - \sin(\theta_0 - 45^\circ) = \sqrt{2} \pi \frac{E_1}{V_0} \left[ \frac{\omega_e/2 - \omega_0}{\omega_0} + \frac{1}{r_1^2} \int_0^{r_1} \frac{B_0 - B(r)}{B_0} d(r^2) + \frac{E_1}{2m_0c^2} \right] \quad (1)$$

where  $\omega_e$  is the frequency of the R. F. voltage applied to the dees,  $\omega_0$  is the rotation frequency of an ion,  $B_0$  is the magnetic field and  $\theta_0$  is the phase of an ion at the center of the magnet, respectively.  $E_1$  is the energy of an ion at the radius of  $r_1$ ,  $m_0c^2$  is the relativistic expression for mass and energy and  $V_0$  is half of the peak to peak R. F. voltage.

If  $\theta_0$ ,  $B_0$  and  $B(r)$  are given,  $\theta_1$  can be calculated by using equation (1). However, Garren and Smith<sup>1)</sup> have developed experimental method for the determination of  $\theta_1$  as a function of radius. In Fig. 1, a calculated phase history of 9.4 MeV proton accelerated by the 2nd harmonic mode is shown together with experimental results measured by the method of Garren and Smith.

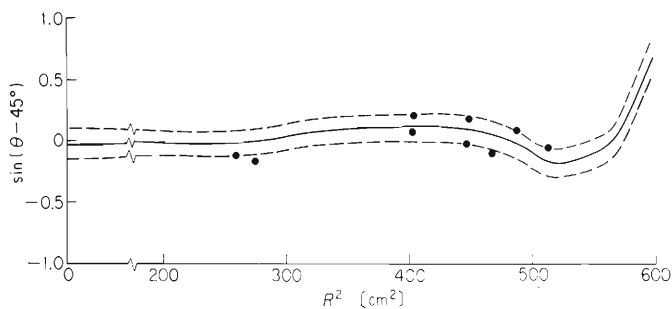


Fig. 1. Displacement of the orbit center for three different positions of the ion source. Data points for the displacement correspond to ion source positions. Figures attached to the points indicate the number of revolution.

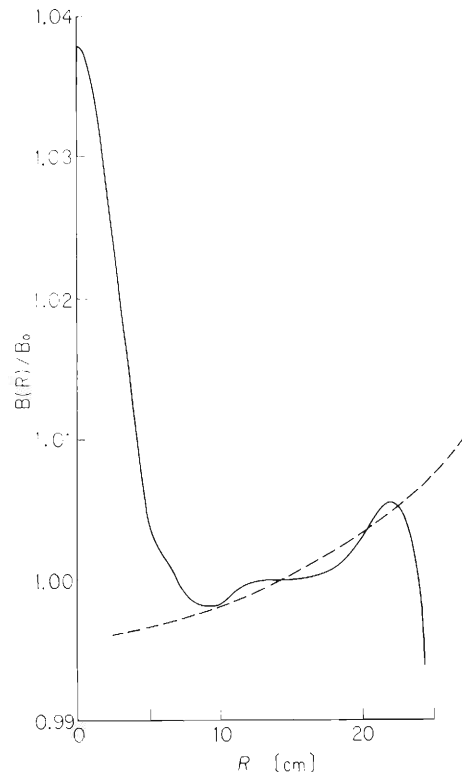


Fig. 2. Magnetic field distribution. Dotted line shows isochronous field for 9.4 MeV proton.

The magnetic field distribution is shown in Fig. 2. In the case of 9.4 MeV protons,  $\theta_0$  is suitable for the maximum energy gain per turn and isochronism is sufficient up to nearly the maximum radius, as shown in Fig. 1.

While, in the case of 4.7 MeV deuteron accelerated by the 4th harmonic mode, wider spread of  $\theta_0$  and large phase excursion from +90 degrees to -90 degrees were observed.

(2) Displacement of orbit center from the magnetic center at higher harmonic mode acceleration

It is well known that an orbit center of an ion is displaced by the first harmonic in the magnetic field.<sup>2)</sup> At the higher harmonic mode acceleration, orbit center displacement is caused by occurrence of asymmetries of both the magnetic field and the acceleration field. The latter is generated by phase difference of the ion arriving at the acceleration gaps.<sup>3)</sup>

According to Hagedoorn and Vester,<sup>4)</sup> the displacement of orbit center from the magnetic center is written as given by polar coordinates  $\rho$  and  $\varphi$ . For the 2nd harmonic acceleration with two 45-degree dees in push-push excitation, variation of  $\rho$  and  $\varphi$  per revolution of an ion,  $\Delta\rho$  and  $\Delta\varphi$ , can be given by following equations

$$\left. \begin{aligned} \Delta\rho &= -\frac{V_0}{E}\rho\sin(2\varphi+\theta+45^\circ) + \pi r C_1 \sin(\varphi-\psi_1) \\ \Delta\varphi &= -\frac{V_0}{E}[\sqrt{2}\sin(\theta-45^\circ) - \sin(2\varphi+\theta-45^\circ)] \\ &\quad + \pi \frac{r}{\rho} C_1 \cos(\varphi-\psi_1) + 2\pi(\nu_r-1) \end{aligned} \right\} \quad (2)$$

where  $V_0$ ,  $E$ ,  $\theta$  and  $r$  are the same meaning in the Eqn. (1).  $C_1$  and  $\psi_1$  are the amplitude and phase of the first term in a Fourier expansion of the azimuthal variation in the magnetic field.  $\nu_r$  is the radial betatron oscillation frequency.

Figure 3 shows the results of computation of the orbit center displacement at the 2nd harmonic mode acceleration for three different positions of the ion source. The ion source position works as an initial condition for the Eqn. (2).

It is seen that a small change of the ion source position is responsible for a large displacement of the orbit center. We are now searching for an optimum accelerating condition, carrying out detailed numerical calculations and experimental study using shadow technique.<sup>5)</sup>

The author would like to acknowledge the collaboration of the cyclotron group at the Muroran Plant of Japan Steel Works in Hokkaido.

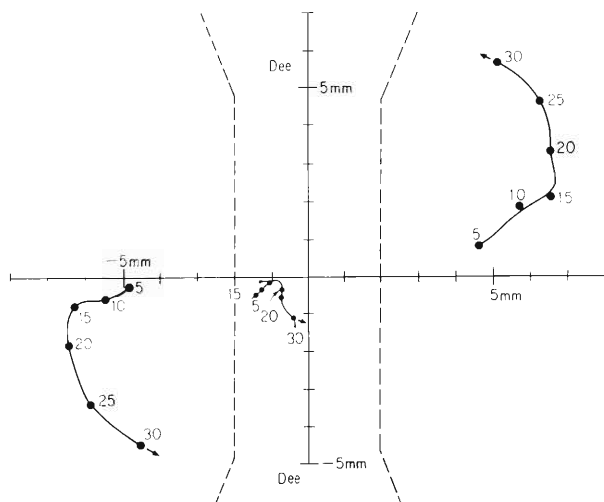


Fig. 3. Phase of a 9.4 MeV proton vs. square of radius.

## References

- 1) A. A. Garren and L. Smith: CERN 63-19, p. 18 (1963).
- 2) J. M. Nieuland: Phillips Res. Repts. Suppl., No. 2. (1972).
- 3) T. Karasawa and Y. Kaneda: Reports of I.P.C.R., (in Japanese), 53, 35 (1977).
- 4) H. L. Hagedoorn and N. F. Verster: N. I. M. 18-19, p. 217 (1962).
- 5) J. R. Richardson: Progress in Nucl. Techniques & Instrumentation (I), p. 66, 1965 North-Holland Publ. Amsterdam.

## 4. NUCLEAR PHYSICS

## Scattering and Reactions

4-1. Spin Flip in the Inelastic Scattering of Polarized Protons on  $^{12}\text{C}$ 

T. Fujisawa, S. Motonaga, F. Soga, M. Yasue,\*  
 N. Ueda,\* T. Hasegawa,\* M. Nakamura,\*\*  
 T. Wada, H. Toba, and H. Kamitsubo

The spin flip probability of polarized protons exciting the  $2^+$  state of  $^{12}\text{C}$  was measured using the  $(pp'\gamma)$  method, i.e., by measuring the angular correlation between protons scattered inelastically from the  $2^+$  excited state and the  $E2(2^+ \rightarrow 0^+ \text{ ground})$  de-excitation  $\gamma$ -rays emitted perpendicularly to the scattering plane.<sup>1),2)</sup> The polarized proton beam extracted from the atomic beam type polarized ion source which was constructed at The Institute of Physical and

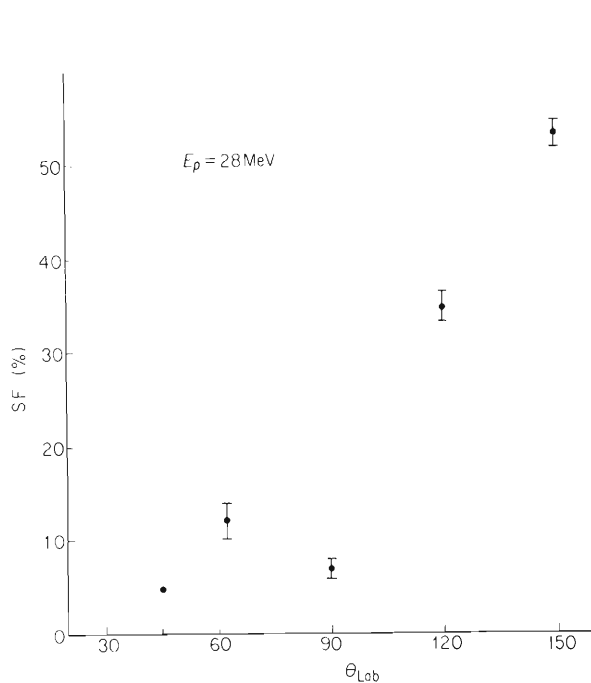


Fig. 1. Proton spin flip probability(SF) in the reaction  $^{12}\text{C}(pp')^{12}\text{C}^*(4.43 \text{ MeV})$  at  $E_p = 28 \text{ MeV}$ .

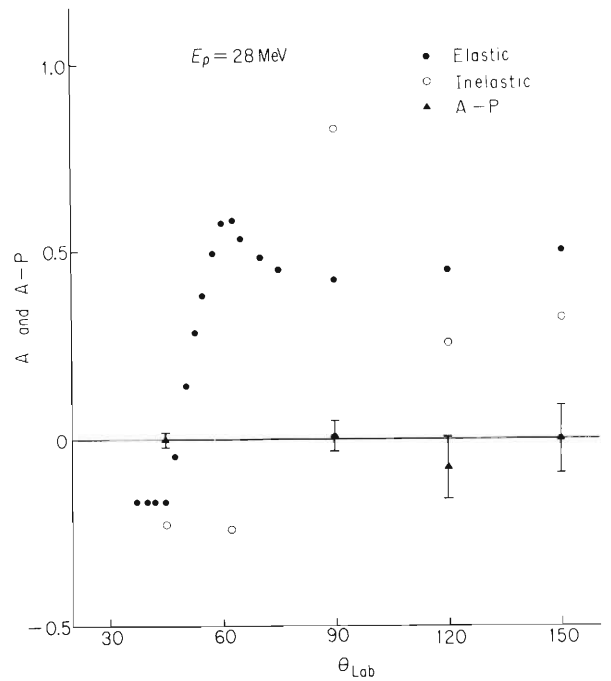


Fig. 2. Analyzing power of the elastic and inelastic scattering of proton by  $^{12}\text{C}$  at 28 MeV(A). And difference between analyzing power and polarization of the inelastic scattering (A-P). The open and closed circles represent the analyzing powers of the inelastic and elastic scattering, respectively. The triangle represents A-P.

\* Institute for Nuclear Study, University of Tokyo.

\*\* Department of Physics, Kyoto University.

Chemical Research was accelerated to 28 MeV in the SF Cyclotron of Institute for Nuclear Study.<sup>3)</sup> The beam current at the scattering chamber named SF 80 was about 1 nA and the size of the beam spot on the target was 2 mm × 3 mm. The  $\gamma$ -rays were detected with a 7.6 cm × 7.6 cm NaI(Tl) crystal mounted on a 56 AVP photomultiplier which was situated above the chamber. It had a slit made of lead 10 cm thick with an aperture of 57 mm $\phi$ . The scattered protons were detected by ORTEC 5000  $\mu$ m surface barrier and 5000  $\mu$ m Li-drift SSDS with defining slits of 6 mm $\phi$  placed symmetrically to the beam direction at points 11 cm from the target. The detectors monitoring the beam polarization which were consisted of two 2000  $\mu$ m surface barrier units with aluminum absorbers 2 cm thick and defining slits of 6 mm $\phi$  were situated at angles of 62.5 degrees from the beam direction symmetrically in the same scattering chamber because the analyzing power of  $^{12}\text{C}$  for the proton is known at the same energy.<sup>4)</sup> Difference in the efficiencies of two detectors and the difference of solid angles were compensated by measuring the asymmetry of the polarized and unpolarized beams alternately. Figures 1 and 2 show the preliminary result.

#### References

- 1) F. H. Schmidt, R. F. Brown, J.B. Gerhart, and W. A. Kolasinski: Nucl. Phys., 52, 253 (1964).
- 2) T. Fujisawa: Genshikaku Kenkyu (in Japanese), 21, No.4, p. 849 (1976).
- 3) T. Fujisawa, S. Motonaga, N. Ueda, S. Yamada, T. Hasegawa, T. Wada, H. Toba, and H. Kamitsubo: IPCR Cyclotron Progr. Rep., 11, 8 (1977).
- 4) R. M. Craig, J. C. Dore, G. W. Greenlees, J. Lowe, and D. L. Watson: Nucl. Phys., 83, 493 (1966).

## 4-2. Two-Step Process in Proton Inelastic Scattering

H. Amakawa, A. Mori,\* and K. Yazaki\*\*

The reaction mechanism of single particle excitation reaction induced by protons is studied using the three-body model. In this model, the target nucleus is assumed to consist of a neutron and inert core nucleus. Employing the two-step approximation, the reaction amplitude  $T_{fi}$  of this model is decomposed into three terms: the DWBA term, the  $(p, d, p')$  term (pickup-stripping process via the ground state deuteron ( $d$ ) propagation) and the  $(p, d^*, p')$  term (pickup-stripping process via the continuum  $p$ - $n$  system ( $d^*$ ) propagation). Thus,  $T_{fi}$  is expressed as follows:

$$T_{fi} = \langle \chi_f^{(-)} | t | \chi_i^{(+)} \rangle ,$$

$$t = v_{pn} + v_{pn} | \phi_d \rangle \frac{1}{E - H_0 - \epsilon_0 - U_d + i\epsilon} \langle \phi_d | v_{pn}$$

$$+ \int v_{pn} | \phi_{\vec{k}}^{(+)} \rangle \frac{1}{E - H_0 - \epsilon_k - U_d + i\epsilon} \langle \phi_{\vec{k}}^{(+)} | v_{pn} d\vec{k} ,$$

where  $\chi$ 's are distorted waves,  $\vec{k}$  is a relative momentum between  $p$  and  $n$ ,  $H_0$  and  $v_{pn}$  are kinetic energy operator and  $p$ - $n$  interaction, respectively.  $\phi_d$  and  $\phi_{\vec{k}}^{(+)}$  denote the internal wave functions for  $d$  and  $d^*$  whose energies are  $\epsilon_0$  and  $\epsilon_k$ , respectively.  $U_d$  is an appropriate potential

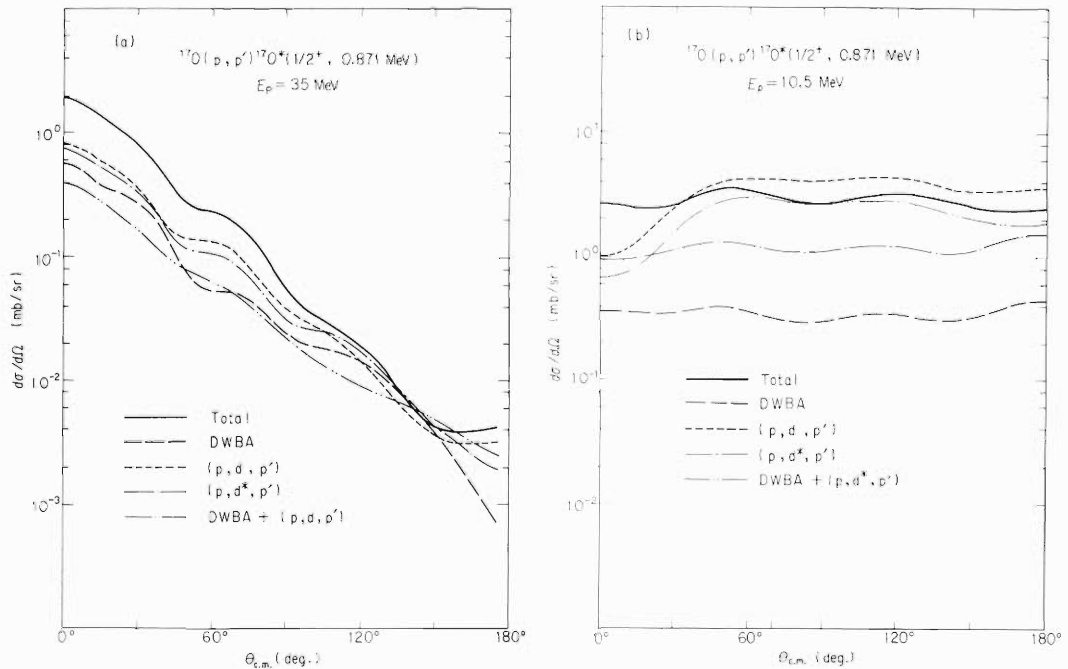


Fig. 1. Calculated cross sections for  $^{17}\text{O}(p, p')^{17}\text{O}^*(1/2^+, 0.871 \text{ MeV})$  reactions at  $E_p = 35 \text{ MeV}$  (Fig. 1(a)) and  $10.5 \text{ MeV}$  (Fig. 1(b)). Solid curves denote the coherent sum of the DWBA,  $(p, d, p')$  and  $(p, d^*, p')$  cross sections. Spectroscopic amplitudes are assumed to be 1.0.

\* Numazu Technical College.

\*\* Department of Physics, University of Tokyo.

which depends only on the p-n center-of-mass coordinate relative to the core nucleus. In the following numerical calculations, we use the optical potentials for  $U_d$  which reproduce the elastic scatterings of deuteron.

We calculate these three terms in the case of  $^{17}\text{O} (p, p') ^{17}\text{O}^* (1/2^+, 0.871 \text{ MeV})$  reactions at 35 and 10.5 MeV bombarding energies. It has previously been pointed out that the finite range effect of the pickup-stripping transition is important.<sup>1)</sup> Therefore, we have performed the exact finite range calculations using the computer code TWOFNR.<sup>2)</sup> For the p-n continuum state, only the s-state was included. The integration over  $\vec{k}$  was replaced by the summation over  $\epsilon_k$ . The parameters of the optical potentials were taken from Ref. 3 and 4.

In the 35 MeV case (Fig. 1(a)), the  $(p, d^*, p')$  term has a magnitude comparable to other two terms. If one does not include the  $(p, d^*, p')$  term in the reaction amplitude, the cross section (double-dotted-solid curve of Fig. 1 (a)) at forward angles is reduced by a factor of 1/4. This clearly shows the importance of the  $(p, d^*, p')$  term at this bombarding energy.

On the other hand, in the 10.5 MeV case (Fig. 1 (b)), the  $(p, d, p')$  term almost dominates over the reaction amplitude. The DWBA and  $(p, d^*, p')$  terms do not play an important role at this bombarding energy.

## References

- 1) P. D. Kunz and L. A. Charlton: Phys. Lett., 61B, 1 (1976).
- 2) M. Igarashi: unpublished.
- 3) M. D. Cooper, W. F. Hornyak, and P. G. Roos: Nucl. Phys., A218, 249 (1974).
- 4) E. Newman, L. C. Becher, B. M. Preedom, and J. C. Hilbert: *ibid.*, A100, 225 (1967).

### 4-3. DWBA Analysis of Proton Inelastic Scattering from $^{28,29,30}\text{Si}$ and Blocking Effects in the Core-Excitation of $^{29}\text{Si}$

Y. Toba, N. Nakanishi, H. Sakaguchi,\* A. Goto,\*  
F. Ohtani,\* N. Kishida, M. Yasue,\*\* and T. Hasegawa\*\*

In order to investigate the blocking effect in the core-excitation of  $^{29}\text{Si}$  caused by the Pauli principle, proton inelastic scattering experiments on  $^{28,29,30}\text{Si}$  were performed with a 16.2 MeV proton beam from the IPCR cyclotron and a 51.9 MeV proton beam from the INS synchrocyclotron. The experimental results at IPCR have already been reported.<sup>1)</sup> In the experiments at INS, a broad range magnetic spectrograph<sup>2)</sup> was used for the detection of scattered particles. The targets which were used in the  $^{28,30}\text{Si}$  (p, p') experiment were a 1.02 mg/cm<sup>2</sup> thick foil of natural silicon ( $^{28}\text{Si}$  92.2% abundant) and a 0.165 mg/cm<sup>2</sup> thick foil of enriched silicon oxide ( $^{30}\text{Si}$  95.6% abundant) with 0.5 mg/cm<sup>2</sup> Mylar backing. These were prepared by a centrifugal precipitation method.<sup>3)</sup> A  $^{29}\text{Si}$  0.135 mg/cm<sup>2</sup> self-supporting foil of enriched silicon oxide ( $^{29}\text{Si}$  92.2% abundant) was prepared by vacuum evaporation.

Figures 1, 2, and 3 show 51.9 MeV and 16.2 MeV data together with results of the DWBA calculations, respectively. In the DWBA calculations of the inelastic scatterings to the  $2^+$  states of  $^{28,30}\text{Si}$ , a macroscopic form factor was used. In the case of the  $3/2_1^+$  1.27 MeV,  $5/2_1^+$  2.03 MeV,  $3/2_2^+$  2.43 MeV, and  $5/2_2^+$  3.07 MeV states of  $^{29}\text{Si}$ , wave functions calculated with the intermediate-coupling model by Castel et al.<sup>4)</sup> were used. On that occasion, core-excitations were calculated

Table 1. Optical potential parameters used in  
the optical model and DWBA calculations.

$E_p$	$V_O(\text{MeV})$	$r_O(\text{fm})$	$a_O(\text{fm})$	$W_V(\text{MeV})$	$W_V(\text{MeV})$	$r_I(\text{fm})$	$a_I(\text{fm})$	$V_{SO}(\text{MeV})$
51.9 MeV	36.456	1.18	0.7	7.043	1.394	1.182	0.692	5.4
16.2 MeV	53.575	1.186	0.65	0.659	10.249	1.085	0.533	5.424

$r_c = 1.25$  fm, and  $r_{SO}$  and  $a_{SO}$  are the same as  $r_O$  and  $a_O$ , respectively, except  $a_{SO} = 0.6$  fm for  $E_p = 16.2$  MeV

Table 2.  $\beta_2$ -value deduced from the DWBA calculations.

$E_p$	$^{28}\text{Si}$	$^{29}\text{Si}$	$^{30}\text{Si}$
51.9 MeV	0.42	0.364	0.36
16.2 MeV	0.51	0.434	—

\* Faculty of Science, Kyoto University.

\*\* Institute for Nuclear Study, University of Tokyo.

with macroscopic form factors and single particle excitations were calculated microscopically with the Blatt-Jackson potential for the two-body interaction. Optical potentials used in the calculations are shown in Table 1. Collective  $2^+$  strengths  $\beta_2$  deduced from the analyses are shown in Table 2. Apart from the 16.2 MeV data which are affected remarkably by giant resonances, the 51.9 MeV data show that the core-excitation of  $^{29}\text{Si}$  is reduced by about 25% compared with  $^{28}\text{Si}$ , but is almost the same as  $^{30}\text{Si}$ .

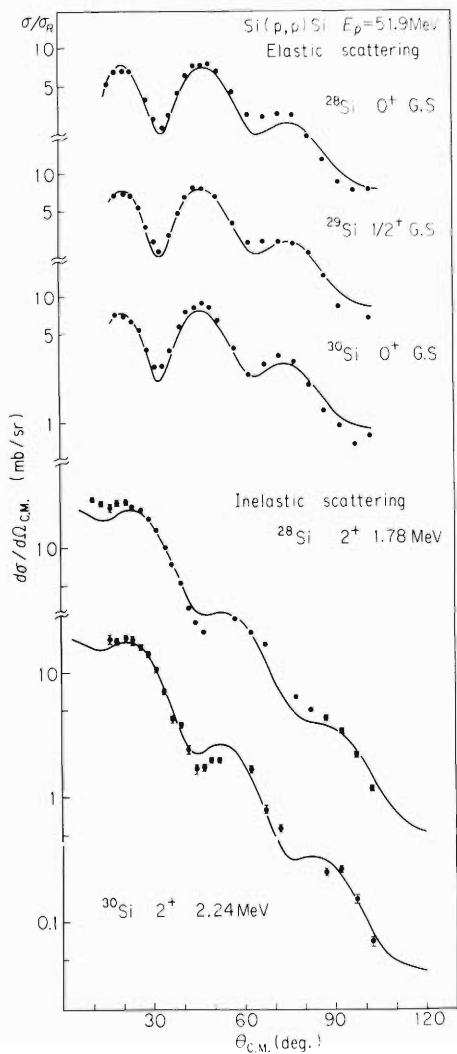


Fig. 1. Angular distributions of 51.9 MeV elastic proton scattering on  $^{28,29,30}\text{Si}$  and inelastic scattering to the  $2^+$  state of  $^{28,30}\text{Si}$ . The solid curves represent the optical model fits and DWBA calculations.

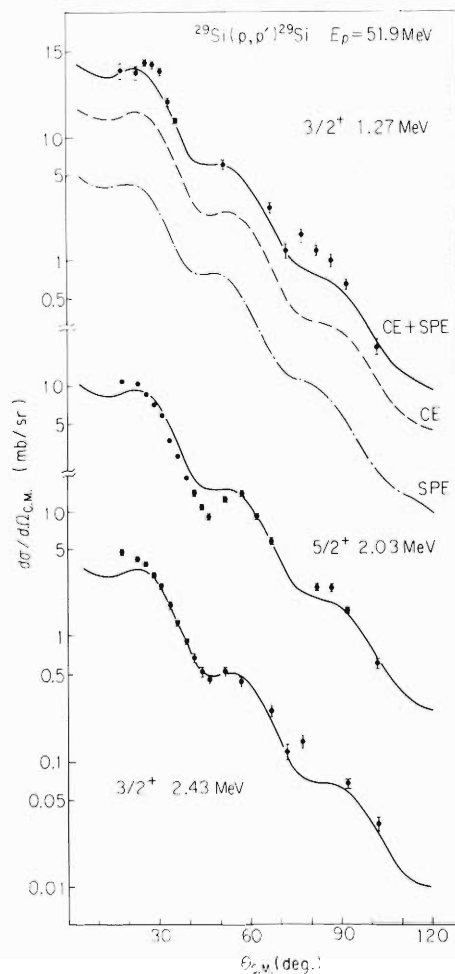


Fig. 2. Angular distributions of 51.9 MeV inelastic proton scattering to the  $3/2_1^+$ ,  $5/2_1^+$ ,  $3/2_2^+$ , and  $5/2_2^+$  states of  $^{29}\text{Si}$ . The solid lines represent DWBA calculations. In the case of  $3/2_1^+$  state, the contributions of the core-excitation (CE) and the single particle excitation (SPE) are represented by a dashed and a dash-dotted curve respectively.

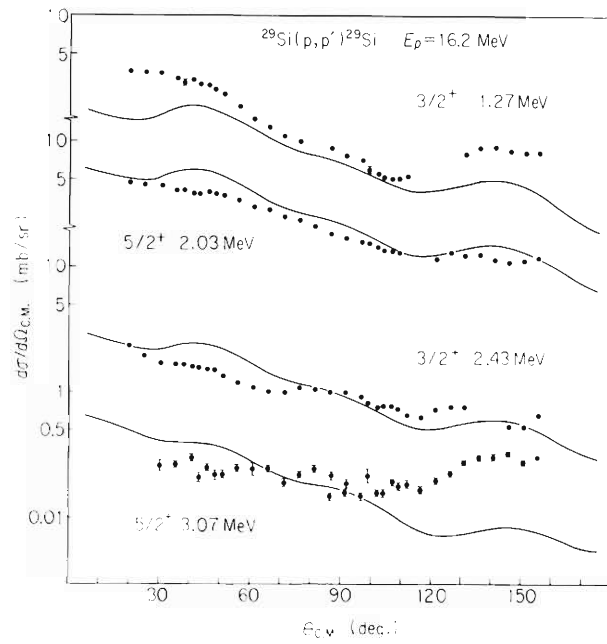


Fig. 3. Angular distributions of 16.2 MeV inelastic proton scattering to the  $3/2_1^+$ ,  $5/2_1^+$ ,  $3/2_2^+$ , and  $5/2_2^+$  states of  $^{29}\text{Si}$  and DWBA curves.

#### References

- 1) Y. Toba, N. Nakanishi, H. Sakaguchi, A. Goto, N. Kishida, and F. Ohtani: IPCR Cyclotron Progr. Rep., 10, 21 (1976).
- 2) K. Yagi, H. Ogawa, Y. Ishizaki, T. Ishimatsu, J. Kokame, and K. Matsuda: Nucl. Instr. Meth., 52, 29 (1967).
- 3) I. Sugai: *ibid.*, 145, 409 (1977).
- 4) B. Castel, K. W. C. Stewart, and Harvey: Can. J. Phys., 48, 1490 (1970).

## 4-4. Analysis of (p, t) Reaction Induced by Polarized Protons

T. Kammuri

Some (p, t) and (p,  $^3\text{He}$ ) reactions using a 49.5 MeV polarized proton beam were studied by Nelson et al.<sup>1)</sup> Only poor fits to the experimental cross sections and analyzing powers were obtained by the zero-range DWBA calculation. Here we present the analysis for the  $^{12}\text{C}(p, t)^{10}\text{C}$  ground state reaction by the DWBA method which includes the effects of the finite-range force and the sequential transfer.<sup>2)</sup> Simultaneous transfer process is treated by the sum of interaction method, thus making it convenient to see the competition between one- and two-step processes.

The parameters of the optical potentials used are listed in Table 1. In treating the finite-range force, we take the Yukawa interaction ( $V_0 = 100$  MeV,  $\mu = 1$  fm) together with the Hulthen type wave functions for light ions, and the Gaussian force ( $V_0 = 70$  MeV,  $\mu = 1.58$  fm) with the Gaussian wave functions. Zero-range strengths  $D_0^2$  (in unit of  $10^4$  MeV<sup>2</sup> fm<sup>3</sup>) are 8.8, 1.02, and 3.37 for (p, t) (p, d) and (d, t) respectively.

Table 1. Optical parameters for  $^{12}\text{C}(p, t)^{10}\text{C}$  calculations.

	V	$r_0$	$a_0$	W	$r_I$	$a_I$	$V_s$	$r_s$	$a_s$	$r_C$
t	132.9	1.54	0.57	19.5	1.82	0.22	0			0.81 <sup>a)</sup>
t	131.2	"	"	19.7	"	"	5.0	1.54	0.57	0.81 <sup>b)</sup>
p	35.2	1.15	0.68	4.87	1.10	1.14	3.42	0.62	0.24	1.25 <sup>c)</sup>
d	109.2	1.0	0.9	22.3	1.52	0.50	0			1.0 <sup>d)</sup>

Imaginary part of triton and proton potentials are of volume type, while that of deuteron has surface-peaked shape.

Potentials a), b), and c) are taken from Ref. 1, referred there as HB3, 5HB3, and PEC, respectively.

Firstly we discuss results of simultaneous transfer. Oscillations in the differential cross sections cannot be obtained by the zero-range calculation while they are stronger than the data in the finite-range case (Fig. 1). Inclusion of the spin-orbit term in the triton potential affects the analyzing power  $A(\theta)$  but the fit to the data becomes worse (Fig. 2). It can be seen that all one-step results cannot dissolve disagreement with experimental  $A(\theta)$ .

Secondly we consider the results obtained by assuming the sequential transfer. Differential cross sections show oscillatory behavior with shapes similar for the zero- and finite-range calculations (Fig. 3). Good agreement with experimental cross sections can be seen. Predicted  $A(\theta)$  differs considerably from the one-step results and gives better fit to the data (Fig. 4).

In summing one- and two-step transition amplitudes expressed in the prior and prior-prior representations respectively, the one-step amplitude is reduced considerably by the non-orthogonality term, leaving 1/4 of the original magnitude. This is the reason why the composite cross section resembles very much with the latter, although the one-step cross section has the

comparable magnitude with that of the two-step process. Therefore the conclusions obtained in the two-step calculations can be applied to the composite case.

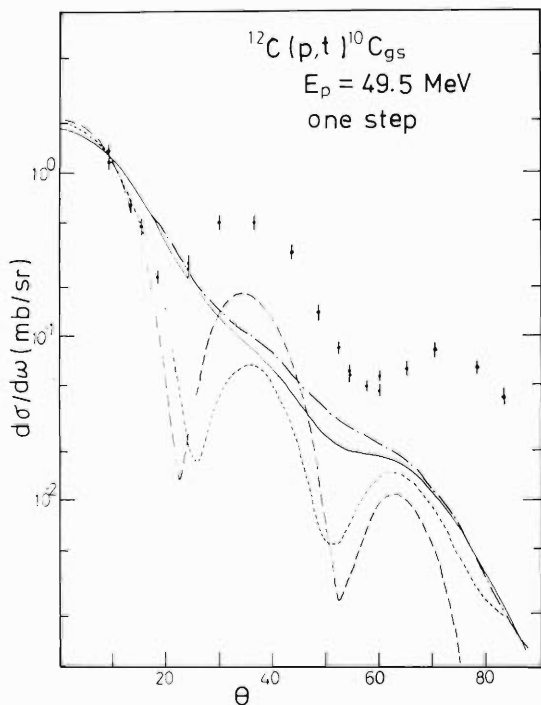


Fig. 1. Comparison of experimental cross sections and one-step DWBA calculations for the  $^{12}\text{C}(p, t)^{10}\text{C}_{\text{g.s.}}$  reaction at 49.5 MeV incident energy. Solid and dot-dashed curves are zero-range results with HB3 and 5HB3 potential respectively, while dashed and dotted curves are finite-range results with Gaussian and Yukawa interactions respectively.

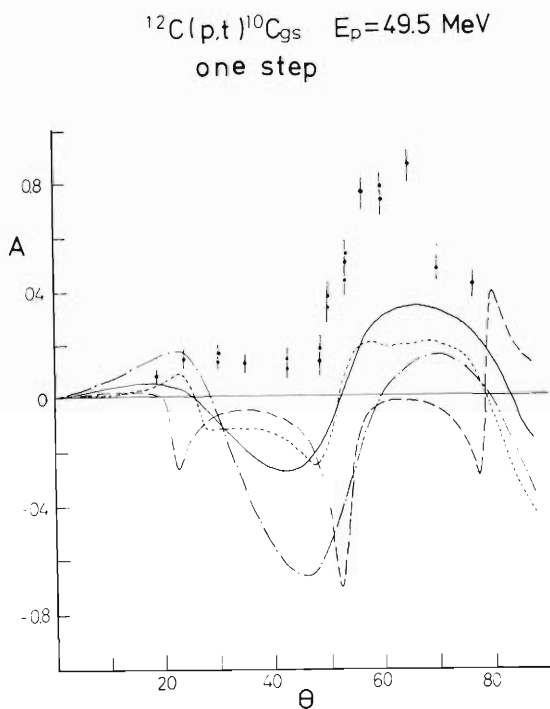


Fig. 2. Same as Fig. 1 except for the analyzing power.

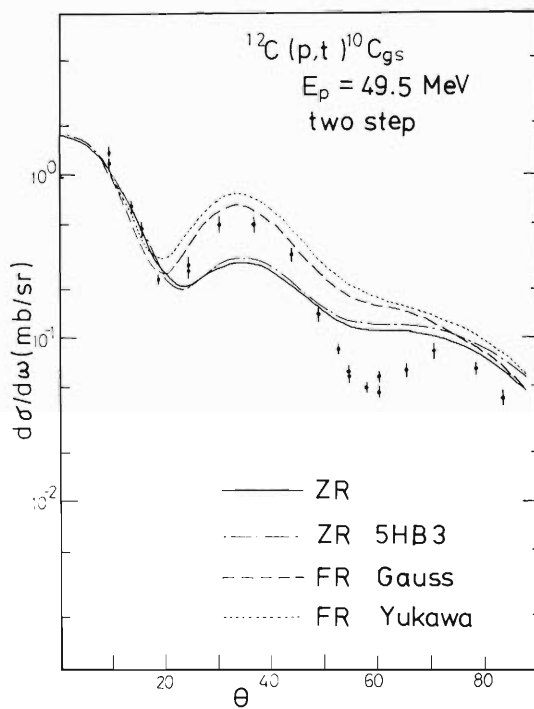


Fig. 3. Same as Fig. 1 except for the two-step calculations.

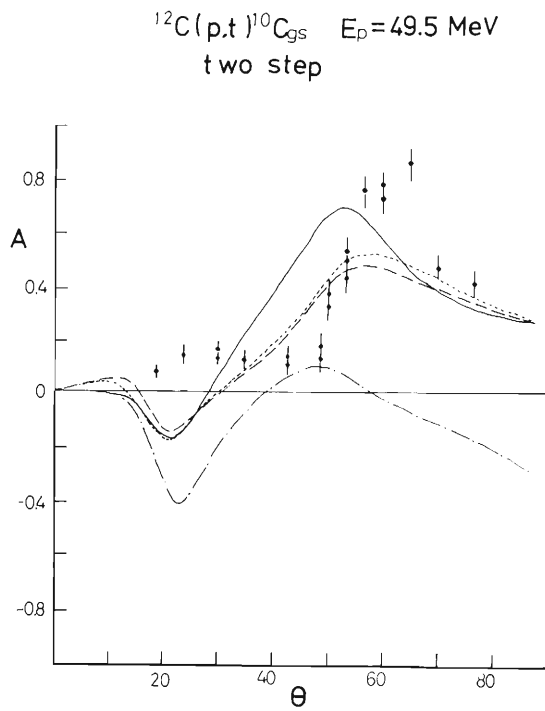


Fig. 4. Same as Fig. 2 except for the two-step calculations.

#### References

- 1) J. M. Nelson, N. S. Chant, and P. S. Fisher: Nucl. Phys., A156, 406 (1970).
- 2) T. Kammuri: to be published.
- 3) J. R. Shepard, W. R. Zimmerman, and J. J. Kraushaar: Nucl. Phys., A275, 189 (1977).
- 4) C. M. Perey and F. G. Perey: Phys. Rev., 132, 755 (1963).

4-5. Analyses of the  $^{54}\text{Fe}(d, p)^{55}\text{Fe}$  Reaction Data at  $E_d=24$  MeV

N. Kishida, N. Nakanishi, Y. Toba, and H. Ohnuma

More detailed analyses of the  $^{54}\text{Fe}(d, p)^{55}\text{Fe}$  angular distributions for the low-lying levels in  $^{55}\text{Fe}$  in terms of DWBA, CCBA and the adiabatic theory for deuteron breakup (ADB) have been made since the last report.<sup>1)</sup>

Various distorting potentials are used in the calculations. The deuteron potential D1 is an optical potential which fits the elastic angular distribution, D2 is the same as D1 but without spin-orbit potential, D3 is an adiabatic potential,<sup>2)</sup> D4 is obtained from Ref. 3, and D5 from Ref. 4. The proton potential P1 is obtained from Ref. 5, P2 is a set without spin-orbit potential searched for so as to reproduce the elastic angular distribution calculated with P1.

The potential sets D1, D4 and D5 reproduce the elastic angular distribution well. Thus those potentials are used in DWBA calculations for the ground state transition (Fig. 1). As the potential sets D4-P1 presented the best result, they are primarily used in the following calculations.

G. S. ( $3/2^-$ ). The results of DWBA and ADB calculations are shown in Fig. 2. Only the

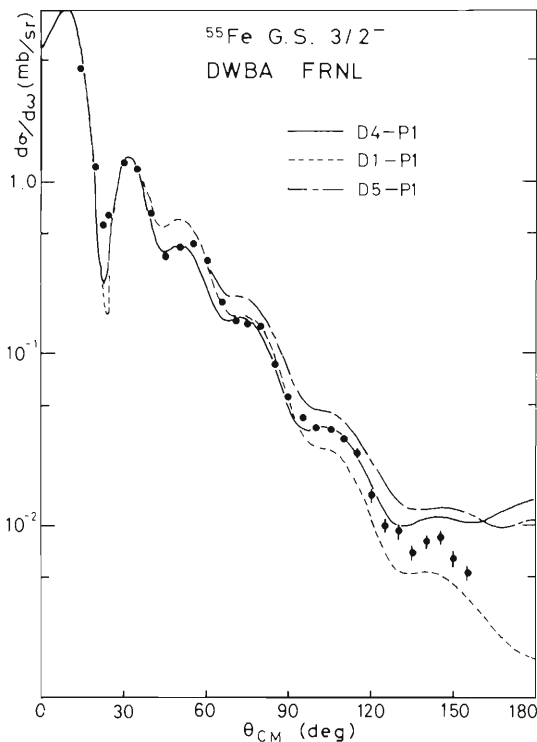


Fig. 1. Comparison of DWBA calculations with various distorting potentials.

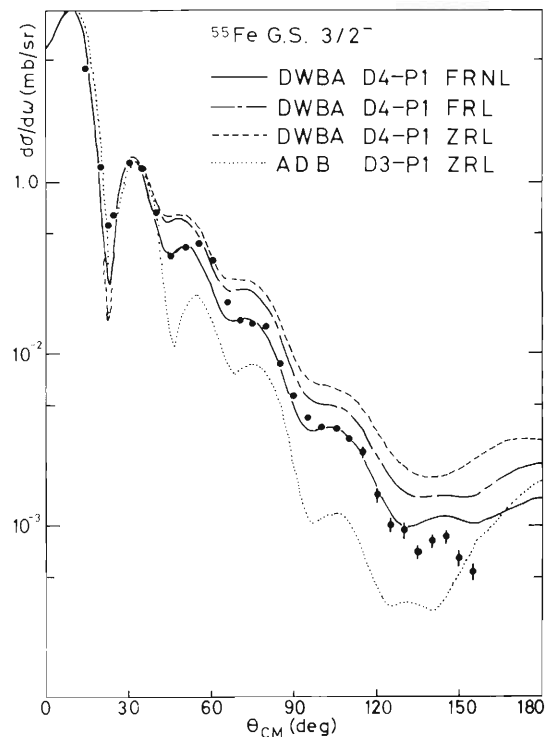


Fig. 2. DWBA and ADB calculations compared with the experimental angular distribution for ground state ( $3/2^-$ ). ZRL, FRL, and FRNL denote zero-range local, finite-range local, and finite-range nonlocal calculations, respectively. Local energy approximation has been used in FR and NL corrections.

FRNL DWBA calculation can reproduce the experimental angular distribution. Especially it should be noted that the effect of nonlocality is very large.

0.411 MeV state ( $1/2^-$ ). Fig. 3 shows the results of calculations. The ADB calculation gives a good fit. The FRNL DWBA calculation reproduces an overall shape, but it does not fall off beyond the third maximum.

0.941 MeV state ( $5/2^-$ ). FRNL DWBA calculation without spin-orbit potential (D2-P2) reproduces the angular distribution very well (Fig. 4), although its significance is not clear. We are inclined to think that this is related to the fact that  $\ell = 3$  j-dependence cannot be reproduced in (p, d) and (d, p) reactions at relatively high incident energies.

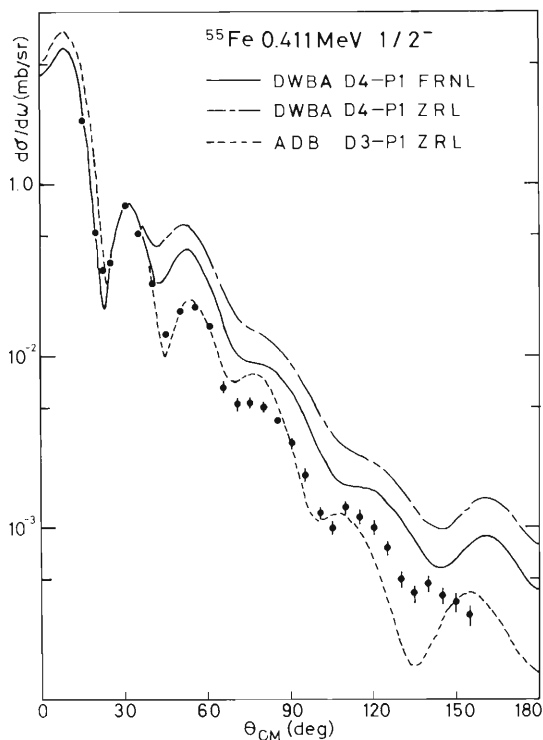


Fig. 3. DWBA and ADB calculations for the 0.411 MeV ( $1/2^-$ ) state compared with the experiment.

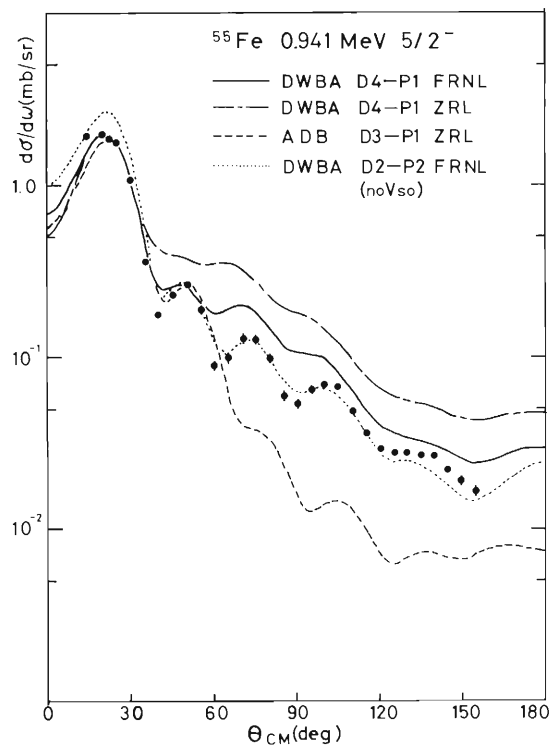


Fig. 4. DWBA and ADB calculations for the 0.941 MeV ( $5/2^-$ ) state compared with the experiment.

1.317 + 1.409 MeV states ( $7/2^-$ ). DWBA and ADB calculations cannot reproduce this angular distribution (Fig. 5). These states are not good  $f_{7/2}$  single-neutron states, because  $^{54}\text{Fe}$  is an  $f_{7/2}$  closed shell nucleus. At least one of them can rather be regarded as a phonon-particle coupled state. Indeed a good fit is obtained by CCBA calculation as shown by solid line in Fig. 6, if a small direct  $f_{7/2}$  amplitude is included. The CCBA calculation has been made without FRNL correction whose effects are very large for other transitions. Moreover a sophisticated form factor is required when the configuration mixing is large and the direct amplitude is small. Nevertheless the calculation suggests the presence of the ground state correlation in  $^{54}\text{Fe}$  ( $1\nu p_{3/2}^2 f_{7/2}^{-2}$  configuration etc.).

Exact-finite-range DWBA calculations are also performed in which D-state of the deuteron ground state is included. It is found that the inclusion of the deuteron D-state has very small effects on calculated angular distributions.

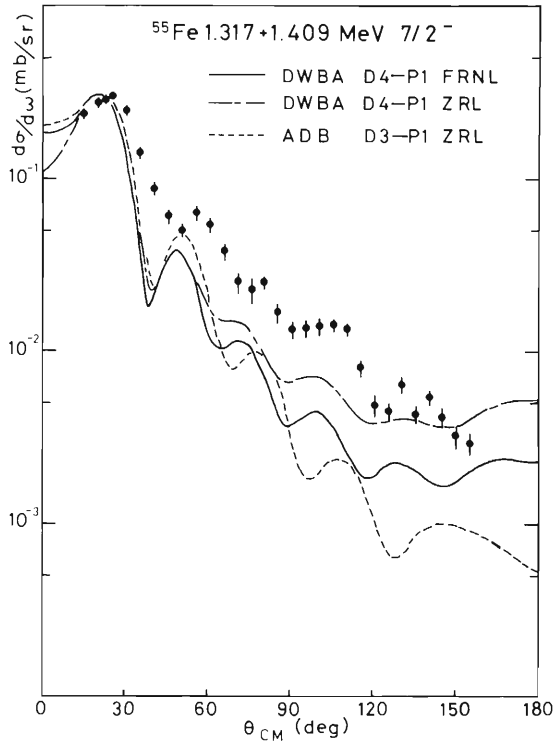


Fig. 5. DWBA and ADB calculations for the 1.317 + 1.409 MeV ( $7/2^-$ ) states compared with the experiment.

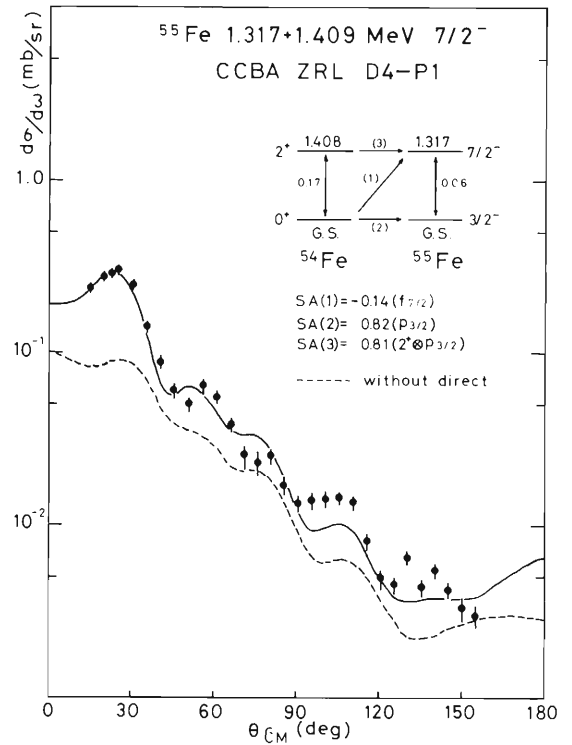


Fig. 6. ZRL CCBA calculations compared with the experimental angular distribution for the 1.317 + 1.409 MeV ( $7/2^-$ ) states.

## References

- 1) N. Kishida, N. Nakanishi, Y. Toba, and H. Ohnuma: IPCR Cyclotron Progr. Rep., 10, 23 (1976).
- 2) J. D. Harvey and R. C. Johnson: Phys. Rev., C3, 636 (1971); R. C. Johnson and P. J. R. Soper: *ibid.*, C1, 976 (1970).
- 3) J. D. Childs, W. W. Daehnick, and M. J. Spisak: *ibid.*, C10, 217 (1974).
- 4) E. Newman, L. C. Becker, B. M. Preedom, and J. C. Hiebert: Nucl. Phys., A100, 225 (1976).
- 5) F. D. Becchetti and G. W. Greenlees: Phys. Rev., 182, 1190 (1976).

## 4-6. Coupled Channel Effects on (d, p) Reactions

M. Ichimura, B. Imanishi, and M. Kawai

Rearrangement collisions are studied in a frame work of coupled channel formalism (CC) in which rearranged channels couple to each other. The purpose of this work is to investigate the effects of multistep transfer processes and thus to get some insight on limitation of the validity of DWBA and further to clarify the role of non-orthogonality terms which is characteristic of the coupling between rearranged channels.

(d, p) reactions are taken as an example, because they involve fairly simple system (a proton, a neutron and the core nucleus) and they have been studied quite well by DWBA. For simplicity, we only consider a process in which the neutron goes back and forth between the proton and the core. Namely, only the coupling between the initial deuteron (d) channel and the final proton (p) channel is taken into account.

Following the formalism presented before,<sup>1)</sup> the coupled equations for the wave functions,  $\chi_\alpha(\mathbf{r}_\alpha)$ , of the relative motion of the channels are written as

$$(T_\alpha + U_\alpha - E_\alpha)\chi_\alpha(\mathbf{r}_\alpha) = - \int \{V_{\alpha\beta}^{np}(\mathbf{r}_\alpha, \mathbf{r}_\beta) + N_{\alpha\beta}(\mathbf{r}_\alpha, \mathbf{r}_\beta)\} \chi_\beta(\mathbf{r}_\beta) d^3 r_\beta \quad (\alpha, \beta = d, p, \alpha \neq \beta),$$

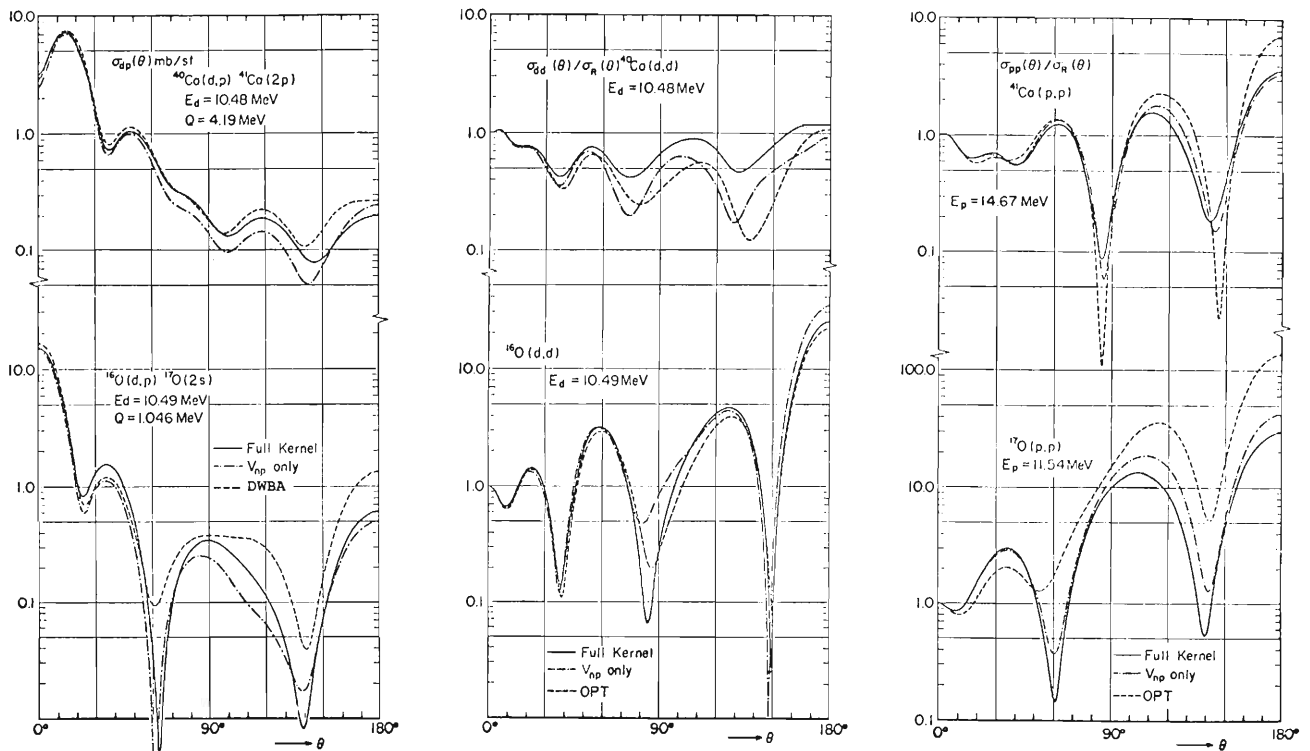


Fig. 1. The cross sections calculated by CC with full kernel (full line), by CC without non-orthogonality (dash-dot-dashed line) and by DWBA or OPT (dotted line).

where the coupling kernel is decomposed into the interaction kernel  $V_{\alpha\beta}^{np}$  due to neutron-proton interaction and the so-called non-orthogonality kernel  $N_{\alpha\beta}$ .

Numerical analyses have been done for the reactions (1)  $^{16}\text{O}(d, p)^{17}\text{O}(\text{s-state})$  with  $Q$ -value  $Q = 1.046$  MeV and the incident energy  $E_{\text{c.m.}} = 10.49$  MeV and (2)  $^{40}\text{Ca}(d, p)^{41}\text{Ca}(\text{p-state})$  with  $Q = 4.19$  MeV, and  $E_{\text{c.m.}} = 10.48$  MeV, and the (d, d) and (p, p) scattering associated with the above (d, p) reactions through the coupling. The results obtained by CC with the full kernel ( $V_{\alpha\beta}^{np} + N_{\alpha\beta}$ ), with only  $V_{\alpha\beta}^{np}$  kernel and by DWBA or the optical model (OPT) are compared<sup>2)</sup> in Fig. 1. This clearly shows appreciable effects of the coupling as well as the importance of the non-orthogonality.

In order to investigate how many steps should be taken into account, we solved the coupled equations, the kernels of which are artificially multiplied by a constant  $\lambda$ , for several values of  $\lambda$ . Then, the S-matrix elements for a given total angular momentum  $J$  are simulated by a polynomial with respect to  $\lambda$ . The power,  $n$ , of  $\lambda$  corresponds to the number of steps if the series converges. In particular,  $n = 0$  corresponds to OPT and  $n = 1$  corresponds to DWBA. An estimate of number of necessary steps is shown in Table 1 for the case of oxygen. (Calculation has also been done for calcium,) Effects of the coupling are stronger for lower partial waves. It must be noted that number of steps depends very much on the process.

We also investigated the energy dependence of the effects of the coupling by performing similar calculations for various incident energies (2 – 30 MeV) with the fixed distorting potentials  $U_{\alpha}$ . Comparing the S-matrix elements obtained by CC with those by DWBA (or OPT), one can distinguish, in  $(E_{\text{c.m.}} - J)$  plane, a CC-region and a distorted wave (DW)-region where DWBA and

Table 1. Number of steps for the reaction  $^{16}\text{O} + d \leftrightarrow ^{17}\text{O}(\text{s}) + p$  at  $E_d = 10.5$  MeV.

J	(d,d)	(d,p)	(p,p)
0	8	>11	>10
1	0	5	8
2	2	3	2
3	0	5	4
4	0	1	2
5	0	1	2

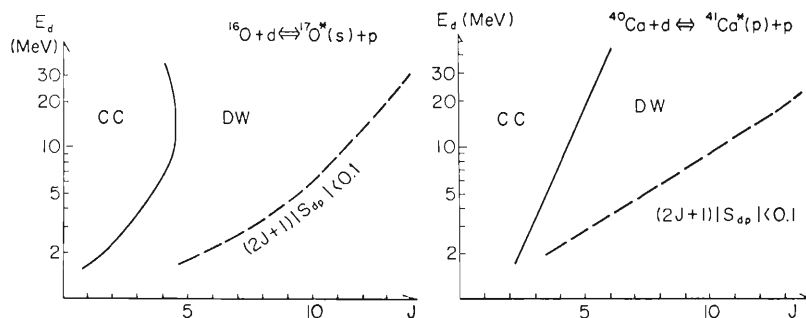


Fig. 2. Decomposition into the CC-region and the DW-region.

OPT are valid. The analysis is summarized in Fig. 2.

Judging from the calculated cross sections, one concludes that the effects of the coupling is smaller as the incident energy increases. This is partly explained from Fig. 2. Namely, the ratio of the CC-region to the DW-region becomes smaller as the energy increases. We also recognized that the absolute value of the difference between the S-matrix element obtained by CC and that by DWBA relative to the absolute value of the S-matrix element of DWBA itself becomes smaller.

#### References

- 1) T. Ohmura, B. Imanishi, M. Ichimura, and M. Kawai: *Prog. Theor. Phys.*, 41, 391 (1969).
- 2) B. Imanishi, M. Ichimura, and M. Kawai: *Phys. Letts.*, 52B, 267 (1974).

4-7. Quasimolecular Resonance by the  $^{24}\text{Mg}(\alpha, ^{12}\text{C})^{16}\text{O}$  Reaction

F. Soga, J. Shimizu, N. Takahashi, K. Takimoto,  
R. Wada, T. Wada, T. Fujisawa, and H. Kamitsubo

Since the discovery of the  $E_{\text{c.m.}} = 19.7$  MeV resonance in the  $^{12}\text{C} + ^{16}\text{O}$  system, there is a growing accumulation of experimental evidences to suggest that anomalies not consistent with statistical fluctuations exist in the compound system  $^{28}\text{Si}$ . However, in many cases the spin assignments have not been firmly established. To confirm the existence of resonances and determine their spin-parities, we have made an experiment on  $\alpha$ -induced reaction on  $^{24}\text{Mg}$  target, which produces the intermediate states of the same excitation energies as those reached by the heavy-ion incident reaction.

The  $^{24}\text{Mg}(\alpha, ^{12}\text{C})^{16}\text{O}$  reaction was studied using the  $\alpha$ -beam accelerated by the cyclotron. The  $^{12}\text{C}$  ion ranging from 15 to 7 MeV was detected and identified with a  $\Delta E$ -E counter telescope of  $6.8 \mu\text{m}$  and  $30 \mu\text{m}$  Si detectors. The carbon recoil from the elastic and inelastic  $\alpha$ -scattering on the small amount of C contaminant which had approximately the same energy as the true event was dropped off by the anticoincidence with the associated  $\alpha$ -particles scattered at the backward angles.

The measured excitation function, the energy ranges of which were selected with consideration of the existence of anomalies, is shown in Fig. 1. Two peaks correspond to anomalies at  $E_{\text{c.m.}} = 10.7$  and  $12.7$  MeV in the  $^{12}\text{C} + ^{16}\text{O}$  reaction. (Refs. 1 and 2). Figure 2 is the angular

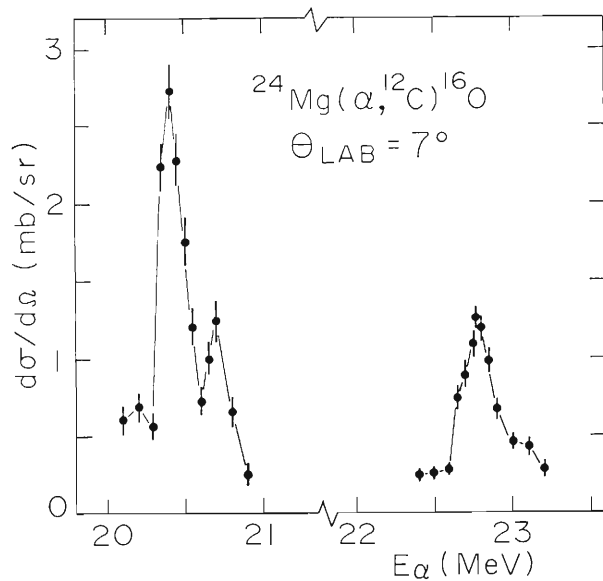


Fig. 1. Excitation function for  $^{24}\text{Mg}(\alpha, ^{12}\text{C})^{16}\text{O}$  reaction.

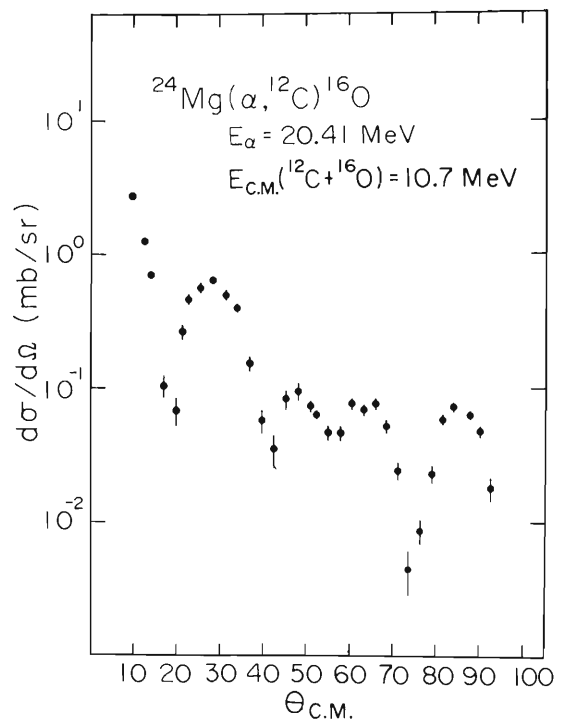


Fig. 2. Angular distribution for  $^{24}\text{Mg}(\alpha, ^{12}\text{C})^{16}\text{O}$  reaction at  $E_{\text{c.m.}} = 10.7$  MeV.

distribution at  $E_{c.m.} = 10.7$  MeV. This angular distribution reflects the interference effect probably due to the presence of the neighboring smaller peak in Fig. 1. If this anomaly can be attributed to a resonance, the possible value of spin may be 7 or 8.

Figure 3 is the angular distribution taken at  $E_{c.m.} = 12.7$  MeV. The existence of the resonance at this energy has already been established in exit channels of neutron, proton, duetron and  $\alpha$ -particles from the  $^{12}\text{C} + ^{16}\text{O}$  reaction.<sup>2)</sup> Solid line shows the  $\chi^2$  fit curve obtained by using linear expansion with Legendre polynomials up to 16th order. The coefficient of 14th order is much larger than those of the other terms. Dashed line shows the square of Legendre polynomial of 7th order and it can be said that the spin-parity of this resonance is  $7^-$ .

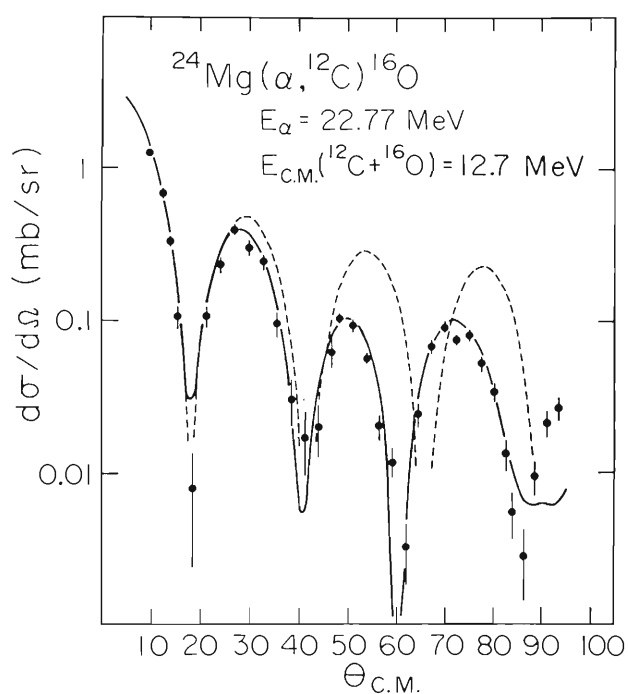


Fig. 3. Angular distribution for  $^{24}\text{Mg}(\alpha, ^{12}\text{C})^{16}\text{O}$  reaction at  $E_{c.m.} = 12.7$  MeV. Solid line shows the  $\chi^2$  fit curve with Legendre polynomial expansion. Dashed line shows  $P_7^2(\cos \theta)$  curve.

## References

- 1) M. L. Halbert, F. E. Durham, and A. Van der Woude: Phys. Rev., 162, 899 (1967).
- 2) P. Taras, G. Rao, N. Schulz, J. P. Vivien, B. Haas, J. C. Merdinger, and S. Landsberger: Phys. Rev., C15, 834 (1977).

4-8. Quasimolecular Resonances Formed by the System  $^{12}\text{C} + ^{13}\text{C}$ 

B. Imanishi

In the elastic scattering of  $^{12}\text{C} + ^{13}\text{C}$ , non-statistical structures have been observed by several authors<sup>1)-4)</sup> in the excitation function in the energy region above the Coulomb barrier. In the system  $^{12}\text{C} + ^{13}\text{C}$  one of the nuclei has an additional neutron which is not so tightly bound as the other neutrons. Of the inelastic scattering induced by  $^{12}\text{C}$  and  $^{13}\text{C}$  those going to the channels concerned with this neutron excitation, are strongly enhanced.<sup>5)</sup> This suggests the possibility of the quasimolecular formation, in which the valence neutron plays an important role through the interaction between  $n$  and  $^{12}\text{C}$ .

Here, by assuming that the resonance system is formed in the system spanned by the channels,  $^{12}\text{C}_1 + ^{13}\text{C}$  ( $1/2^-$ , gr.),  $^{12}\text{C}_1 + ^{13}\text{C}^*$  ( $1/2^+$ , 3.086 MeV),  $^{12}\text{C}_1 + ^{13}\text{C}^*$  ( $5/2^+$ , 3.854 MeV) and their "core-exchange" channels ( $^{13}\text{C} \rightarrow ^{12}\text{C}_2 + n$ ), we carried out the coupled-channel calculation. The potentials between  $n$  and  $^{12}\text{C}$  and between two  $^{12}\text{C}$  nuclei<sup>6)</sup> are assumed as

$$V_{nc}(R) = \frac{-56.7 - 6.1\pi(\hat{R})}{1 + \exp\{(R - 2.26)/0.705\}} - 28.4(\vec{\ell} \cdot \vec{s}) \frac{1}{R} \frac{d}{dR} \frac{1}{1 + \exp\{(R - 2.26)/0.705\}}, \quad (1)$$

and

$$U_{cc}(x) = 100e^{-0.1x^2} - V_0/[1 + \exp\{(x - 6.2)/0.55\}] - W' E_{cm} / [(1 + \exp\{(x - 5.82)/0.21\})], \quad (2)$$

with

$$\begin{array}{lll} V_0 = 13.8 \text{ MeV}, & W' = 0.24 \text{ MeV} & \text{for ground channel,} \\ V_0 = 15.3 \text{ MeV}, & W' = 0.1 \text{ MeV} & \text{for other channels.} \end{array}$$

In Fig. 1 the results of preliminary calculation for the real part of the elastic scattering phase shifts  $\delta_{J\ell}$  ( $J = 11/2, 13/2$  and  $15/2$ ) are shown as functions of the incident energy. Resonant behaviour is seen in each curve. Especially, in the curve for  $J^\pi = 13/2^+$  ( $\ell = 7$ ) there appear two prominent resonances, i. e., the one with narrow width at  $E_{cm} = 10.2$  MeV and the other with broad width at  $E_{cm} = 9.3$  MeV. The broad one seems to be single-particle resonance of the elastic channel which may correspond to the one ( $\ell = 7$ ) derived by Crozier and Legg<sup>3)</sup> from the resonance analysis of the elastic scattering, and the narrow one seems to be the doorway-state resonance enhanced by the above broad resonance through the double resonance mechanism.<sup>7)</sup>

In our present calculation of  $\delta_{J\ell}$  for  $J = 11/2 - 17/2$ , we could not find marked resonance at the energy region near  $E_{cm} \sim 8$  MeV, where Willet et al. have observed prominent structures.

Strong coupled-channel effects are seen in the curves of  $\delta_{J\ell}$  (elastic). The difference between  $\delta_{J=\ell+1/2, \ell}$  (elastic) and  $\delta_{J=\ell-1/2, \ell}$  (elastic) in Fig. 1 is due to the coupling effects between the elastic and other channels. If there are no coupling effects on the elastic channel, these phase

shifts must agree with each other in the heavy-ion approximation.

Resonances with such strong coupled-channel effects cannot be understood only by the distorting potentials for respective channels. However, such resonances can be plainly explained by the following potential<sup>8)</sup> (adiabatic potential) which is defined by the diagonalization:

$$\xi_i(r) = \sum_{k,l} \{A^{-1}(r)\}_{ik} \{U(r) + \epsilon\}_{kl} A_{li}(r) + \epsilon_i, \quad (3)$$

where  $\epsilon = [\epsilon_i \delta_{ik}]$  is a matrix consisting of the excitation energies  $\epsilon_i$  of  $^{13}\text{C}^*$ .

In Fig. 2 the lowest two of the adiabatic potentials  $\xi_i^{(J^\pi = 13/2^+)}(r)$  are shown. These potentials explain the nature of the resonances with the coupled-channel calculations. What we would like to pay particular attention to is that the lowest adiabatic potential  $\xi_1(r)$  describing the elastic scattering is pushed down from the potential  $U_{11}(r)$  by about 6 MeV at  $r = 5.5$  fm and by about 1 MeV at the barrier peak. Decrease of the barrier height make the resonance width at  $E_{\text{cm}} = 9.2$  MeV broad.

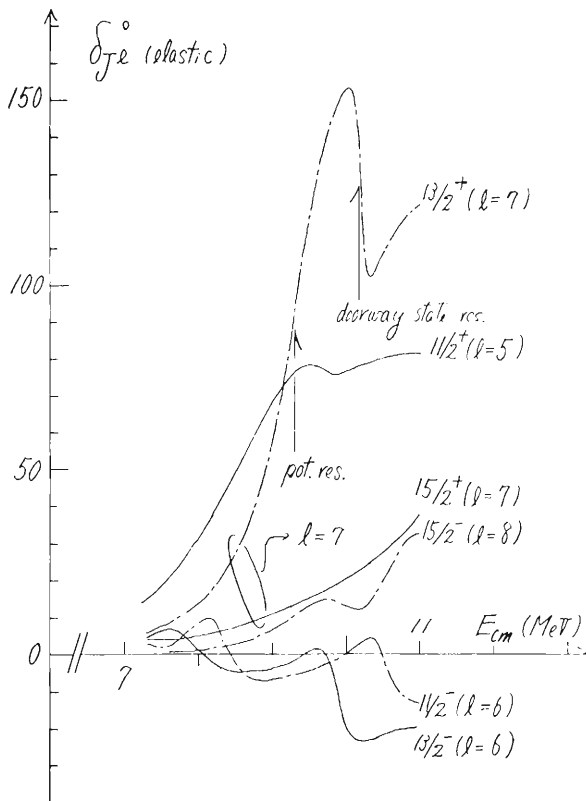


Fig. 1. Real part of the elastic scattering phase shifts  $\delta_{J\ell}$ , where  $J(= \ell \pm 1/2)$  represents the angular momentum of the total system and  $\ell$  the partial-wave angular momentum for the relative motion between  $^{12}\text{C}(\text{O}^+, \text{gr.})$  and  $^{13}\text{C}^*(1/2^-, \text{gr.})$ .

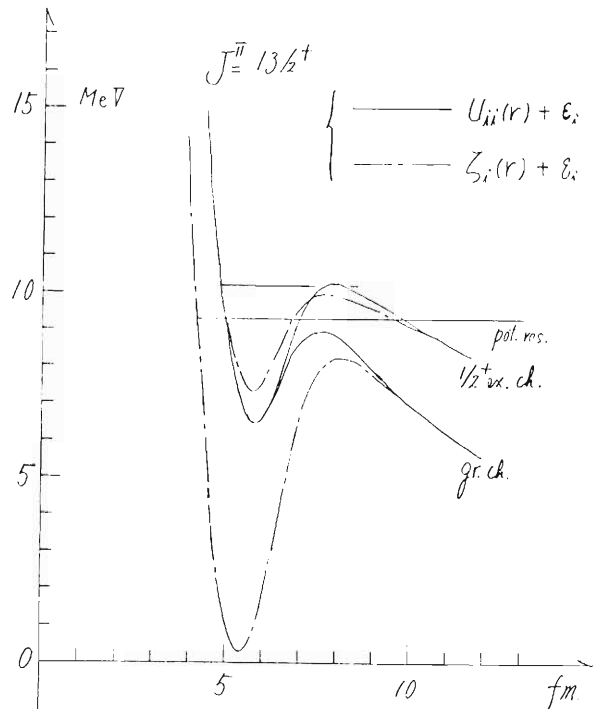


Fig. 2. Distorting potentials  $U_{ii}^{(J^\pi)}(r)$  ( $i = 1, 2$ ) and adiabatic potentials  $\xi_i^{(J^\pi)}(r)$  ( $i = 1, 2$ ) for the elastic and inelastic  $\{^{13}\text{C}(^{12}\text{C}, ^{12}\text{C})^{13}\text{C}^*(1/2^+, 3.854 \text{ MeV})\}$  channels belonging to the angular momentum for  $J^\pi = 13/2^+$ .

## References

- 1) U. Weiss, D. Fick, K. D. Hildenbrand, and W. Weiss: Nucl. Phys., A274, 253 (1976).
- 2) D. Fick: in Proc. of the Intern. Conf. on the Resonances in Heavy Ion Reactions (Hvar, Yugoslavia, 1977) to be published.
- 3) D. J. Crozier and J. C. Legg: Phys. Rev. Lett., 33, 782 (1974).
- 4) D. A. Bromley: in Proc. of the Intern. Conf. on the Resonances in Heavy Ion Reactions (Hvar, Yugoslavia, 1977) to be published; S. J. Willet, S. K. Korotky, K. A. Erb, M. M. Hindi, and D. A. Bromley: in Proc. of the Intern. Conf. on Nucl. Structure - Contributed Paper - Tokyo, p.641 (1977).
- 5) L. T. Chua: in Doctor thesis of Yale University (1974).
- 6) G. Michaud and E. Vogt: Phys. Rev., C5, 350 (1972).
- 7) W. Scheid, W. Greiner, and R. Lemmer: Phys. Rev. Lett., 25, 176 (1970).
- 8) M. Nogami: in Proc. of the INS-IPCR Symp. on Cluster Structure of Nuclei and Transfer Reactions Induced by Heavy-Ions, Tokyo, p.401 (1975).

4-9. Fusion Reaction in  $^{12}\text{C} + ^{14}\text{N}$  and  $^{16}\text{O} + ^{10}\text{B}$  Systems

T. Motobayashi, S. M. Lee, T. Shimoda,  
H. Utsunomiya, M. Yanokura, and I. Kohno

In order to study the behavior of the fusion reaction at high energies, especially to investigate its incident channel dependence, we have measured the yield of  $^6\text{Li}$  particles emitted through  $^{12}\text{C} + ^{14}\text{N}$  and  $^{16}\text{O} + ^{10}\text{B}$  reactions. The results were analyzed using the Hauser-Feshbach theory to extract critical angular momenta for fusion ( $J_{\text{cr}}$ ) as reported previously [1, 2]. They indicated some difference in the behavior of  $J_{\text{cr}}$  values arising from the difference in the incident channel (Fig. 1). This suggests that the fusion reaction process is mainly governed by the reaction dynamics of the two colliding nuclei and not by the property of the compound nucleus  $^{26}\text{Al}$ .

To re-examine this incident channel dependence of the  $J_{\text{cr}}$  values in a different way, we measured here the cross section of the evaporation residue for the same systems ( $^{14}\text{N} + ^{12}\text{C}$  and  $^{16}\text{O} + ^{10}\text{B}$ ).

The experiments were performed with  $^{14}\text{N}$  and  $^{16}\text{O}$  beams from the cyclotron and the energies were 91.3 MeV and 97.9 MeV, respectively. These values were chosen so as to produce the  $^{26}\text{Al}$  compound nucleus with the same excitation energy (57.2 MeV) in both cases of  $^{14}\text{N} + ^{12}\text{C}$  and  $^{16}\text{O} + ^{10}\text{B}$ . The emitted particles with  $Z = 6 - 12$  were detected with a counter telescope which consists of a gas proportional  $\Delta E$  counter and a Si E detector. Since the evaporation residue are emitted in the forward direction, special attention was paid upon the forward angle measurement and consequently detection at  $3.5^\circ$  was achieved. Targets were of self-supported  $^{10}\text{B}$  ( $40 \mu\text{g}/\text{cm}^2$ ) and  $^{12}\text{C}$  ( $70 \mu\text{g}/\text{cm}^2$ ) foils. To eliminate the contribution from the contaminant in these targets, we also measured the systems of  $^{16}\text{O} + ^{16}\text{O}$ ,  $^{16}\text{O} + ^{12}\text{C}$ , and  $^{14}\text{N} + ^{16}\text{O}$ , to know such contribution. A  $\text{TiO}_2$  foil ( $60 \mu\text{g}/\text{cm}^2$ ) was used for  $^{16}\text{O}$  target.

Data analysis is now in progress.

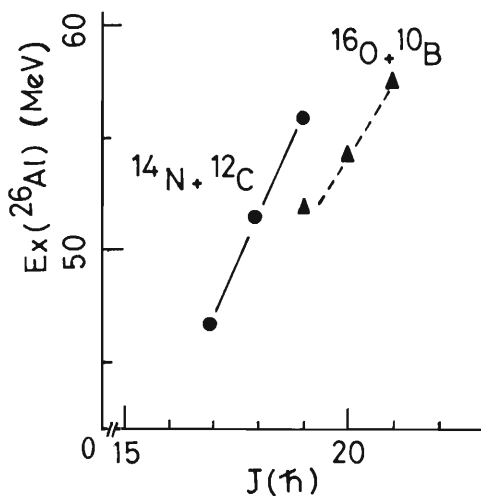


Fig. 1. Values of  $J_{\text{cr}}$  extracted from the Hauser-Feshbach calculations on the reactions  $^{12}\text{C}(^{14}\text{N}, ^6\text{Li})^{20}\text{Ne}$  and  $^{10}\text{B}(^{16}\text{O}, ^6\text{Li})^{20}\text{Ne}$ .

## References

- 1) T. Ooi, T. Motobayashi, I. Kohno, M. Ishihara, T. Numao, T. Fukuda, and S. M. Lee: IPCR Cyclotron Progr. Rep., 9, 10 (1975).
- 2) I. Kohno, T. Motobayashi, T. Ooi, M. Ishihara, T. Numao, T. Fukuda, and S. M. Lee: *ibid.*, 10, 38 (1976).

4-10.  $\alpha$ -Transfer Reactions between 1p or 2s-1d Shell Nuclei (2)

T. Motobayashi, I. Kohno, T. Ooi, and S. Nakajima

In spite of recent progress in the DWBA theory for heavy-ion induced reaction, the mechanism of the  $\alpha$ -transfer reaction has not been fully understood yet. The calculated cross sections have always been much smaller than the experimental ones. To investigate this discrepancy, we performed a series of experiments on  $\alpha$ -transfer reaction between light nuclei ( $^{10}\text{B}$ ,  $^{12}\text{C}$ ,  $^{14}\text{N}$ ,  $^{16}\text{O}$ , and  $^{20}\text{Ne}$ ). For these nuclei the  $\alpha$ -cluster structure has been well studied theoretically with the shell model<sup>1),2)</sup> or the cluster model.<sup>3),4)</sup> The experimental procedure and the experimental results were already reported.<sup>5)</sup> We present here some results of the DWBA analysis.

Some results of the DWBA calculations are shown in Fig. 1 together with the experimental data. The exact finite range code SATURN-MARS<sup>6)</sup> was revised so as to be suitable for the calculation of the  $\alpha$ -transfer reactions.<sup>7)</sup> The bound state wave functions were obtained with Woods-Saxon potentials ( $a = 0.7$  fm and  $R = 1.3 \cdot A^{1/3}$  fm) by the separation-energy procedure. The distorting potentials were that of the optical model which reproduce the angular distributions of the elastic scatterings. The values in parenthesis in the right hand side of each curve in Fig. 1.

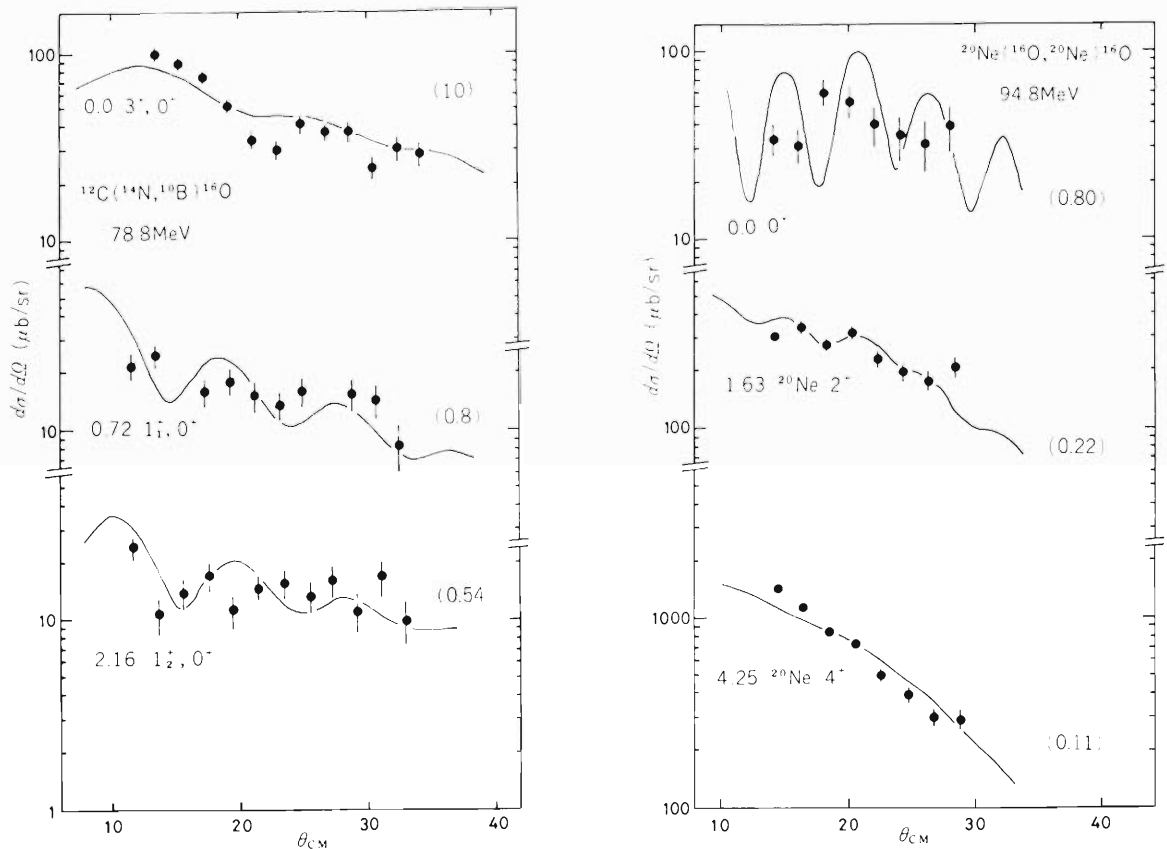


Fig. 1. Angular distributions for some alpha transfer reactions. The solid curves correspond to the DWBA calculations with the normalization constants written in parenthesis in the right hand side of each curve.

are the values of the normalization constant  $n$ , which were obtained by comparing the calculated cross section with the experimental ones as

$$\left(\frac{d\sigma}{d\Omega}\right)_{\text{exp}} = n \cdot \left(\frac{d\sigma}{d\Omega}\right)_{\text{DWBA}} \quad (1)$$

The values of  $n$  obtained for various reactions are listed in Table 1. If the DWBA calculations performed here are correct in describing these reactions,  $n$  should be equal to the products of two  $S$ -factors corresponding to two  $\alpha$ -core systems involved in the reactions. Hence, we can extract the values of  $S$ -factor for each  $\alpha$ -core system from the analysis of the case of elastic transfer

Table 1. The values of  $n$  and  $S$  for various reactions.

Reactions	$n$	$0.21^{1)}$	$0.21^{1)}$	$0.19^{1)}$	$0.23^{2)}$	$0.69^{2)}$
		$S$ $0^+$	$^{20}\text{Ne}$ $2^+$	$4^+$	$^{16}\text{O}$ $0^+$	$^{14}\text{N}$
$^{20}\text{Ne}(^{16}\text{O}, ^{20}\text{Ne})^{16}\text{O}$	$0^+$	0.80	0.89			
	$2^+$	0.22	0.89	0.25		
	$4^+$	0.11	0.89		0.12	
$^{16}\text{O}(^{12}\text{C}, ^{16}\text{O})^{12}\text{C}$	$0^+$	1.0			1.0	
$^{10}\text{B}(^{14}\text{N}, ^{10}\text{B})^{14}\text{N}$	82					9.1

	$n$	$n(\text{cal})$
$^{12}\text{C}(^{14}\text{N}, ^{10}\text{B})^{16}\text{O}$	10	9.1
$^{16}\text{O}(^{16}\text{O}, ^{12}\text{C})^{20}\text{Ne}$	$0^+$	0.62
	$2^+$	0.34

( $n = S^2$ ; see also in Table 1). Using these extracted values of  $S$ , we can calculate the values of  $n$  for other reactions. As is seen in Table 1, these values agree fairly well with the ones extracted directly from Eqn. (1). This fact provides an evidence for the consistency of the DWBA analysis for these  $\alpha$ -transfer reactions.

However, values of  $S$ -factor extracted here are much larger than the ones predicted by the theory (listed in Table 1). We have now to re-examine the  $\alpha$ -core wave function. In Fig. 2 the microscopic wave function<sup>8)</sup> for the ground state of  $^{20}\text{Ne}$  is shown. This wave function includes the effects of the anti-symmetrization between the nucleons in the  $\alpha$ -particles and the ones in the core-nucleus. For comparison, the wave function corresponding to the Woods-Saxon potential (which was used in the present calculations) and the same function multiplied by the square root of  $S$  ( $= 0.21$  [1]) are also shown in Fig. 2. It is clearly seen that the microscopic wave function has damped amplitude in the interior region of the nuclei, and has amplitude as large as the simple Woods-Saxon wave function in the nuclear surface region. Therefore, we can conclude that the  $S$ -factor obtained from the analysis of the experimental data is not the  $S$ -factor itself predicted by the theory, because the transfer cross sections is affected strongly by the nuclear surface on account of the strong absorptive nature of the heavy-ion scattering, and the behavior of the  $\sqrt{S}u(r)$  is very different from that of  $y(r)$  in the nuclear surface region. Therefore, it is not

surprising that the S-factors obtained are much larger than ones predicted by the theory. To understand more precisely the mechanism of the  $\alpha$ -transfer reactions, microscopic wave function itself could be used in the analysis.

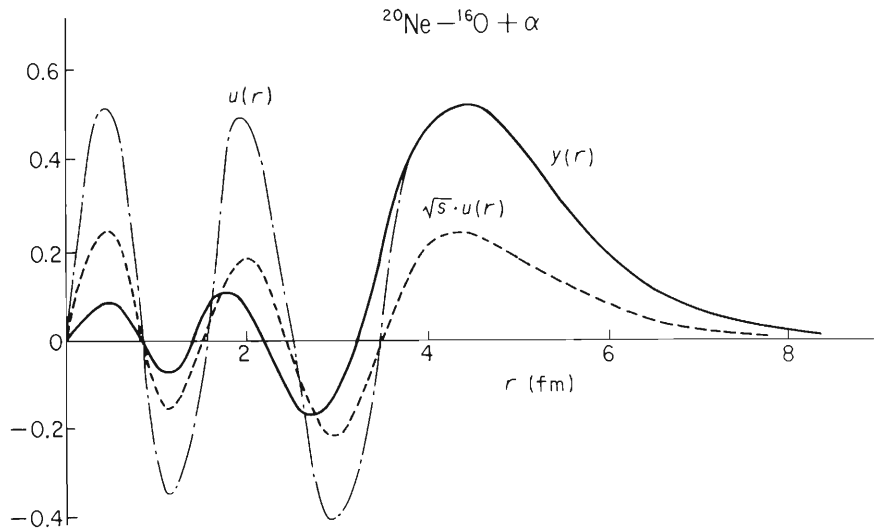


Fig. 2. Comparison of the various kinds of the alpha-core wave function. The solid curve corresponds to the microscopic wave function [8], the dashed-dotted one corresponds to the simple Woods-Saxon wave function, and dashed one Woods-Saxon wave function multiplied by the square root of the theoretical values of  $S (=0.21)$ .

## References

- 1) M. Ichimura, A. Arima, E. C. Halbert, and T. Terasawa: Nucl. Phys., A204, 225 (1973).
- 2) D. Kurath: Phys. Rev., C-7, 1390 (1973).
- 3) T. Matsuse, M. Kamimura, and Y. Fukushima: Progr. Theor. Phys., 53, 706 (1975).
- 4) I. Shimodaya, R. Tamagaki, and H. Tanaka: *ibid.*, 27, 793 (1962).
- 5) T. Motobayashi, I. Kohno, T. Ooi, and S. Nakajima: IPCR Cyclotron Progr. Rep., 10, 35 (1976).
- 6) T. Tamura and K. S. Low: Comput. Phys. Commun., 8, 349 (1974).
- 7) T. Matsuura: Private communication.
- 8) K. I. Kubo, F. Nemoto, and H. Bando: Nucl. Phys., A224, 573 (1974).

#### 4-11. Spin Polarization of $^{12}\text{B}$ in ( $^{10}\text{B}$ , $^{12}\text{B}$ ) and ( $^{12}\text{C}$ , $^{12}\text{B}$ ) Reactions on $^{100}\text{Mo}$

M. Ishihara, K. Tanaka, H. Kamitsubo, N. Takahashi, Y. Miake, Y. Nojiri  
T. Minamisono,\* A. Mizobuchi,\* and K. Sugimoto\*

In previous papers (1) we reported on the measurement of spin polarization of  $^{12}\text{B}$  performed to study the mechanism of energy and angular momentum transfer in the heavy ion collisions. In that experiment the polarization  $P$  as a function of reaction  $Q$ -value was determined for the reaction  $^{100}\text{Mo}(^{14}\text{N}, ^{12}\text{B})^{102}\text{Ru}$  at 90 and 125 MeV by measuring  $\beta$ -ray asymmetry of the decaying  $^{12}\text{B}$  products. The results obtained may be summarized as follows:

(i) In the high energy region of the energy spectrum, where the quasi-elastic hump dominates,  $P$  varies smoothly from large negative ( $P = -0.3$  to  $-0.5$  at highest energies) to positive as the  $Q$ -value becomes more negative. ( $P > 0$  when  $\vec{P} // \vec{k}_f \times \vec{k}_i$ )

(ii) Zero crossing of  $P$  occurs around the  $Q$ -value corresponding to the peak of the quasi-elastic hump.

(iii) In the low energy region, where the deep inelastic hump becomes dominant,  $P$  is negative but relatively small ( $|P| < 0.1$ ).

A remarkable aspect about these results is that they generally do not conform to the predictions from the classical model (2) of heavy ion collisions in terms of frictional forces. Especially the  $Q$  dependence of  $P$  in high energy region as described in (i) is opposite to the classical prediction. On the other hand, a microscopic consideration based on the kinematical matching conditions (1, 3) for the particle-transfer reaction well accounted for qualitative features of experimental results.

This indicates for the reaction studied that mass transfer is the main mechanism responsible for the energy and angular momentum transfers rather than the process of inelastic nature (not accompanied with mass transfer) which may be phenomenologically represented by frictional forces.

To confirm the validity of the microscopic model employed, the measurement of  $P$  was extended to pick-up and mass-exchange reactions, for which the model predicts different  $Q$  dependence of  $P$  from that for the stripping reaction ( $^{14}\text{N}$ ,  $^{12}\text{B}$ ). The reactions  $^{100}\text{Mo}(^{10}\text{B}$ ,  $^{12}\text{B})^{98}\text{Mo}$  at  $E(^{10}\text{B}) = 67$  MeV and  $^{100}\text{Mo}(^{12}\text{C}$ ,  $^{12}\text{B})^{100}\text{Tc}$  at  $E(^{12}\text{C}) = 90$  MeV were used.

Figure 1 shows  $P$  and the yield of  $^{12}\text{B}$  as a function of  $Q$ -value obtained for the ( $^{10}\text{B}$ ,  $^{12}\text{B}$ ) reaction. A characteristic feature of the energy spectrum is that the peak position of the quasi-elastic hump is pushed towards the small  $Q$  value close to  $Q_{\text{gg}} = 0.6$  MeV. This complies with the expectation from the matching conditions that the cross section is favoured towards positive  $Q$  values for pick-up reactions, though it is towards negative  $Q$  values for stripping reactions; the optimum  $Q_{\text{eff}}$  value  $\bar{Q}_{\text{eff}}$  may be expressed as

$$\bar{Q}_{\text{eff}} = \frac{1}{2} mv^2 - \hbar v \frac{\lambda_2}{R_2}, \quad (1)$$

for pick-up reactions as compared to

\* Faculty of Science, Osaka University.

$$\bar{Q}_{\text{eff}} = -\frac{1}{2}mv^2 + \hbar v \frac{\lambda_1}{R_1}, \quad (2)$$

for stripping reactions, where  $v$  is the relative velocity of the colliding nuclei and  $\lambda_2$  and  $\lambda_1$  are the  $z$ -component of the orbital angular momentum of the transferred cluster with respect to center of mass of  $^{10}\text{B}$  and  $^{14}\text{N}$ , respectively.

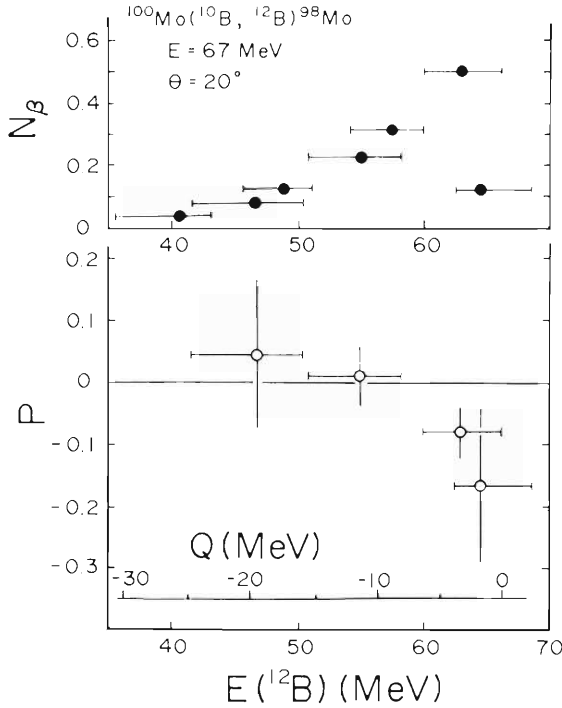


Fig. 1. Yield (upper part) and polarization (lower part) of  $^{12}\text{B}$  as a function of  $Q$  value obtained in the  $^{100}\text{Mo}(^{10}\text{B}, ^{12}\text{B})^{98}\text{Mo}$  reaction at  $E_{\text{lab}}(^{10}\text{B}) = 67 \text{ MeV}$  and  $\theta_{\text{lab}} = 20^\circ$ .

The low energy portion ( $Q \lesssim -15 \text{ MeV}$ ) of the cross section may be attributed to some other complex reaction mechanism.

The polarization observed for the region of QE hump ( $Q = 0 \sim -10 \text{ MeV}$ ), may also be explained by Eqn. (1), which indicates that the component of  $\lambda_2 = +2$  is most responsible for this region of negative  $Q$  values while those of  $\lambda_2 = 0$  and  $-2$  for the region of positive  $Q$  values. Considering the fact that the ground state spin of  $^{10}\text{B}$  is  $J^\pi = 3^+$  and thus the sign of  $P$  of  $^{12}\text{B}_{\text{g.s.}}$  should be inverse to that of  $\lambda_2$  ( $\ell_2 = 2$  assumed), we obtain  $P < 0$  in agreement with experiment. The small positive  $P$  values obtained for the lower energy region remain to be explained.

For the exchange reaction ( $^{12}\text{C}, ^{12}\text{B}$ ), small positive  $P$  values less than 0.1 were obtained over the most part of energy spectrum.

## References

- 1) K. Sugimoto, N. Takahashi, A. Mizobuchi, Y. Nojiri, T. Minamisono, M. Ishihara, K. Tanaka, and H. Kamitsubo: *Phys. Rev. Lett.*, **39**, 323 (1977); K. Tanaka, M. Ishihara, H. Kamitsubo, N. Takahashi, A. Mizobuchi, Y. Nojiri, T. Minamisono, and K. Sugimoto: *Proc. of Intern. Conf. Nucl. Struct.*, Tokyo, 1977, Vol. 11 (in press).
- 2) J. Wilczynski: *Phys. Lett.*, **47B**, 484 (1973).
- 3) D. M. Brink: *ibid.*, **40B**, 37 (1972); M. Ishihara, K. Tanaka, T. Kammuri, K. Matsuoka, and M. Sano: *ibid.*, (in press).

4-12. On the Mechanism of Two-Nucleon Transfer Reactions  
Induced by Heavy Ions

T. Takemasa and H. Yoshida

Two-nucleon transfer reactions are analyzed here to clarify the reaction mechanism. For that purpose, the one-step (simultaneous) and two-step (successive) transfer processes are taken into account in the analyses. Denoting the reaction as  $A(a, b)B$ , the corresponding transition amplitudes for one- and two-step processes are

$$T_{ba}^1 = \int dr_a dr_b \chi_b^{(-)*}(r_b) \langle Bb | V_b | Aa \rangle \chi_a^{(+)}(r_a), \quad (1)$$

$$T_{ba}^2 = \int dr_a dr_b \chi_b^{(-)*}(r_b) V_{b-a}(r_b, r_a) \chi_a^{(+)}(r_a), \quad (2a)$$

$$V_{b-a}(r_b, r_a) = \sum_c \int dr_c dr'_c \langle Bb | V_b | Cc \rangle G_c^{(+)}(r'_c, r_c) \langle Cc | V_a | Aa \rangle, \quad (2b)$$

where  $\chi^{(\pm)}(r)$  and  $G^{(+)}(r', r)$  are the distorted wave and Green functions respectively. In Eqn. (2), the transition amplitude  $T_{ba}^{(2)}$  for the two-step process is written in the prior-post form so that the non-orthogonality term may not appear. The finite-range calculations with full recoil are performed here both for  $T_{ba}^{(1)}$  and  $T_{ba}^{(2)}$ . The one-step amplitude  $T_{ba}^{(1)}$  is calculated by the usual exact finite-range DWBA where the microscopic form factor is constructed by the generalized method<sup>1)</sup> of Bayman and Kallio<sup>2)</sup> and the single particle wave functions with half the separation energy of the transferred two nucleons are generated from the Woods-Saxon potential with the geometrical parameters  $r_0 = 1.25$  fm and  $a = 0.65$  fm. For form factors of the two-step process, the usual separation energy method is used corresponding to the one-nucleon transfer reaction at each step. The reaction considered here are  $^{12}\text{C}(^{18}\text{O}, ^{16}\text{O})^{14}\text{C}$ ,  $^{48}\text{Ca}(^{18}\text{O}, ^{16}\text{O})^{50}\text{Ca}$  and  $^{48}\text{Ca}(^{16}\text{O}, ^{14}\text{C})^{50}\text{Ti}$ . Structure wave functions for p-shell nuclei,  $^{18}\text{O}$ ,  $^{50}\text{Ca}$ , and  $^{50}\text{Ti}$  are taken

Table 1. Optical potential parameters used in the analyses.

	V	W	$r_R$	$r_I$	$a_R$	$a_I$	Ref.
$^{12}\text{C}(^{18}\text{O}, ^{16}\text{O})^{14}\text{C}$	200	10	1.28	1.28	0.45	0.45	1)
$^{48}\text{Ca}(^{18}\text{O}, ^{16}\text{O})^{50}\text{Ca}$	97	59.7	1.21	1.14	0.497	0.422	7)
$^{48}\text{Ca}(^{16}\text{O}, ^{14}\text{C})^{50}\text{Ti}$	37	78	1.35	1.27	0.42	0.28	8)

from Refs.3-6. The optical potential parameters for each reaction are listed in Table 1. They are the parameters that fit the elastic scattering at entrance channels. In the present analyses, the common parameter set is used for the entrance, intermediate and exit channels in each reaction. The results of the calculations are shown in Figs. 1-3 together with the experiments. The dashed

line is the calculated cross section due to the one-step process. The dot-dash line is the calculated cross section due to the two-step process and the solid line is the coherent sum of these two processes.

The results can be summarized as follows: The two-step process competes with the one-step process and the interference of two processes is important to reproduce the angular distributions as well as the absolute magnitude of the cross sections. The shift of the grazing peak and the large normalization factors predicted by the usual DWBA calculations have largely been improved by the inclusion of the two-step process. One exception is the case of the reaction  $^{48}\text{Ca}(^{16}\text{O}, ^{14}\text{C})^{50}\text{Ti}$ , where the normalization factor  $N$  from 10 to 25 is still needed.<sup>9), 10)</sup> The use of the more refined structure wave functions does not seem to improve the present results. Probably the other reaction mechanisms are playing the role in this case.<sup>10)</sup> As for the role of the intermediate states in the two-step process, the ground states give generally the dominant contribution to the cross section with the exception of the reaction  $^{48}\text{Ca}(^{18}\text{O}, ^{16}\text{O})^{50}\text{Ca}$ , where the excited  $1/2^+$  state of  $^{17}\text{O}$  has the dominant effect on the cross section. This is partly due to the fact that  $1s_{1/2}$ -orbit has large amplitude in the nuclear interior and the two-step process is generally affected by the nuclear interior region.

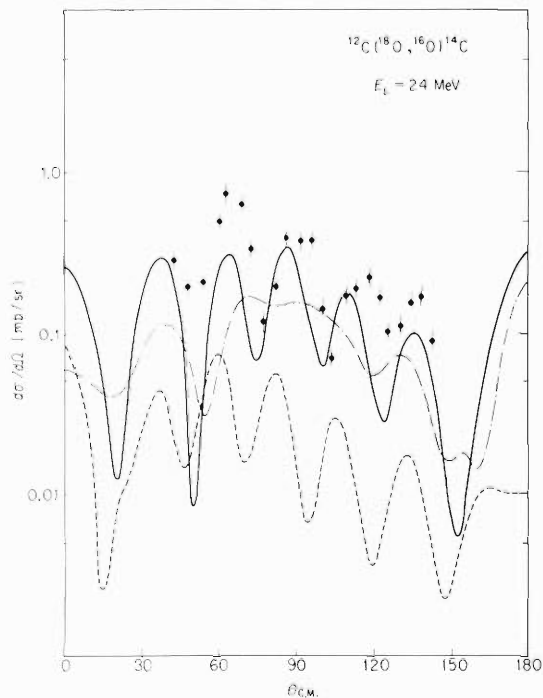


Fig. 1. Angular distributions of the reaction  $^{12}\text{C}(^{18}\text{O}, ^{16}\text{O})^{14}\text{C}$ . The dashed line is the calculated cross section due to the one-step process. The dot-dash line is the calculated cross section due to the two-step process and the solid line is the coherent sum of these two processes.

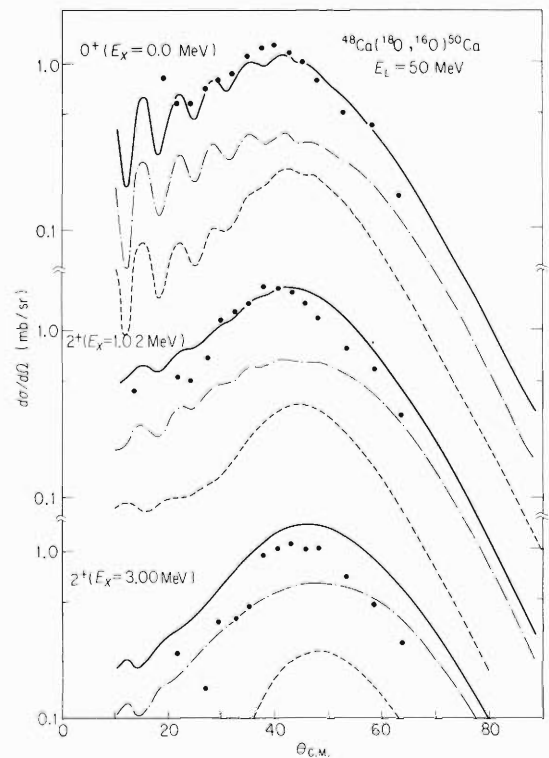


Fig. 2. Angular distributions of the reaction  $^{48}\text{Ca}(^{18}\text{O}, ^{16}\text{O})^{50}\text{Ca}$ . See the caption to Fig. 1 for details.

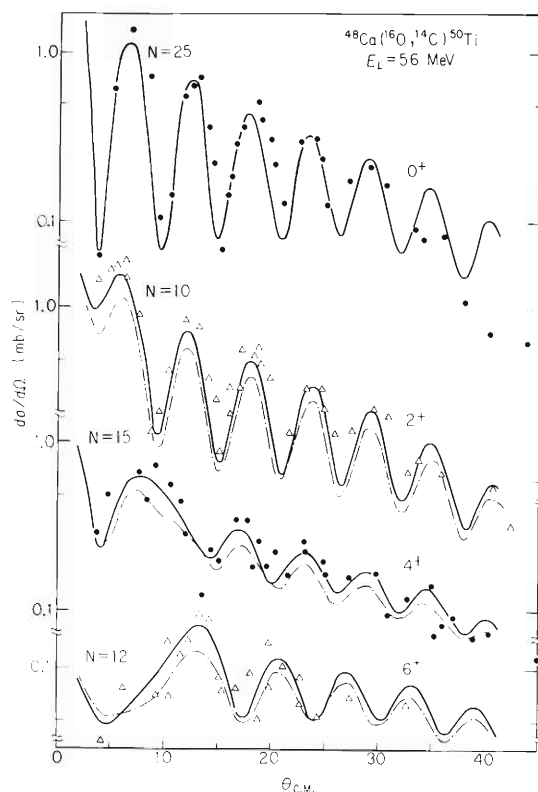


Fig. 3. Angular distributions of the reaction  $^{48}\text{Ca}(^{16}\text{O}, ^{14}\text{C})^{50}\text{Ti}$ . See the caption to Fig. 1 for details.

## References

- 1) T. Takemasa: *Phys. Lett.*, 55B, 28 (1975).
- 2) B. F. Bayman and A. Kallio: *Phys. Rev.*, 156, 1121 (1967).
- 3) A. N. Boyarkina: *Bull. Acad. Sci. USSR (Sov. Phys.)*, 28, 255 (1964).
- 4) T. Inoue, T. Sebe, H. Hagiwara, and A. Arima: *Nucl. Phys.*, 59, 1 (1964); 85, 184 (1966).
- 5) R. A. Broglia, P. Federman, Ole Hansen, K. Hehl, and C. Riedel: *ibid.*, A106, 421 (1968).
- 6) T. T. S. Kuo and G. E. Brown: *ibid.*, A114, 241 (1968).
- 7) J. F. Petersen, D. A. Lewis, D. Dehnhard, H. P. Morsch, and B. F. Bayman: *Phys. Rev. Lett.*, 36, 307 (1976).
- 8) W. Henning, D. G. Kovar, B. Zeidman, and J. R. Erskin: *ibid.*, 32, 1015 (1974).
- 9) T. Kammuri: *Nucl. Phys.*, A259, 343 (1976).
- 10) D. H. Feng., T. Udagawa, and T. Tamura: *ibid.*, A274, 262 (1976).

### 4-13. Calculation of Friction Force in the Collision $^{28}\text{Si} + ^{20}\text{Ne}$ on the Basis of the Linear Response Theory

A. Iwamoto,\* K. Harada,\* K. Sato,  
S. Yamaji, and S. Yoshida\*\*

Hofmann and Siemens<sup>1)</sup> formulated deep-inelastic collisions of heavy-ions based on the linear response theory. This theory is rather simple and is suitable for numerical calculation. Also it provides a relation to the classical friction model used successfully to describe these phenomena. However, the numerical calculation of heavy-ion reaction based on this model is done hitherto only for a very simple system.<sup>2)</sup> We give here some results of calculation carried out on a more realistic case.

We adopt the two-center harmonic oscillator Hamiltonian<sup>3)</sup> in which the center separation  $R$  and the deformations  $\delta$  ( $\delta = \delta_1 = \delta_2$ ) of two fragments appear as parameters. The expression of the friction coefficient  $\gamma_{\mu\nu}$  is given as

$$\gamma_{\mu\nu} = -4I\hbar \sum_{j,k} I_{jk} \frac{(e_j - e_k) \langle j | F_\mu | k \rangle \langle k | F_\nu | j \rangle}{\{(e_j - e_k)^2 + I^2\}^2} \quad (1)$$

where the quantity  $F_\mu$  stands for the derivative of two-center Hamiltonian  $H_{TC}$  with respect to the dynamical variable  $\mu$  ( $R$  or  $\delta$ ),

$$F_\mu = \frac{\partial H_{TC}}{\partial \mu} \quad (2)$$

and  $I_{jk}$  is given by

$$I_{jk} = \frac{1}{1 + \exp\left(\frac{e_j - \lambda}{kT}\right)} \left\{ 1 - \frac{1}{1 + \exp\left(\frac{e_k - \lambda}{kT}\right)} \right\} \quad (3)$$

In the above expressions,  $e_j$  stands for the single-particle energy of  $j$ -th orbit,  $kT$ , the nuclear temperature and  $\lambda$ , the chemical potential. We have included a smearing width  $\Gamma$  in Eqn. (1), which is necessary when we deal with a finite system with discrete energy levels.<sup>2)</sup> The quantity  $\Gamma$  is taken to be a free parameter in our numerical calculation.

The introduction of  $\Gamma$  in the expression for  $\gamma_{\mu\nu}$  causes a difficulty in the theory. That is, we have a finite value of energy dissipation arising from the relative motion of two fragments even when they are far apart. In order to eliminate this difficulty, we subtracted from  $F_R$  a term which arises by the simple translation of two centers of the potential. So the remaining terms in  $F_R$  are such as those caused by the changes of neck shape and the oscillator parameter due to the volume conservation, etc. This procedure is correct in the asymptotic region, but is only an approximation when  $R$  is small. The numerical calculation was done for the system  $^{28}\text{Si} + ^{20}\text{Ne}$ .

\* Japan Atomic Energy Research Institute.

\*\* Tohoku University.

Figure 1 shows the quantity  $\gamma_{RR}$  as a function of center separation  $R$  for three different values of  $\Gamma$  at zero temperature. In this and the following figures,  $\Gamma$  is given in the unit of  $\hbar\omega_0$ , the oscillator constant of the compound nucleus. We see clearly the surface-peaked feature of  $\gamma_{RR}$ . In this system, the scission configuration is at  $R \sim 8$  fm. Also seen is the fact that  $\gamma_{RR}$  decreases as  $\Gamma$  increases.

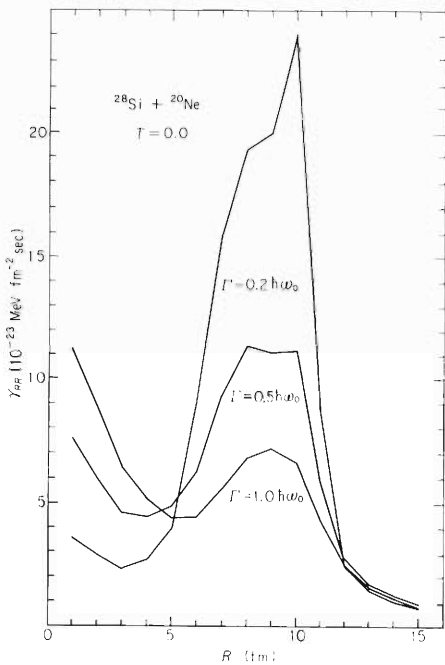


Fig. 1. Radial-radial friction coefficient  $\gamma_{RR}$  as a function of center separation  $R$ . Temperature  $kT$  is zero and three curves correspond to  $\Gamma = 1.0 \hbar\omega_0$ ,  $\Gamma = 0.5 \hbar\omega_0$  and  $\Gamma = 0.2 \hbar\omega_0$ , respectively.

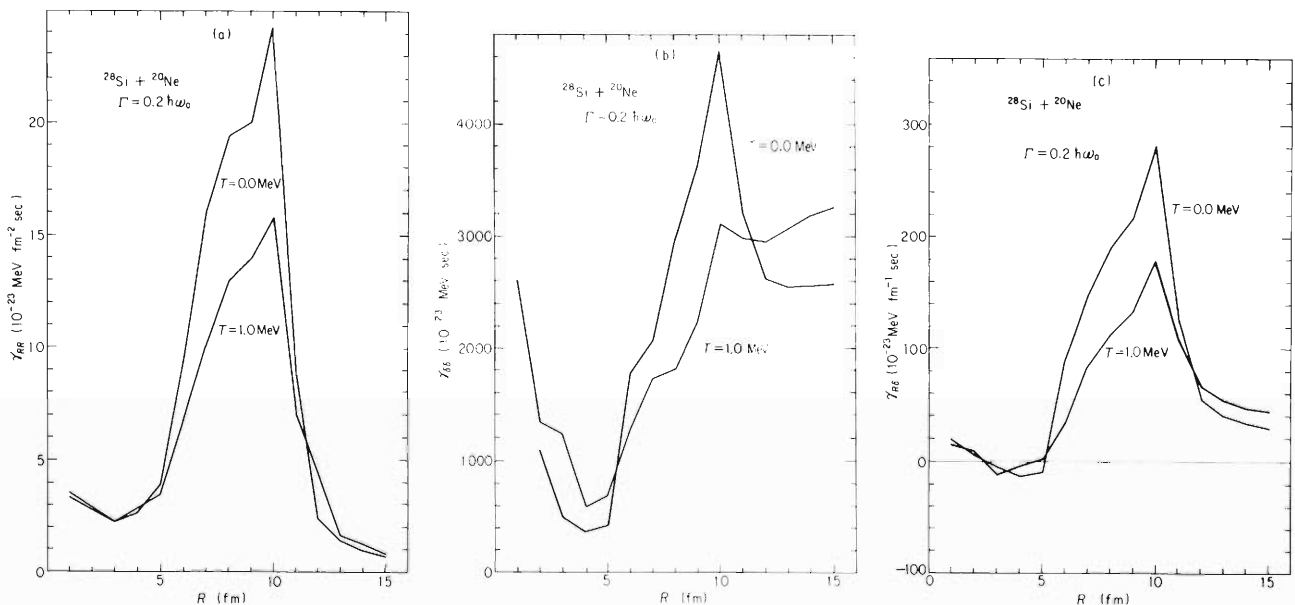


Fig. 2. Friction coefficients as a function of center separation  $R$ . Smearing width  $\Gamma$  is  $0.2 \hbar\omega_0$  and two curves correspond to  $kT = 0.0$  MeV and  $kT = 1.0$  MeV. Figs. 2(a), 2(b) and 2(c) correspond to the radial-radial coefficient  $\gamma_{RR}$ , the deformation-deformation coefficient  $\gamma_{\delta\delta}$ , and the radial-deformation coefficient  $\gamma_{R\delta}$ , respectively.

Figure 2 shows the quantities  $\gamma_{RR}$ ,  $\gamma_{\delta\delta}$  and  $\delta_{R\delta}$  as a function of center separation R for temperatures of zero and 1 MeV, respectively. The smearing width  $\Gamma$  of  $0.2 \hbar \omega_0$  is used in both cases. The effect of finite temperature is seen to reduce the magnitude of  $\gamma_{RR}$ ,  $\gamma_{\delta\delta}$  and  $\gamma_{R\delta}$  at surface region. This tendency is opposite to the result of Ref. 2. We also find that the cross term  $\gamma_{R\delta}$  is rather large, that is, the relation  $\gamma_{R\delta} \sim \sqrt{\gamma_{RR} \gamma_{\delta\delta}}$  holds approximately at the surface region, which means that the coupling of R and  $\delta$  motions is important.<sup>4)–6)</sup>

As to the absolute magnitude of  $\gamma$ , we compared our value with the results of two other calculations. One is the value of Gross-Kalinowski,<sup>7)</sup> which was used in the classical friction model calculation. The other is the one calculated by Glas-Mosel<sup>8)</sup> using a microscopic model. They are given by

Gross-Kalinowski	$\gamma_{RR} \sim 400 \times 10^{-23} \text{ MeV fm}^{-2} \text{ sec},$
Glas-Mosel	$\gamma_{RR} \sim 5 \times 10^{-23} \text{ MeV fm}^{-2} \text{ sec},$
ours	$\gamma_{RR} \sim 20 \times 10^{-23} \text{ MeV fm}^{-2} \text{ sec}.$

Thus our value is not very different from that of Glas-Mosel, but much smaller than that of Gross-Kalinowski. But this discrepancy between ours and that of Gross-Kalinowski does not mean directly that the microscopic model is useless, because the coupling between R and  $\delta$  motions may cause a very large effect.

## References

- 1) H. Hofmann and P. J. Siemens: Nucl. Physics, A257, 165 (1976).
- 2) P. J. Johansen, P. J. Siemens, A. S. Jensen, and H. Hofmann: Preprint, to be published in Nucl. Physics A.
- 3) A. Iwamoto, S. Yamaji, S. Suekane, and K. Harada: Progr. Theor. Physics, 55, 115 (1976).
- 4) R. Eggers, M. N. Namboodiri, P. Gonthier, K. Geoffroy, and J. B. Natowitz: Phys. Rev. Letters, 37, 324 (1976).
- 5) H. H. Deubler and K. Dietrich: Nucl. Physics, A277, 493 (1977).
- 6) A. Iwamoto and K. Harada: Phys. Letters, 68B, 7 (1977).
- 7) D. H. E. Gross and H. Kalinowski: *ibid.*, 48B, 302 (1974).
- 8) D. Glas and U. Mosel: Nucl. Physics, A264, 268 (1976).

#### 4-14. Canonical Quantization from the Time-Dependent Hartree-Fock Theory in the Lipkin Model

T. Hoshino, K. Yazaki\* and T. Yukawa\*\*

In recent years, many calculations on heavy-ion reactions have been done based on the time-dependent Hartree-Fock (TDHF) method.<sup>1)</sup> Since the TDHF method is suitable to describe the large amplitude collective motion, it has also been investigated theoretically in many aspects.<sup>2)-5)</sup> Reviewing the theoretical studies of TDHF, we consider that interesting points to be investigated are mainly the followings: (1) How to derive from TDHF an appropriate collective coordinate and construct a classical Hamiltonian apart from the adiabatic assumption.<sup>2)</sup> (2) How to quantize the classical collective Hamiltonian and to what an extent the quantized Hamiltonian and its energy eigenvalues approximate the exact ones. In order to clarify these points, we adopt here the exactly solvable Lipkin model<sup>6)</sup> which has often been used as a testing ground of various theoretical methods of the collective motion.<sup>4),5)</sup>

The Lipkin model consists of  $N$  fermions which occupy two  $N$ -fold degenerate levels with energies  $\frac{1}{2}\epsilon$  and  $-\frac{1}{2}\epsilon$  respectively. We denote the upper (lower) orbit by a quantum number  $+p$  ( $-p$ ) ( $p = 1, 2, \dots, N$ ) and define a slightly generalized Lipkin model Hamiltonian by

$$\hat{H} = \epsilon \hat{K}_3 + \frac{V}{2} (\hat{K}_-^2 + \hat{K}_+^2) + V' \hat{K}_3^2, \quad (1)$$

where  $\hat{K}_3 \equiv \frac{1}{2} \sum (a_p^\dagger a_p - a_{-p}^\dagger a_{-p})$ ,  $\hat{K}_+ \equiv \sum a_p^\dagger a_{-p}$ ,  $\hat{K}_- \equiv (\hat{K}_+)^\dagger$  and  $a_{\pm p}^\dagger$  ( $a_{\pm p}$ ) is a creation (annihilation) operator of a particle in the  $\pm p$  orbit. For later use, we define a Hermitian operator  $\hat{K}_2: \hat{K}_2 \equiv \frac{1}{2i} (\hat{K}_+ - \hat{K}_-)$ . Since  $\hat{K}_3$  and  $\hat{K}_\pm$  obey the quasi-spin algebra, the eigenstates of  $\hat{H}$  are characterized by the eigenvalues of  $\hat{K}^2$  ( $\hat{K}^2 \equiv \hat{K}_3^2 + \frac{1}{2} (\hat{K}_+ \hat{K}_- + \hat{K}_- \hat{K}_+)$ ). It is therefore convenient to adopt for basis vectors the eigenvectors of  $\hat{K}^2$  and  $\hat{K}_3: \hat{K}^2 |J, M\rangle = J(J+1) |J, M\rangle$  and  $\hat{K}_3 |J, M\rangle = M |J, M\rangle$ , where  $M = -J, -J+1, \dots, J$ . We define the vacuum state of the  $N$  particle system by  $|J, -J\rangle$  ( $J=N/2$ ), in which all the  $N$  particles occupy the lower orbits. We restrict our concern to those collective states which contain a component of the vacuum state.

A single Slater determinant can be defined by  $|\theta\phi\rangle \equiv \exp(-i\phi\hat{K}_3) \exp(-i\theta\hat{K}_2) |J, -J\rangle$ , where  $\theta, \phi$  are time-dependent parameters.  $\hat{H}$  consists purely of  $\hat{K}_3$  and  $\hat{K}_\pm$ , and  $|\theta\phi\rangle$  is the single Slater determinant generated by rotating  $|J, -J\rangle$  in the quasi-spin space. Consequently,  $|\theta\phi\rangle$  satisfies all the necessary conditions to be a solution of the TDHF variational equation  $\delta \langle \theta\phi | i \frac{\partial}{\partial t} - \hat{H} | \theta\phi \rangle = 0$ . As is well known, the above variational equation is equivalent to the variational equation for the action integral  $\delta I = \delta \int L dt = 0$ , where  $L$  is the classical Lagrangian:<sup>3)</sup>

$$L = \langle \theta\phi | i \frac{\partial}{\partial t} - \hat{H} | \theta\phi \rangle \\ = -J \cos \theta \cdot \dot{\phi} - [-\epsilon J \cos \theta + \frac{\chi}{2} J \cos(2\phi) (1 - \cos^2 \theta) + \frac{\chi'}{2} J \cos^2 \theta + \frac{2J}{2J-1} \chi'] , \quad (2)$$

where  $\chi = V(2J-1)$  and  $\chi' = V'(2J-1)$ . Since  $L$  contains only the time-derivative of the parameter  $\phi$ , we first assume  $\phi$  as a coordinate. Then the momentum canonically conjugate to  $\phi$  is  $p_\phi = \partial L / \partial \dot{\phi} = -J \cos \theta$ , and therefore the classical collective Hamiltonian is derived as

\* Department of Physics, University of Tokyo.

\*\* National Laboratory for High Energy Physics.

$$H_{\text{TDHF}} = p_\phi \cdot \dot{\phi} - L = \epsilon p_\phi + \frac{\chi}{2J} \cos(2\phi) (J^2 - p_\phi^2) + \frac{\chi'}{2J} p_\phi^2 + \frac{2J}{2J-1} \chi' \quad (3)$$

According to Ref. 7, for example, the quantal transformation matrix element

$$F(q't'; qt) = {}_H \langle q't' | qt \rangle_H = {}_S \langle q' | \exp[-i\hat{H}(t-t')] | q \rangle_S \quad (4)$$

is equal to the Feynman path integral

$$F(q't'; qt) = \frac{1}{2\pi} \int dq dp \exp\left[ i \int_t^{t'} \{ p \cdot \dot{q} - \hat{H}(p, q) \} dt \right] \quad (5)$$

In Eqn. (4),  $|qt\rangle_H$  ( $|q\rangle_S$ ) is an eigenstate of a coordinate operator  $\hat{Q}_H(t)$  ( $\hat{Q}_S$ ) with eigenvalue  $q$  in the Heisenberg (Schrödinger) picture ( ${}_S \langle q' | q \rangle_S = \delta(q' - q)$ ). The integrand on the exponent of the expression (5) is a classical Lagrangian, in which the classical Hamiltonian is defined by

$$H(p, q) = H\left(p, \frac{q' + q''}{2}\right) = \int d(q' - q'') \exp[-ip(q' - q'')] {}_S \langle q' | \hat{H} | q'' \rangle_S \quad (6)$$

While the quantal effect is taken into account by the integration over  $p$  and  $q$ , a classical trajectory is obtained by taking the variation of the action integral on the exponent. Thus we consider it as the minimum condition in quantization that the quantized Hamiltonian reproduces the classical Hamiltonian through Eqn. (6). Therefore the present quantization prescription is in general

$$H(p, q) = \hat{H}(\hat{P}, \hat{Q}) = \frac{1}{2\pi} \int dq d\rho dp \exp(i\frac{\rho}{2}\hat{P}) |q\rangle_S \langle q| \exp(i\frac{\rho}{2}\hat{P}) \exp(i\rho p) H(p, q) \quad (7)$$

where  $\hat{Q}$  and  $\hat{P}$  are quantum operators satisfying the commutation relation  $[\hat{P}, \hat{Q}] = \frac{1}{i}$ . Applying this prescription to  $H_{\text{TDHF}}$ , we finally obtain a collective Hamiltonian quantized from TDHF:

$$\hat{H}_{\text{TDHF}} = \epsilon \hat{P} + \frac{\chi}{4J} \sum_{\pm} \exp(\pm i\hat{Q}) (J^2 - \hat{P}^2) \exp(\pm i\hat{Q}) + \frac{\chi'}{2J} \hat{P}^2 + \frac{2J}{2J-1} \chi' \quad (8)$$

This Hamiltonian is diagonalized within the space of eigenstates  $|m\rangle\rangle$  of  $\hat{P}$  ( $\hat{P}|m\rangle\rangle = m|m\rangle\rangle$ ), where  $m$  is finite ( $m = -J+1, -J+3, \dots, J-1$ ):  $\langle\langle -J-1 | \hat{H}_{\text{TDHF}} | -J+1 \rangle\rangle = \langle\langle J-1 | \hat{H}_{\text{TDHF}} | J+1 \rangle\rangle = 0$  and  $\langle\langle m | \hat{H}_{\text{TDHF}} | m' \rangle\rangle \neq 0$  only for  $m-m' = \pm 2$  or  $0$ . The finiteness of  $m$  is consistent with the fact that  $p_\phi$  is bounded by  $+J$  and  $-J$ , i.e.,  $p_\phi = -J \cos \theta$ . It should be noted that the above property of  $\hat{H}_{\text{TDHF}}$ , which leads to the finiteness of  $m$ , is not produced by the ordinary Hermitian ordering, though we do not show a proof here.

The exact collective Hamiltonian, on the other hand, is derived as

$$\hat{H}_{\text{exact}} = \epsilon \hat{P} + \frac{\chi}{2(2J-1)} \sum_{\pm} \exp(\pm i\hat{Q}) [(J^2 - \hat{P}^2) \{(J+1)^2 - \hat{P}^2\}^{1/2}] \exp(\pm i\hat{Q}) + \frac{\chi'}{2J-1} \hat{P}^2 \quad (9)$$

by using the Nodvik's expression for the quasi-spin operators:<sup>8)</sup>

$$\hat{K}_3 = \hat{P} = \frac{1}{i} \frac{\partial}{\partial Q} \quad \hat{K}_\pm = \exp(\pm \frac{1}{2} \hat{Q}) [(J + \frac{1}{2})^2 - \hat{P}^2]^{1/2} \exp(\pm \frac{1}{2} \hat{Q})$$

The comparison of  $\hat{H}_{\text{TDHF}}$  and  $\hat{H}_{\text{exact}}$  shows that  $\hat{H}_{\text{TDHF}}$  approximates  $\hat{H}_{\text{exact}}$  to the 2nd order in  $\hat{P}$  with errors in the coefficients of  $O(1/J)$  with respect to the main parts. Since the quantal effect in this model is roughly  $1/J$ , i.e.  $m$  is bounded by  $-J+1$  and  $J-1$  differing by 2, the error in the coefficients comes partly from the ambiguity in the quantization procedure of the classical  $\hat{H}_{\text{TDHF}}$ . This error in the first interaction term makes the number of the eigenstates of  $\hat{H}_{\text{TDHF}}$  less than that of  $\hat{H}_{\text{exact}}$  by 1, which is again  $O(1/J)$  with respect to the total number. It is not only due to the ordering

ambiguity but also is inherent in the TDHF approximation itself. Although there is no problem of the operator ordering when  $\chi = 0$ , one still finds the error in the coefficient of the second interaction term. In the absence of the two-body interactions ( $\chi = \chi' = 0$ ),  $\hat{H}_{\text{TDHF}}$  is equal to  $\hat{H}_{\text{exact}}$ , which can be proved in general.

Now we proceed to discuss the results of the numerical calculation. Figure 1 shows the energy spectra of the  $N = 40$  system, in which  $\chi$  is varied while  $\chi'$  is fixed to zero. As is mentioned above, the TDHF spectrum agrees with the exact spectrum in the limit of small  $\chi$ . Although the difference between the two spectra becomes larger as  $\chi$  increases, their deviation is never seriously large. In Fig. 2, we show the spectra of the  $N = 20$  system for various combinations of  $\chi$  and  $\chi'$  ( $\chi' \neq 0$ ). In spite of the fact that all the spectra are changed much from the unperturbed spectrum, in which levels are equally spaced with the energy difference of 2, and moreover the measure of the error of  $O(1/J)$  in this case is twice as large as that in Fig. 1, the agreement of the TDHF spectra with the exact spectra is still remarkable. We note again, however, that there occurs an inherent error in TDHF in the presence of the two-body interaction, which we see in the case  $\chi = 0$  and  $\chi' = 1$  of this figure.

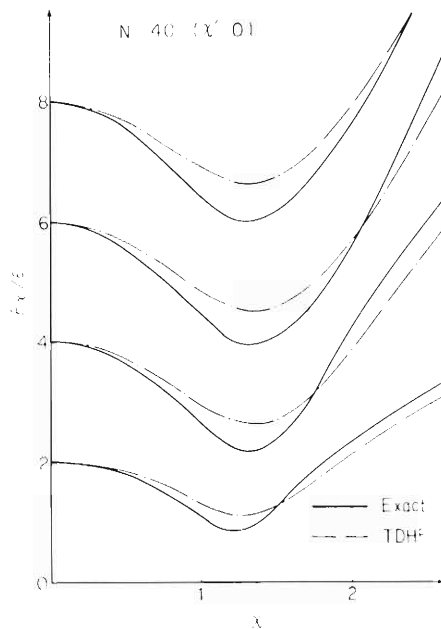


Fig. 1. TDHF and exact energy spectra for  $N = 40$ .

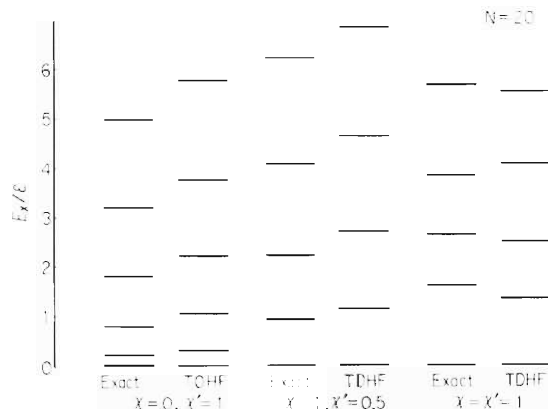


Fig. 2. TDHF and exact energy spectra for  $N = 20$ .

## References

- 1) See for example, J. A. Maruhn, and R. Y. Cusson: Nucl. Phys., A270, 471 (1976) and references therein.
- 2) D. M. Brink, M. J. Giannoni, and M. Veneroni: Nucl. Phys., A258, 237 (1976).
- 3) A. K. Kerman and S. E. Koonin: Ann. Phys., 100, 332 (1976).
- 4) G. Holtzwarth: Nucl. Phys., A207, 545 (1973).
- 5) S. J. Krieger: *ibid.*, A276, 12 (1977).
- 6) H. J. Lipkin, N. Meshkov, and A. J. Glick: *ibid.*, 62, 188 (1965).
- 7) E. S. Abers and B. W. Lee: Phys. Reports, 9C, 1 (1973).
- 8) J. S. Nodvik: Ann. Phys., 51, 251 (1969).

#### 4-15. $\alpha$ -Particle and Light Product Correlation in the $^{14}\text{N} + ^{93}\text{Nb}$ Reaction

T. Shimoda, M. Ishihara, H. Kamitsubo,  
T. Motobayashi, and T. Fukuda\*

Recent correlation experiments<sup>1)-4)</sup> on heavy ion reactions have revealed that  $\alpha$ -particles are emitted with appreciable probability in company with reaction residues of the quasi-elastic (QE) and deep inelastic (DI) collisions. Because of the exclusive nature of the information provided by such correlations, the study of the  $\alpha$  accompanying process has attracted much interest as a promising probe to explore the detailed reaction mechanism of the energy dissipating collisions.

Among the different  $\alpha$ -emission mechanisms proposed for the coincidence events, the process due to the fragment decay succeeding to the primary reaction appears to be most likely. In fact the present experiment on the  $^{14}\text{N} + ^{93}\text{Nb}$  system has shown that the sequential decay of the projectile-like residues from the QE and DI collisions is the major origin of the coincident  $\alpha$  particles. This conclusion is in contrast to the results<sup>2)</sup> on relatively light reaction systems, where the importance of the decay of target-like residues was suggested. It does not either conform to the prompt  $\alpha$ -emission mechanism by the dissipative force suggested theoretically<sup>5)</sup> and experimentally.<sup>3)</sup>

The experimental procedures were almost the same as those in Ref. 1. The energy and angular correlations between the  $\alpha$ -particle and the projectile-like fragments (from proton to  $^{16}\text{O}$ ) were measured in the bombardment of a  $^{93}\text{Nb}$  metallic target by 90 and 110 MeV  $^{14}\text{N}$  ions. The projectile-like fragments were detected at lab angle  $\theta_1 = 35^\circ$  and the coincident particles were detected at various angles  $\theta_\alpha$  in the scattering plane defined by the beam axis and the fragment detector.

Figure 1 shows some of the energy-integrated angular correlations obtained at  $E_{1ab} = 115$  MeV. It is seen that the correlations for different channels are essentially the same as those at  $E_{1ab} = 90$  MeV reported previously.<sup>1)</sup> It should be noted that there is no particular enhancement in the cross section for the  $^{10}\text{B} - \alpha$  channel. The strong backward-forward asymmetry and the location of the peak of the correlation indicate the dominance of sequential  $\alpha$ -decay from excited light fragments. Especially, the fact that the peak angle  $\theta_\alpha$  and  $\theta_1$  are generally on the same side of the beam axis (except for  $^{13}\text{C} - \alpha$ ) is contradictory to the prediction for the heavy fragment sequential decay and of the "piston" model.<sup>5)</sup>

A more straightforward evidence for the light fragment sequential decay is obtained from the energy correlations. A typical example of such correlation is presented in Fig. 2, where coincidence yields for the  $^{10}\text{B} - \alpha$  channel are shown by contour lines in the plane of  $\alpha$ -particle c.m. energy versus  $^{10}\text{B}$  c.m. energy. Loci for given values of relative kinetic energy  $E_{1-2}$  between  $\alpha$  and  $^{10}\text{B}$ , and c.m. kinetic energy  $E_0$  of the primary excited nucleus  $^{14}\text{N}^*$ , are also indicated in the plane by dotted and dashed lines, respectively. The excitation energy of the decaying  $^{14}\text{N}^*$  may be given by the relative energy  $E_{1-2}$  and  $\alpha$  separation energy. It is seen that the coincidence yields mainly fall into two regions. Although these two regions are separated from each other, they correspond to the kinematical zones defined by the same energy band of  $E_{1-2} = 1.2 \pm 0.5$  MeV

\* Department of Physics, Osaka University.

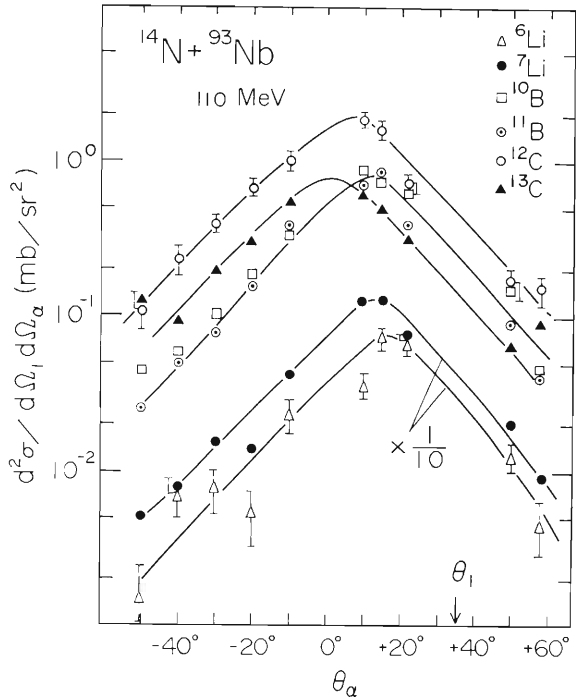


Fig. 1. The energy-integrated in-plane angular correlations between  $\alpha$  and various light products at  $E_{\text{lab}} = 115$  MeV. The light fragments were detected at the fixed laboratory angle of  $\theta_1 = 35^\circ$ .

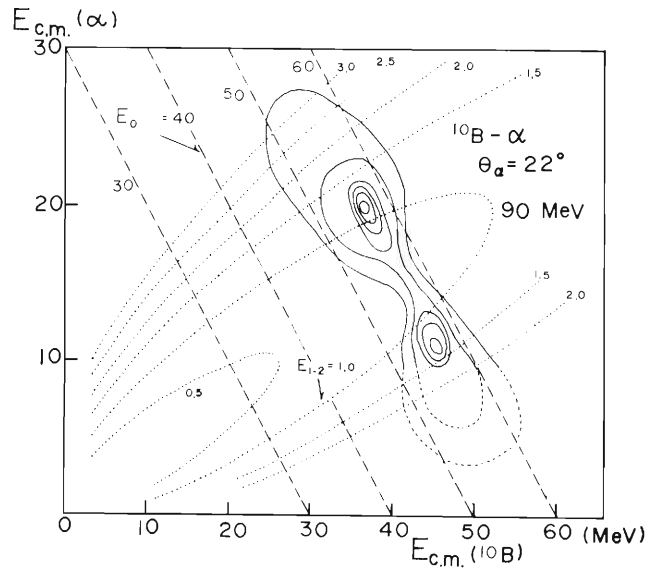


Fig. 2. An example of the contour plot of the energy correlations is displayed in the plane of c.m. energies of  $\alpha$  particle and  $^{10}\text{B}$ .

and  $E_0 = 55 \pm 5$  MeV. Essentially the same feature was observed in the other channels except for few channels like  $\alpha$ - $\alpha$ . This double-fold nature of the contour map is apparently a property characteristic of the light fragment sequential decay.

## References

- 1) H. Kamitsubo, M. Ishihara, T. Shimoda, T. Fukuda, T. Motobayashi, T. Ooi, and I. Kohno: IPCR Cyclotron Progr. Rep., 10, 26 (1976); H. Kamitsubo: in Proc. of the Colloque Franco-Japonais de Spectroscopie Nucléaire et Réaction Nucléaire and INS Symposium on Nuclear Collectivity, Dogashima and Tokyo, 1976, p. 235.
- 2) J. W. Harris, T. M. Cormier, D. F. Geesman, L. L. Lee, Jr., R. L. McGrath, and J. P. Wurm: Phys. Rev. Lett., 38, 1460 (1977).
- 3) H. Ho, R. Albrecht, W. Dünneweber, G. Graw, S. G. Steadman, J. P. Wurm, D. Disdier, V. Rauch, and F. Scheibling: Z. Physik, A283, 235 (1977); C. K. Gelbke, M. Bini, C. Olmer, D. L. Hendrie, J. L. Laville, J. Mahoney, M. C. Mermaz, D. K. Scott, and H. H. Wieman: Phys. Lett., 77B, 83 (1977).
- 4) R. Ost, N. E. Sanderson, S. Mordechai, J. B. A. England, B. R. Fulton, J. M. Nelson, and G. C. Morrison: Nucl. Phys., A265, 142 (1976).
- 5) D. H. E. Gross and J. Wilczyński: Phys. Lett., 67B, 1 (1977).

4-16. Light Fragment Excitation in the  $^{14}\text{N} + ^{93}\text{Nb}$  Reaction

T. Shimoda, M. Ishihara, H. Kamitsubo,  
T. Motobayashi, and T. Fukuda\*

We have reported<sup>1)</sup> that the light-fragment sequential decay is the dominant mechanism for the coincidence process between light product and  $\alpha$  particle in the  $^{14}\text{N} + ^{93}\text{Nb}$  reaction. Appreciable yields observed for the coincidence process imply that a considerable fraction of the light products are populated in their excited states above the  $\alpha$  separation energies when they are produced in the primary two-body reaction. Thus the cross section of light fragment excitation is related to the mechanism which determines how the light and heavy products share the internal energy supplied from dissipation of relative kinetic energy in the primary quasi-elastic and deep inelastic process.

The total cross section of light fragment excitation above the  $\alpha$  separation energy  $S_\alpha$  is deduced as a function of the scattering angle  $\theta_0$  of the primary excited light fragment by

integrating the coincidence yields  $\frac{d^4\sigma}{dE_1 dE_\alpha d\Omega_1 d\Omega_\alpha}$  over the energy plane obtained at a given set

of angles  $\theta_1$  and  $\theta_\alpha$ . (subscripts 1 and  $\alpha$  refer to the light fragment and  $\alpha$  particles, respectively.) To accomplish this integration the coordinate system referring to center of mass of the decaying light fragment was used as shown in Fig. 1. This coordinate system consists of four variables, i.e.,

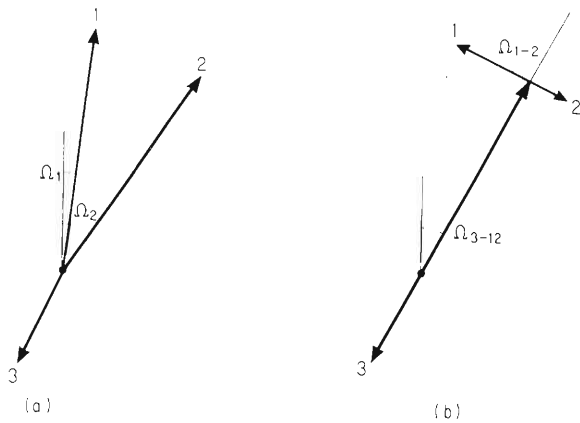


Fig. 1. The velocity diagrams of three body system displayed in (a) the laboratory system and (b) the center of mass system of the decaying light fragment. Particles denoted by 1 and 2 are observed. The primary product (1 + 2) decays into particle 1 and 2.

energies  $E_{1-\alpha}$ ,  $E_0$  and corresponding angular variables  $\Omega_{1-\alpha}$ ,  $\Omega_0$ , where  $E_{1-\alpha}$  is the relative kinetic energy between  $\alpha$  particle and the final light product and  $E_0$  is the kinetic energy of the primary excited light fragment. For given values of  $\theta_1$  and  $\theta_\alpha$ ,  $\Omega_0$  may be considered to be

constant for a large range of  $E_1$  and  $E_\alpha$ . The cross section  $\frac{d\sigma^{ex}}{d\Omega_0}$  is given as  $\frac{d\sigma^{ex}}{d\Omega_0} = \iiint dE_{1-2}$

$dE_0 d\Omega_{1-2} J \frac{d}{dE_1 dE_\alpha d\Omega_1 d\Omega_\alpha}$ , where  $J$  is the Jacobian relevant to the transformation of the

\* Department of Physics, Osaka University.

coordinate system. In the integration over  $\Omega_{1-2}$ , isotropic angular distributions of the break-up particles are assumed.

Figure 2 shows the cross section of the light fragment excitation probability thus obtained. The angles  $\theta_0$  of the primary products are  $29^\circ \sim 31^\circ$  for all channels. The points are labelled by the corresponding primary light product. The abscissa represents the threshold Q-value  $Q_{ggg}$  for the three-body process, which is related to the two-body ground state Q-value  $Q_{gg}$  as  $Q_{ggg} = Q_{gg} + S_\alpha$ . It is clearly seen that the relative cross sections for different isotopes with a given Z are well represented by the expression  $\frac{d\sigma^{ex}}{d\Omega_0} = f(z) \exp(Q_{ggg}/T_{eff})$ , which is analogous to the expression<sup>2)</sup> for the singles cross section. The value of effective temperature  $T_{eff}$  is about 3.5 MeV for all of the B, C, N, and O isotopes, and is comparable with the value of  $T_{eff} = 2.9 \sim 3.5$  MeV for singles cross section.

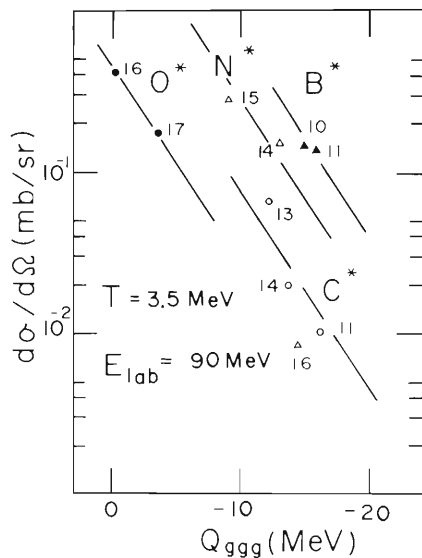


Fig. 2. The cross section for light fragment excitation above  $\alpha$  separation energy are plotted versus the threshold Q value for the three body process, where the excited primary products are emitted at the laboratory angle of  $29^\circ - 31^\circ$ . The solid lines represent the function  $f(z)\exp(Q_{ggg}/T_{eff})$  for the case of  $T_{eff} = 3.5$  MeV. The normalizations of the function are arbitrary for each isotopes.

## References

- 1) H. Kamitsubo, M. Ishihara, T. Shimoda, T. Fukuda, T. Motobayashi, T. Ooi, and I. Kohno: IPCR Cyclotron Progr. Rep., 10, 26 (1976).  
T. Shimoda, M. Ishihara, H. Kamitsubo, T. Motobayashi, and T. Fukuda: *ibid.*, 11, 54 (1977).
- 2) V. V. Volkov: Proc. Int. Conf. on Reactions between Complex Nuclei, Nashville, 2, 363 (1974).  
J. P. Bondorf, F. Dickmann, D. H. E. Gross, and P. J. Siemens: J. de Phys., C6, 145 (1971).

#### 4-17. Angular Distribution and Energy Spectrum of "Direct" $\alpha$ -Particles Emitted from the $^{159}\text{Tb} + 95 \text{ MeV } ^{14}\text{N}$ Reaction

T. Inamura, K. Hiruta, S. Ise, T. Shimoda,  
T. Nomura, and M. Ishihara

We have measured angular distributions of  $\alpha$ -particles and other ejectiles from the  $^{159}\text{Tb} + 95 \text{ MeV } ^{14}\text{N}$  reaction to study how "direct"  $\alpha$ -particles are emitted from the reaction. This was initiated by finding that the starting population for  $\gamma$ -deexcitation following forward-peaking fast  $\alpha$ -particle emission is different from that in the compound reaction.<sup>1)</sup>

To detect particles a  $\Delta E$ -E counter telescope was used, consisting of  $30 \mu\text{m}$  and  $2000 \mu\text{m}$  thick Si surface-barrier detectors. The  $^{159}\text{Tb}$  target was a self-supporting metallic foil  $2.1 \text{ mg/cm}^2$  thick.

Figure 1 shows the observed angular distribution of  $\alpha$ -particles with  $E_\alpha \geq 30 \text{ MeV}$  in the laboratory system, together with the angular distributions observed for typical ejectiles heavier than  $\alpha$ -particle. The followings are noted: for  $^{11}\text{C}$  the distribution shows a bell shape whose peak coincides with the grazing angle ( $\theta_{\text{gr}} = 43^\circ$  in lab.), being typically quasi-elastic; from  $^{10}\text{B}$  to

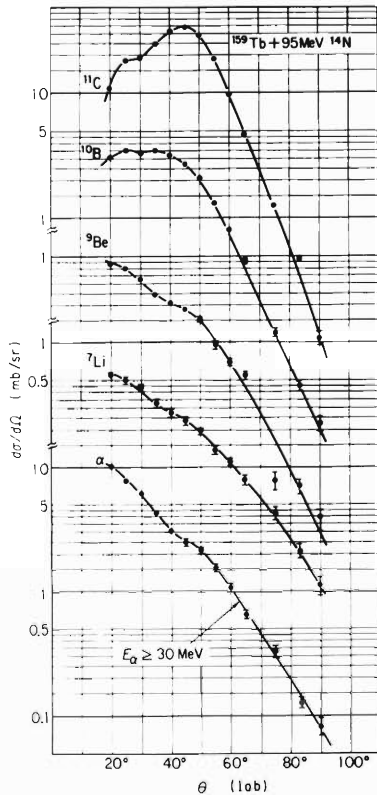


Fig. 1. The laboratory angular distributions of  $\alpha$ -particles with  $E_\alpha \geq 30 \text{ MeV}$  and other typical ejectiles heavier than  $\alpha$ -particle from the  $^{159}\text{Tb} + 95 \text{ MeV } ^{14}\text{N}$  reaction.

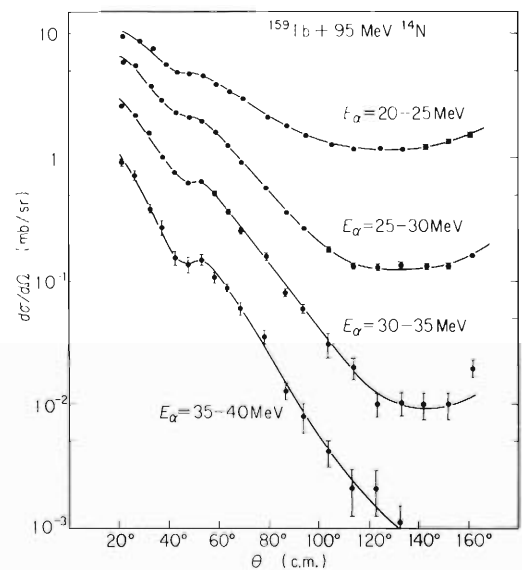


Fig. 2. Angular distributions of  $\alpha$ -particles integrated over small ranges of the kinetic energy.

$\alpha$ -particle there are rising cross sections at forward angles with increasing transferred mass and small bumps near the grazing angle; and, except for  ${}^1\text{O}$ B, the position of the bumps moves toward larger angle than the grazing angle with increasing transferred mass.

Figure 2 shows angular distributions of  $\alpha$ -particles integrated over small ranges of the kinetic energy. The rising cross section at backward angles is considered to be due to evaporation process.

The energy spectrum of "direct"  $\alpha$ -particles observed at  $20^\circ$  to the beam ( $22^\circ$  in c.m.) is shown in Fig. 3. This was obtained by subtracting the evaporation component from the total energy spectrum recorded. The evaporation component was deduced from the data taken at  $160^\circ$  to the beam ( $162^\circ$  in c.m.) with a reduction factor  $\sin 162^\circ/\sin 158^\circ$ . Here we assumed that the angular distribution of evaporated  $\alpha$ -particles is symmetric about  $90^\circ$  in c. m., following the  $1/\sin\theta$  rule.

It should be noted that the shape of the "direct"  $\alpha$  spectrum is likely to be described by a Gaussian (or Maxwell-Boltzmann) distribution, showing a sort of statistical nature. As was suggested by Britt and Quinton,<sup>2)</sup> this might be explained by a vector coupling between the projectile velocity (group velocity) and the intrinsic  $\alpha$ -particle velocity in the region of reaction because the latter distribution may be approximately given by a Gaussian distribution as is the velocity distribution of nucleons. This idea is applicable so long as the memory of the initial linear momentum is not lost.

The reaction of interest looks as if the target nucleus absorbs the transferred  ${}^1\text{O}$ B nucleus, while  $\alpha$ -particles are emitted directly, i. e.,  ${}^{14}\text{N} + {}^{159}\text{Tb} = (\alpha + {}^1\text{O}\text{B}) + {}^{159}\text{Tb} \rightarrow \alpha + ({}^1\text{O}\text{B} + {}^{159}\text{Tb}) = \alpha + {}^{169}\text{Yb}^*$ . Because of this we have applied an idea of the two-body reaction mechanism<sup>3),4)</sup> to describe the optimum Q-value and the angular momentum of the residual nucleus. By assuming the kinematical conditions  $\Delta k = 0$  and  $\Delta L = 0$  (see Ref. 4), the residual angular momentum is estimated to be  $\lambda_2 \simeq 21 \hbar$ . If "direct"  $\alpha$ -particles are emitted tangentially from the colliding system in the reaction plane, the incoming partial wave is estimated to be  $\ell_{\text{in}} \simeq 39 \hbar$ . This result is in accord with the conclusion about the angular momentum distribution of the entrance channel on the basis of "direct"  $\alpha$ - $\gamma$  coincidence measurement.<sup>1)</sup>

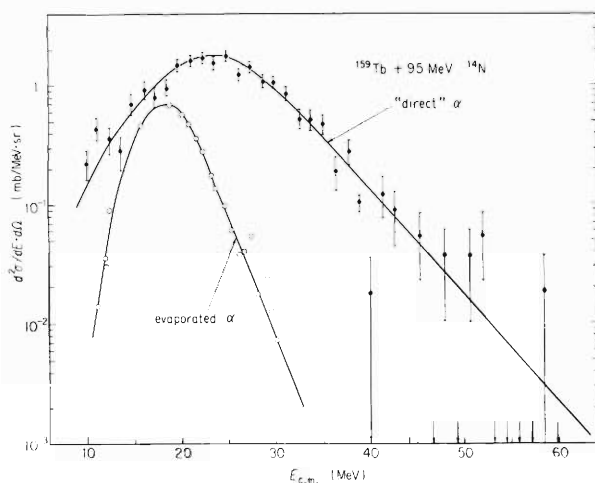


Fig. 3. Energy spectrum of "direct"  $\alpha$ -particles emitted to  $22^\circ$  (c.m.) from the  ${}^{159}\text{Tb} + 95 \text{ MeV } {}^{14}\text{N}$  reaction, together with the one of evaporated  $\alpha$ -particles.

## References

- 1) T. Inamura, M. Ishihara, T. Fukuda, T. Shimoda, and K. Hiruta: Phys. Lett., **68B**, 51 (1977).
- 2) H. C. Britt and A. R. Quinton: Phys. Rev., **124**, 877 (1961).
- 3) P. J. Siemens, J. P. Bondorf, D. H. E. Gross, and F. Dickmann: Phys. Lett. **36B**, 24 (1971).
- 4) D. M. Brink: *ibid.*, **40B**, 37 (1972).

4-18. Energy Relaxation of a Composite System  
Deduced from Preequilibrium  $\alpha$ -Particle  
Spectra in  $^{209}\text{Bi} + ^{14}\text{N}$  Reactions

T. Nomura and H. Utsunomiya

Weiner and Weström<sup>1)</sup> have recently attempted to describe preequilibrium phenomena in terms of diffusion of heat in nuclear matter, starting from a “hot spot” created by a reaction at a nuclear surface. They have shown that evaporated particles from such a locally excited system are expected to show enhancement of high-energy parts and a large asymmetry in the angular distributions. The angular and energy distributions of  $\alpha$ -particles emitted in the  $^{209}\text{Bi} + ^{14}\text{N}$  reaction described in the preceding paper<sup>2)</sup> seem to be consistent with this interpretation, i.e., evaporation from a locally heated system. We thus decided to analyze the experimental  $\alpha$ -particle spectra by the following simple statistical formula of Ericson<sup>3)</sup>

$$N(E_\alpha) \propto E_\alpha \sigma_c(E_\alpha) \exp(-E_\alpha/T). \quad (1)$$

Here,  $E_\alpha$  is the kinetic energy of an  $\alpha$ -particle,  $\sigma_c$  the inverse cross section, and  $T$  the nuclear temperature of the residual nucleus, which is related to the usual level density parameter  $a$  and the averaged excitation energy of the residual nucleus  $U_{av}$  with  $T^2 \approx U_{av}/a$ .  $U_{av} \approx 30$  and  $40$  MeV in cases of  $85$  and  $95$  MeV incident energies, respectively. In Eqn. (1), we assume the spin-independent constant nuclear temperature. This may be justified because we are treating high excitation energies and relatively low angular momenta; the maximum spin calculated from the sharp cut-off approximation is  $39 \hbar$  ( $85$  MeV) and  $52 \hbar$  ( $95$  MeV). In fact, the spin-dependent temperature defined by Williams and Thomas<sup>4)</sup> as  $T_j \simeq T(1 - E_{rot}(j)/U_{av})^{1/2}$  is close to  $T$  provided the rotational energy  $E_{rot}(j)$  is calculated by the rigid-body moment of inertia.

As for  $\sigma_c(E_\alpha)$ , we used reaction cross sections calculated by Igo,<sup>5)</sup> who showed the results as a function of  $E_\alpha/B_\alpha$ , where  $B_\alpha$  is the barrier height of the optical potential used. A spherical nucleus is assumed in Ref. 5, in which  $B_\alpha \simeq 21.5$  MeV. Eqn. (1) turned out to reproduce well the spectral shape at backward angles when  $T$  is taken to be a “compound nucleus value” described later, but the calculated peak position is by  $2$ - $3$  MeV higher than the experimental one. The similar discrepancy has been pointed out by Knox et al.<sup>6)</sup> and was attributed to the nuclear distortion resulting in a smaller Coulomb barrier. In order to take this effect into account in the calculation of  $\sigma_c$ , we treat  $B_\alpha$  as a parameter to be determined and assume, for simplicity, the same dependence of  $\sigma_c$  on  $E_\alpha/B_\alpha$  as in the case of a spherical nucleus. It turned out that all the observed spectra could be fitted excellently by Eqn.(1) when we assume  $B_\alpha = 19.5$  MeV and treat  $T$  as another fitting parameter. To show this, we plotted the quantity  $N(E_\alpha)/E_\alpha \sigma_c(E_\alpha)$  versus  $E_\alpha$  on a semilog scale in Fig. 1, where  $N(E_\alpha)$  were taken from experimental spectra. If Eqn. (1) can reproduce experiment, the resultant plot must be a straight line. This is indeed the case at all angles as seen in Fig. 1. The slope of a straight line at each angle gives the best value of nuclear temperature. The values of  $T$  thus determined are shown in Fig. 2. The temperature

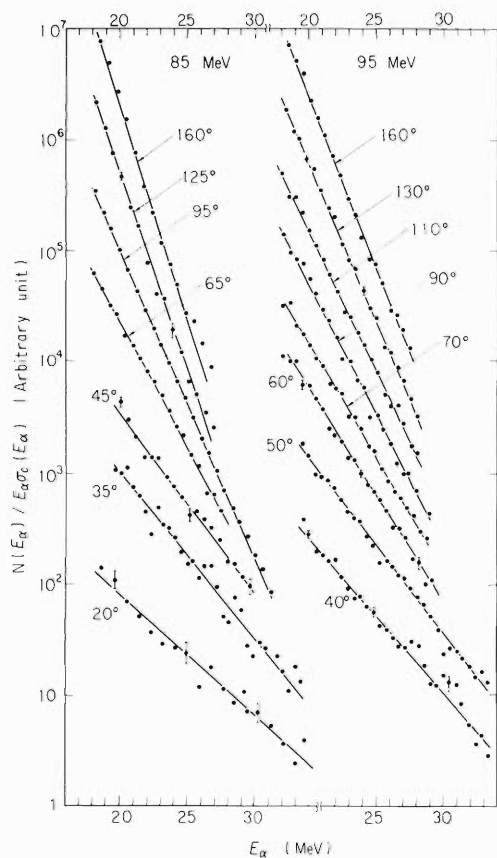


Fig. 1. Plot of  $N(E_\alpha)/E_\alpha\sigma_c(E_\alpha/B_\alpha)$  versus  $E_\alpha$ , where  $N(E_\alpha)$  are taken from experimental spectra and  $\sigma_c$  are calculated under the assumption of  $B_\alpha = 19.5$  MeV. The lab. angles are indicated.

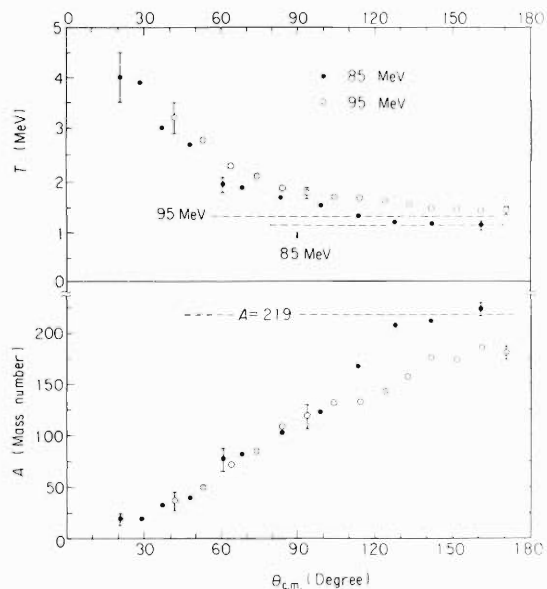


Fig. 2. The nuclear temperature  $T$  and size  $A$  of a hot spot versus emission angles.

decreases monotonically with increasing angles and almost reaches, at very backward angles, a “compound nucleus value”, a value expected from an energetically equilibrated system, which is calculated from  $T^2 \approx U_{av}/a$  and  $a = A/9 \text{ MeV}^{-1}$  with  $A = 219$ .

A possible origin of the local heating may be the following. There is some experimental evidence that the  $\alpha$ -particle emission of interest originates from reactions occurring at nuclear surfaces. Quite recently, Inamura et al.<sup>7)</sup> suggested that the associated initial channel spins are localized just above the critical angular momentum for complete fusion, being similar to deeply inelastic reactions, where relaxation phenomena become important. At such reactions, a “hot spot” is formed as soon as the two colliding nuclei touch each other due to large radial frictional forces, and the relative angular momenta are transformed mainly to the rotation of a heavier nucleus, i.e.,  $^{209}\text{Bi}$  in our case, due to its large moment of inertia. The hot spot sitting on the surface of this rotating system is an origin of the observed  $\alpha$ -particles, which are emitted, in average, in the direction of the rotational velocity at the surface. Let us assume that the hot spot is directed to forward angles when the system starts to rotate. Then, we may relate the emission angle somehow to the reaction time in the similar manner as suggested in deeply inelastic

collisions (e.g., negative deflection angle).<sup>8)</sup> It seems, therefore, that the nuclear temperature deduced from the present analysis can be interpreted to have physical significance, i.e., to show the degree of energy relaxation of the hot spot versus the time lapse measured from the initial collision. The size of the hot spot can be obtained from  $T^2 \approx U_{av}/a$  and  $a=A/9$ , assuming that these equalities hold even in the local heating. The results are shown in Fig. 2.

#### References

- 1) R. Weiner and M. Weström: Phys. Rev. Lett., 34, 1523 (1975); Nucl. Phys., A286, 282 (1977).
- 2) H. Utsunomiya, T. Nomura, T. Motobayashi, T. Inamura, and M. Yanokura: IPCR Cyclotron Progr. Rep., 11, 63 (1977).
- 3) T. Ericson: Advan. Phys., 9, 425 (1960).
- 4) D. C. Williams and T. D. Thomas: Nucl. Phys., 53, 577 (1964).
- 5) G. Igo: Phys. Rev., 115, 1665 (1959).
- 6) W. J. Knox, A. R. Quinton, and C. E. Anderson: Phys. Rev., 120, 2120 (1960).
- 7) T. Inamura, M. Ishihara, T. Fukuda, T. Shimoda, and H. Hiruta: Phys. Lett., 68B, 51 (1977).
- 8) J. Wilczynski: *ibid.*, 40B, 37 (1972).

4-19. Preequilibrium  $\alpha$ -Particle Emission from  
 $^{209}\text{Bi} + ^{14}\text{N}$  Reactions

H. Utsunomiya, T. Nomura, T. Motobayashi,  
 T. Inamura, and M. Yanokura

In reactions induced by relatively light "heavy ions" (e. g.,  $^{12}\text{C}$ ,  $^{14}\text{N}$ , and  $^{16}\text{O}$ ) at bombarding energies well above the Coulomb barrier,  $\alpha$ -particles are known to be emitted with large probabilities. The  $\alpha$ -particle emission occurs predominantly in the forward direction with appreciable enhancement of the high-energy part when compared to an evaporation spectrum observed in compound reactions.<sup>1),2)</sup> The reaction process involved, however, has not yet been well understood. In order to throw more light on this phenomenon, we have studied  $^{209}\text{Bi} + ^{14}\text{N}$  reactions at relatively low bombarding energies, i. e., at  $E_{\text{lab.}} = 85$  and  $95$  MeV, with emphasis on energy and angular distributions of  $\alpha$ -particles. The Coulomb barrier of the entrance channel estimated from the systematics generally adopted is around 65 MeV.

A self-supporting  $^{209}\text{Bi}$  target of about  $1 \text{ mg/cm}^2$  thickness was bombarded with 85 and 95 MeV  $^{14}\text{N}$  ions from the cyclotron. The following measurements were carried out: 1) Charged particles with  $Z \leq 8$  detected with conventional counter telescopes were measured between  $20^\circ$  and  $160^\circ$  at 85 MeV and between  $40^\circ$  and  $170^\circ$  at 95 MeV. 2) Fission fragments were measured between  $10^\circ$  and  $170^\circ$  at both incident energies; we identified high-energy particles stopped within a thin ( $30 \mu \text{ Si}$ )  $\Delta E$  counter as fission fragments. 3) Cross sections for the production of heavy residual nuclei following fusion or fusion-like reactions such as ( $^{14}\text{N}, xn$ ) and ( $^{14}\text{N}, \alpha xn$ ) were

Table 1. Summary of experimental cross section.

	Cross sections (mb)	
	85 MeV	95 MeV
$\alpha$ -particles <sup>a)</sup>	$42 \pm 6$	(63)
Fission	$890 \pm 65$	$1350 \pm 100$
( $^{14}\text{N}, xn$ )	$5 \pm 1$	$3 \pm 1$
( $^{14}\text{N}, \alpha xn$ )	$31 \pm 3$	$49 \pm 8$
( $^{14}\text{N}, 2\alpha xn$ )	$3 \pm 1$	$3 \pm 1$

- a) Estimated from the smooth extrapolation of the observed angular distributions at very forward and backward angles. In the case of 95 MeV, the given value has a large error due to lack of statistics at forward angles.

measured by detecting  $\alpha$ -decays of their ground states in-beam in the same way as described in Ref. 3.

The measured cross sections are summarized in Table 1. The following points are to be noted. 1) Fission is the almost exclusive mode of the deexcitation of the compound nucleus, neutron evaporation being negligibly small. Since  $\alpha$ -particle evaporation is far less probable than neutron

evaporation in this mass region, we expect no significant contribution from the compound reaction to the observed  $\alpha$ -particles. 2) The cross section for the emitted  $\alpha$ -particles is roughly equal to the sum of cross sections for heavy residual nuclei produced in ( $^{14}\text{N}, \alpha xn$ ) and ( $^{14}\text{N}, 2\alpha xn$ ) reactions; this shows that the rest of a composite system after the  $\alpha$ -particle emission mostly fuses each other.

The measured angular and energy distributions of  $\alpha$ -particles were transformed into those in the c. m. system under the assumption of a binary reaction, i. e.,  $^{209}\text{Bi} + ^{14}\text{N} \rightarrow \alpha + ^{219}\text{Th}$ , which seems reasonable from the above mentioned facts. The present angular distributions are very similar to those reported in similar reactions by Britt and Quinton.<sup>1)</sup> The yield decreases rapidly with increasing angles up to around  $70^\circ$ , and still continues to decrease slowly at more backward angles; in particular, there is no such rise near  $180^\circ$  as expected from the compound reaction. A main difference between the present angular distributions and those reported in Ref. 1 is that we observed a small bump or shoulder, at both incident energies, near grazing angles, i. e., at around  $100^\circ$  (85 MeV) and  $80^\circ$  (95 MeV), in which typical transfer reactions have peaks in their angular distributions as shown in Fig. 1. We therefore consider these bumps as originating from the most direct  $\alpha$ -particle or  $^8\text{Be}$  emission corresponding to  $^{10}\text{B}$  or  $^6\text{Li}$  transfer reaction, respectively. In fact, the difference between on- and off-peak spectra shows a broad peak at energies corresponding to the initial velocities in both cases as shown in Fig. 2. A preliminary measurement on the  $^{181}\text{Ta} + ^{14}\text{N}$  and  $^{197}\text{Au} + ^{14}\text{N}$  reactions at 85 MeV has shown the same features.

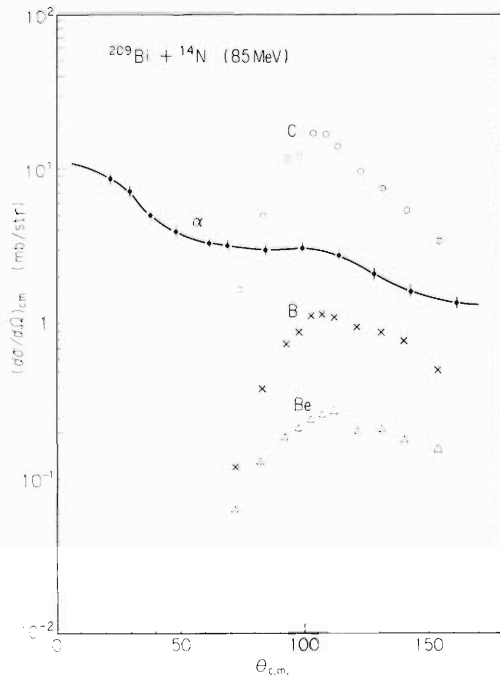


Fig. 1. Angular distributions of  $\alpha$ -particles, Be, B, and C isotopes taken in the  $^{209}\text{Bi} + ^{14}\text{N}$  reaction at 85 MeV.

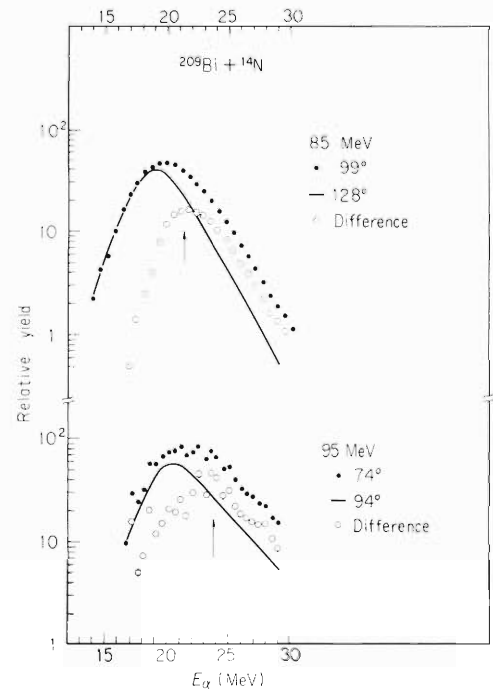


Fig. 2. Difference spectra between those taken at a bump in the angular distribution and at an off-peak angle. See also Fig. 3.

The measured  $\alpha$ -particle spectra at 85 MeV are shown in Fig. 3. At backward angles, they are peaked at around 19.5 MeV and have nearly exponential tails toward high energies; this is a familiar feature generally known in the evaporation process from the compound reaction. The forward spectra are very broad and apparently quite different from the evaporation spectrum;

however, we can still note the existence of high-energy tails which also decay almost exponentially but very slowly, indicating high “nuclear temperature” of the associated composite system. The experimental spectra at 95 MeV have nearly the same tendency. The most probable energy, i. e., energy at the peak position and the averaged energy at each observed angle are shown in Fig. 4.

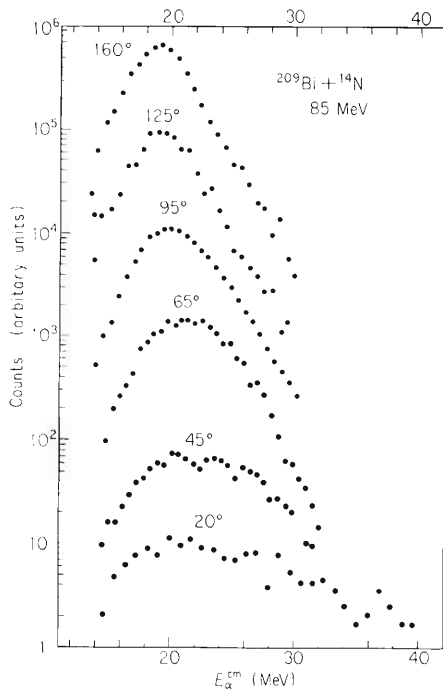


Fig. 3.  $\alpha$ -particle spectra at various angles taken in the  $^{209}\text{Bi} + ^{14}\text{N}$  reaction at 85 MeV.

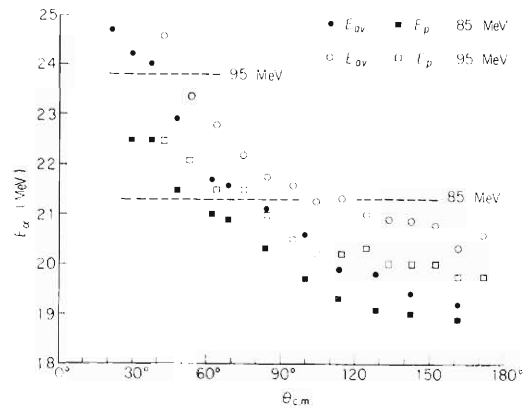


Fig. 4. The most probable ( $E_p$ ) and averaged energies of  $\alpha$ -particles emitted in the  $^{209}\text{Bi} + ^{14}\text{N}$  reaction at 85 and 95 MeV. The energies corresponding to initial velocities are shown by dashed lines.

## References

- 1) H. C. Britt and A. R. Quinton: Phys. Rev., 124, 877 (1961).
- 2) J. Galin, B. Gatty, D. Guereau, C. Rousset, U. C. Schlotthauer-Voos, and X. Tarrago: *ibid.*, C9, 1126 (1974).
- 3) T. Nomura, K. Hiruta, T. Inamura, and M. Odera: Nucl. Phys., A217, 253 (1973).

## 5. NUCLEAR PHYSICS

## Nuclear Spectroscopy

5-1. Cross Section for the  $^{40}\text{Ca}(^{16}\text{O}, p)^{55}\text{Co}$  Reaction

H. Morinaga, M. Yanokura, J. Imazato,\*  
T. Nomura, and M. Ishihara

Recently studies of precompound process with heavy-ion beam have revealed some new aspects of heavy-ion reaction mechanism.<sup>1),2)</sup> In the present work the cross section for one proton emission in case of  $^{16}\text{O}$  ions was measured in order to investigate such a reaction. A radiochemical method was employed to determine the yield of  $^{55}\text{Co}$  after the bombardment of  $^{40}\text{Ca}$  with  $^{16}\text{O}$  beam of 89 MeV for 3 h. The target was highly enriched isotope (>99.99%) and also chemically very pure, so that we had not to worry about contaminative reaction. Its thickness corresponds to the range of beam energy  $E_{\text{lab}} = 89$  to 63 MeV. A  $^{55}\text{Co}$  source was prepared by ion exchange for the HCl solution of the target and the recoil stopper, and completely separated from other strong activities. The  $\gamma$  transition of 931 keV from the  $^{55}\text{Co}$  decay with a half-life of 18 h was observed in a Ge(Li) spectrum obtained by  $\beta$ - $\gamma$  coincidences to suppress the background. The cross section turned out to be  $1.75 \pm 0.5 \mu\text{b}$  for the  $^{40}\text{Ca}(^{16}\text{O}, p)^{55}\text{Co}$  reaction. Other activities observed were  $^{48}\text{Cr}$ ,  $^{49}\text{Cr}$ ,  $^{52}\text{Mn}$ ,  $^{43}\text{Sc}$ , and  $^{44}\text{Sc}$ , they are summarised in the table.

Table 1. Cross section for the activity production in  $^{40}\text{Ca} + ^{16}\text{O}$ .

Nucleus	Cross section
$^{55}\text{Co}$	$1.75 \pm 0.5 \mu\text{b}$
$^{52}\text{Mn}$ (ground state)	$42 \pm 8 \text{ mb}$
(isomer)	$73 \pm 15 \text{ mb}$
$^{49}\text{Cr}$	$244 \pm 40 \text{ mb}$
$^{48}\text{Cr}$	$4.1 \pm 1.0 \text{ mb}$
$^{44}\text{Sc}$	$0.21 \pm 0.4 \text{ mb}$
$^{43}\text{Sc}$	$9.0 \pm 0.2 \text{ mb}$

## References

- 1) M. Blann: Nucl. Phys., A235, 211 (1974); M. Blann, A. Mignerey, and W. Scobel: Nucleonika, 21, 335 (1976), and references therein.
- 2) T. Nomura, J. Delaunay, C. Tosello, and N. Bendjaballah: preprint; T. Nomura, H. Utsunomiya, T. Motobayashi, and T. Inamura: Proc. of Intern. Conf. on Nucl. Structure, Tokyo, (Contributed Papers) p. 736 (1977); J. W. Harris, P. Braun-Munzinger, T. M. Cormier, D. F. Geesaman, L. L. Lee, Jr., R. L. Mcgrath, and J. P. Wurm: *ibid.*, p. 698.

\* Department of Physics, University of Tokyo.

## 5-2. $\gamma$ -Rays Following Fast $\alpha$ -Particles Emitted in the $^{159}\text{Tb} + 95 \text{ MeV } ^{14}\text{N}$ Reactions

T. Inamura, K. Hiruta, S. Ise, T. Shimoda,  
M. Ishihara, and T. Nomura

We have already pointed out:<sup>1),2)</sup> (1) for the  $^{159}\text{Tb} + 95 \text{ MeV } ^{14}\text{N}$  reaction, unlike compound nucleus formation, the fact  $\alpha$ -particle emitting reaction involves incoming partial waves with angular momenta restricted to values just above the critical angular momentum  $\ell_{\text{cr}}$  for fusion reaction; (2) because of this, high-spin states are populated selectively and they decay to the ground-band without feeding side-band members. We have also inferred that fast “direct”  $\alpha$ -particles are emitted tangentially from the colliding system in a peripheral collision between heavy ions. This conclusion is in accord with the observed angular distributions of “direct”  $\alpha$ -particles, which show features characteristic of a peripheral collision between heavy ions.<sup>3)</sup>

Concerning the reaction mechanism of fast  $\alpha$ -particle emission, Gross and Wilczynski have recently suggested that fast  $\alpha$ -particles are emitted along the direction of the radial frictional force (from the opposite side of the target nucleus) in heavy ion reactions.<sup>4)</sup> In this case there should be the following characteristic features: (1) the angular momentum removed by the fast  $\alpha$ -particle is zero; (2) the associated incoming partial waves are identified by the direction of the  $\alpha$ -particle emission; and (3) the angular momentum deposited on the residual nucleus is almost identical with the angular momentum of the incoming partial wave. Accordingly one can expect that if it is observed in coincidence with fast  $\alpha$ -particles, the starting population for  $\gamma$ -deexcitation depends on the position and the finite solid angle of the  $\alpha$ -particle detector; the starting population will move towards higher spin states for  $\alpha$ -particles emitted to larger angles than for those to smaller angles. The finite solid angle will determine the width of angular momentum window of the associated entrance channel. That is to say, one may have a  $\gamma$ -transition yield curve similar to our observation<sup>1),2)</sup> but with a different critical point (see Fig. 1) depending on the  $\alpha$ -detector position.

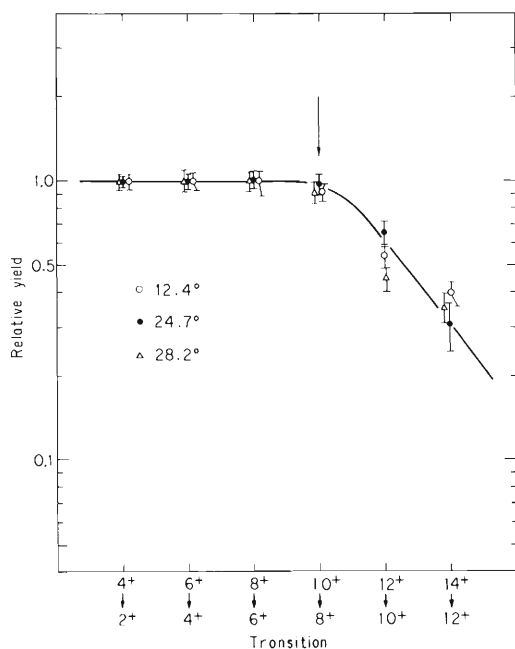


Fig. 1. Gamma-transition yields relative to the  $4^+ \rightarrow 2^+$  transition in  $^{166}\text{Yb}$  that is produced via the fast  $\alpha$ -particle emission process in the  $^{159}\text{Tb} + 95 \text{ MeV } ^{14}\text{N}$  reaction: ● is for  $\gamma$ -rays coincident with  $\alpha$ -particles recorded at  $24.7^\circ$  to the beam, ○ is for  $28.2^\circ$  and △ is for  $12.7^\circ$ . The energy of recorded  $\alpha$ -particles is  $E_\alpha \geq 33 \text{ MeV}$  in lab. The arrow indicates a critical point from where the yields of successive transitions decrease considerably.

We have measured  $\gamma$ -rays from the  $^{159}\text{Tb} + 95 \text{ MeV } ^{14}\text{N}$  reaction in coincidence with energetic  $\alpha$ -particles ( $E_{\alpha} \geq 33 \text{ MeV}$  in lab.) recorded at  $\theta_1 = 12.4^\circ$  (the angular width  $\Delta\theta = 8^\circ$ ) and  $\theta_2 = 28.2^\circ$  ( $\Delta\theta = 8^\circ$ ) to the beam direction (in lab.); in terms of Gross-Wilczynski model<sup>4)</sup> the angular momenta of incoming partial waves corresponding to these directions are estimated to be  $\ell_1 = 13 \hbar$  and  $\ell_2 = 26 \hbar$  by assuming  $r_0 = 1.25 \text{ fm}$ . However, nothing different has been found between the observed  $\gamma$ -transition yield curves at two different angles as is shown in Fig. 1. The previously observed  $\gamma$ -transition yield curve ( $\theta = 24.7^\circ$ ,  $\Delta\theta = 16^\circ$ ) is also shown in Fig. 1. This result contradicts the expectation mentioned above, indicating that there exists an angular momentum window in the entrance channel which leads to the fast  $\alpha$ -particle emission, independently of its direction.

In conclusion the present observation of  $\gamma$ -rays in coincidence with fast  $\alpha$ -particles is not in accord with the mechanism suggested by Gross and Wilczynski,<sup>4)</sup> in which the fast  $\alpha$ -particle is emitted along the direction of the radial frictional force.

#### References

- 1) T. Inamura, K. Hiruta, M. Ishihara, T. Fukuda, and T. Shimoda: IPCR Cyclotron Prog. Rep., 10, 59 (1976).
- 2) T. Inamura, M. Ishihara, T. Fukuda, T. Shimoda, and K. Hiruta: Phys. Lett., 68B, 51 (1977).
- 3) T. Inamura, K. Hiruta, S. Ise, T. Shimoda, T. Nomura, and M. Ishihara: IPCR Cyclotron Prog. Rep., 11, 58 (1977).
- 4) D.H.E. Gross and J. Wilczynski: Phys. Lett., 67B, 1 (1977).

5-3. High Spin States of  $^{162}\text{Yb}$ 

A. Hashizume, T. Katou, Y. Tendow, and H. Kumagai

Levels of  $^{162}\text{Yb}$  were populated by means of the compound-evaporation reaction  $^{155}\text{Gd}(^{12}\text{C}, 5n)^{162}\text{Yb}$ . De-excitation  $\gamma$ -rays were detected with Ge (Li) detectors. In this type of reaction, the incident heavy-ion carries a large amount of angular momentum into the compound system ( $\ell = 46 \hbar$ ) for a classical grazing collision of 95 MeV  $^{12}\text{C}$  on  $^{155}\text{Gd}$ . The evaporated nucleons and de-exciting  $\gamma$ -rays, on the other hand, carry away relatively little angular momentum, amounting to at most a few  $\hbar$  per nucleon. Thus these compound-evaporation reactions are very suitable for the study of the high spin states.

The excited states in  $^{162}\text{Yb}$  were studied previously by the  $^{164}\text{Er}(\alpha, 6n\gamma)$  reaction and the ground state rotational band up to the  $14^+$  state has been established.<sup>1)</sup> This result makes some contrast to that of  $^{166}\text{Yb}$  where the ground state band up to the  $20^+$  state has been known. A self-supporting and isotopically enriched target  $^{155}\text{Gd}$  was prepared by use of vacuum evaporation technique where  $\text{Gd}_2\text{O}_3$  was reduced by thorium. Figure 1 (a) shows the excitation functions obtained by measuring  $\gamma$ -rays between the transitions in the ground state band. These  $\gamma$ -rays were observed at  $90^\circ$  to the beam direction. Examples of excitation functions of another  $\gamma$ -rays assigned to the transitions in  $^{162}\text{Yb}$  are also shown in Fig. 1(b).

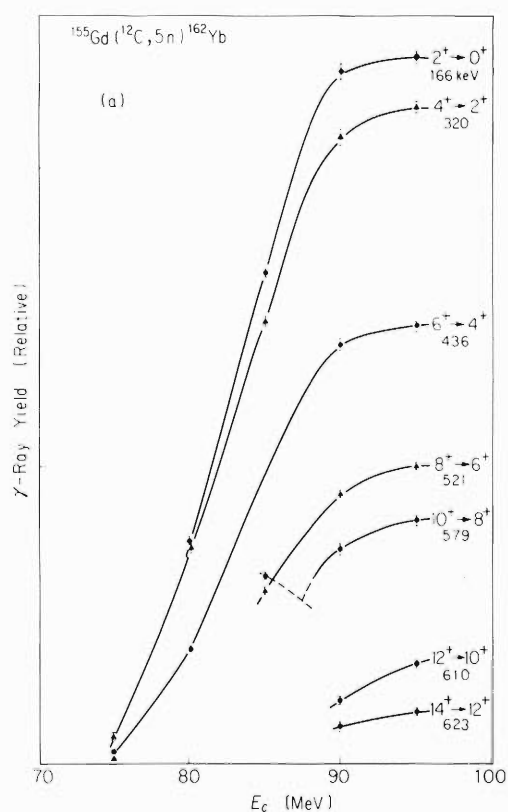


Fig. 1(a) Excitation functions of levels of the ground state rotational band in  $^{162}\text{Yb}$ .

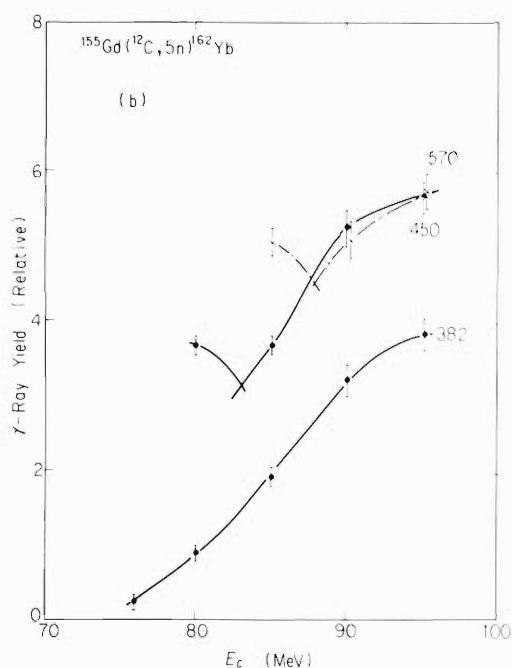


Fig. 1(b) Examples of excitation functions of another  $\gamma$ -rays also, assigned to  $^{162}\text{Yb}$ .

The angular distributions of  $\gamma$ -rays were studied from  $90^\circ$  to  $30^\circ$  at every  $15^\circ$ . In  $\gamma$ - $\gamma$  coincidence experiments, a magnetic tape recorder system developed for this purpose<sup>2)</sup> was employed. Figure 2 shows the sum of 7 background-subtracted  $\gamma$ - $\gamma$  coincidences resulting from gates placed on each individual ground state band transition up to  $14^+ \rightarrow 12^+$ . All the transitions in the ground state band up to  $14^+$  are in good agreement with the results reported by Banaschik et al.<sup>1)</sup> Further, the  $14^+ \rightarrow 12^+$  transition is supposed to be a doublet, because the peak still appeared even when the gate was opened by the same energy. This fact suggests that the energy of  $16^+ \rightarrow 14^+$  transition nearly coincides on that of  $14^+ \rightarrow 12^+$  transition. Other  $\gamma$ -rays such as 382, 452, 634 and probably 570 keV coincide to members of transitions in the ground state

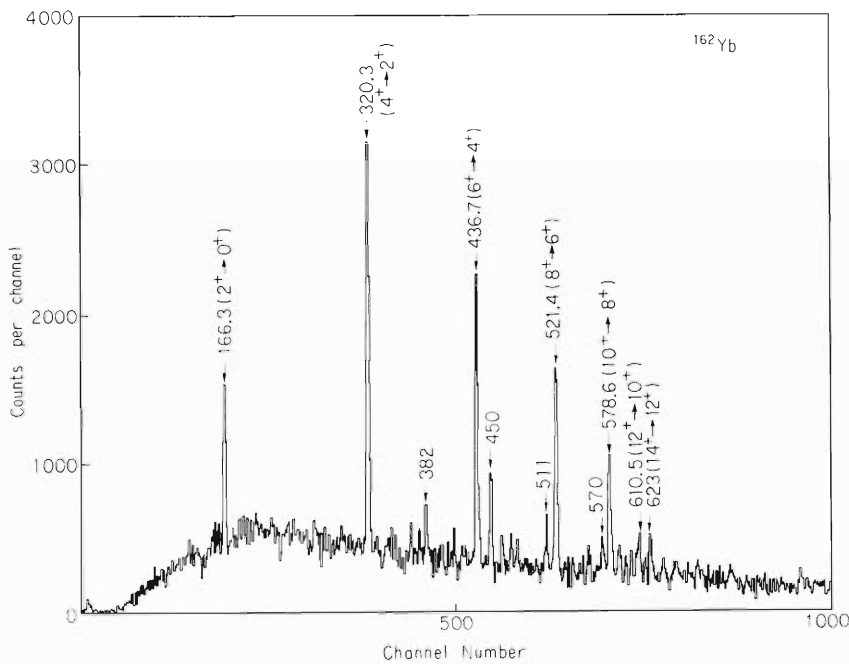


Fig. 2. Sum of  $\gamma$ - $\gamma$  coincidence spectra gated by the transitions in the ground-state rotational band.

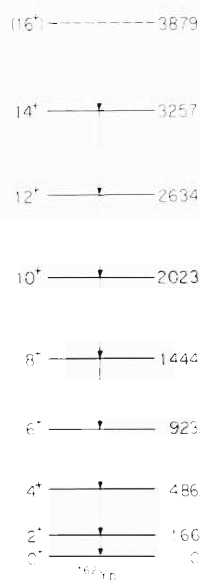


Fig. 3. States in  $^{162}\text{Yb}$ .

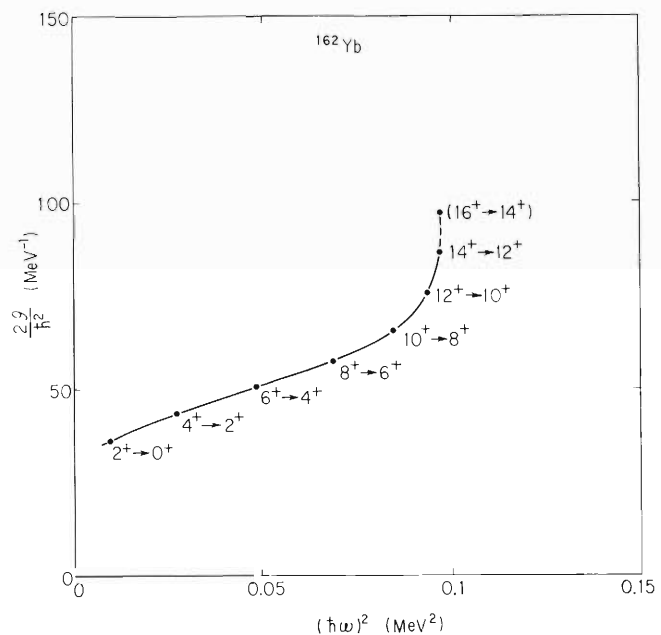


Fig. 4. Apparent moment of inertia as a function of the square of the rotational frequency.

band. From their intensities, these  $\gamma$ -rays are presumed to originate from the transitions in side bands. Studies of the structures of the side bands are in progress.

The level structure of the ground band in  $^{162}\text{Yb}$  is shown in Fig. 3. In the well deformed region to which  $^{162}\text{Yb}$  belongs, the lower levels of the ground state band can be described by simple rotational model. However at high spin states, the sudden increase of moment of inertia was observed in the nuclei of deformed region. This fact is now believed to be the crossing of different bands. Figure 4 shows the curve, giving the relation between the moment of inertia and square of angular rotational frequency of  $^{162}\text{Yb}$  nucleus. The curve does not show the so-called backbending shape as that of  $^{166}\text{Yb}$  does.

### References

- 1) M.V. Banaschik, C. Gunther, H. Hubel, A.C. Rester, G. Nowicki, and J.J. Pinajan: Nucl. Phys., A222, 459 (1974).
- 2) H. Kumagai and A. Hashizume: IPCR Cyclotron Progr. Rep., 9, 70 (1975).

A. Hashizume, H. Kumagai, T. Katou, and Y. Tendow

This study is one of the series experiments on high spin states in Yb isotopes. The  $^{164}\text{Yb}$  was excited by means of the  $^{155}\text{Gd} (^{12}\text{C}, 3n)$  reaction. The target is the same as that used for the study on  $^{162}\text{Yb}$ . Excitation functions, angular distributions of  $\gamma$ -rays and  $\gamma$ - $\gamma$  coincidences were taken by the same experimental set-up as in the case of  $^{162}\text{Yb}$ . The high spin states in  $^{164}\text{Yb}$  have been studied by Lieder<sup>1)</sup> and by Stelson<sup>2)</sup> and states up to  $22^+$  have been reported. No side band has yet been found.

The  $\gamma$ - $\gamma$  coincidence has been studied at the incident energy of 70 MeV C-ions. By examining each spectrum gated at the transitions in the ground state band, the spin states up to  $18^+$  were confirmed. Figure 1 shows the sum of 9 coincidence spectra gated by the members of the ground state band from the  $18^+$  state except the  $8^+ \rightarrow 6^+$  (468 keV) transition. The peak of the 468 keV transition coincides accidentally with that of a  $\gamma$ -ray of another origin and its spectrum (Fig. 2) shows the coincidence with several  $\gamma$ -rays indicated by asterisks. The origin of

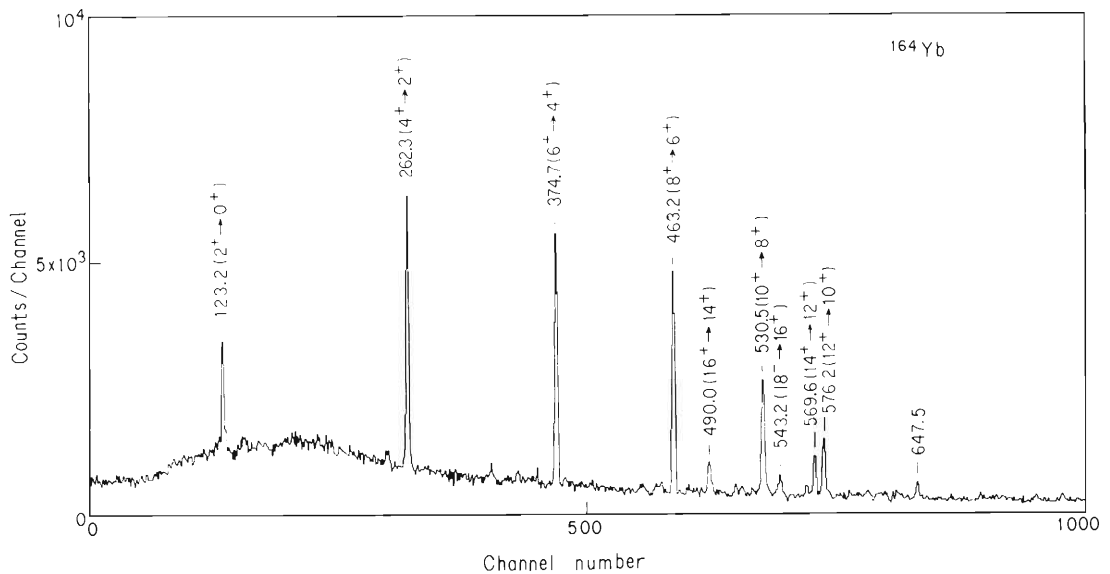


Fig. 1. The sum of 9 spectra of  $\gamma$ - $\gamma$  coincidence gated by the cascade transitions from  $18^+$  to ground state except the  $8^+ \rightarrow 6^+$  transition.

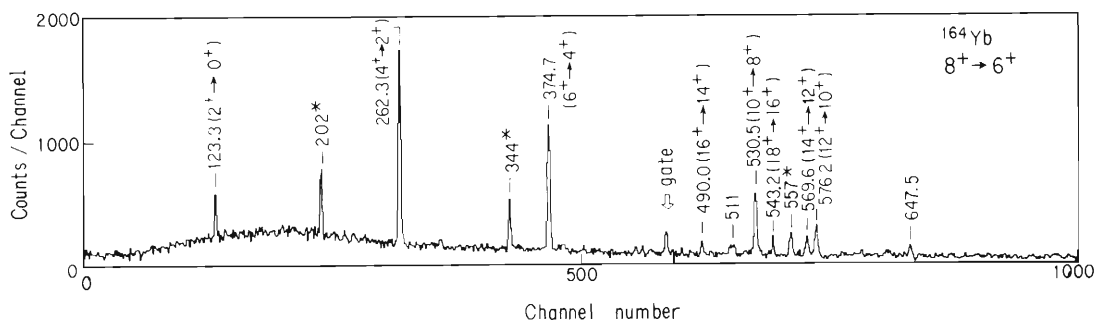


Fig. 2. Coincidence spectrum gated by  $8^+ \rightarrow 6^+$  transition  $\gamma$ -ray.

these  $\gamma$ -rays is not yet elucidated. The peak at 633 keV reported as  $20^+ \rightarrow 18^+$  transition<sup>2)</sup> coincides also with one of the above  $\gamma$ -rays of unknown origin and it was difficult from the coincidence spectrum gated by 633 keV  $\gamma$ -ray to conclude it as  $20^+ \rightarrow 18^+$  transition. Furthermore, the 713 keV  $\gamma$ -ray has not been confirmed as  $22^+ \rightarrow 20^+$  transition because of appreciable statistical errors of the data.

In addition to the  $\gamma$ -rays in the ground state band, there was reported<sup>1)</sup> a 647.5 keV  $\gamma$ -ray which has nearly equal intensity as that of  $16^+ \rightarrow 14^+$  transition. Following our coincidence experiment, a existence of 2.4015 MeV state is suggested which de-excites to 1.7540 ( $10^+$ ) state by emitting the 647.5 keV  $\gamma$ -ray. Figure 3 shows the behaviour of apparent moment of inertia as a function of angular rotational frequencies. Further analyses of data is in progress.

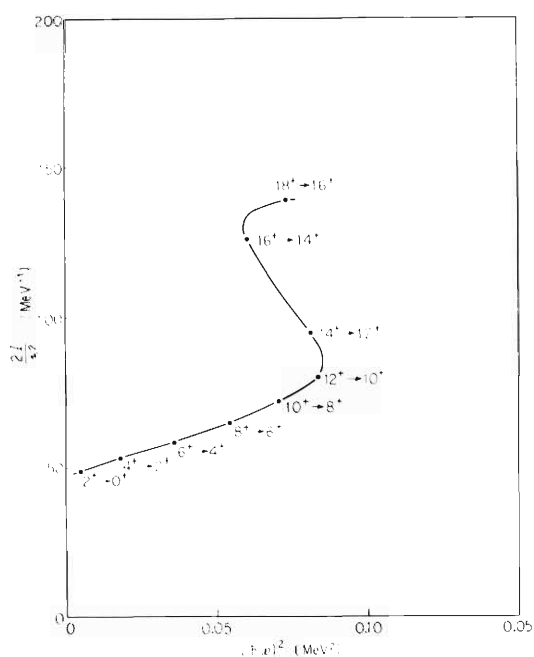


Fig. 3. Backbending curve for  $^{164}\text{Yb}$ .

## References

- 1) R. M. Lieder, H. Beuscher, W. F. Davidson, P. Jahn, H. -J. Probst, C. M. Borike: *Z. Phys.*, **257**, 147 (1972).
- 2) P. H. Stelson: Private communication to *Nucl. Data. Sheets*, *Nucl. Data Sheets*, **11**, 376 (1974).

A. Hashizume, Y. Tendow, H. Kumagai, and T. Katou

This study is one of the series of experiments on high spin states in Yb isotopes. The experimental set-up is the same as used in the preceding reports. The  $^{166}\text{Yb}$  was excited by means of the  $^{158}\text{Gd} (^{12}\text{C}, 4n)$  reaction. A thick, self-supporting and isotopically enriched target was used. Excitation functions, angular distributions of  $\gamma$ -rays and  $\gamma$ - $\gamma$  coincidences were studied.

Figure 1 shows the sum of 9 spectra of  $\gamma$ - $\gamma$  coincidences gated by the successive cascade transitions from  $20^+$  to the ground state. In this spectrum coincidences with the background have been subtracted by setting a window near the gating peak. The  $18^+ \rightarrow 16^+$  transition, as its energy being 509 keV, could not be resolved from the annihilation  $\gamma$ -rays. Therefore, the spectrum gated by the 509 keV  $\gamma$ -ray was not involved in the above sum spectrum. By investigating each spectrum gated at the transitions in the ground state band, the spin states up

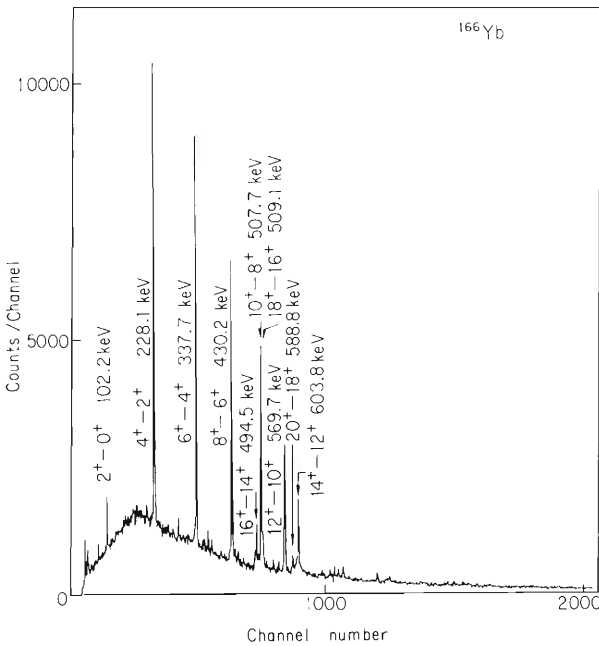


Fig. 1. The sum of 9 spectra of coincidences gated by  $\gamma$ -rays in the ground-state rotational band.

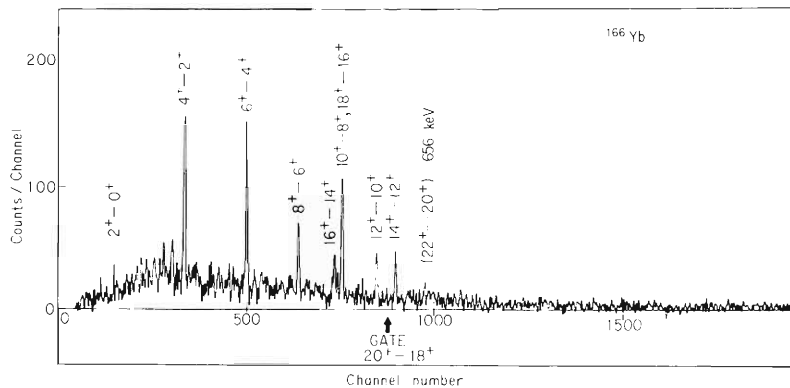


Fig. 2.  $\gamma$ - $\gamma$  coincidence spectrum gated by the  $20^+ \rightarrow 18^+$  transition.

to  $20^+$  were clearly confirmed.<sup>1)</sup> Further, there is an indication that the 656 keV  $\gamma$ -ray coincides with those of ground state band. Figure 2 shows a coincidence spectrum gated by  $20^+ \rightarrow 18^+$  transition  $\gamma$ -ray. We propose tentatively that the 656 keV transition goes to the  $20^+$  state from higher energy level. The peak is so weak that we could not determine E2 character of this transition. However, if it is assumed that the  $22^+$  state de-excites to  $20^+$  state emitting 656 keV  $\gamma$ -ray, the backbending curve representing change of moment of inertia as a function of the square of rotational frequency can be extrapolated smoothly as shown by dashed line in Fig. 3. Figure 4 shows the ground state rotational band in  $^{166}\text{Yb}$ .

Besides the transitions in the ground state band, there were found about 20 weak  $\gamma$ -rays which could be able to attribute to transitions in  $^{166}\text{Yb}$ . These  $\gamma$ -rays may be emitted by the de-excitation process from the states in side bands. Further study is in progress.

In Yb isotopes of the mass numbers from 162 to 170, there is an interesting behavior concerning the moment of inertia of high spin states. In  $^{162}\text{Yb}$ , the moment of inertia of high spin states change rather rapidly, but the values as a function of square of angular rotational frequency do not make the backbending shape. Whereas the curves for  $^{164}\text{Yb}$  and  $^{166}\text{Yb}$  show large backbending. In contrast, the values of  $2\mathcal{I}/\hbar^2$  rest nearly constant in  $^{168}\text{Yb}$ , and  $^{170}\text{Yb}$  shows again rapid change of  $2\mathcal{I}/\hbar^2$ , though the latter doesn't show S shape.<sup>2)</sup> It is a surprising fact that the small change of neutron number results in the large anomalies of angular momentum. These anomalies have been studied by the theorists<sup>3),4)</sup> in the framework of Hartree-Fock-Bogoliubov cranking model or utilizing deformed BCS trial wave functions. They could explain the anomalies qualitatively, though it seems that some discrepancies yet exist between experimental and theoretical results. Further study on high spin states in lighter Yb isotopes will be interesting.

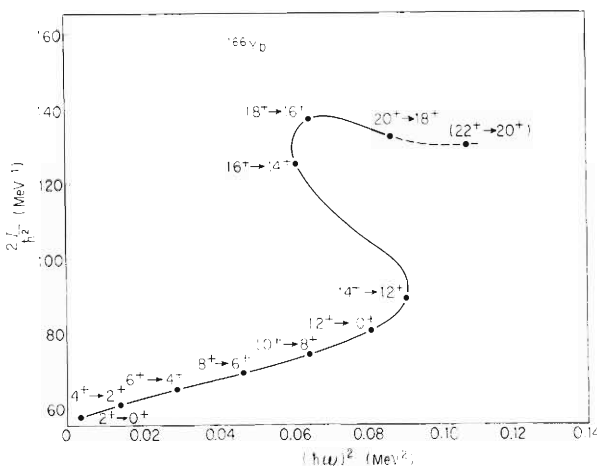


Fig. 3. Relation between the moment of inertia and the square of rotational frequency.

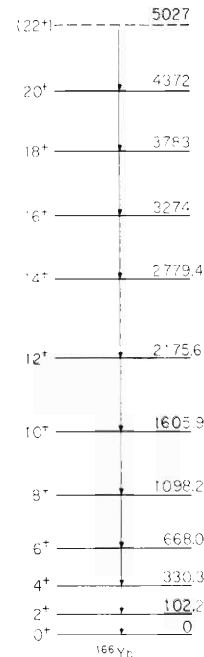


Fig. 4. The ground state rotational band in  $^{166}\text{Yb}$ .

## References

- 1) R. M. Lieder, H. Buscher, W. F. Davidson, P. Jahn, H. -J. Probst, and C. Mayer-Brorike: *Z. Phys.*, 257, 147 (1976).
- 2) H. Beuscher, W. F. Davidson, R. M. Lieder, and C. Mayer-Boricke: *Phys. Lett.*, 40B, 44 (1972); A. J. Hartley, R. Chapman, G. D. Dracoulis, S. Flanagan, W. Gelletly, and J. N. Mo: *J. Phys.*, 6, L60 (1973).
- 3) A. Faessler, F. Grummer, L. Lin, and J. Urbano: *Phys. Lett.*, 48B, 87 (1974).
- 4) A. L. Goodman and J. P. Vary: *Phys. Rev. Lett.*, 35, 504 (1975).

## 5-6. Populations of the Particle-Hole K Isomer and the Ground State Rotational Level

H. Ejiri,\* T. Shibata,\* S. Nakayama,\* and A. Hashizume

Recently we have found that particle-hole K isomer is populated strongly by (p, xn $\gamma$ ) reactions with large input angular momenta per projectile nucleon, and that the ground band rotational level with K = 0 is well populated by complex projectiles with small input angular momenta per projectile nucleon. It provides firstly an evidence that excitations of states with same spin but different K (microscopic structure) depend on the projectile velocity. We define the K isomer ratio  $P_K(J)/R_0(J)$ , where  $P_K(J)$  and  $P_0(J)$  are the population of the K isomer and the ground band (K = 0) levels with the spin J. Here the  $P_0(J)$  is corrected for the contribution from the isomer.

Population of isomers following (i, xn $\gamma$ ) reactions was previously investigated by various authors.<sup>1),2)</sup> The K isomer ratios,  $P_K(J)/P_0(J)$ , have been found to increase<sup>1),2)</sup> as the input angular momentum of the projectile increases for low incident energies because of the increase of the fraction of large K levels which preferentially feed the K isomers according to the K-band deexcitation model.<sup>3)</sup>

Therefore measurement of the K isomer ratios for two different mass projectiles with nearly the same input angular momentum is crucial in order to establish the projectile (velocity) dependence rather than the previously noted angular momentum dependence. In the previous work the  $P_8(8)/P_0(8)$  were measured for the  $J^\pi K = 8^-8$  particle-hole state (1832.5 keV) and the  $8^+8$  ground band level (1278.5 keV) in  $^{182}\text{Os}$ . They were excited by the (p, 4n $\gamma$ ) reaction with 40 MeV P, the ( $^3\text{He}$ , 3n $\gamma$ ) reactions with 24 - 26 MeV  $^3\text{He}$ , the ( $\alpha$ , 6n $\gamma$ ) reaction with 90 MeV  $\alpha$  and the ( $^{14}\text{N}$ , p7n) reaction with 120 MeV  $^{14}\text{N}$ . The experiments were carried out by using the  $^3\text{He}$  beam provided from the Osaka Univ. energy variable cyclotron, and the  $\alpha$  and HI beams provided from the RCNP cyclotron. From the view point mentioned above the best comparison can, however, be made for the 40 - 50 MeV (P, 4n $\gamma$ ) data and 28 - 35 MeV ( $^3\text{He}$ , 3n) data. The (P, 4n)  $\gamma$  reactions have been studied previously.<sup>2),4)</sup> The latter reaction, however, has not been studied although ( $^3\text{He}$ , 3n $\gamma$ ) reactions below that energy have been investigated at the Osaka Univ. Dept. Physics, cyclotron. The RCNP cyclotron gives too high energy  $^3\text{He}$ . Thus the IPCR cyclotron is best suited for the purpose.

In the present work the isomer ratio  $P_8(8)/P_0(8)$  for the  $^{182}\text{Os}$  was studied by using the ( $^3\text{He}$ , 3n $\gamma$ ) reaction at E = 31 MeV. The  $^3\text{He}$  beam was provided from the IPCR cyclotron. Singles, prompt and delayed  $\gamma$  ray spectra were measured by two Ge (Li) detectors set at  $125^\circ$  and  $235^\circ$  to the beam. We found the ratio  $P_8(8)/P_0(8) = 0.210 \pm 0.020$ . The present isomer ratio and the previous data<sup>2),4)</sup> are plotted in Fig. 1.

We found that the  $P_8(8)/P_0(8)$  are almost constant for the complex projectiles with various input angular momenta, and that the isomer ratios for protons are definitely larger than those for the complex projectiles. The present result suggests that the 40 - 50 MeV (p, 4n) reactions give an effective K distribution  $\exp(-K^2/2K_0^2)$  with a large  $K_0 = 5$ , while other complex projectiles give the  $\exp(-K^2/2K_0^2)$  with a smaller  $K_0 = 3.8$  (see Fig. 1). The  $P_8(8)/P_0(8)$  increases smoothly as the

\* Department of Physics, Osaka University.

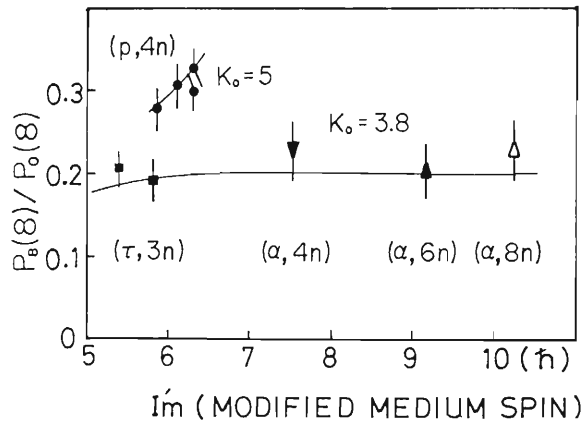


Fig. 1. Isomer ratios as a function of the modified medium spin  $I_m$  defined as  $\Sigma I P(I) / \Sigma P(I)$ . Solid lines are calculated for the exp  $(-K^2/2K_0^2)$  with  $K_0 = 5$  for protons and  $K_0 = 3.8$  for other complex projectiles.

average input angular momentum per projectile nucleon ( $\bar{J}_i$ ) increases. One might guess that each nucleon of the projectile hits each paired target nucleon and has to transfer large angular momentum to get a large  $K$  p-h pair. On the other hand complex projectiles transfer angular momentum to many nucleons, each exciton having rather small  $J$  and  $K$ , and populate well rotational levels with small  $K$ .

The present experiment is one of the works being carried out in collaboration with the Dept. Physics and RCNP inbeam PEP group (Y. Nagai, H. Sakai, T. Itahashi, M. Hoshi, T. Kishimoto, and K. Maeda).

## References

- 1) H. Ejiri, Y. Nagai, H. Sakai, T. Itahashi, T. Shibata, M. Hoshi, S. Nakayama, T. Kishimoto, and K. Maeda: Contribution to the Tokyo Intern. Conf. Nuclear Structure, Tokyo (1977).
- 2) H. Ejiri, G. B. Hagemann, and T. Hammer: Proc. Intern. Conf. on statistical properties of Nuclei, Albany (1971).
- 3) M. Ishihara, N. Yoshikawa, H. Kawakami, and M. Sakai: Nucl. Phys., A179, 769 (1972).
- 4) H. Ejiri and I. Halpern: Bull. Am. Phys. Soc., 13, 700 (1968); S. M. Ferguson, H. Ejiri, and I. Halpern: Nucl. Phys., A188, 1 (1972).

5-7. Half-life of  $^{207}\text{Bi}$ 

M. Yanokura, H. Nakahara,\* and K. Miyano\*\*

The radioactive isotope  $^{207}\text{Bi}$  is widely used as a  $\gamma$ -ray standard source. However, its reported half-life ranges from 28 to 50 years.<sup>1)-4)</sup> In the method of determination of the half-life by specific activity, one has to use data such as photon intensities per disintegration,  $\gamma$ -ray detection efficiencies which are likely to become source of large errors. Therefore, it is advisable to find a method which requires as few auxiliary data as possible.

We propose a method which requires no knowledge of the number of the atoms of  $^{207}\text{Bi}$ , the  $\gamma$ -ray detection efficiencies and geometry. Figure 1 shows the partial decay scheme of  $^{211}\text{At}$  relevant to the present work. The 570 keV level in  $^{207}\text{Pb}$  is fed both by alpha decay of

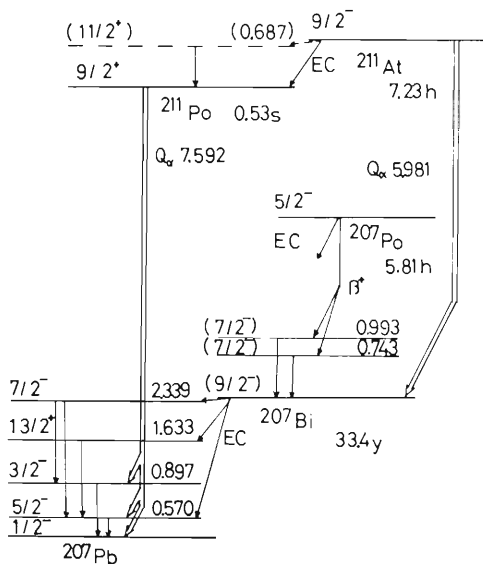


Fig. 1. Decay schemes of  $^{211}\text{At}$ ,  $^{211}\text{Po}$ , and  $^{207}\text{Bi}$ . Only the levels related to the present work are shown. The dashed level in  $^{211}\text{Po}$  is the new level, but not discussed in this report.

$^{211}\text{Po}$  and by EC decay of  $^{207}\text{Bi}$ . Since the half-life of  $^{211}\text{At}$  ( $^{211}\text{Po}$ ) is very different from the that of  $^{207}\text{Bi}$ , the photopeak area ratio of  $A_1$  and  $A_2$ , which due to  $^{211}\text{Po}$  and  $^{207}\text{Bi}$ , respectively, can be determined from the analysis of the decay curve of the 570 keV  $\gamma$ -ray. This ratio satisfy the following equation.

$$\frac{A_1(^{211}\text{Po})}{A_2(^{207}\text{Bi})} = \frac{\lambda_0 N_0 b_{\text{EC}} \alpha_1}{\lambda_2 N_0 b_{\alpha} \gamma_2}, \quad (1)$$

where  $N_0$  is the number of  $^{211}\text{At}$  atoms at the end of chemical separation,  $b_{\text{EC}}/b_{\alpha}$  is EC/ $\alpha$  ratio of  $^{211}\text{At}$ ,  $\alpha_1$  is the branching ratio of the 6.868 MeV  $\alpha$ -ray emitted from  $^{211}\text{Po}$ ,  $\gamma_2$  is the intensity of the 570 keV  $\gamma$ -ray per disintegration of  $^{207}\text{Bi}$ , and  $\lambda_0$  and  $\lambda_2$  are the decay constant of  $^{211}\text{At}$  and  $^{207}\text{Bi}$ , respectively.

\* Faculty of Science, Tokyo Metropolitan University.

\*\* Faculty of Science, Niigata University.

A metallic bismuth target (99.999% purity) about 1 mm thick was bombarded with  $\alpha$  beam of about 1  $\mu$ A from the cyclotron for one hour to produce  $^{211}\text{At}$  through the reaction  $^{209}\text{Bi}(\alpha, 2n)^{211}\text{At}$ .

The alpha energy was set below 28 MeV so as not to produce  $^{210}\text{At}$ . The target was dissolved in conc-HCl, and astatine was extracted into the organic phase by diisopropylether and again back-extracted into aqueous phase by distilled water. An aliquot of the aqueous sample solution was pipetted to a glass vial, and the decay of  $\gamma$ -ray from  $^{211}\text{Po}$  and  $^{207}\text{Bi}$  populated by the decay of  $^{211}\text{At}$  were followed for several days by a heavily shielded Ge(Li) detector. A thin bismuth target, which was vacuum-evaporated onto an aluminium foil, was also bombarded, and reaction products recoiled out the target were collected onto a catcher foil. The  $\alpha$ -ray from  $^{211}\text{At}$  and  $^{211}\text{Po}$  in the catcher foil were measured by a Si-detector.

The half-life of  $^{211}\text{At}$  was evaluated from the decay curves of the 897 keV photopeak and 7.868 and 7.448 MeV alpha peaks. The results of the least-squares analysis yielded  $7.23 \pm 0.02$  h. The EC/ $\alpha$  ratio of  $^{211}\text{At}$  was calculated to be 0.583/0.417 from the measured spectrum. Branching ratio of the three  $\alpha$  decay from  $^{211}\text{Po}$  and  $\alpha$  energies were determined. The results obtained are shown in Table 1. The 570 keV  $\gamma$ -ray, turned out to have two components in its decay curve, from which we estimated the ratio of  $A_1/A_2$ . The branching ratio of the 570 keV  $\gamma$ -ray from  $^{207}\text{Bi}$  is taken from Ref. 5, since the decay schemes of  $^{207}\text{Bi}$  is well known.

The half-life of  $^{207}\text{Bi}$  evaluated from Eqn. (1) was  $33.4 \pm 0.8$  years. The quoted error was mainly due to the counting statistics associated with the photopeak area of the 570 keV  $\gamma$ -ray emitted from  $^{207}\text{Bi}$ .

Table 1. Experimental results of energies and intensities of the  $\gamma$ -rays and  $\alpha$ -rays.

Nuclide	Half-life	$E_\gamma$ (keV)	$E_\alpha$ (MeV)	Intensity (%)	EC/ $\alpha$
$^{211}\text{At}$	$7.23 \pm 0.2$ h	$686.7 \pm 0.48$	(5.868)	$41.7 \pm 0.01$	0.581/0.417
$^{211}\text{Po}$	(0.53 s)	(569.7)	$6.568 \pm 0.001$	$0.58 \pm 0.01$	
		(897.3)	$6.891 \pm 0.001$	$0.60 \pm 0.01$	
			(7.448)	$98.82 \pm 0.01$	

The parenthesized values were taken from Ref. 5.

## References

- 1) H. M. Neumann and I. Perlman: Phys. Rev., 81, 958 (1951).
- 2) G. Irbottle: J. Inorg. Nucl. Chem., 12, 6 (1959).
- 3) I. Sosniak and R. E. Bell: Can. J. Phys., 37, 1 (1959).
- 4) E. H. Appelman: Phys. Rev., 121, 253 (1961).
- 5) Nuclear Data Sheets, Sec., B 5, No. 3 (1971).

## 6. NUCLEAR INSTRUMENTATION

### 6-1. A Particle Identification Program for the On-Line Use

T. Nomura

A simple on-line program to identify mass and atomic numbers of heavy particles has been made for the OKITAC 4500C (32 K core memories) data processing system. The code assumes two different experimental arrangements for the particle identification (PI): (1)  $\Delta E$ -E counter telescope and (2) time-of-flight. For the first method, we used the empirical formula proposed in Ref. 1, which was slightly modified and approximated by

$$PI = n \Delta E [(E + 0.49 \Delta E) / 300]^{n-1}, \quad (1)$$

with 
$$n = 1.84 - 0.046 \Delta E / T. \quad (2)$$

Here,  $\Delta E$  and  $E$  are pulse heights (in unit of MeV) from  $\Delta E$  and  $E$  counters, respectively;  $T$  is thickness of the  $\Delta E$  detector, measured in unit of  $\text{mg}/\text{cm}^2$  in the case of a Si counter. Eqn. (1) turned out to show remarkable improvement for PI compared to a conventional electrical circuit used for PI. The principle of the second method is the same as described in Ref. 2. The above two PI methods can be used separately, or if desired, can be combined together.

The program can be applied to experimental data taken in the coincidence mode with up to four parameters stored on a disk pack in an event-by-event wise. This code is usually stored in another disk pack as one of the utility programs of the PHA system, and can be called any time during or after the data accumulation. "Gates" can be set on a calculated PI spectrum displayed in log or linear scale in order to represent the corresponding energy spectra ( $\Delta E$ ,  $E$  and / or  $\Delta E + E$ ) and other possible spectra depending on other parameters in coincidence. Inversely, gates can be set on energy spectra and others to obtain the corresponding PI spectrum. The parameters for PI and gates are inputted from the teletype and can be changed any time even during the data accumulation; When they are changed, the calculation starts from the beginning of the data stored in the disk pack.

#### References

- 1) G. W. Butler, A. M. Poskanzer, and D. A. Landis: Nucl. Instr. Methods, 89, 189 (1970).
- 2) F. S. Goulding and B. G. Harvey: Ann. Rev. Nucl. Sci., 25, 167 (1975).

## 6-2. Determination of the Etching Rate Versus Restricted Energy Loss Curves in CN Films and CTA Films by Using N-Ion Beams

T. Doke, T. Hayashi,\* T. Yanagimachi,\*\* and I. Kohno

For determination of the flux of heavy charged particles with  $Z > 40$  in the primary cosmic rays at the top of atmosphere in Japan, where the energy of the incident cosmic ray particles is in the relativistic region, we have recently tried a series of balloon experiments using plastic nuclear track detector arrays with a large detection area.<sup>1)-3)</sup> In these experiments, the nuclear charge of cosmic ray particle passed through the plastic detectors was determined by measuring the etching rate ( $V_t$ ) of the particle track and by referring it to the curve of REL (restricted energy loss)<sup>4)</sup> versus  $V_t$  obtained by using known heavy charged particles. In the balloon experiments, three kinds of nuclear track detectors were used. One was a  $190 \mu\text{m}$  thick cellulose nitrate (CN, Daicel) film, the second, a  $250 \mu\text{m}$  thick cellulose triacetate (CTA, Fuji) film, and the third, a  $200 \mu\text{m}$  thick polycarbonate (PC, Teijin) film. To obtain the curves (so-called calibration curves) of REL- $V_t$  for these plastic films, the films were irradiated with N-ions of  $6.43 \text{ MeV/n}$ . Two geometrical arrangements of the plastic films used for the N-ion irradiation are shown in Fig. 1(a) and (b).

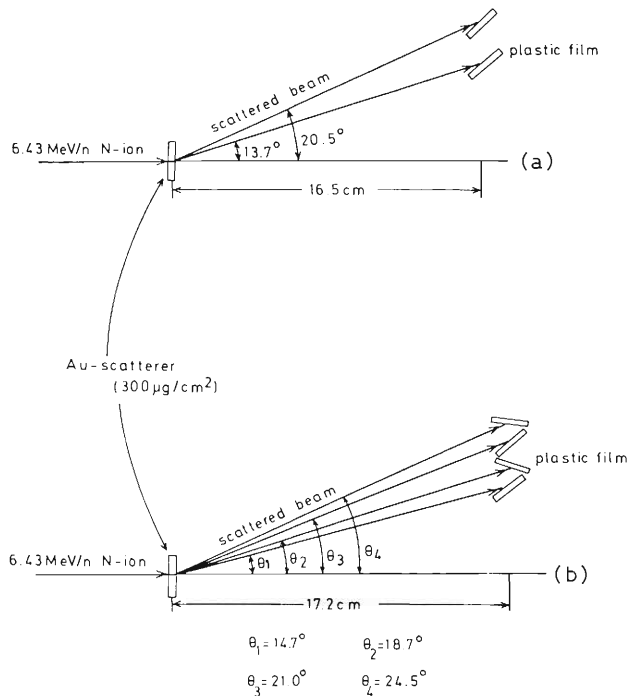


Fig. 1. Two geometrical arrangements of plastic films and the scatterer (Au-foil of  $300 \mu\text{g}/\text{cm}^2$ ) for the N-ion irradiation. For CTA and PC, films were enveloped in  $16 \mu\text{m}$  thick Al-absorber. The injection angle of the scattered N-ion to the plastic films is  $19^\circ - 41^\circ$ .

After N-ion irradiation, the plastic films were immersed in the solution of  $6.0 - 6.7\text{N}$  NaOH, which was kept at  $30^\circ$  or  $45^\circ\text{C}$  for various lengths of time. Thus, the growth curves of the etched track length ( $L(t)$ ) for  $6.43 \text{ MeV/n}$  N-ion was obtained as a function of etching time ( $t$ ). From

\* Science and Engineering Research Laboratory, Waseda University.

\*\* Faculty of Science, Rikkyo University.

this growth curve, the  $REL-V_t$  relation can easily be obtained. Calibration curves for CN and for CTA thus obtained are shown in Figs. 2 and 3, respectively. In these figures, the results recently obtained by using Ar-ions of 400 MeV/n from Bevalac are also shown.<sup>5)</sup>

As seen in Fig. 2, the result by N-ions is in agreement with that by Ar-ions within the experimental errors.

In the results by Ar-ions,<sup>5)</sup> a remarkable difference in the response curve between the front and back surfaces, of CTA was found, while, in the results by N-ions, no difference could be found presumably due to large experimental errors. For N-ions, therefore, the mean values of  $V_t$  in both surfaces are shown in Fig. 3. The curve obtained by using N-ions seems to be roughly consistent with that by Ar-ions.

These results were used for the determination of the charge of particles detected in the balloon experiments carried out in 1973 and in 1976.

The calibration curve for PC could not be obtained because of the short registration range of N-ion.

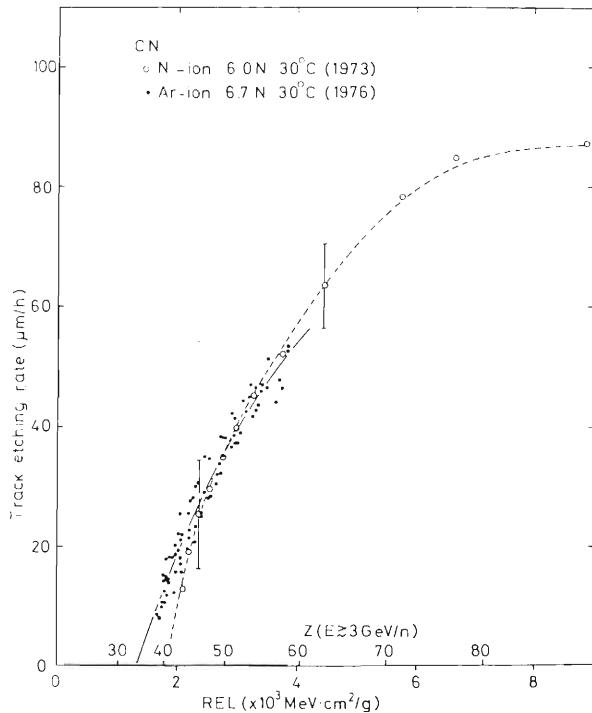


Fig. 2.  $V_t$  REL(or Z) relations in CN. REL in the relativistic region depends only on the nuclear charge (Z). The solid curve is represented by the relation,  $V_t = V_0 [1 - \exp(-A(REL - REL_c))]^2$ , where  $A = 0.356$ ,  $V_0 = 87.5$  ( $\mu\text{m/h}$ ) and  $REL_c = 1.32$  ( $\times 10^3$  MeV $\cdot\text{cm}^2/\text{g}$ ).

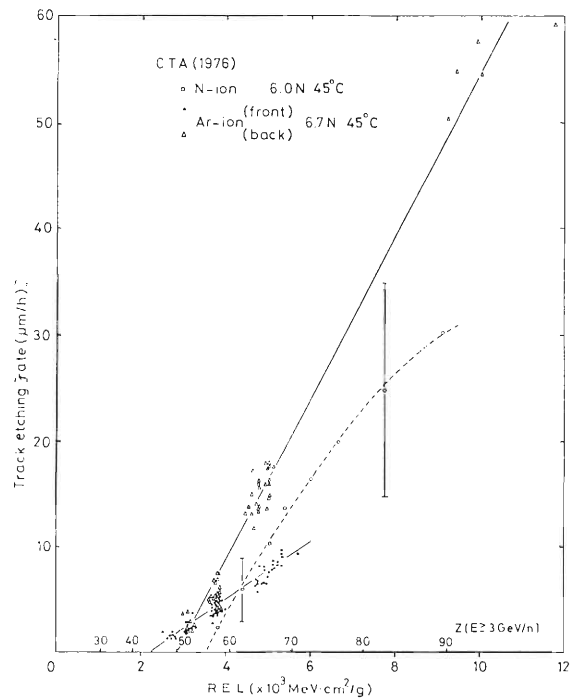


Fig. 3.  $V_t$  REL(or Z) relations in CTA. The solid lines are represented by the relation,  $V_t = B \cdot REL + C$ , where  $B = 2.81$ ,  $C = 6.53$  for the front surface and  $B = 7.67$ ,  $C = 22.1$  for the back surface, respectively.

## References

- 1) T. Doke, H. Okamoto, E. Shibamura, T. Hayashi, K. Ito, T. Yanagimachi, S. Kobayashi,

- K. Nagata, M. Miyajima, and T. Saito: Bull. Inst. Space and Aeronautical Sci., Univ. of Tokyo, 11, 497 (1975).
- 2) T. Doke, H. Okamoto, E. Shibamura, T. Hayashi, K. Ito, T. Yanagimachi, S. Kobayashi, M. Miyajima, T. Saito, and K. Nagata: Proc. 14th Intern. Cosmic Ray Conf., Munich, OG 6-19, 4123 (1975).
  - 3) T. Doke, T. Hayashi, K. Ito, T. Yanagimachi, K. Hisano, K. Nagata, and M. Miyajima: Bull. Inst. Space and Aeronautical Sci., Univ. of Tokyo, 13, 875 (1977).
  - 4) E. V. Benton and W. D. Nix: Nucl. Instr. and Meth., 67, 343 (1969).
  - 5) T. Hayashi, K. Takayama, T. Yanagimachi, and S. Kobayashi: Ionizing Radiation, Japan Soc. Appl. Phys., 4, No. 3, 22 (1977).

### 6-3. Target Chamber for Recoil-distance Lifetime Measurements

T. Katou, H. Kumagai, Y. Tendow,  
Y. Awaya, and A. Hashizume

A target chamber for recoil-distance measurements of nuclear lifetime in the range from 1 ps to 1  $\mu$ s was constructed. An outline of the chamber is described in this report.

A schematic diagram of the plunger apparatus and the electronics are shown in Fig. 1. The beam from the cyclotron enters the target chamber and passes through the collimators and focusses at the target. The stopper foil is held firmly in position by a holder which is electrically insulated from a support attached to the base of the chamber. The equipment for controlling the linear movement of the target is also mounted on the same base of the chamber in order to reduce the possible relative movement between the target and the stopper when the chamber is evacuated or the room temperature changes. The linear movement of the target is provided by a sliding stage moved by a pulse motor (240 pulses correspond to 1  $\mu$ m).

The control system has the following functions: a) setting of the direction and distance of movement: b) detection of the touch of the target to the stopper: c) detection of the maximum limit of the movement.

To measure the distance of movement the output pulses from a commercially available "MAGNESCALE" are counted by UP/DOWN scaler or the advance pulses to the pulse motor are counted.

A MAGNESCALE graduated to 1  $\mu$ m is used to measure the distance between the stopper and the target foil. The zero distance determination can be done in the same way as in Ref. 1 with capacitance method. Figure 2 shows an example of a plot of  $C^{-1}$  versus the MAGNESCALE reading. The expected linear relation is found. The target was able to approach to the stopper within 5  $\mu$ m. For a typical recoil velocity of 1% of the light velocity and a lifetime of 1 ps, the mean path is about 3  $\mu$ m. The capacity is also used to monitor the thermal expansion of the system when the beam is present.

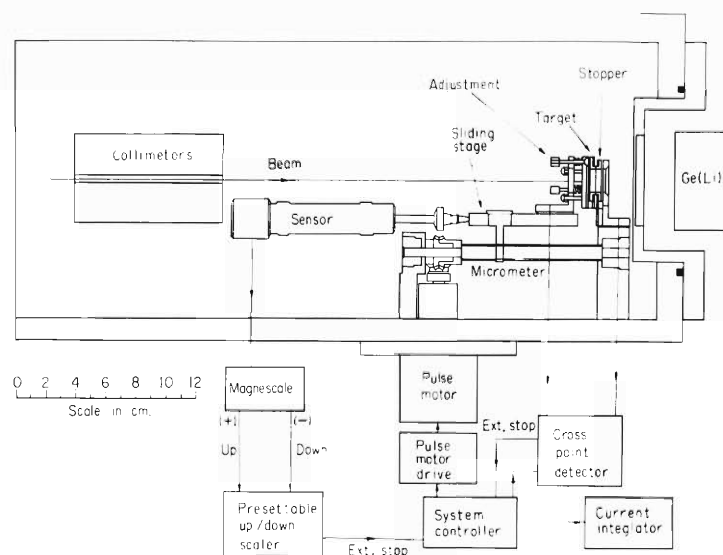


Fig. 1. Schematic view of the plunger apparatus.

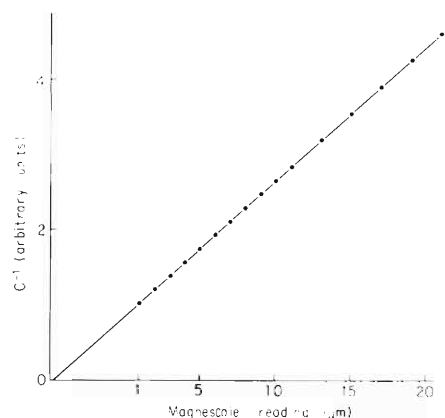


Fig. 2. A graph giving  $C^{-1}$  vs the distance.

The procedure adopted for pre-aligning the target parallel to the stopper surface is to adjust the reflected laser lights from the stopper and the target using an adjuster.

The foil-stretching technique is consisted of pressing an area of foil with a frame over the circular end of a cylindrical tube and further stretching the foil surface from the opposite direction with a metal insert which slides inside the tube. This double stretching technique improves a flat foil surface and eliminates nonuniformities at the edge. The frame for mounting the foil is shown schematically in Fig. 3.

Figure 4 shows an example of interferogram of gold target foil obtained by a He-Ne light with wavelength 663 nm. The height difference between neighboring fringes is half a wavelength, that is,  $0.3 \mu\text{m}$ .

The test experiments using HI beam are now in progress.

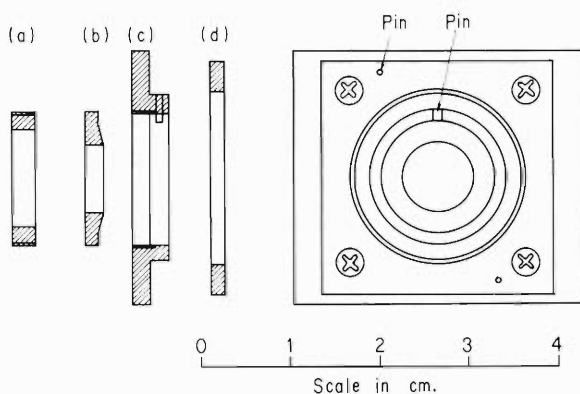


Fig. 3. A schematic diagram of the mounting frame: a) locking nut; b) stretching insert; c) mounting frame; d) pressing frame.

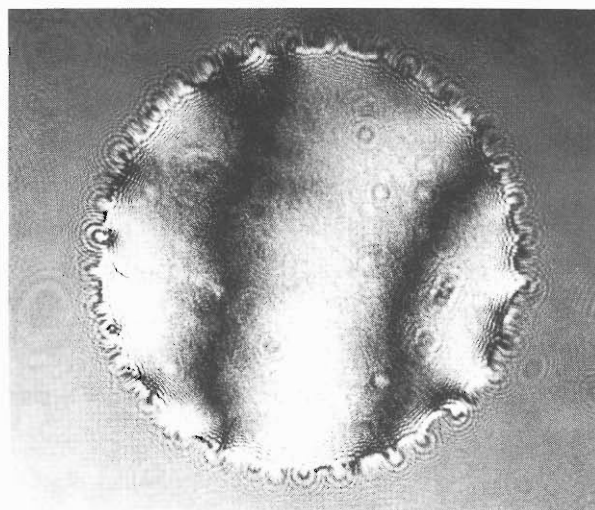


Fig. 4. Interferogram of a gold target foil.

#### Reference

- 1) T. K. Alexander and A. Bell: Nucl. Instr. and Meth., 81, 22 (1970).

#### 6-4. Gas $\Delta E$ -E Telescope for the Particle Identification of Heavy Ions

M. Yanokura, I. Kohno, T. Motobayashi,  
H. Nakahara,\* and K. Yamakoshi\*\*

One of the most common techniques for the particle identification is the  $\Delta E$ -E method, where  $\Delta E$  is specific energy loss and E is total energy. For the detection of light particles with  $Z < 9$  solid-state detector telescopes are widely used, while Gas detectors are used for the  $dE/dX$  measurement at low energy of heavier particles. Both ionization chamber and proportional counter have been used as the gas detectors. General advantages of the gas counters are the following: (i) by adjusting the gas pressure the thickness of  $\Delta E$  detector can be varied, according to the requirements of a given specific experiment; (ii) the homogeneity of the gas  $\Delta E$  detector can be better than 1%. On the other hand, the gas detector have some defects. First is the difficulty in handling the gas flow system and the mechanical weakness of the window material. Second, resolution of  $\Delta E$  spectrum is affected significantly by the uniformity of the electric field.

Photograph of the gas counter was shown in Fig. 1. It has three advantages: (1) Various length of outer tube of  $\Delta E$  detector can be selected; (2) A thin window film can be easily exchanged without changing the counter setting; (3) The same counter can be used as an ionization chamber and a proportional counter, only by exchange of the anode parts. A simplified diagram of the telescope was shown in Fig. 2. The outer tube of gas counter, entrance housing and SSD housing are machined from brass. The grid and anode are made of Au-coated tungsten wires of  $10 \mu\text{m}$ . These wires are parallel to the trajectory of the particles. The outer tube, grid and anode are mounted on insulators. The space between outer tube and anode is 20 mm and between grid and anode is 5 mm. The entrance window is made from VYHH film, copolymerization resin of 90% Vinyl acetate and 10% Vinyl chloride, of  $10\text{-}30 \mu\text{g}/\text{cm}^2$  thickness. Typical outer tube length is 70 mm. The entrance window is  $1.5 \times 5 \text{ mm}$  and can safely support a gas pressure of 42 Torr.

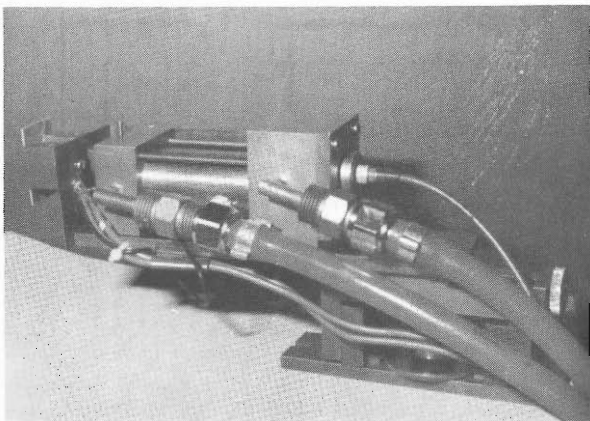


Fig. 1. Photograph of the gas  $\Delta E$ -E counter. The gas pipes, magnet and shielding wall are set.

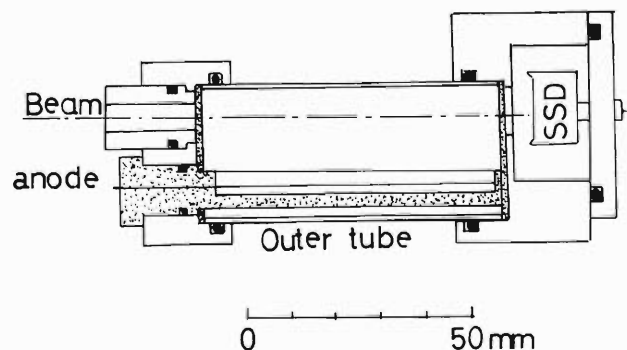


Fig. 2. The gas counter. Typical length of the counter was 115 mm.

\* Tokyo Metropolitan University.

\*\* Cosmic Ray Laboratory, The University of Tokyo.

Gas flow system is shown in Fig. 3. The gas counter was operated with a steady flow of PR gas containing of 90% argon and 10% methane. The gas pressure was stabilized with the mass flow controller and a reservoir of large volume. For gas pressure 7 to 30 Torr, the stability was better than 1% over a time of 12 h. The pressure was measured by an alphasatron vacuum gauge and monitored throughout the experiment.

The test experiment were performed with a 82 MeV carbon beam from the cyclotron. The target was a self-supporting  $^{54}\text{Cr}$  foil. A 1 mm thick Si-detector was used as a E counter. For  $\Delta E$  detector the proportional counter was used with operating gas pressure of 17 Torr, window thickness of  $20 \mu\text{g}/\text{cm}^2$  and operating anode voltage of 150 V. As is shown in a  $\Delta E$  spectrum gated with a constant E (Fig. 4), light particles are reasonably resolved by these conditions.

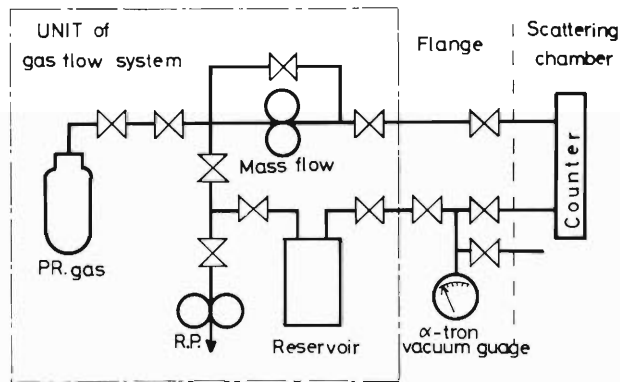


Fig. 3. Gas flow system.

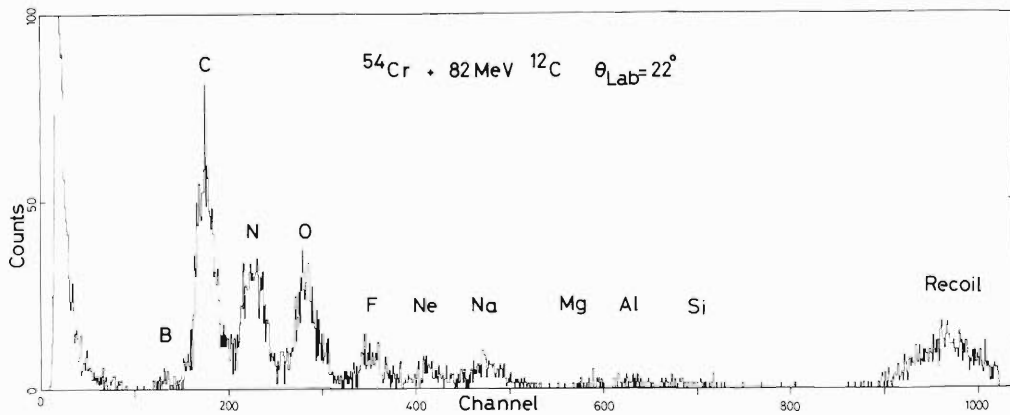


Fig. 4. One of the typical  $\Delta E$  spectrum.

## 7. ATOMIC AND SOLID-STATE PHYSICS

### 7-1. Energy Loss and Straggling of C and He Ions in Metal Foils

T. Takahashi, Y. Awaya, T. Doke, T. Hamada, A. Hashizume,  
K. Izumo, H. Kumagai, T. Tonuma, and S. Uchiyama

According to Ashley, Ritchie and Brandt,<sup>1)</sup> and Jackson and McCarthy,<sup>2)</sup> the energy loss of a heavy particle of charge  $Z_1e$  and velocity  $v = \beta c$  can be written as

$$\frac{dE}{dx} = Z_1^2 K + Z_1^3 J$$

where  $J/K$  is a small positive quantity, of the order of a few hundredths for  $\beta = v/c = 0.1$ . To test the  $Z_1^3$  dependence, we made preliminary experiment on Al, Ni, Ag, Au, and Pb foils, using C and He ions of  $0.10 < \beta < 0.11$ . Results are shown in Table 1 and Table 2, where interpolated values from Northcliffe and Schilling's data<sup>3)</sup> are also shown. Our data are in accordance with Northcliffe and Schilling's data within the experimental accuracy, except for Pb. Because of experimental errors, no conclusion can be drawn about the  $Z_1^3$  dependence, but it seems somewhat smaller than that predicted by the theory. Experiments at higher energies, where the  $Z_1^3$  dependence is expected to be more clearly observed, are now in progress.

According to Sofield et al.,<sup>4)</sup> energy straggling of 5.486 MeV He ions in Al is in excellent agreement with the Bethe-Livingstone theory.<sup>5)</sup> Our results on the straggling of 22 MeV He ions show 20 – 40% larger values than those predicted by the theory. The reason for this is not explained yet.

Table 1. Electronic stopping power of C ions in units of MeV/(mg/cm<sup>2</sup>).

Material	Energy (MeV/nucleon)	Our experiments	Northcliffe and Schilling
Al	5.301	1.953 ± 0.018	1.96 ± 0.02
Ni	5.273	1.597 ± 0.021	1.60 ± 0.02
Ag	5.288	1.260 ± 0.015	1.27 ± 0.02
Au	5.082	0.956 ± 0.017	0.98 ± 0.01
Pb	5.345	0.974 ± 0.025	0.92 ± 0.01

Table 2. Electronic stopping power of He ions in units of MeV/(mg/cm<sup>2</sup>).

Material	Energy (MeV/nucleon)	Our experiment	Northcliffe and Schilling
Al	5.295	0.222 ± 0.002	0.219 ± 0.002
Ni	5.273	0.179 ± 0.004	0.180 ± 0.002
Ag	5.300	0.145 ± 0.004	0.141 ± 0.002
Au	5.076	0.107 ± 0.003	0.108 ± 0.002

## References

- 1) J. C. Ashley, R. H. Ritchie, and W. Brandt: Phys. Rev., B5, 2393 (1972).
- 2) J. D. Jackson and R. L. McCarthy: *ibid.*, B6, 4131 (1972).
- 3) L. C. Northcliffe and R. F. Schilling: Nuclear Data Tables, A7, 233 (1970).
- 4) C. J. Sofield, N. E. B. Cowern, J. M. Freeman, and K. Parthasaradhi: Phys. Rev., A15, 2221 (1977).
- 5) M. S. Livingston and H. A. Bethe: Rev. Mod. Phys., 9, 245 (1937).

## 7-2. X-Rays Following Multiple Inner-Shell Ionization (1)

Y. Awaya, T. Katou, H. Kumagai, T. Tonuma,  
Y. Tendow, K. Izumo, T. Takahashi,  
A. Hashizume, M. Okano, and T. Hamada

The dependence of the  $K\alpha$  X-ray spectrum pattern on the incident energy ( $E$ ) of the projectile has been studied by exciting a Ti target with N ions of 66, 71, 84, 95, and 108 MeV and C ions of 61, 72, and 82 MeV. The dependence on the atomic number of the projectile ( $Z_1$ ) has also been studied by exciting the Ti target with 6 MeV/amu  $\alpha$  particles, C, N, and O ions.

The  $\alpha$  particles,  $C^{4+}$ ,  $N^{4+}$  ( $N^{5+}$  for 108 MeV) and  $O^{5+}$  ions were accelerated by the cyclotron. The Ti target was a self-supporting metallic foil. Its thickness was  $1.35 \text{ mg/cm}^2$  except for the case of 95 MeV N-ion bombardment where a foil of  $1.8 \text{ mg/cm}^2$  was used. The target was placed at  $60^\circ$  with respect to the beams. The estimated energy loss of the projectile in the target is less than 6% of the incident energy. X-rays were measured with an automatically controlled step-scanning Bragg crystal spectrometer<sup>1),2)</sup> employing a flat crystal of LiF (200). The detection system of the scintillation counter (SC) was used in most of the measurements. When the X-ray yield was not enough to use SC, the detection system of the proportional counter (PC) was used.

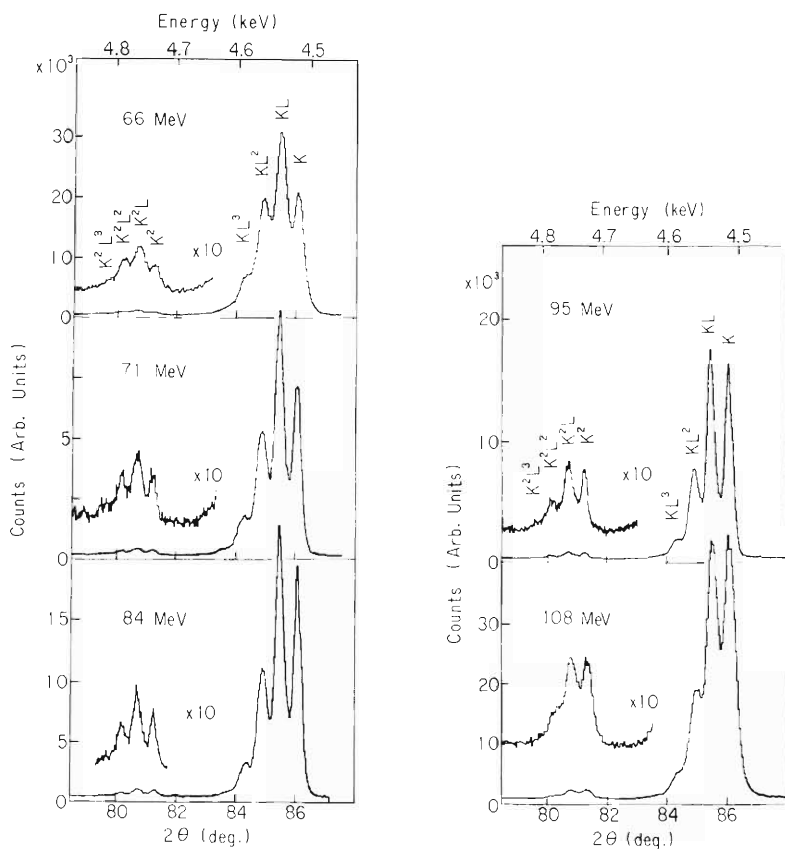


Fig. 1. Ti  $K\alpha$  X-ray spectra excited by N ions of the indicated incident energy.

The efficiency of the spectrometer utilizing PC system is ten times larger than that utilizing SC system for Ti K X-rays whereas the resolution of the former is worse than the latter. This depends on the angular divergence of the Soller slit and the absorption of the X-rays by the Mylar window of the chamber<sup>1),2)</sup> besides the efficiency of each counter.

The spectra of Ti K $\alpha$  X-rays induced by 66, 71, 84, 95, and 108 MeV N-ion impact and those induced by 6 MeV/amu  $\alpha$  particles, C, N, and O ions are shown in Figs. 1 and 2. Symbol K<sup>m</sup>L<sup>n</sup> denotes the m K-shell and n L-shell vacancies in the initial state. For some cases the K $\beta$  X-ray spectra were also measured. They are shown in Fig. 2. The symbol  $\alpha$  or  $\beta$  attached to each peak means that the peak belongs to K $\alpha$  or K $\beta$  transition.

The analysis of the spectra will be made in part (II).

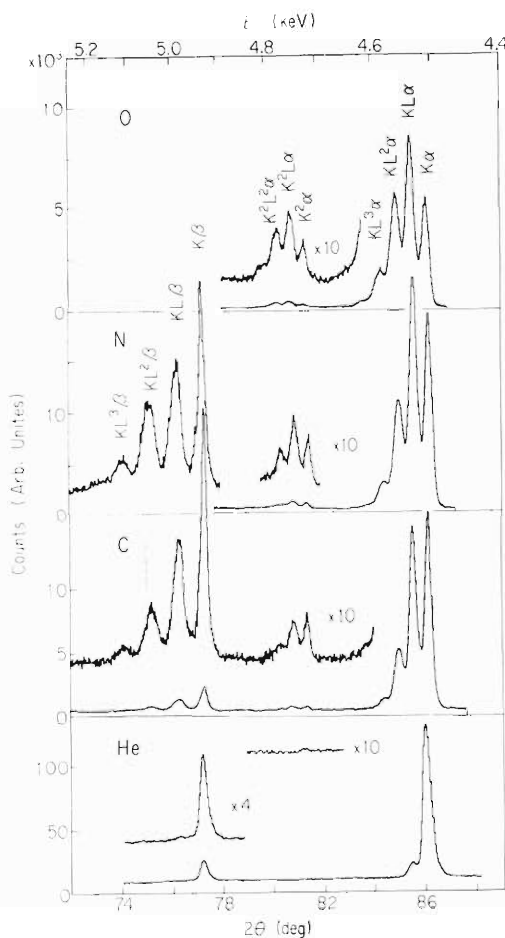


Fig. 2. Ti K X-ray spectra excited by 6-MeV/amu  $\alpha$  particles, C, N, and O ions.

## References

- 1) Y. Awaya, Y. Tendow, H. Kumagai, M. Akiba, T. Katou, and T. Hamada: IPCR Cyclotron Progr. Rep., 9, 79 (1975).
- 2) H. Kumagai, Y. Awaya, Y. Tendow, T. Katou, and M. Akiba: Reports I.P.C.R., (in Japanese), 53, 153 (1977).

## 7-3. X-Rays Following Multiple Inner-Shell Ionization (2)

Y. Awaya, K. Izumo, T. Hamada, M. Okano, A. Hashizume,  
T. Takahashi, Y. Tendow, H. Kumagai, T. Katou, and T. Tonuma

The previously reported data<sup>1)</sup> on the dependence of K X-ray spectrum pattern on the atomic number of the target element ( $Z_2$ ) as well as the present data described in part (I) are analysed.

(1) The diagram and satellite X-rays

Relative peak intensity obtained for N-ion bombardment are shown in Fig. 1 and those for C-ion bombardment in Fig. 2. In Fig. 2, data at lower energies and the result of theoretical calculation, in solid curves, are those of Hill et al.<sup>2)</sup>

By assuming that there is no correlation between electrons and that the probability for ionizing each sub-shell electron of the L shell is the same, the ionization cross section of  $m$  K-shell and  $n$  L-shell electrons  $\sigma_{mK,nL}$  is given by the following expression,<sup>3),4)</sup>

$$\sigma_{mK,nL} = \int_0^{\infty} \binom{2}{m} P_K^m(b) [1 - P_K(b)]^{2-m} \binom{8}{n} P_L^n(b) [1 - P_L(b)]^{8-n} 2\pi b db, \quad (1)$$

where  $P_L(b)$  is the probability of single ionization for the L shell with  $N$  electrons,  $b$  is the impact parameter and  $\binom{N}{X}$  is the binomial coefficient. For the expression of single K-shell and  $n$  L-shell ionization cross section  $\sigma_{1K,nL}$ , a factor  $[1 - P_K(b)]$  is approximated to one and, in the region where  $P_K(b) \neq 0$ ,  $P_L(b)$  is almost constant and can be approximated by  $P_L(0)$ . Then,

$$\sigma_{1K,nL} \cong \binom{8}{n} P_L^n(0) [1 - P_L(0)]^{8-n} \cdot 2 \int P_K(b) 2\pi b db = \binom{8}{n} P_L^n(0) [1 - P_L(0)]^{8-n} \cdot \sigma_K \quad (2)$$

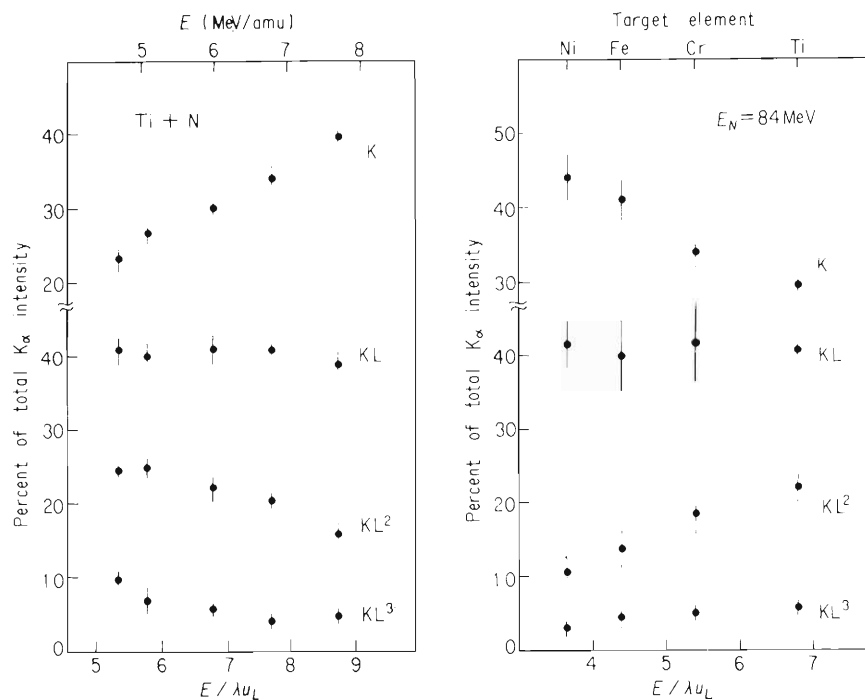


Fig. 1. Percent of total  $K\alpha$  intensity in the diagram line and satellites vs.  $E/\lambda u_L$ . Left: the Ti target was bombarded by N-ions of energy  $E$ , Right: the Ti, Fe, Cr, and Ni targets were bombarded by 84 MeV N-ions.

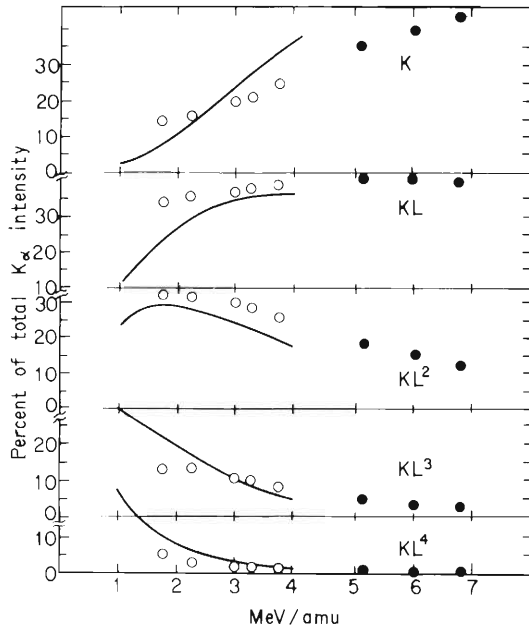


Fig. 2. Percent of total  $K\alpha$  intensity in the diagram line and satellites vs. energy of per amu of projectile for C-ions. The open circles and solid curves are taken from Ref.2.

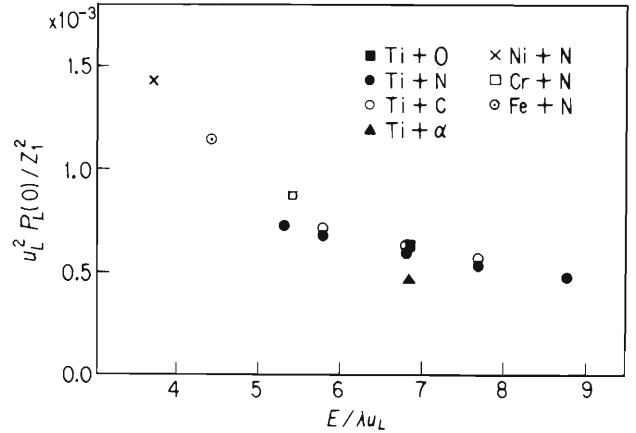


Fig. 3. Plot of  $P_L(O)$ .

The relative intensity of  $KL^n$  X-rays has been converted to the relative ionization cross section by using the calculated fluorescence yield  $\omega_{KL^n}$ . The value of  $\omega_{KL^n}$  was calculated by a statistical scaling procedure by assuming no initial M-shell vacancies and by using values of radiative transition probability calculated by Scofield<sup>5)</sup> and those of Auger transition probability by Kostroum et al.<sup>6)</sup> The estimated values are listed in Table 1. From the relative ionization cross section for each  $KL^n$  configuration, the parameter  $P_L(O)$  has been determined by the least square fitting. It was found that the curve  $u_L^2 P_L(O)/Z_1^2$  vs.  $E/\lambda u_L$  shows the same relation which can be applied universally as is obtained for single inner-shell ionization, where  $u_L$  is the binding energy of the L electron and  $\lambda$  is the mass of projectile in electron mass unit. The result is shown in Fig. 3.

Table 1. Scaled K-shell fluorescence yield  $\omega_{KL^n}$  of Ti, Fe, and Zn for various combination of 2s ( $n_1$ ) and 2p ( $n_2$ ) vacancies ( $n = n_1 + n_2$ ). Interpolated values are used for Cr and Ni.

$n_1 \setminus n_2$	0	1	2	3	4	5	
Ti	0	0.194	0.197	0.197	0.189	0.168	0.118
	1	0.257	0.272	0.286	0.296	0.295	0.252
	2	0.324	0.352	0.383	0.418	0.450	0.447
Fe	0	0.319	0.325	0.327	0.319	0.291	0.217
	1	0.395	0.414	0.433	0.448	0.449	0.400
	2	0.467	0.499	0.533	0.570	0.604	0.603
Zn	0	0.453	0.461	0.467	0.460	0.431	0.340
	1	0.532	0.553	0.573	0.590	0.593	0.547
	2	0.598	0.628	0.661	0.694	0.724	0.726

## (2) The hypersatellite X-rays

The relative intensity of hypersatellite to the diagram plus satellite lines,  $\sigma_X(K^2)/\sigma_X(K)$ , increases with either the increase of  $E$  or the decrease of  $Z_2$ , when  $Z_1$  is constant (N-ions). It is found that when the values of  $\sigma_X(K^2)/\sigma_X(K)$  are plotted against the reduced parameter  $E/\lambda u_K$ , these two kinds of points, one with increasing  $E$  and the other with decreasing  $Z_2$ , are connected smoothly as is seen in Fig. 4, where  $u_K$  is the K-electron binding energy of the target atom. The points marked by atomic symbols were obtained for 84-MeV N-ion impact to the corresponding target element and those without the marks are for bombardment of the Ti target with N and C ions of corresponding value of  $E$ .

The plot of  $\sigma_X(K^2)/\sigma_X(K)$  vs.  $Z_1^2$  is shown in Fig. 5. This result shows that the value of  $\sigma_X(K^2)/\sigma_X(K)$  is proportional to  $Z_1^2$ . Since the value of  $\sigma_X(K)$  is proportional to  $Z_1^2$ , as long as the ionization is caused by the direct Coulomb interaction, this shows that the value of  $\sigma_X(K^2)$  is proportional to  $Z_1^4$ . This fact provides another evidence of  $Z_1^4$ -scaling for double ionization of K shell obtained by Kawatsura et al.<sup>7)</sup>

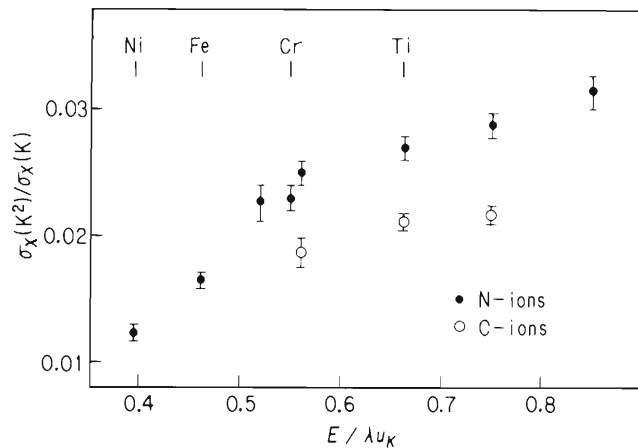


Fig. 4. Total  $K^2L^{\alpha}X$ -ray intensity relative to total  $KL^{\alpha}X$ -ray intensity vs  $E/\lambda u_K$ .

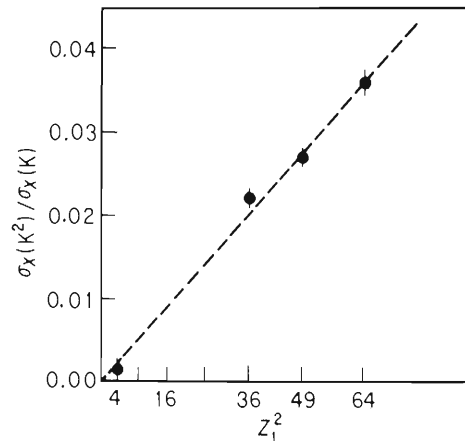


Fig. 5.  $\sigma_X(K^2)/\sigma_X(K)$  as a function of  $Z_1^2$ .

## References

- 1) Y. Awaya, M. Akiba, T. Katou, H. Kumagai, Y. Tendow, K. Izumo, T. Takahashi, A. Hashizume, M. Okano, and T. Hamada: Phys. Letters, 61A, 111 (1977); IPCR Cyclotron Progr. Rep., 10, 78 (1976).
- 2) K. W. Hill, B. L. Doyle, S. M. Shafroth, D. H. Madison, and R. D. Deslattes: Phys. Rev., A13, 1334 (1976).
- 3) J. M. Hansteen and O. P. Mosebekk: Phys. Rev. Lett., 29, 1361 (1973).
- 4) J. H. McGuire and P. Richard: Phys. Rev., A8, 1374 (1973).
- 5) J. H. Scofield: *ibid.*, 179, 9 (1969).
- 6) V. O. Kostroum, M. H. Chen, and B. Crasemann: *ibid.*, A3, 533 (1971).
- 7) K. Kawatsura, K. Ozawa, F. Fujimoto, and M. Terasawa: Proc. 10th Intern. Conf. on Physics of Electronic and Atomic Collisions Abstracts, Paris, p. 50 (1977).

## 7-4. Gas Target System for Study of X-Rays Induced by Heavy Ions

T. Tonuma, Y. Awaya, T. Kambara, H. Kumagai, and I. Kohno

A gas target system equipped with gas cell was made and used in the study of K x-rays induced by ions. It is advantageous in our case of using the cyclotron beam to employ a closed gas target system equipped with windows because of following reasons: 1) thickness of gas target is easily controlled and also it is easy to get high pressure that can not be attained by a differential pumping system; 2) after passing through a window, heavy ions (C, N) accelerated by the cyclotron are almost naked ions. Therefore, an initial charge state of heavy ions are regarded as a fully stripped charge state.

Figure 1 illustrates the gas cell and the gas feeding system. Two windows through which the beam passes are covered with  $7\ \mu\text{m}$  thick aluminium foils and the other window facing an x-ray detector with  $50\ \mu\text{m}$  thick beryllium foil. Each window has a diameter of 12 mm. The vessel itself is made of aluminium. The cell is able to withstand the gas pressure of about 300 Torr when placed in vacuum. The pressure was monitored by an  $\alpha$ -tron gauge throughout the experiment. The size of the beam spot was less than 3 mm in diameter at the entrance window.

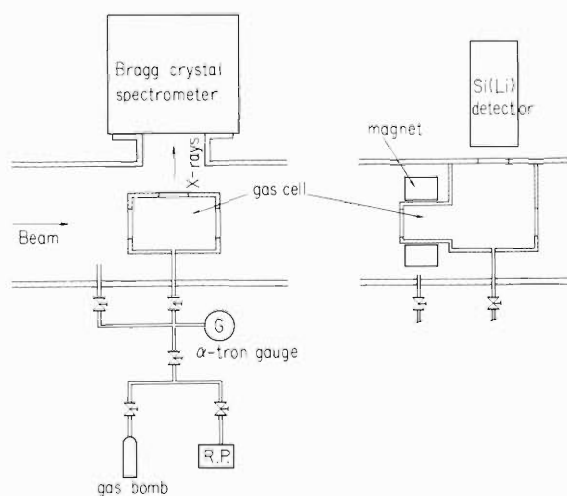


Fig. 1. Gas target and gas feeding system.

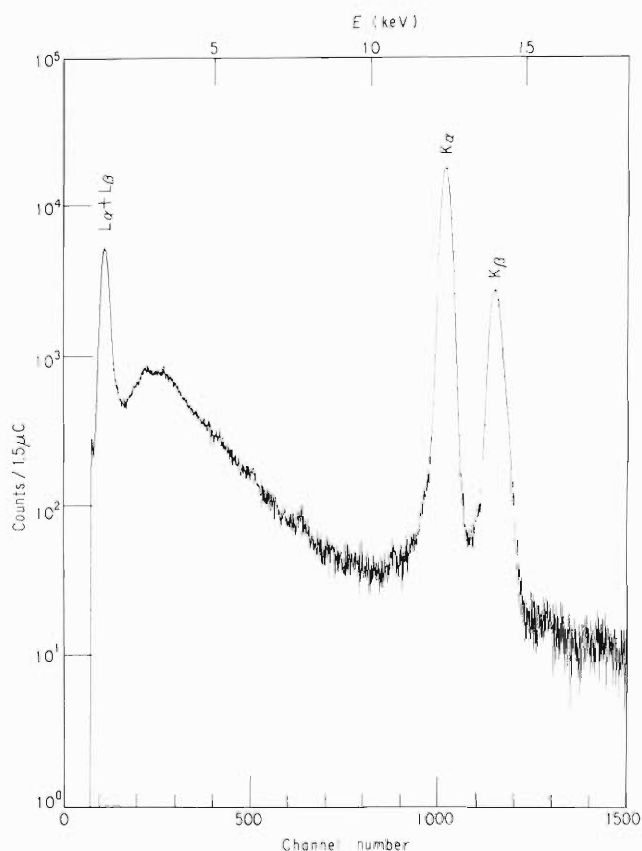


Fig. 2. The Kr K X-ray spectrum induced by 84 MeV N-ions measured with a Si(Li) detector.

The x-rays from the gas target, emitted by the beam bombardment, were detected by a Si(Li) x-ray detector<sup>1)</sup> and by a Bragg crystal spectrometer.<sup>2)</sup>

The first example of the x-ray energy spectrum obtained by using this gas target system is shown in Fig. 2. The  $K_{\alpha}$  and  $K_{\beta}$  spectra from a Kr gas target induced by 84 MeV N-ions were measured using the Si(Li) detector which was placed perpendicular to the beam direction. Air space of about 7 mm existed between the window of the target and that of detector. Each window was covered with 50  $\mu\text{m}$  Be foil. The pressure of the Kr gas was kept at 4.0 Torr during the measurement. In the low energy region of x-ray spectra continuous background was observed. This may be due to the bremsstrahlung induced by recoil electrons created by the projectiles in the target and windows.<sup>1)</sup>

The second example of the x-ray energy spectrum is shown in Fig. 3. The  $K_{\alpha}$  diagram and satellite line spectra of Ar gas target induced by 84 MeV N-ions were measured by the Bragg crystal spectrometer, which had a Ge(111) crystal and a proportional counter. In the measurement, Bragg angle( $2\theta$ ) was increased by steps of  $0.05^{\circ}$  after counting was done for integrated current of  $1.5 \mu\text{C}$  at each step. The beam current was about 10 nA up to 15 nA. The pressure of Ar gas varied from 203 Torr to 210 Torr during three and a half hours required for the measurement. Each peak in the figure is labelled by symbol  $KL^n$  which denotes the corresponding initial configuration having one K-shell vacancy and n L-shell vacancies.

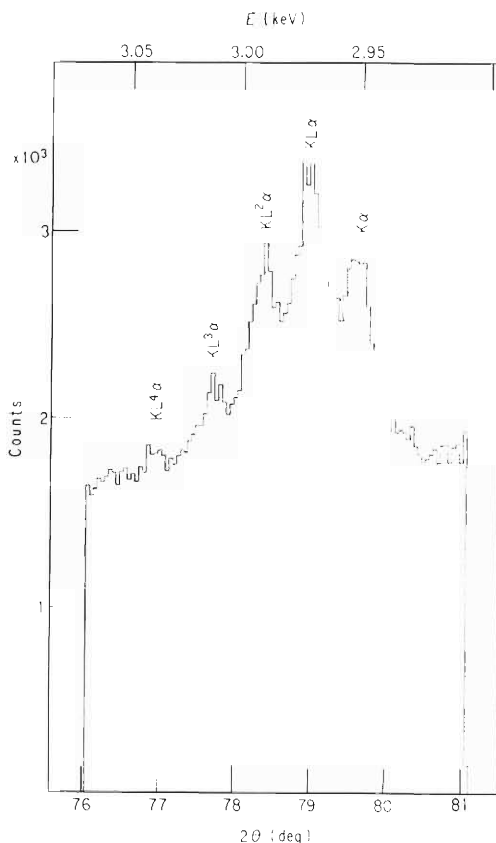


Fig. 3. The Ar  $K_{\alpha}$  X-ray spectrum induced by 84 MeV N-ions measured with a Bragg crystal spectrometer.

Using the Si(Li) detector, the yield of Ar x-rays was determined with and without a magnet which suppressed secondary electrons emitted from an Al foil window by the beam bombardment. From the measurement it was found that the secondary electrons created little Ar x-rays. The yield of x-rays created by  $\gamma$ -rays emitted from an Al foil might be also negligible because the cross

section were very small. The determination of target thickness requires the knowledge of the temperature as well as the pressure of the gas. However, it is difficult to know the exact temperature of gas during the experiment because the temperature may rise locally due to heating by the beam. Hence, the x-ray yield or the elastic scattering yield will have to be monitored by another counter instead of measuring the temperature.<sup>3)</sup> The ratio S/N was rather unsatisfactory as shown in the figure. Improvement of the S/N ratio is being tried.

#### References

- 1) Y. Awaya, K. Izumo, T. Hamada, M. Okano, T. Takahashi, A. Hashizume, Y. Tendow, and T. Katou: Phys. Rev., A13, 992 (1975).
- 2) Y. Awaya, Y. Tendow, H. Kumagai, M. Akiba, T. Katou, and T. Hamada: IPCR Cyclotron Progr. Rep., 9, 79 (1975).
- 3) T. Motobayashi: *ibid.*, 10, 72 (1976).

## 7-5. Chemical Effect in X-Ray Spectra Produced by Fast Ions

M. Uda, K. Maeda, Y. Awaya, M. Kobayashi,  
Y. Sasa, H. Kumagai, and T. Tonuma

X-ray emission spectra induced by 84 MeV  $N^{4+}$ , 72 MeV  $C^{4+}$ , 24 MeV  $He^{2+}$ , and 6 MeV  $H^+$  ions generated in the cyclotron were measured with an on-line Bragg spectrometer.<sup>1)</sup> Integrated beam current was kept constant for each angular setting. Target materials used here were in the form of thin films, thickness of which was in the range of 1–5 mg/cm<sup>2</sup>. Insulators were made conducting by coating with a thin layer (200 Å) of carbon.

The present study deals with chemical effects reflected in X-ray spectra emitted from F, Na, S, Fe, Ni, and Cu in different kinds of chemical environments. Target materials used for this purpose were as follows: (1) for transitions between inner shells such as Fe  $K\alpha$ , S  $K\alpha$  and Al  $K\alpha$ ; Fe,  $\alpha$ -Fe<sub>2</sub>O<sub>3</sub>, Cu<sub>2</sub>S, Na<sub>2</sub>SO<sub>4</sub>, Al and AlF<sub>3</sub>, and (2) for transitions between inner shell and valence band such as (a) F  $K\alpha$ , Na  $K\alpha$ , Al  $K\beta$ , S  $K\beta$ , Fe  $K\beta$ , and Ni  $K\beta$ ; NaF, Na<sub>3</sub>AlF<sub>6</sub>, AlF<sub>3</sub>, (CF<sub>2</sub>)<sub>n</sub>, NaSCN, Na<sub>2</sub>S<sub>2</sub>O<sub>6</sub>, Cu<sub>2</sub>S, Na<sub>2</sub>SO<sub>4</sub>, Al, Fe,  $\alpha$ -Fe<sub>2</sub>O<sub>3</sub>, Ni, and NiO, and (b) Fe  $L\alpha,\beta$ , Ni  $L\alpha,\beta$  and Cu  $L\alpha,\beta$ ; Fe, FeO,  $\alpha$ -Fe<sub>2</sub>O<sub>3</sub>, Ni, NiO, Cu, Cu<sub>2</sub>O, and CuO.

The centroid energies and intensities of X-ray lines in F  $K\alpha$  and Na  $K\alpha$  spectra were determined by least-square fitting of the multiple Gaussian curves to the overlapping peaks.

S  $K\alpha$  and  $K\beta$  spectra obtained from Cu<sub>2</sub>S and Na<sub>2</sub>SO<sub>4</sub> are shown in Fig. 1.  $K^mL^n\alpha$  denotes  $K\alpha$  spectra emitted from S atom with  $mK$  and  $nL$  vacancies at the initial state. Same is true for  $KL^n\alpha$ .

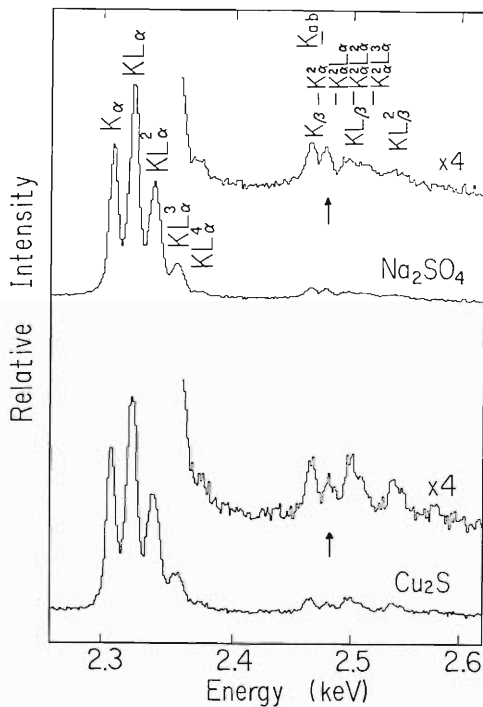


Fig. 1. S  $K\alpha$  and  $K\beta$  spectra from Na<sub>2</sub>SO<sub>4</sub> and Cu<sub>2</sub>S induced by 84 MeV<sup>4+</sup>. X-rays were measured with the gas flow proportional counter through EDDT (020).

The spectra in  $KL^{n\alpha}$  region are, both in intensities and centroid energies, quite similar to each other. On the other hand, somewhat different intensity distributions can be seen in  $K\beta$  region. If components of  $K^2L^{n\alpha}$  named hypersatellite could be subtracted from this region, difference in  $KL^{n\beta}$  spectra in these two compounds would readily be noticeable. This is because the number of electrons in 2p level which are responsible for  $K^{m}L^{n\alpha}$  emission is the same but that in 3p responsible for the emission of  $KL^{n\beta}$  is different in these compounds.

Marked difference in  $L\alpha_{1,2}$  and  $L\beta_1$  band spectra modified with the high energy satellites from the metals and the oxides can also be seen in Fig.2(a)–(c). No appreciable difference in  $K\alpha$  and  $K\beta$  spectra between Fe and  $\alpha\text{-Fe}_2\text{O}_3$ , and also between Ni and NiO could, however, be observed under our experimental condition.

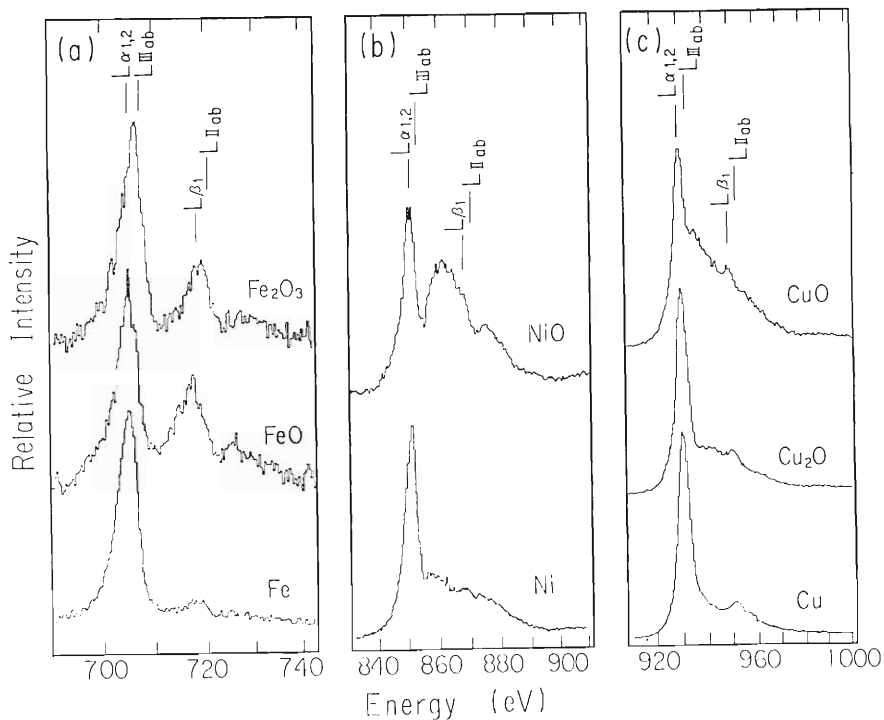


Fig. 2(a)-(c).  $L\alpha_{1,2}$  and  $L\beta_1$  band spectra of Fe, Ni, and Cu taken from Fe, FeO, and  $\text{Fe}_2\text{O}_3$  (a), Ni and NiO (b), and Cu and  $\text{Cu}_2\text{O}$  (c) which were induced by 84 MeV  $\text{N}^{4+}$ . RAP(001) and the proportional counter were here employed.

The centroid energies and the relative intensities of F  $K\alpha$  and Na  $K\alpha$  spectra are summarized in Tables 1 and 2. The bonding effect is clearly reflected in F  $KL^{n\alpha}$  spectra but is indistinct in Na  $K\alpha$ . Study to get the relationship between the intensity distributions of the satellite lines and ionic characters of the compounds used is under way.

Table 1. Centroid energies, full width at half maxima (FWH) and relative intensities of F K $\alpha$  spectra induced by 84 MeV N $^{4+}$ , 72 MeV C $^{4+}$ , 24 MeV He $^{2+}$  and 6 MeV H $^{+}$ .

Target	KL $^2\alpha$			KL $\alpha$			K $\alpha^{(1)*}$			K $\alpha^{(2)*}$			
	Energy (eV)	FWHM (eV)	I	Energy (eV)	FWHM (eV)	I	Energy (eV)	FWHM (eV)	I	Energy (eV)	FWHM (eV)	I	
N $^{4+}$	NaF	684.8	3.4	85	680.1	2.5	149	676.3	2.3	100	673.8	3.6	17
	Na $_3$ AlF $_6$	684.8	3.7	70	679.9	2.8	120	676.4	2.6	100	674.1	4.0	31
	AlF $_3$	684.6	3.8	63	680.1	2.9	89	676.9	2.8	100	673.9	3.5	36
	teflon	683.8	3.8	44	679.6	2.9	58	676.6	2.5	100	674.1	3.5	38
C $^{4+}$	NaF	684.4	3.4	57	679.7	2.6	145	675.9	2.0	100	673.8	3.0	23
	Na $_3$ AlF $_6$	684.6	3.7	53	679.6	2.6	94	676.2	2.6	100	673.9	3.6	35
	AlF $_3$	684.4	4.0	54	679.8	2.8	80	676.6	2.7	100	673.8	3.6	46
	teflon	684.3	4.0	32	680.0	3.2	48	676.6	2.6	100	673.7	3.6	34
He $^{2+}$	NaF	684.5	3	7	680.0	2.7	60	676.1	2.1	100	674.1	3.2	35
	Na $_3$ AlF $_6$	684.4	4	10	679.9	2.3	37	676.3	2.8	100	673.8	4.2	50
	AlF $_3$	683.6	7	14	680.1	2.8	33	676.7	2.9	100	673.7	4.1	67
	teflon	—	—	—	679.5	2.4	30	676.6	2.4	100	673.7	5.1	75
H $^{+}$	NaF	684.1	3	6	679.9	2.4	48	675.9	2.0	100	674.3	5.0	35
	Na $_3$ AlF $_6$	684.1	4	9	679.8	2.4	38	676.3	2.5	100	673.8	3.2	39
	AlF $_3$	683.5	4	11	680.1	2.2	27	676.8	2.6	100	673.8	3.4	54
	teflon	—	—	—	679.6	3.0	31	676.8	2.3	100	673.8	3.4	43

\* K $\alpha$  spectrum is splitted into two components, K $\alpha^{(1)}$  and K $\alpha^{(2)}$ , caused by formation of molecular orbitals.

Table 2. Centroid energies, full width at half maxima (FWH) and relative intensities of Na K $\alpha$  spectra induced by 84 MeV N $^{4+}$ .

	KL $^4\alpha$			KL $^3\alpha$			KL $^2\alpha$			KL $\alpha$			K $\alpha$		
	Energy (eV)	FWHM (eV)	I	Energy (eV)	FWHM (eV)	I	Energy (eV)	FWHM (eV)	I	Energy (eV)	FWHM (eV)	I	Energy (eV)	FWHM (eV)	I
NaF	1076.1	6.0	6	1067.2	5.9	53	1057.5	5.6	121	1049.5	4.5	116	1042.0	5.2	100
Na $_3$ AlF $_6$	1076.3	5.8	7	1067.0	5.9	52	1057.5	5.6	111	1049.5	4.4	116	1042.2	5.2	100
Na $_2$ SO $_4$	1075.9	5.8	7	1067.0	5.7	52	1057.5	5.6	117	1049.5	4.6	122	1042.0	4.9	100
NaSCN	1076.6	5.9	7	1067.0	5.9	52	1057.4	5.6	128	1049.5	4.6	114	1042.0	5.2	100
Na $_2$ S $_2$ O $_6$	1076.1	5.1	11	1067.0	5.5	53	1057.7	5.6	121	1049.5	4.6	130	1042.2	5.1	100

#### Reference

- (1) Y. Awaya, T. Tendow, H. Kumagai, M. Katou, and T. Hamada: IPCR Cyclotron Progr. Rep., 9, 79 (1975).

## 7-6. Lattice Location of Ni Atoms Implanted into Al

E. Yagi, A. Koyama, H. Sakairi, and R. R. Hasiguti

The problem about interstitial sites in f.c.c. metals is fundamental one in lattice defects. In the present work, the location of nickel atoms implanted into aluminum was investigated by means of backscattering. It is expected that the implanted nickel atoms occupy the interstitial sites because nickel has only small solubility in aluminum. If it is the case, the information on the interstitial site will be obtained from the determination of nickel atom location.

Aluminum single crystals were electropolished and annealed in vacuum at  $550^{\circ}\text{C}$  for 7 h. The 180 keV Ni implantation was carried out at room temperature with a dose of  $2 \times 10^{16}$  ions/cm<sup>2</sup>. Channeling effects were investigated with respect to  $\langle 100 \rangle$  and  $\langle 110 \rangle$  axes by means of backscattering with 4.8–5.8 MeV protons accelerated by the cyclotron. The beam was collimated to have divergence less than  $0.019^{\circ}$ . The irradiated area was  $0.2 \text{ mm}^2$ , and the beam current was about 0.5 nA. The backscattered protons were measured by a surface-barrier solid state detector (FWHM $\approx 15$  keV) placed at a scattering angle of about  $150^{\circ}$ . The scattered cone seen by the detector was about  $9^{\circ}$  wide. The target specimen was maintained at room temperature during the channeling experiment.

In order to investigate the location of the implanted nickel atoms an angular scan was performed through  $\langle 100 \rangle$  and  $\langle 110 \rangle$  axes. Figure 1 (a) shows the normalized backscattering yields  $\chi$  from nickel and aluminum atoms as a function of the angle  $\theta$  between the incident beam direction and the  $\langle 100 \rangle$  axial direction. Figure 1 (b) shows the results for the  $\langle 110 \rangle$  axis.

The backscattering yield from nickel atoms shows a dip with minimum yield  $\chi_{\text{min}}$  of about

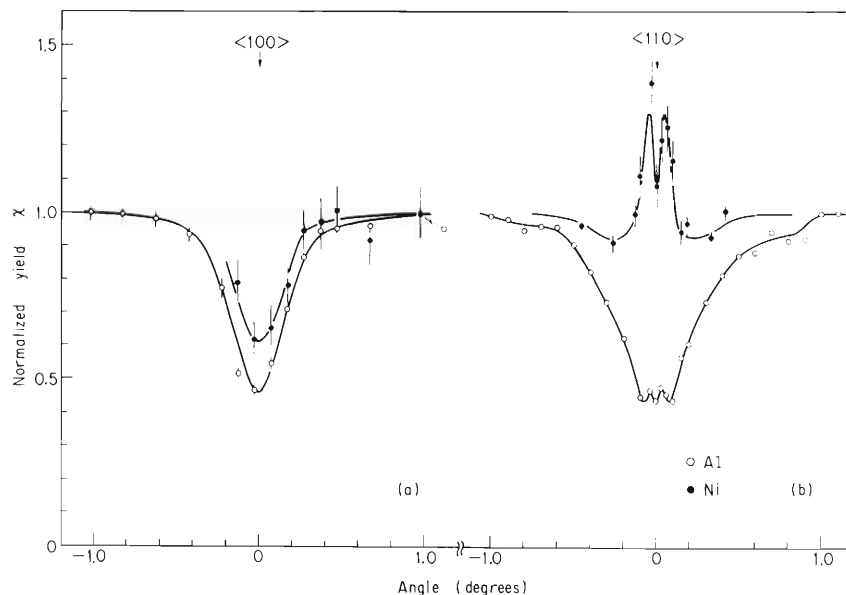


Fig. 1. Normalized backscattering yield from Ni and Al atoms as a function of the angle  $\theta$  between the incident beam direction and the  $\langle 100 \rangle$  axial direction (a), and the  $\langle 110 \rangle$  axial direction (b).

0.62 for the  $\langle 100 \rangle$  axis, while a double peak for the  $\langle 110 \rangle$  axis. The  $\langle 100 \rangle$  Ni-dip has the same half-width at half-minimum as that of the Al-dip. The double peak results from the flux-peaking effect and indicates that nickel atoms are located at interstitial sites. These experimental results suggest that the nickel atom occupies the interstitial site displaced from the normal lattice site in an aluminum crystal by the amount of about one fourth of the lattice constant in the  $\langle 100 \rangle$  direction. In the  $\langle 110 \rangle$  angular scan, an Al-dip has also fine structure consisting of a small double peak at its center. As in the case of nickel, this result suggests the presence of aluminum atoms displaced from normal lattice sites by nearly the same amount in the  $\langle 100 \rangle$  direction. The interstitial nickel atoms displace aluminum atoms at normal lattice sites into interstitial sites.

## 7-7. Damage Production Rate in $\text{TiO}_2$ as Measured by Channeling Method

E. Yagi, A. Koyama, H. Sakairi, and R. R. Hasiguti

The damage production rate of interstitials in  $\text{TiO}_2$  was investigated by channeling method.<sup>1)</sup> Our previous channeling experiments<sup>2)</sup> indicated that in a nonstoichiometric  $\text{TiO}_{2-x}$  crystal main defects are Ti interstitials and they are located along the [001] mid-channel axis. In the [001] angular scan of backscattered protons from Ti ions, a small peak due to Ti interstitials was observed at the center of the Ti-dip.

In the present work, experimental details are the same as those described in the previous paper.<sup>2)</sup> The channeling experiment was carried out with 5.77 MeV protons. The effect of radiation damage by incident protons was investigated. At large irradiation dose, the stoichiometric crystal was colored slightly blue and the increase was observed in both normalized backscattering yield  $\chi_0$  from Ti ions and that from O ions when measured for incidence parallel to the [001] axis. Thus the dose dependence of such increase  $\Delta\chi_0$  was measured by the following procedure. After the measurements of  $\chi_0$ , the irradiation was carried out in the random direction with respect to the [001] axis. This process was repeated successively. Figure 1 shows the increases  $\Delta\chi_0$  obtained for scattering from Ti ions and from O ions at depths between 4000Å and 7000Å. The increasing rate of  $\Delta\chi_0$  is  $1.8 \times 10^{-19}/(\text{particles}/\text{cm}^2)$  for Ti-dip and  $7.9 \times 10^{-19}/(\text{particles}/\text{cm}^2)$  for O-dip. These increases of  $\chi_0$  are attributed to the production of Frenkel pairs of Ti ions and that of O ions, respectively.

As previously reported,<sup>2)</sup> the normalized beam flux density amounts to about 4.2 at the center of the [001] channel as a result of flux-peaking effect. Using this value, the damage production rate of Frenkel pairs for Ti ions can be estimated to be about  $4.4 \times 10^{-20}/(\text{particles}/$

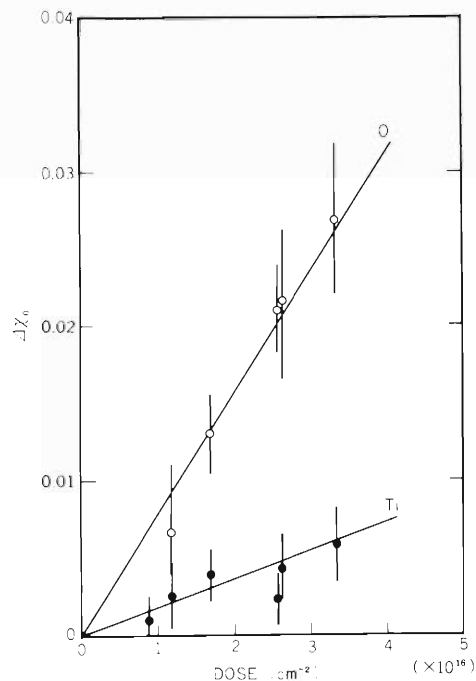


Fig. 1. Dose dependence of the irradiation-induced increase of normalized scattering yield  $\chi_0$  from Ti ions and O ions measured for incidence parallel to the [001] axis.

$\text{cm}^2$ ) in atomic fraction. This is of the same order of magnitude as that obtained in Cu for irradiation with 4.9 MeV protons at liquid-helium temperature by electrical resistivity measurement [i.e.  $\sim 1 \times 10^{-20}/(\text{particles}/\text{cm}^2)$ ].<sup>3)</sup> For O ions the damage rate cannot be estimated exactly since the location of interstitial oxygen ion is unknown. But its lowest limit is estimated to be  $1.9 \times 10^{-19}/(\text{particles}/\text{cm}^2)$ , because the normalized beam flux density can be considered to be less than 4.2 at any sites other than the center of a [001] axial channel.

#### References

- 1) E. Yagi, A. Koyama, H. Sakairi, and R. R. Hasiguti: Radiation Effects in Semiconductors 1976, Inst. Phys., London, p. 485 (1977).
- 2) E. Yagi, A. Koyama, H. Sakairi, and R. R. Hasiguti: J. Phys. Soc. Japan, 42, 939 (1977).
- 3) H. Sakairi, E. Yagi, A. Koyama, T. Karasawa, and R. R. Hasiguti: *ibid.*, 43, 999 (1977).

## 7-8. Perturbed Angular Correlation of $\gamma$ -Rays Emitted from $^{111}\text{Cd}$ in $\text{NiFe}_2\text{O}_4$

H. Sekizawa, K. Asai, T. Okada,  
N. Sakai, N. Shiotani, and E. Yagi

It is well known that large hyperfine magnetic fields are observed at the nuclei of non-magnetic ions in a magnetic material below its magnetic transition temperature. Since the origin of the hyperfine magnetic fields at the nuclei is the electron-spin polarization induced by the neighboring magnetic ions, the investigation of the hyperfine magnetic fields at the nuclei of non-magnetic ions supplies important information about the cation-cation magnetic interactions. In a previous report we presented experimental data on the time-differential perturbed angular correlation (PAC) of  $\gamma$ -rays emitted from  $^{111}\text{Cd}$  in  $\text{NiFe}_2\text{O}_4$  at room temperature.<sup>1)</sup> According to our results, the hyperfine magnetic field at  $^{111}\text{Cd}$  is distributed around 93 kOe at room temperature. In this report we present similar experimental data at 110K and discuss the origin of the distribution of the hyperfine magnetic field.

The procedure of sample preparation and the setup of the counter and magnet system were the same as that described in the previous report. The sample was packed in an aluminum tube. The normalized anisotropy of the coincidence counting rates  $R(t)$  is shown in Fig. 1. Definition of  $R(t)$  is as follows:

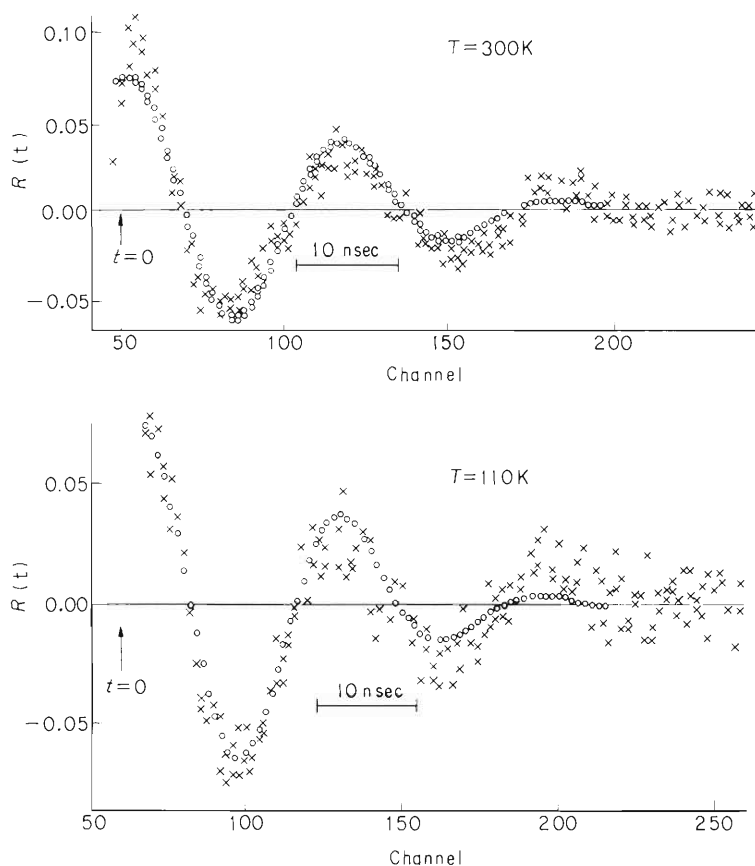


Fig. 1. The normalized anisotropy of the coincidence counting rates  $R(t)$  at 300K and at 110K. The experimental data are shown by the symbol X, and the computer fits of  $f(H)$  (see the text) by O.

$$R(t) = \frac{W(90^\circ, t) - W(180^\circ, t)}{W(90^\circ, t) + W(180^\circ, t)},$$

where  $W(\theta, t)$  denotes the coincident counts,  $\theta$  the angle between the two cascade  $\gamma$ -rays,  $t$  the time interval between these  $\gamma$ -rays. The physical meaning of  $R(t)$  is as follows:  $R(t)$  oscillates with the frequency twice the Larmor frequency of the hyperfine magnetic field perpendicular to the plane defined by the two cascade  $\gamma$ -rays. It is shown in Fig. 1 that the amplitude of  $R(t)$  decreases as the time interval increases. The decrease of the amplitude can be ascribed to the distribution of the hyperfine magnetic field at the  $^{111}\text{Cd}$  nuclei. If we assume a Gaussian distribution of the hyperfine magnetic field  $f(H) \propto \exp[-(H - H_0)^2 / (\sqrt{2}\Delta H)^2]$ , then,  $H_0 = 96$  kOe and  $\Delta H = 17$  kOe are obtained from the computer fits of 110K spectrum. These values are nearly the same as those at room temperature except that  $H_0$  at 110K is a little larger than that at room temperature. Figure 2 shows the distribution of the hyperfine magnetic field at  $^{111}\text{Cd}$  (our results) and  $^{115}\text{In}$  (Ref. 3).

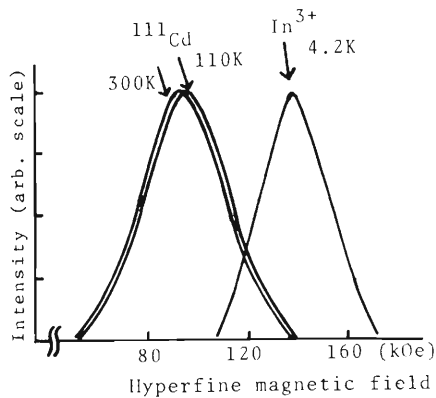


Fig. 2. The hyperfine field of diamagnetic ions on A site in  $\text{NiFe}_2\text{O}_4$ . The data on  $\text{In}^{3+}$  are the NMR data at 4.2K quoted from Ref. 2 and Ref. 3.

We are interested in the origin of the distribution of precession frequencies  $\Delta\omega$ .  $\text{In}^{3+}$  ions occupy preferentially tetragonal (A) sites ( $\sim 80\%$ ) according to the magnetic measurement.<sup>3)</sup>  $\text{In}^{3+}$  ion at A site is surrounded by twelve B site ions. Each B site is considered to be occupied at random by  $\text{Fe}^{3+}$  or  $\text{Ni}^{2+}$  ion. The hyperfine magnetic field of non-magnetic ion at A site is contributed mainly by the neighboring magnetic ions at B sites.<sup>2),3)</sup> The contribution of  $\text{Fe}^{3+}$  ion and that of  $\text{Ni}^{2+}$  ion are considered to be different. The fluctuation of the number of the neighboring  $\text{Fe}^{3+}$  and  $\text{Ni}^{2+}$  ions on the B sites will produce the distribution of the hyperfine field at  $^{111}\text{Cd}$ . This is an important mechanism to account for the distribution of precession frequencies. If we assume that situations are not much different between  $\text{In}^{3+}$  and  $\text{Cd}^{2+}$ , simple considerations lead to an expected apparent width  $\Delta H$  of 24 kOe for  $\text{Cd}^{2+}$ , which is a little smaller than the experimental value of 40 kOe.

In the above discussion we considered only the distribution of magnetic fields. It is reported that a quadrupole splitting is observed in the Mössbauer spectra of  $^{57}\text{Fe}$  nucleus at A site in  $\text{NiFe}_2\text{O}_4$  in the paramagnetic region. Its value is 0.37 mm/sec. If we assume that electric field gradient of the same magnitude acts on  $^{111}\text{Cd}$  nucleus, then, the quadrupole frequency will be  $6 \times 10^7$  rad/sec. This quadrupole effect in polycrystalline sample can give rise to an apparent width of the hyperfine magnetic field comparable to the observed one.

Further studies on the effect of the electric quadrupole field to the PAC spectra are in progress. It seems to be necessary to investigate the PAC spectra in the paramagnetic temperature range.

#### References

- 1) H. Sekizawa, K. Asai, T. Okada, N. Shiotani, E. Yagi, and S. Ambe: IPCR Cyclotron Progr. Rep., 10, 99 (1976).
- 2) Y. Miyahara and S. Iida: J. Phys. Soc. Japan, 32, 858 (1972).
- 3) Y. Miyahara and S. Iida: *ibid.*, 37, 1248 (1974).
- 4) V. A. Gordienko, V. I. Nikolaev, and S. S. Yakimov: Sov. Phys. -JETP, 39, 551 (1974).

## 7-9. On the Use of $^{48}\text{V}$ Source for the Study of Positron Annihilation

K. Hinode, S. Tanigawa, M. Doyama,\* and N. Shiotani

For the positron lifetime measurement, the birth signals of positrons are required, so that not all the  $\beta^+$  decay nuclide can be used as a positron source for the lifetime measurement. Fortunately, the disintegration scheme of  $^{48}\text{V}$  enables one to perform the lifetime measurement in addition to the  $\gamma$ - $\gamma$  angular correlation and Doppler broadening measurements. As the birth signal, one of the two  $\gamma$ -rays with energies of 1.31 and 0.98 MeV emitted from excited states of  $^{48}\text{Ti}$  can be used. (Fig. 1.)

The  $^3\text{He}$  bombardment of 0.1 Coulomb ( $E_{^3\text{He}} = 30 \text{ MeV}$ ) created  $^{48}\text{V}$  of about  $10 \mu\text{Ci}$  in a Ti foil with the thickness of  $1 \mu\text{m}$  through the nuclear reaction  $\text{Ti} (^3\text{He}, \text{pxn})^{48}\text{V}$ . (Fig. 2.)

This source is superior to the usual  $^{22}\text{NaCl}$  source in various points. 1) The fraction of the annihilation in the source foil is negligible, or less than a few percent. Positrons of higher energy ( $E_{\text{max}} = 0.696 \text{ MeV}$ ) are emitted by  $^{48}\text{V}$  than by  $^{22}\text{Na}$  ( $E_{\text{max}} = 0.545 \text{ MeV}$ ) and source wrapping materials are not required because of the imbedded form of the sources in Ti foil. 2) Long lifetime components due to the annihilation of positrons in the source itself (e.g. NaCl) and in the source foil materials do not appear in the lifetime spectrum. This enables us to obtain more reliable data for long lifetime components. For example, Figure 3 shows lifetime spectra for neutron-irradiated Mo measured with a  $^{48}\text{V}$  source in Ti foil and with a  $^{22}\text{NaCl}$  source of equivalent intensity wrapped with  $3.5 \mu\text{m}$  Mylar. 3) This source can be used under many measuring conditions (e.g. at low temperature or high temperature,<sup>1)</sup> in a vacuum<sup>1)</sup> or for liquid metals, etc.)

However, almost simultaneously with the positron emission, a pair of  $\gamma$ -rays with energies of 1.31 and 0.98 MeV are emitted to nearly isotropic directions.<sup>2)</sup> When one of these  $\gamma$ -rays enters

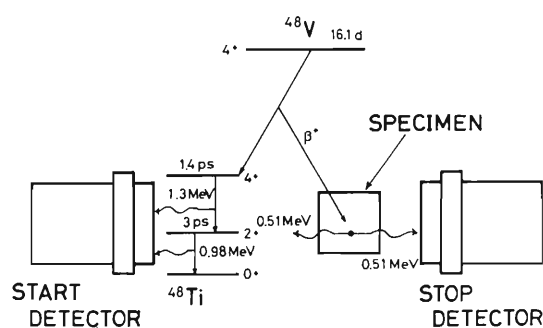


Fig. 1. Principle of lifetime measurement using  $^{48}\text{V}$  source.

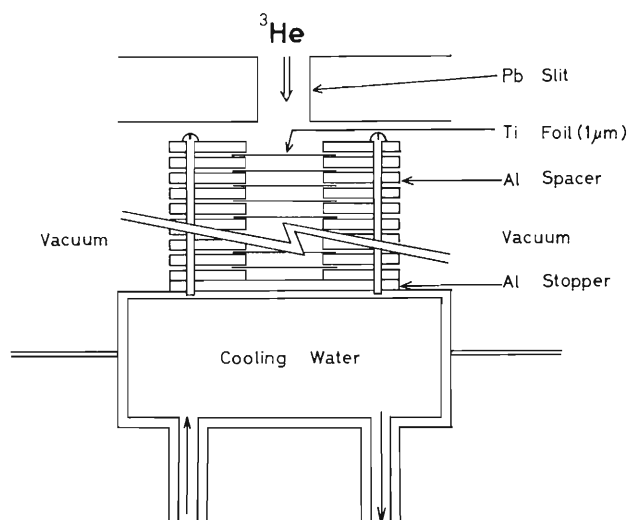


Fig. 2. Schematic drawing of the target for the production of  $^{48}\text{V}$  in Ti foil.

\* Department of Metallurgy and Materials Science, Faculty of Engineering, The University of Tokyo.

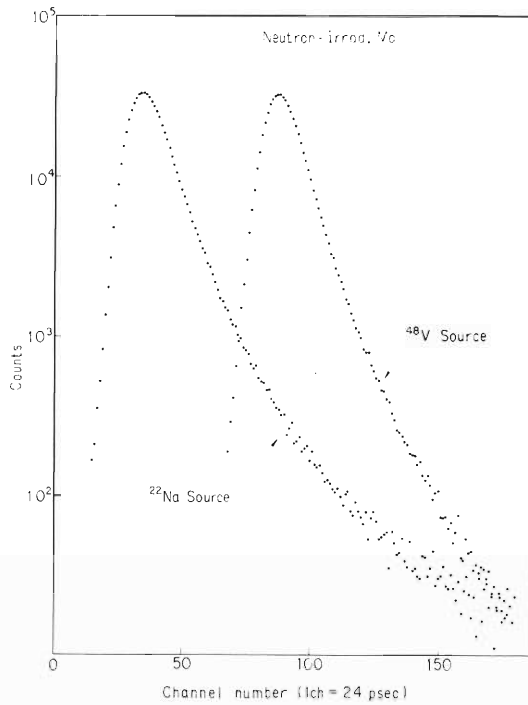


Fig. 3. Typical lifetime spectra of neutron-irradiated Mo measured with  $^{48}\text{V}$  source in  $1\mu\text{m}$  Ti foil and  $^{22}\text{NaCl}$  source wrapped with  $3.5\mu\text{m}$  Mylar.

into the start detector and the other into stop detector, a prompt component may be added to the original lifetime spectrum. This may degrade the spectra. The separation of this prompt component is possible in principle. Such an analysis is now in progress.

#### References

- 1) S. Tanigawa, K. Hinode, R. Nagai, M. Doyama, and N. Shiotani: IPCR Cyclotron Progr. Rep., 11, 111 (1977).
- 2) P. L. Roggenkamp, C. H. Pruett, and R. G. Wilkinson: Phys. Rev., 88, 1262 (1952).

## 7-10. Thermal Equilibrium Measurements of Positron Annihilation Line Shapes in KCl, KBr, and Ge

S. Tanigawa, K. Hinode, R. Nagai,  
M. Doyama,\* and N. Shiotani

Line shape measurements of spectra of positron annihilation radiations were carried out for KCl, KBr and Ge to study the interaction of positrons with lattice vacancies at thermal equilibrium. The experimental set-up was similar to the previous one.<sup>1)</sup> The energy resolution of Ge(Li) detector used was 1.45 keV at FWHM for 512 keV  $\gamma$ -ray from  $^{106}\text{Ru}$ .  $^{48}\text{V}$  produced in a  $1\ \mu\text{m}$  thick Ti foil by  $^3\text{He}$  bombardment was used as the positron source. Merits of this source are described in a preceding report.<sup>2)</sup>

Figures 1 and 2 show the temperature dependence of parameter H, counts of the central portion of the annihilation line normalized to the total counts, for KCl and KBr as a function of temperature. Both KCl and KBr show similar temperature dependence. In the low temperature region (region I) i.e. in the region below  $270^\circ\text{C}$  for KCl and below  $160^\circ\text{C}$  for KBr, H decreased linearly with temperature. In the intermediate region (region II) i.e.  $270^\circ\text{C} - 480^\circ\text{C}$  for KCl and  $160^\circ\text{C} - 450^\circ\text{C}$  for KBr, the increase of H was found. In high temperature region (region III), H again decreased. The increase of H in region II can be thought as the result of trapping of positrons by vacancies at thermal equilibrium. The slopes of H in regions I and III are nearly the same. If it is assumed that H in region I represents  $H_p$  (H in perfect crystal sites) and H in region III represents  $H_v$  (H in vacant sites) and that they have the same negative temperature dependence, one obtains Figs. 3 and 4 by the subtraction of  $H_p$  from the observed value of H. In this way, the formation energy of the Schottky pair (the pair of neutral cation and anion vacancies) was estimated to be  $2.00 \pm 0.1\ \text{eV}$  for KCl and  $1.84 \pm 0.1\ \text{eV}$  for KBr, respectively, by the use of trapping model of positrons by lattice defects.<sup>3)</sup> Although the interpretation of the negative temperature dependence of  $H_p$  and  $H_v$  has not yet been clear, it may be plausible that the lattice expansion effect and the temperature dependence of positronium states<sup>4)</sup> are involved.

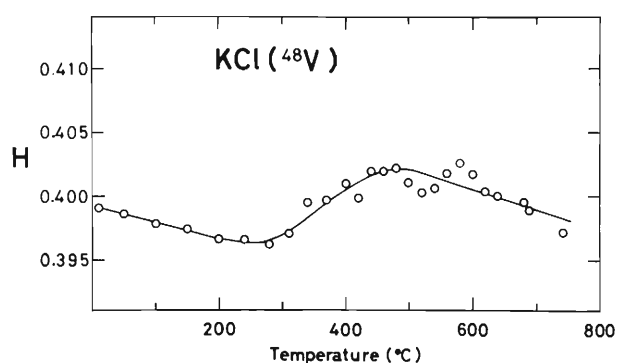


Fig. 1. The temperature dependence of H for KCl.

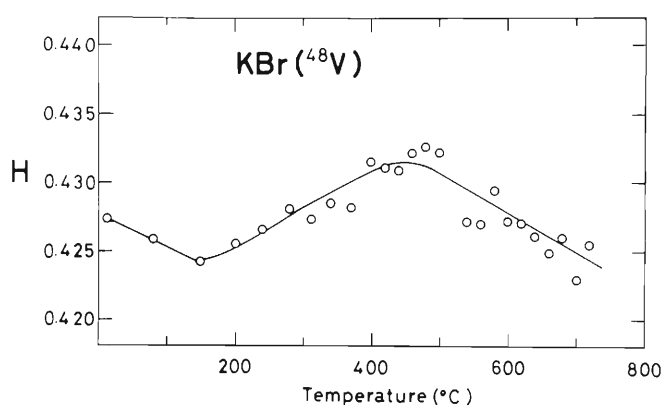


Fig. 2. The temperature dependence of H for KBr.

\* Department of Metallurgy and Materials Science, Faculty of Engineering, The University of Tokyo.

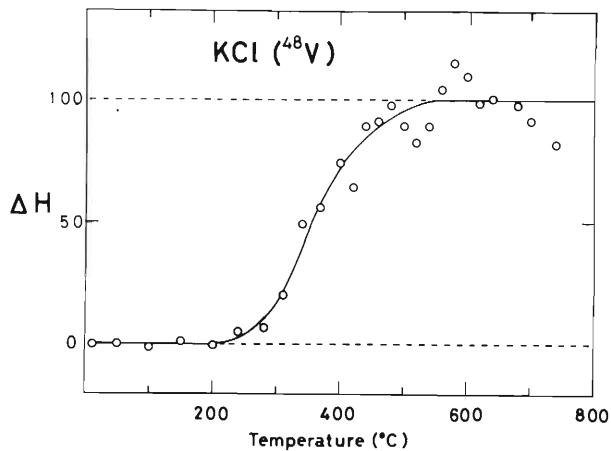


Fig. 3. The plot of  $\Delta H (= H - H_p)$  vs. temperature for KCl.

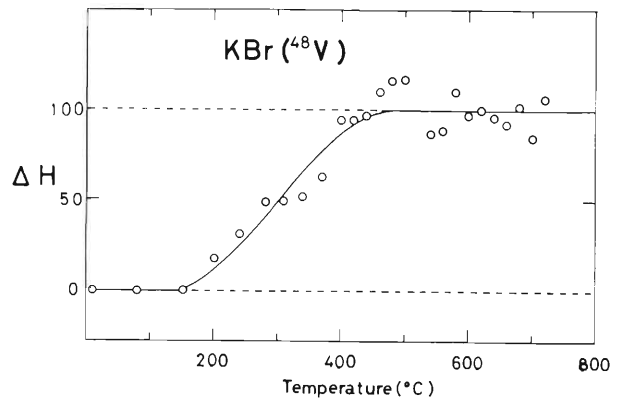


Fig. 4. The plot of  $\Delta H (= H - H_p)$  vs. temperature for KBr.

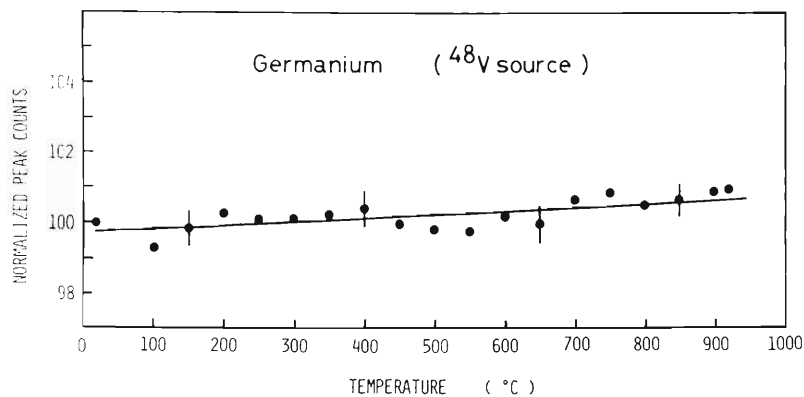


Fig. 5. The temperature dependence of the peak counts  $N(O)$  for Ge.

In Fig. 5, the peak counts  $N(O)$  of the annihilation spectrum in Ge is plotted as a function of temperature.  $N(O)$  shows a linear dependence on temperature, only slightly increasing with temperature, and no vacancy effect can be found. In Ge, the formation energy  $E_F^V$  and migration energy  $E_M^V$  of a vacancy have been expected to be about 1.9 eV<sup>5)</sup> and about 0.15 eV,<sup>6)</sup> respectively. The present results can be interpreted in either of the two alternative ways: (i) the concentration of vacancies  $c_v$  is too low to be detected by the positron technique, or (ii) positrons are not trapped by thermally created vacancies. The mobility of vacancies is expected to be very high because of low  $E_M^V$ . At the melting point a vacancy can migrate over  $5 \times 10^3$  lattice points during the lifetime of positrons. Therefore, even if  $c_v$  is small the number of chances for a positron to meet with vacancies is much enhanced. So, the case (ii) may be more probable. In Ga, similar results were reported by Segers et al.<sup>7)</sup> Due to the loosely packed crystal structure of Ge and Ga, it can be thought that vacancies do not provide strong attractive field for positrons.

## References

- 1) R. Nagai, S. Tanigawa, and M. Doyama: *Scripta Met.*, 10, 529 (1976).
- 2) K. Hinode, S. Tanigawa, M. Doyama, and N. Shiotani: *IPCR Cyclotron Progr. Rep.*, 11, 109 (1977).
- 3) K. Hinode, S. Tanigawa, and M. Doyama: *J. Phys. Soc. Japan*, 41, 2037 (1976).
- 4) T. Hyodo and Y. Takakusa: Abstract F 2 "The 4th Intern. Conf. Positron Annihilation", Helsingor, Denmark (1976).
- 5) A. Hiraki: *J. Phys. Soc. Japan*, 21, 34 (1966).
- 6) G. D. Watkins: *Lattice Defects in Semiconductors* (The Institute of Physics, London and Bristol), p. 1 (1975).
- 7) D. Segers, C. Dauwe, M. Dorikens, and L. Dorikens-Vanpraet: *Appl. Phys.*, 10, 121 (1976).

## 7-11. Effects of Irradiation Temperature, Prestrain, and Helium Concentration on the Helium Embrittlement of Type 316 Stainless Steel

H. Shinno, H. Shiraishi, R. Watanabe,\* H. Kamitsubo,  
I. Kohno, and T. Shikata

It is known that metals or alloys irradiated by fast neutrons show reduction of ductility at high temperature, which is thought to be due to helium produced by nuclear reactions in the materials. This effect is called "helium embrittlement", the study of which is urgently needed since it is one of the important restrictive factors in designing controlled thermonuclear reactors. The aim of this study is to obtain information on the mechanism of the helium embrittlement, and to utilize it for developing new metals and alloys which are highly resistant to neutron irradiation embrittlement.

The helium injection by the cyclotron was conducted, with the variation of the three following parameters which possibly affect the helium embrittlement; irradiation temperature, degree of cold-working, and helium concentration. The material used in this experiment was Type 316 stainless steel commercially obtained. It was cold-rolled and annealed alternately until it became 0.2 mm thick. From this thin plate, tensile test specimens were prepared by punching. Then, they were annealed for 30 min, at 1050°C in vacuum (solution-treatment). After that, some of the specimens were pre-elongated 5% using a tensile testing machine. Details of the helium injection procedure were described elsewhere.<sup>1)</sup> The concentration of helium injected into the specimens was 3 to 10 atomic ppm, and the irradiation was conducted at low (room temperature – 300°C) and high (750–900°C) temperature. The irradiated specimens were tensile tested by an Instron type testing machine with the strain rate of  $5 \times 10^{-4}$  sec<sup>-1</sup>. Specimens were tested at room temperature in air or at 750°C in vacuum of  $2 \times 10^{-6}$  torr. The fractured parts were cut from the tensile test specimens. Then, some pieces were annealed for 24 h at 1100°C in vacuum. These specimens were electrolytically jet polished and observed by a transmission electron microscope (abbreviated TEM hereafter).

Table 1 shows the results of the tensile tests. Each experimental value shows the average of the two tests. The results of the tests at room temperature show no effect of the helium injection, but those at 750°C show the reduction of ductility due to the helium injection in the case of the solution-treated specimens. The effects of varying the above three parameters were summarized as follows: 1) No effect of the irradiation temperature was found as far as this experiment is concerned. 2) Effect of the cold-working was remarkable. The specimens strained 5% before the helium injection did not show the reduction of ductility even at the test temperature

Table 1. Tensile test results on helium injected and control samples of Type 316 stainless steel at 750°C.

	Helium conc.	Irrad. temp.	Yield stress	Ultimate tensile stress	Uniform elong.	Total elong.
	(ppm)	(°C)	(kg/mm <sup>2</sup> )	(kg/mm <sup>2</sup> )	(%)	(%)
Solution- treated	0	r.t. –300 750–900 750–900	7.47	17.6	25.4	56.0
	3		7.96	18.6	26.2	33.3
	3		8.65	19.2	23.4	32.2
	10		8.76	17.2	15.9	18.5
5% pre- strained	0	r.t. –300 750–900 750–900	12.9	18.6	23.3	52.5
	3		12.6	19.3	38.1	48.0
	3		12.8	19.7	22.3	50.4
	10		12.1	18.8	22.4	51.5

\* National Research Institute for Metals.

of 750°C, though the solution-treated specimens showed notable helium embrittlement at the same testing condition. 3) As the helium concentration increased, the reduction of the ductility increased monotonically in the case of the solution-treated specimens, but the 5% prestrained specimens didn't show helium embrittlement up to the helium concentration of 10 ppm, as shown in Fig. 1.

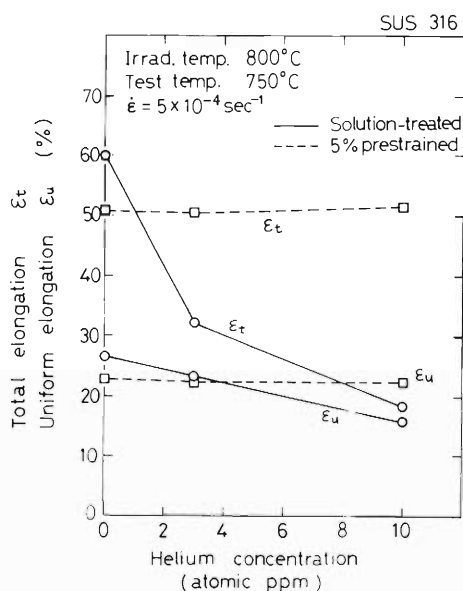


Fig. 1. Total and uniform elongations as functions of helium concentration for Type 316 stainless steel.

An observation by the TEM showed that no helium bubbles appear in the tensile tested specimens unless the heat treatment is carried out. In those samples helium probably exist as small bubbles which are smaller than the resolution limit of the TEM (50 Å). The precipitated carbides were not found in these specimens. Helium bubbles were found in the specimens annealed for 24 h at 1100°C, in the solution-treated specimens as well as in the specimens 5% prestrained before the helium injection.

Prestraining of 5% was very effective to improve the resistivity of Type 316 stainless steel to the helium embrittlement. In other words, dislocations were effective for the prevention of the helium embrittlement. The interaction between dislocations and helium bubbles is well known.<sup>2)</sup> Dislocations probably work as trapping sites of helium bubbles, and prevent the accumulation of helium to the grain boundaries. The reduction of ductility increased with the helium concentration in the case of solution-treated specimens. The results are consistent with the previous data.<sup>3)</sup> The tensile properties of the solution-treated specimens irradiated at different temperatures were very similar, and the TEM observation shows no microstructural differences. These results suggest that injected helium didn't escape from the specimens during the irradiation at temperatures as high as 900°C.

The effects of irradiation temperature, prestrain, and helium concentration on the helium embrittlement of Type 316 stainless steel are concluded as follows: 1) there is no effect of irradiation temperature, 2) 5% prestrained Type 316 stainless steel does not embrittle even in 10 ppm helium level, and 3) the ductility of solution-treated Type 316 stainless steel decreased as the helium concentration increased.

## References

- 1) R. Watanabe, H. Shiraishi, H. Shinno, H. Kamitsubo, I. Kohno, and T. Shikara: IPCR Cyclotron Progr. Rep., 10, 104 (1976).
- 2) W. Beeré: Scripta Metallurgica, 9, 999 (1975).
- 3) K. Matsumoto, T. Kataoka, M. Terasawa, M. Shimada, S. Nakahigashi, H. Sakairi, and E. Yagi: J. Nucl. Materials, 67, 97 (1977).

## 8. RADIOCHEMISTRY AND NUCLEAR CHEMISTRY

## 8-1. Charged Particle Activation Analysis for Surface Oxygen

T. Nozaki and M. Iwamoto

Charged particle activation analysis has begun to be applied to the study of surface oxygen on high purity substances. The apparatus we use is shown in Fig. 1. The sample in the form of two plates in intimate contact with each other is placed on the water-cooled target holder and set in the bombardment vessel which can be evacuated by oil-free pumps. The reactions of  $^{16}\text{O}(p, \alpha)^{13}\text{N}$  and  $^{16}\text{O}(^3\text{He}, p)^{18}\text{F}$  have been adopted for radioactivation, and the incident particle energy is so adjusted as to give the maximum cross section for the given reaction at the inside surfaces of the sample plates. After the bombardment, the inside surfaces of appropriate thickness are removed from the plates and their  $^{13}\text{N}$  or  $^{18}\text{F}$  content is measured.

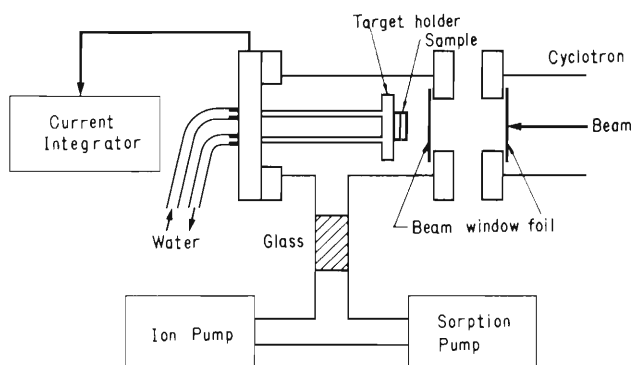


Fig. 1. Apparatus for radioactivation.

This method possesses the following advantages over other types of activation analysis and electron or X-ray spectrometries for surface analysis: (1) freedom from the nuclear recoil effect; (2) relative insensitiveness to the ambient atmosphere, and (3) capability of the determination of impurities in the surface layer of some thickness, such as an epitaxial layer. Only superficial oxygen in high vacuum can be measured by other methods, though information under usual atmospheric condition would often be more important. In the present method, it will be possible to study on the relationship between surface oxygen quantity and oxygen partial pressure of ambient atmosphere.

Our study is still in its beginning stage, and we have so far analysed only high-purity silicon after two different surface treatments. For the selection of the incident particle energy, the excitation curve of the activation reaction should be known precisely. The excitation function for the  $^{16}\text{O}(p, \alpha)^{13}\text{N}$  reaction was measured by the use of stacked Mylar foils. The result is shown in Fig. 2. As for the  $^{16}\text{O}(^3\text{He}, p)^{18}\text{F}$  reaction, reliable excitation function is known.<sup>1)</sup>

High-purity silicon rod (2 – 3 cm, diameter) after zone melting in vacuum was cut into disks (200 or 500  $\mu\text{m}$  thickness). This kind of silicon is known to contain less than 100 ppb of bulk

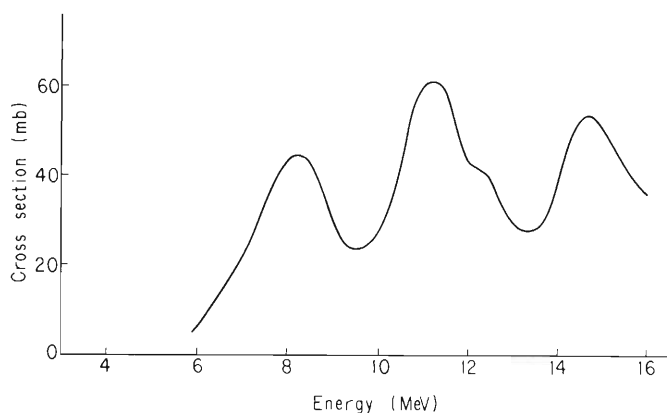


Fig. 2. Excitation function for the  $^{16}\text{O}(p, \alpha)^{13}\text{N}$  reaction.

oxygen.<sup>2)</sup> Thus, its surface layer with  $5 \text{ mg/cm}^2$  thickness contains less than 0.5 ng of bulk oxygen. The wafer was treated with a hot solution of NaOH (10%) or cold mixture of HF and  $\text{HNO}_3$  (1:3), washed in pure water with supersonic waves, and dried. Two of the wafers were set in the bombardment vessel and bombarded with charged particles ( $2\text{--}3 \mu\text{A}$ , 10 min) after the evacuation of the vessel. The vacuum condition was monitored remotely during the bombardment; it was usually  $1\text{--}2 \times 10^{-6}$  Torr throughout the bombardment, but sometimes degassing was observed at its beginning.

After the bombardment, a bar was stuck with wax on the outside surface of each wafer in order to facilitate manual operation for the removal of the inside surface layer by mechanical grinding. The inside surface of about  $5 \text{ mg/cm}^2$  thickness was then ground off on a glass plate with the aid of a small quantity of alumina powder and water. These powders were transferred altogether into a polyethylene tube for activity measurement. The annihilation radiation was measured with a well-type scintillation crystal and a single channel analyser, and its decay followed. The  $^{13}\text{N}$  or  $^{18}\text{F}$  component was always clearly identified in the decay curve. As activation standard, a stack of three thin Mylar foils was bombarded with the incident particles of the same energy as at the inside surface of the analytical sample and the inner foil of the three foils was used.

The result of analysis for float-zone silicon is shown in Table 1. It will be interesting to compare results of the present method with those of the on-line activation analysis in which protons from the  $^{16}\text{O}(d, p)^{17}\text{F}$  reaction are measured. We intend to analyse more variety of samples under different ambient atmosphere.

Table 1. Quantity of surface oxygen ( $\mu\text{g/cm}^2$ ).

Surface treatment Reaction	NaOH	HF-HNO <sub>3</sub>
$^{16}\text{O}(p, \alpha)^{13}\text{N}$	0.21	0.18
	0.17	0.15
	0.11	0.098
$^{16}\text{O}(^3\text{He}, p)^{18}\text{F}$		0.13
$\bar{\chi}$	0.16	0.14
$\sigma$	0.042	0.030

## References

- 1) T. Nozaki, M. Iwamoto, and T. Ido: Intern. J. appl. Radiat. Isotopes, 25, 393 (1974).
- 2) T. Nozaki, Y. Yatsurugi, and N. Akiyama: J. Electrochem. Soc., 117, 1566 (1970).
- 3) E. g., L. Gualia, G. Weber, D. David, J van Audenhove, and J. Pauwels: Eurisotop Rep. ITE-90-E C/III/436/76-E (1976).

8-2. Charge Spectra of  $^{198}\text{Hg}^{n+}$  Ions from the  $^{198}\text{Au}$  Decay

Y. Itoh, M. Aratani, and T. Nozaki

It is highly probable that charge spectra of recoil atoms from a thin surface layer of a solid is affected sensitively by the surface state. We expected the usefulness of charge spectrometry in surface science. We measured charge spectra of  $^{198}\text{Hg}^{n+}$  from  $\beta^-$  decay of  $^{198}\text{Au}$  in a thin gold film evaporated on high purity silicon for different film thicknesses. The effect of surface oxide layer on the charge spectra was compared with that on ESCA spectra.

The silicon substrate was a mirror-polished wafer (13 mm  $\times$  9 mm  $\times$  350  $\mu\text{m}$ ) with resistivity larger than  $10\Omega$  cm and with  $\langle 100 \rangle$  surface orientation. It was washed supersonically with acetone and etched in a 20% HF solution just before being installed in a vacuum evaporation chamber. Gold of 99.99% purity was evaporated onto the wafer from a conical basket heater of tungsten under a vacuum of  $1 \times 10^{-6}$  Torr at a rate of about  $0.2 \text{ nm sec}^{-1}$ . Gold films with 3.6 nm and 1.2 nm thicknesses were thus prepared. Their thicknesses were controlled by a ULVAC DTM-200 type monitor and certified by  $\gamma$ -ray spectrometry after neutron activation. The 3.6 nm sample was irradiated under a neutron flux of  $1.5 \times 10^{12} \text{ n cm}^{-2} \text{ sec}^{-1}$  for 12 h, and the 1.2 nm sample under  $3.5 \times 10^{13} \text{ n cm}^{-2} \text{ sec}^{-1}$  for 11.5 h. Their  $^{198}\text{Au}$  activities at the mass spectrometric measurements were 10  $\mu\text{Ci}$  and 83  $\mu\text{Ci}$ , respectively. The mass spectrometer we used was described previously.<sup>1)</sup> A voltage of 5 kV was applied to the sample for acceleration of the primary ion. Vacuum during the measurement was kept at  $1 \times 10^{-7}$  Torr.

Charge spectra of  $\text{Hg}^{n+}$  from the  $\beta^-$  decay are clearly observed as are shown in Fig. 1 for the two samples. For both samples  $\text{Hg}^{5+}$  was the most abundant and for the 1.2 nm sample  $\text{Hg}^+$  was of higher intensity than for the 3.6 nm sample. The difference of the charge spectra due to the gold film thickness can be attributed to the presence of other atoms than gold on the film. ESCA spectra of the two samples are shown in Fig. 2, which indicates the presence of more

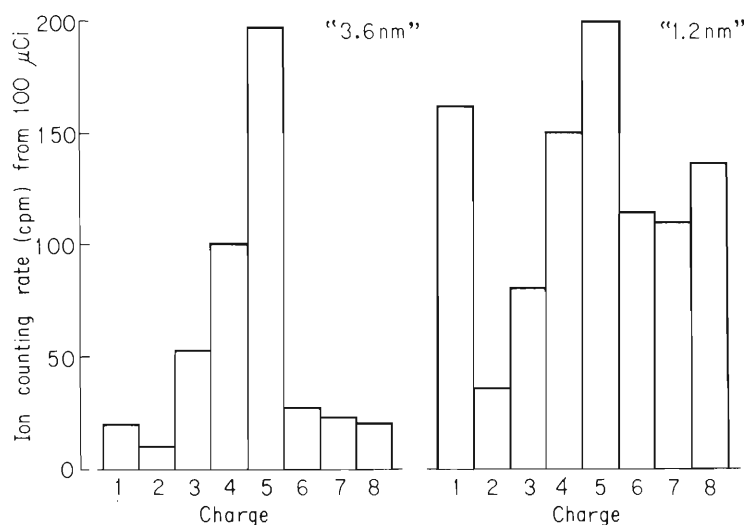


Fig. 1. Charge spectra of  $\text{Hg}^{n+}$  for the two samples.

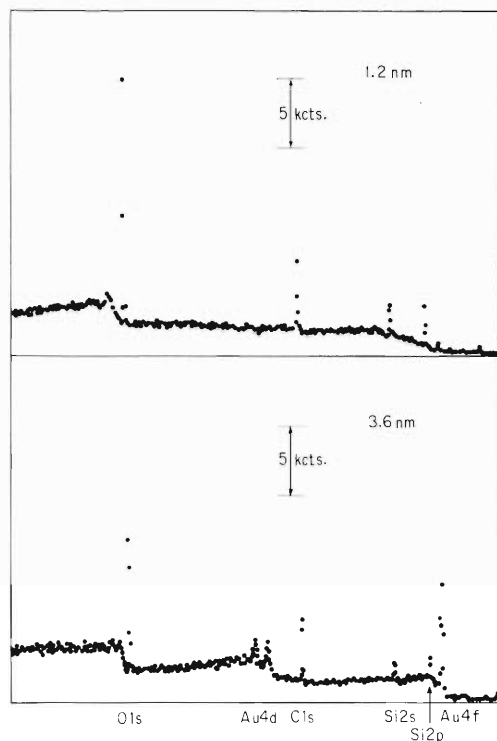


Fig. 2. ESCA spectra of the gold films evaporated on silicon.

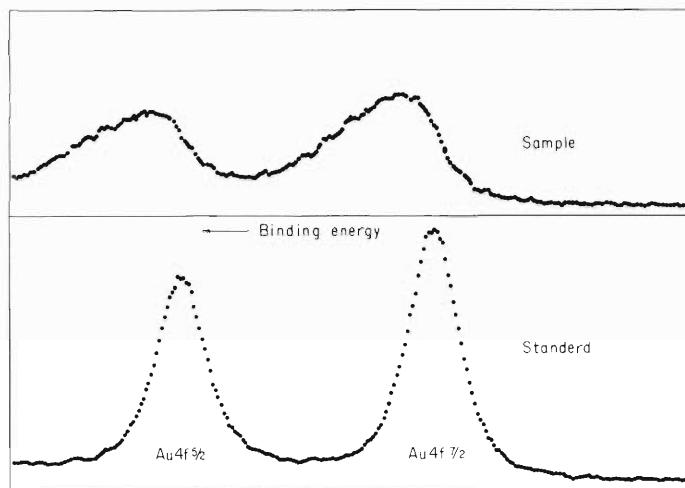


Fig. 3. Shift of binding energy for the gold film.

amount of  $\text{SiO}_x$  on the 1.2 nm sample than on the 3.6 nm sample. The Au4f peaks of the ESCA spectra observed in detail are shown in Fig. 3 for the 1.2 nm sample. These charge and ESCA spectra suggest that the gold surface was covered with a  $\text{SiO}_x$  film formed from surface oxygen atoms and Si atoms having diffused through the gold film, and that metallic gold atoms are mixed with gold atoms of higher binding energies. It is natural that the charge of  $\text{Hg}^{II+}$  is partly neutralized in the  $\text{SiO}_x$  film. The increase of  $\text{SiO}^+$  and decrease of  $\text{Hg}^{5+}$  after exposure of the

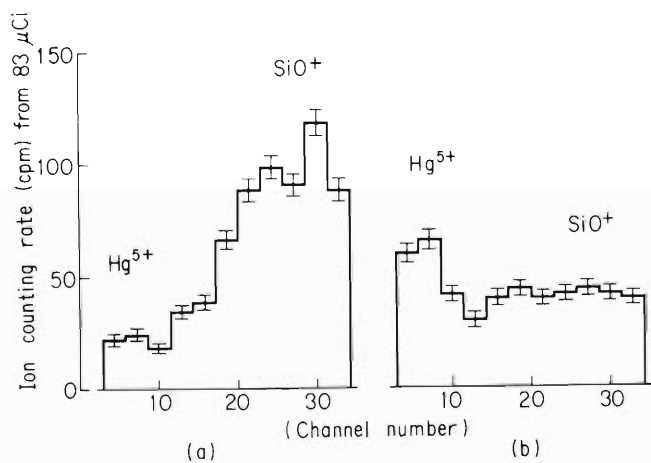


Fig. 4. Change of charge spectra of  $\text{SiO}^+$  and  $\text{Hg}^{5+}$  by air exposure.

- (a) after exposure to air.  
 (b) after preservation under  $1 \times 10^{-7}$  Torr.

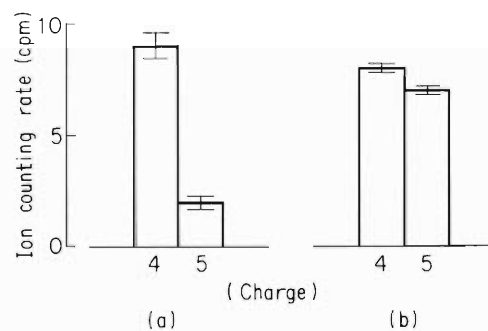


Fig. 5. Change of charge spectra of  $\text{Hg}^{4+}$  and  $\text{Hg}^{5+}$ .

- (a) after exposure to air.  
 (b) after preservation under  $1 \times 10^{-7}$  Torr.

sample to air are shown in Fig. 4 (a), and the decrease of  $\text{SiO}^+$  and increase of  $\text{Hg}^{5+}$  after its preservation under  $1 \times 10^{-7}$  Torr are shown in Fig. 4 (b). The increase of  $\text{Hg}^{4+}$  after air exposure is shown in Fig. 5 (a) and (b); this is attributed to the partial neutralization of  $\text{Hg}^{5+}$  into  $\text{Hg}^{4+}$  in the oxide film. We also detected considerably high peaks which can be assigned to  $\text{HgSiO}_3^{2+}$  and  $\text{HgSiO}_3^{3+}$ .<sup>2)</sup>

These results indicate that charge spectrometry is applicable profitably to surface research in combination with other techniques, such as, ESCA, SEM, and AES.

## References

- 1) Y. Kawana and M. Aratani: *Inst. J. Mass Spectrom. Ion Phys.*, 10, 493 (1972).
- 2) D. G. Engle: *J. Opt. Soc. Am.*, 11, 599 (1925).

## 9. RADIATION CHEMISTRY AND RADIATION BIOLOGY

## 9-1. Emission Spectra of a KBr Single Crystal Irradiated with Heavy Ions at 4.2 K. Time-Dependent Spectra

K. Kimura and M. Imamura

Emission and absorption spectra of a KBr single crystal irradiated with heavy ions have been found to differ substantially from those irradiated with X- or  $\gamma$ -rays at 4.2 K; the outlines of these results were reported in a previous report.<sup>1)</sup>

One of the significant results was that an intensity ratio of the  $\sigma$ - to  $\pi$ -emission increases with increasing LET: 2.1 for X-rays, 6-7 for He-ions, and 10-12 for C-ions. This year, extensive studies were made on this problem by using pulsed heavy-ion beams and stationary beams as well.

For pulse irradiation, 24 MeV He-, 85 MeV C-, and 95 MeV N-ion beams were chopped to pulses of about 40  $\mu$ s in width and the time-dependent emission spectra of a KBr single crystal were recorded at 4.2 K by using an optical multichannel analyzer (OMA); set-up of the measurements is shown in Fig. 1.

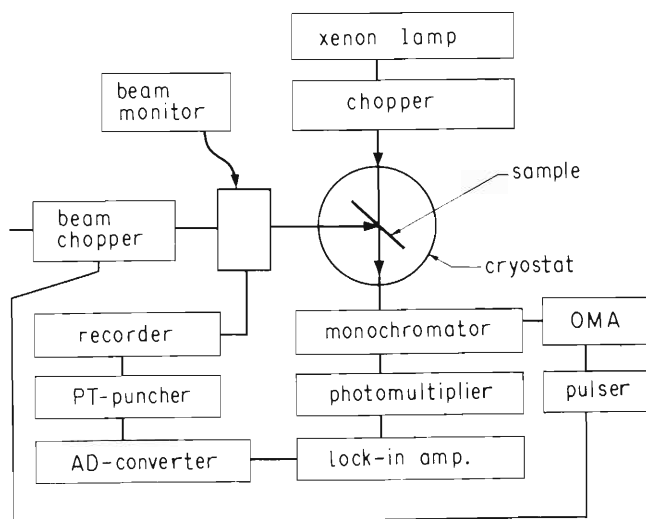


Fig. 1. Experimental set-up.

Figure 2 shows the time-dependent  $\pi$ -emission spectra observed for a KBr single crystal irradiated with 85 MeV C-ions at 4.2 K. The half-life of the emission is 0.2 ms, which is a little longer than 0.1 ms obtained by Pooley and Runciman<sup>2)</sup> using electron pulses.

The intensity ratios of  $\sigma$ - to  $\pi$ -emission,  $I_{\sigma}/I_{\pi}$ , are plotted as a function of absorbed dose of He-, C-, and N-ions in Fig. 3. Since the emission intensities decrease with increasing dose, this result indicates that the  $\sigma$ -emission intensities for heavy-ion irradiated crystals are depressed to a greater extent than are the  $\pi$ -emission intensities at a dose larger than 2  $\mu$ C.

From these results, the increased values of  $I_{\sigma}/I_{\pi}$  in heavy-ion irradiations may presumably be

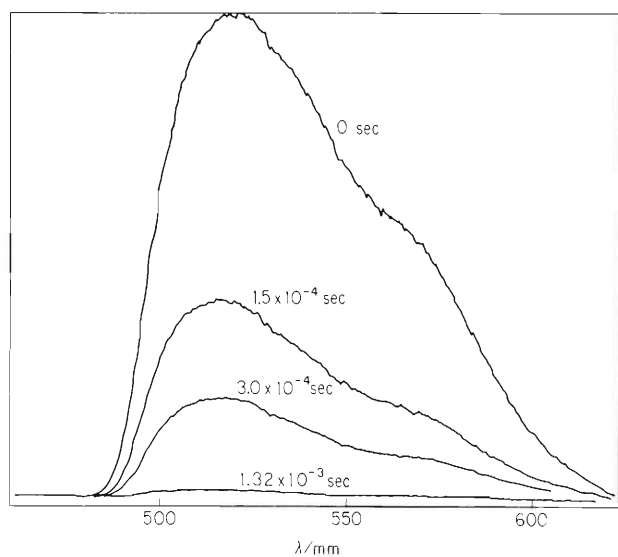


Fig. 2. Time-dependent spectra of  $\pi$ -emission of a KBr single crystal irradiated with 85-MeV C-ions at 4.2 K.

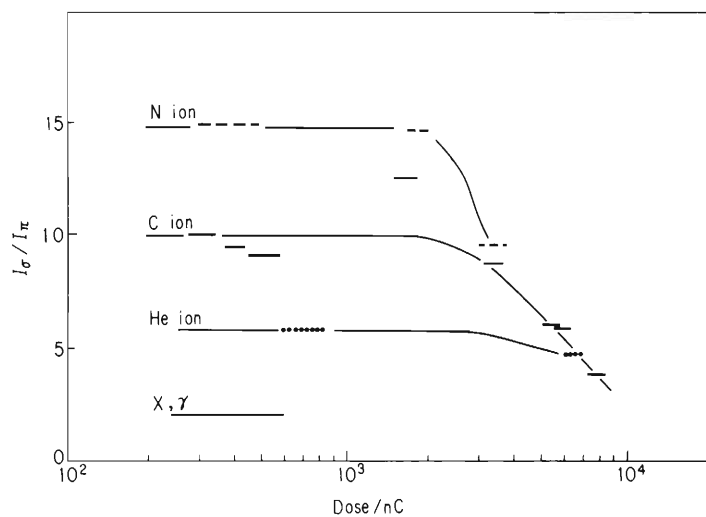


Fig. 3. Dose dependence of  $I_{\sigma}/I_{\pi}$ .

ascribed, not to an increase in nonradiative decay of the  $\pi$ -exciton, but to an increase in radiative decay of the  $\sigma$ -exciton or to higher initial concentration of the  $\sigma$ -exciton than that of the  $\pi$ -exciton.

## References

- 1) K. Kimura and M. Imamura: IPCR Cyclotron Progr. Rep., 10, 112 (1976).
- 2) D. Pooley and W. A. Runciman: J. Phys., C3, 1815 (1970).

## 9-2. Yields of Trapped Electron Produced by Heavy-Ion Irradiation in Ethanol Glass at 77 K

A. Kira, M. Matsui, and M. Imamura

Glassy ethanol at 77 K was subjected to heavy-ion irradiation. Electrons which escape geminate recombination are trapped in the glass and exhibit a characteristic absorption band in the visible region as shown in Fig. 1.

A comparative study has been made on the yields of trapped electrons produced by irradiation of three different heavy ions, He-, C-, and N-ions whose incident energies were 18, 58, and 60 MeV, respectively. Ethanol was frozen on a Suprasil quartz plate attached to a copper plate cooled by liquid nitrogen. Optical densities of irradiated glasses were measured on a Cary 14RI spectrophotometer.

Figure 1 shows the absorption spectrum for ethanol glass irradiated with C-ions. The absorption band does not precisely coincide with that for  $\gamma$ -irradiated ethanol glass at 77 K, unless the  $\gamma$ -irradiated glass was slightly warmed before measuring spectrum, as shown Fig. 1.

This spectral shift, which was also observed for He- and N-ion irradiated glasses, may suggest a temperature rise along heavy-ion tracks in glasses. No absorption band assignable to dielectrons was observed; they might be expected to form in densely ionized regions.

In Fig. 2, optical densities of trapped electrons at 525 nm divided by the range of a heavy-ion are plotted against absorbed dose. The yields of trapped electrons are not linear with dose. Similar dose dependence of the yield has also been observed for the  $\gamma$ -irradiated glass and regarded as being due to electron capture by free radicals whose concentration increases with increasing dose.

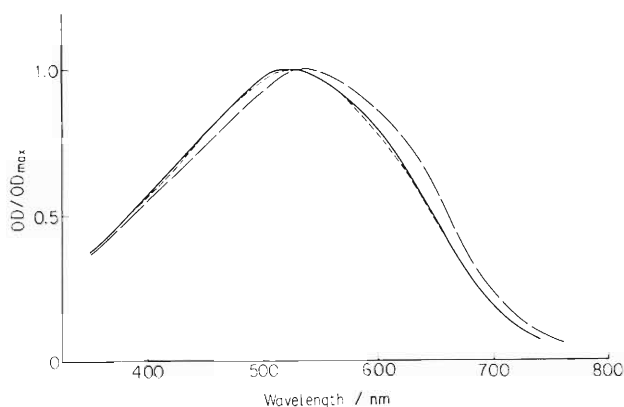


Fig. 1. Absorption spectra of trapped electrons in ethanol glasses irradiated with C-ion (solid curve); irradiated with  $\gamma$ -rays at 77 K (broken curve) and after subsequent warming (dotted curve).

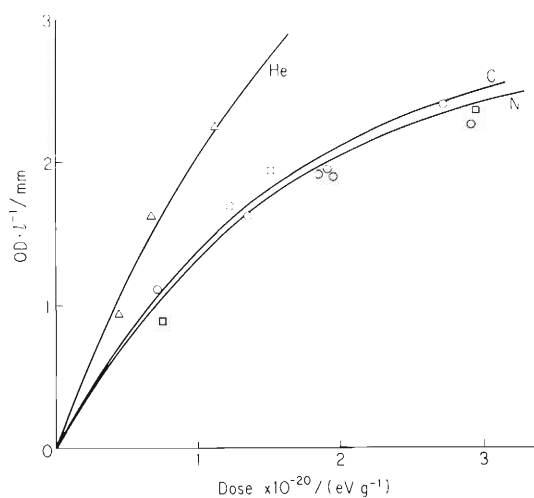


Fig. 2. Trapped-electron yields ( $OD^{525}$  divided by the range of heavy ion) as a function of dose:  $\Delta$ , He;  $\circ$ , C;  $\square$ , N. The curves represent Eqn. 1 by using the values for  $G_e$  and  $\alpha G_R$  listed in Table 1.

On the assumption of the electron capture by free radicals, the concentration of trapped electrons,  $[e_t^-]$ , at a dose of  $r$  is given by

$$[e_t^-] = \frac{G_e}{\alpha G_R} \left\{ 1 - \exp\left(\frac{-10\alpha G_R r}{N_A}\right) \right\} \quad (1)$$

where  $G_e$  and  $G_R$  are G-values of trapped electrons and free radicals, respectively;  $\alpha$  is an electron-capture constant of free radicals;  $N_A$  is the Avogadro number.

In Fig. 2, curves are drawn to give best fit to the experimental values by taking the values for  $G_e$  and  $\alpha G_R$  as listed in Table 1. The value of  $G_e$ , which is the G-value for electrons escaping geminate recombination and trapped in glasses, decreases with increasing LET of radiations. If the value of the capture constant,  $\alpha$ , is assumed independent of radiation quality,  $G_R$  increases slightly with increasing LET.

Table 1. The values for  $G_e$  and  $\alpha G_R$ .

Radiation	$G_e$	$\alpha G_R \times 10^{-2} (M^{-1})$
N	1.1	3.6
C	1.1	3.6
He	1.7	3.3
$\gamma$	3.6	3.1

### 9-3. Further Study of High LET Effect on Template/Primer Activity of DNA in situ

S. Kitayama, F. Yatagai, and A. Matsuyama

We are interested in the difference between radiochemical lesions in DNA caused by low and high LET radiations. The primer/template activity of DNA in bacterial cells can be assayed in situ by the preparation of their permeable cells which can incorporate deoxyribonucleoside triphosphates into DNA.<sup>1)</sup> Irradiation at low LET range, e.g.  $\gamma$ -ray irradiation, induces mostly single-strand breakage in duplex DNA in vivo as well as in vitro. About 30% of such single-strand breaks has free 3'-OH terminal which are priming sites for DNA polymerase. This is one of the reason why  $\gamma$ -ray irradiation stimulates DNA synthesis in permeable cells of bacteria.<sup>2)-4)</sup> As indicated in the previous report,<sup>5)</sup> it is very plausible that high LET irradiation would induce lesions in both strands at or near the complementary strands of duplex DNA. Since DNA which has damages in both strands proximate each other is a poor template/primer for DNA polymerase, it would be expected that high LET irradiation caused a different effect on the DNA synthesis in the permeable cells from that of low LET irradiation. However, no quantitative difference in stimulatory effect between irradiations with  $\gamma$ -rays and N-ions (2.9 MeV/amu) was observed.<sup>5)</sup> This might be due to the irradiation by secondary electrons ejected from the track core whose range is  $\sim 1 \mu\text{m}$  in water and is comparable to the size of bacterial cells. The instability of permeable cells held at room temperature during the irradiation with N-ions is also one of the experimental difficulties. So, we have improved the irradiation apparatus to keep the temperature near  $0^\circ\text{C}$  by circulation of ice-water during irradiation. To avoid the formation of dewdrops on the surface of the samples that cause serious change of LET, permeable cells were spread on a membrane filter and were held on a filter paper pad. Moreover, the samples were covered with a thin filter (polycarbonate filter,  $\sim 5 \mu\text{m}$  in thickness) to eliminate the effect of secondary electrons ejected from air layer in front of the samples. Dose-response curves of M. radiodurans KD830 (Ade<sup>-</sup>, DNAase<sup>-</sup>)<sup>6)</sup> to  $\alpha$ -particles (4.78 MeV/amu) and  $^{60}\text{Co}$   $\gamma$ -rays are shown in Fig. 1. DNA synthetic activity in the permeable cells was compared after the irradiation within shoulder doses of both high- and low-LET radiations. The relative synthetic rates of DNA

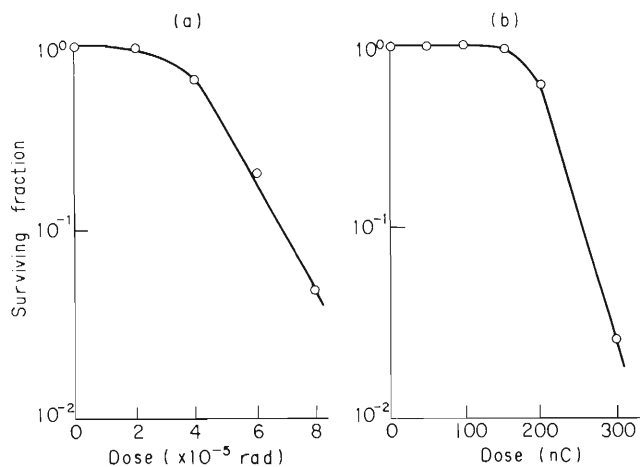


Fig. 1. Dose-response curves of M. radiodurans to  $\gamma$ -rays from  $^{60}\text{Co}$ (A) and  $\alpha$ -particles (4.78 MeV/amu)

Cells of M. radiodurans KD830 at logarithmic phase of growth were washed with M/15 phosphate buffer(pH 7) and irradiated under cooling with ice-water as described in the text.

during initial 20 min of incubation at 37°C are shown in Fig. 2. Although secondary electrons ejected from the track core of  $\alpha$ -particles in water traverse much less than those of secondary electrons produced by N-ions,  $\alpha$ -particles showed stimulatory effect on the DNA synthesis in the permeable cells. However, the stimulation by  $\alpha$ -particles was less than that by  $\gamma$ -rays especially at the low doses. This result may imply that  $\alpha$ -particles as well as  $\gamma$ -rays induce single-strand breaks which have free 3'-OH, a priming site for DNA polymerase, but percentage of such terminal in whole lesions is somewhat different between two radiations. In other words, if any characteristic biological lesions are induced by irradiation of high LET particles utilizing track-segment method, such lesions would be accompanied by many lesions similar to those induced by low LET radiations such as  $^{60}\text{Co}$   $\gamma$ -rays.

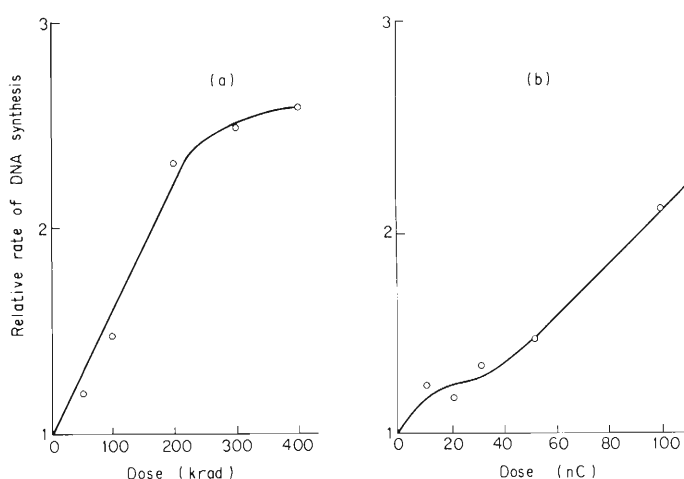


Fig. 2. Irradiation effect of  $\gamma$ -rays(A) or  $\alpha$ -particles(B) on DNA synthesis in permeable cells of *M. radiodurans*.

Permeable cells of *M. radiodurans*<sup>1)</sup> were irradiated with (A)  $\gamma$ -rays from  $^{60}\text{Co}$  or (B)  $\alpha$ -particles (4.78 MeV/amu) under cooling with circulating ice-water. Vertical lines indicate relative rate of DNA synthesis observed at initial 20 min of incubation at 37°C.

## References

- 1) S. Kitayama and A. Matsuyama: *Biochim. Biophys. Acta*, 418, 321 (1976).
- 2) D. Billen and G. R. Hellermann: *ibid*, 361, 166 (1974).
- 3) D. Billen and G. R. Hellermann: *ibid*, 383, 379 (1975).
- 4) E. A. Waldstein and R. B. Setlow: *ibid*, 442, 154 (1976).
- 5) S. Kitayama, F. Yatagai, and A. Matsuyama: *IPCR Cyclotron Progr. Rep.*, 9, 98 (1975).
- 6) S. Kitayama and A. Matsuyama: *Mut. Res.*, 29, 327 (1975).

## 9-4. Induction of Mutations in Bacteriophage $\phi$ X 174 by $\alpha$ -particles and N-ions

F. Yatagai, S. Kitayama, and A. Matsuyama

It has been reported that the inducible post-replication repair (sos repair) of overlapping daughter strand gaps appears to be necessary for UV-induced mutagenesis to occur in a *uvrA* strain of *E. coli*.<sup>1)</sup> The overlapping daughter strand gaps are thought to be refractory to both excision and recombination repair. In fact, the fraction of mutants measured in a population of UV-irradiated phage  $\phi$ X 174 increased with increasing UV-dose when the mutation frequency was assayed on host cells which had been irradiated with a small dose of UV, while there was no increase when unirradiated cells were used for assay.<sup>2)</sup> On the other hand,  $\gamma$ -irradiation of the amber mutants induced the reverse mutation to wild-type even when unirradiated host cells were used for assay.<sup>3)</sup> Higher efficiency was obtained under irradiation in the presence of oxygen than under anoxic condition.<sup>3)</sup> Our interest is to find out the relation between the damages in single-strand DNA by charged particles and the induction of mutation.

In the present study, *am3* mutant of  $\phi$ X 174 has been irradiated with  $\alpha$ -particles and N-ions in order to determine the efficiency of reverse mutation to (pseudo) wild-type. The phage samples which were spread on a thin filter and covered with another filter of the same type, were irradiated with charged particles. After irradiation the surviving fraction was assayed on *E. coli* HF4714, which has an amber suppressor (*su*<sup>+</sup>). Wild-type and pseudo wild-type revertants were assayed on both UV-irradiated and unirradiated *E. coli* C<sub>N</sub> (*su*<sup>-</sup>). Further experimental details will be given elsewhere.

Figures 1 and 2 show that survival curves of the amber mutant are almost exponential against fluence for  $\alpha$ -particles and N-ions of 4.6 MeV/amu. For both ion beams, the efficiency of

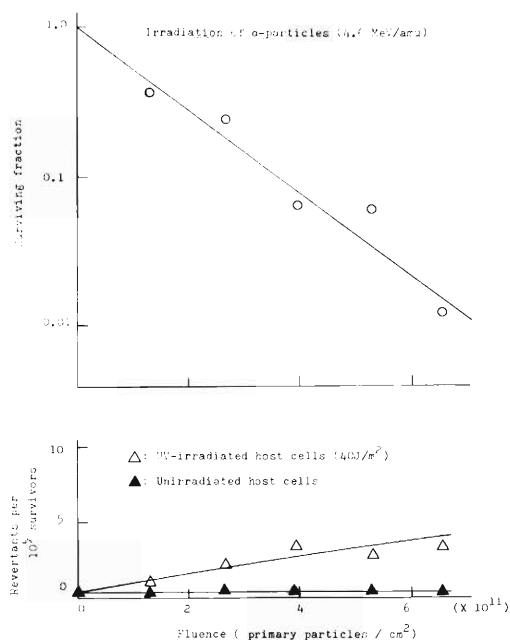


Fig. 1. Induction of mutation in  $\phi$ X 174 *am3* by  $\alpha$ -particles (see text.):

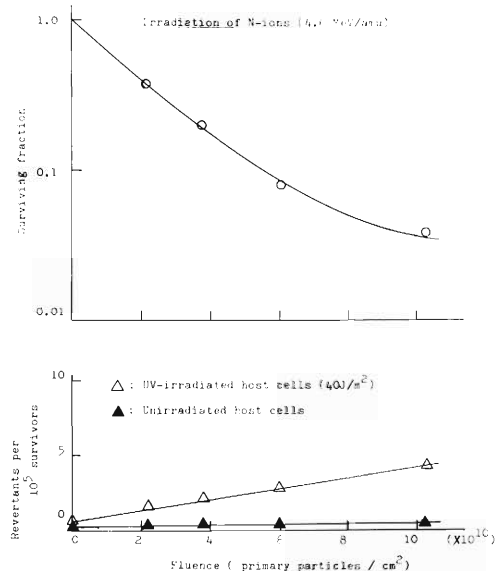


Fig. 2. Induction of mutation in  $\phi$ X 174 *am3* by N-ions (see text.).

induction to (pseudo) wild-type, which was assayed on both UV-irradiated and unirradiated host cells, shows the same mode of dose-dependence as that of UV mentioned above (Figs. 1 and 2). Almost no difference in the efficiency was found between  $\alpha$ -particles and N-ions (Figs. 1 and 2); the efficiency for these charged particles was rather low but of the same order as that of UV- or  $\gamma$ -irradiation obtained in our separate experiments (Table 1). Since DNA strand breakage in  $\phi$ X 174 is lethal, this result suggests that irradiation with charged particles induces not only strand breakage but also many other premutational damages in DNA, comparable with that of UV per lethal hit.

Table 1. Comparison of efficiencies of mutation induction caused by different types of radiation.

Type of Radiation	Revertants per $10^5$ Survivors*
UV-light	5.6
$\gamma$ -rays	3.9
$\alpha$ -particles	2.5
N-ions	2.5

\* Survival of am3 mutant of  $\phi$ X 174 was assayed on E. coli C HF 4714 ( $su^+$ ) for different radiations indicated above. To determine the values of revertants/ $10^5$  survivors for 10% survival, the irradiated phages were infected to uv irradiated E. coli C ( $su^-$ ).

## References

- 1) S. G. Sedgwick: *Mutat. Res.*, 41, 185 (1976).
- 2) J. F. Bleichrodt and W. S. D. Verheij: *Molec. gen. Genet.*, 135, 19 (1974).
- 3) J. F. Bleichrodt and W. S. D. Verheij: *Int. J. Radiat. Biol.*, 25, 505 (1974).

## 9-5. Inactivation of Ribonuclease A in Aqueous Solution by Cyclotron Beams

Y. Hattori, F. Yatagai, and A. Matsuyama

In the framework aiming to reveal specific features of the damage on biological substances caused by heavy-ion radiations, experiments have been started on the inactivation of bovine pancreatic ribonuclease A (EC 2.7.7.16) by cyclotron beams.

Ribonuclease (RNase) A, of which purified commercial preparation is easily available, has been used as an object of radiation biochemistry by many investigators. Recently Lynn<sup>1)</sup> reported that RNase A was protected against  $\gamma$ -radiolytic destruction when the enzyme was associated with deoxyribonucleic acid (DNA) under conditions such that the nucleic acid was not acting as a scavenger. Using the same model systems the effect of N-ion radiation on RNase A activity is studied. The present experiment is done, with its attention particularly focused on the modification of radiosensitivity of RNase by the associated DNA.

Sample solutions to be irradiated were prepared according to Lynn<sup>1)</sup>: (1)  $5 \times 10^{-6}$  M aqueous solution of RNase A (crystalline preparation of Sigma Chemical Co.); (2)  $5 \times 10^{-6}$  M RNase A plus salmon sperm DNA (10  $\mu\text{g}/\text{ml}$ ) -- RNase-DNA complex; (3)  $5 \times 10^{-6}$  M RNase A in 0.1 M  $\text{NaClO}_4$  plus DNA (10  $\mu\text{g}/\text{ml}$ ) -- dissociated complex. The irradiation of the solutions was done in Pyrex glass cells with a window of aluminum foil (20  $\mu$ ) under agitation in the presence of atmospheric oxygen at room temperature. The ion beam was shot into the solution through the cell window. Energies of N-ions and  $\alpha$ -particles entering solutions were 4.5 and 4.6 MeV/amu, respectively. Irradiated RNase solutions were subjected to the assay of residual activity according to the method of Anfinson et al.<sup>2)</sup> with modification.

Experimental results obtained so far are as follows: (a) RNase A, when associated with DNA, was not protected against the inactivation by N-ions, but showed higher sensitivity than without DNA; (b) the enzyme activity was protected when DNA and  $\text{NaClO}_4$  were added in the solution. These relationships are shown in Fig. 1.<sup>3)</sup> Thus the effect of DNA added to RNase solution in

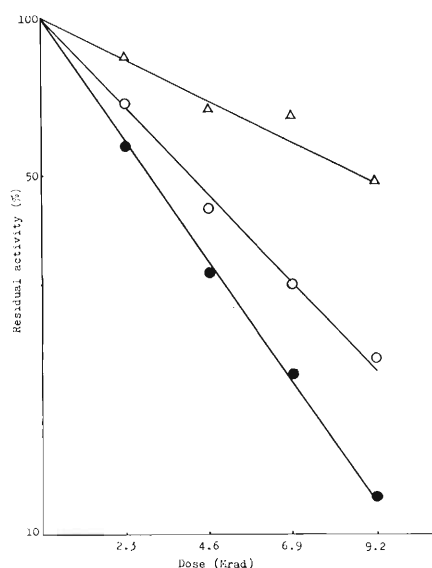


Fig. 1. Inactivation of RNase A in aqueous solution by N-ion irradiation at room temperature under the presence of air.

○  $5 \times 10^{-6}$  M RNase A; ●  $5 \times 10^{-6}$  M RNase A + DNA (10  $\mu\text{g}/\text{ml}$ ); △  $5 \times 10^{-6}$  M RNase in 0.1M  $\text{NaClO}_4$  + DNA (10  $\mu\text{g}/\text{ml}$ ). Energy of N-ions entering solution was 4.5 MeV/amu.

case of N-ion irradiation was found to be different from that in  $\gamma$ -irradiation.<sup>1)</sup> Data on the effect of  $\alpha$ -particles are not yet sufficiently accumulated. Further experiments are in progress.

#### References

- 1) K. R. Lynn: *Radiat. Res.*, 66, 644 (1976).
- 2) C. B. Anfinsen, R. R. Redfield, W. L. Choate, J. Page, and W. R. Carroll: *J. Biol. Chem.*, 207, 201 (1954).
- 3) Y. Hattori, F. Yatagai, and A. Matsuyama: 20th Annual Meeting of Japan Radiat. Res. Soc., Sendai, Oct. (1977).

## 9-6. The Effects of High LET Radiations on Mammalian Cells

S. Sawada, M. Sasaki, S. Okada, F. Yatagai,  
I. Kaneko, and A. Matsuyama

For clinical radiation therapy, fundamental studies on cellular level are requested to get information on the radiobiological effects of ionizing radiations to be used. The advantages of high LET radiations, such as  $\alpha$ -particles and heavy ions, over x-rays and  $\gamma$ -rays because of their high RBE values in inducing cell death are well known.

Studies with cultured Chinese hamster cell V-79 were carried out last year to solve the technical problems which do not arise in x- or  $\gamma$ -ray experiments. The following programs are now in progress on the basis of the last year's results.

(1) Molecular autoradiography of high LET radiation-induced double-strand cuts of DNA and their rejoining in mouse leukemic L5178 cells.

DNA was labeled by incubating the exponentially-growing cells for 60 minutes with  $^3\text{H}$ -thymine. The labeled cells suspended in a cold medium were placed on a Sartorius membrane filter and most of the medium was thus removed. Immediately before irradiation, the cells on the filter were covered with a polycarbonate filter to exclude the effects of secondary electrons which emerged into the air layer above the cells. The cells were irradiated at room temperature with  $\alpha$ -particles and N-ions accelerated in the cyclotron (4.6 MeV/amu at sample).

Immediately after irradiation, the polycarbonate filter was removed and the Sartorius filter with cells was placed in a stainless steel holder. The holder was capped and the cells were then removed by flushing through the filter from a syringe attached to the cap. Nearly 50% of the cells on each filter were thus collected.

To examine the rejoining of broken DNA strands, cells, together with the Sartorius filter, were placed in a plastic culture dish and incubated in a  $\text{CO}_2$ -incubator at  $37^\circ\text{C}$ . At various times of post-irradiation incubation, the cells were removed from the filter by the method described above.

For DNA fiber autoradiography, an aliquot of cell suspension, containing approximately 3000 cells, was placed on a glass slide, which was coated with a mixture of gelatin and chromium sulfate, and mixed with sodium lauryl sulfate. The slides were left at room temperature to lyse the cells. The lysate was then spread over the surface of the slide. The slides were dipped into Sakura NR-M2 liquid emulsion. After drying, the slides were kept in a light-proof box with silica gel and allowed to expose at  $4^\circ\text{C}$  for at least 5 months in the dark-room (The slides are still allowed to expose at the present time).

(2) Production of chromosome aberrations by  $\alpha$ -rays in human lymphocytes.

Peripheral blood lymphocytes obtained from normal person were layered between polycarbonate films and exposed to  $\alpha$ -rays (4.6 MeV/amu) accelerated in the cyclotron. The irradiated cells were collected and incubated with the phytohemagglutinin-containing medium for 50 h so that chromosomes were analysed in the first post-irradiation mitosis. The  $\alpha$ -irradiation efficiently produced chromosome aberrations such as dicentrics, rings, and acentric fragments.

Although the experiments are now at the preliminary stage, the  $\alpha$ -rays are about 1.6 and 4.8 times more efficient in producing dicentrics and rings than 2 MeV and 14 MeV fast neutrons, respectively. Detailed analysis regarding the distribution of dose in lymphocyte nuclei and dose-yield kinetics of chromosome aberrations are now in progress.

(3) Setting up of the equipments and apparatuses for preservation of cultured mammalian cells.

As a constant supply system of cells for the further investigation to confirm the preliminary results obtained last year on the dose effectiveness curves of Chinese hamster cell V-79 for the studies on recovery from the cell damages caused by high LET radiations, and for comparative studies on strand breakage of DNA in the mammalian cells due to heavy ions as well as other types of radiations, a sterilizing room, a CO<sub>2</sub>-incubator, and a liquid nitrogen vessel were set up and the preservation of the cultured mammalian cells was started.

## 10. PREPARATION OF RADIOISOTOPES AND LABELED COMPOUNDS

## 10-1. Production of Radioisotopes and Preparation of Labelled Compounds for Medical and Agricultural Use

T. Nozaki, Y. Itoh, M. Iwamoto, T. Karasawa,  
K. Fukushi, T. Irie, and T. Hara\*

Studies have been continued on the production of  $^{77}\text{Br}$  and  $^{73}\text{Se}$  and the preparation of radiohalogen derivatives of cholesterol and phenylalanine. The excitation curves for the formation of  $^{77}\text{Br}$  or  $^{73}\text{Se}$  by the following reactions have been measured up to proton energy of about 50 MeV and  $^3\text{He}$  and  $\alpha$ -particle energy of about 40 MeV, together with those for simultaneous formation of  $^{76}\text{Br}$  or  $^{72}\text{Se}$ : (1)  $\text{Se} + \text{p} \rightarrow ^{77}\text{Br}$ , (2)  $\text{Br} + \text{p} \rightarrow ^{77}\text{Kr} \rightarrow ^{77}\text{Br}$ , (3)  $^{75}\text{As}(\alpha, 2\text{n})^{77}\text{Br}$ , (4)  $^{75}\text{As}(\text{p}, 3\text{n})^{73}\text{Se}$ , (5)  $\text{Ge} + ^3\text{He} \rightarrow ^{73}\text{Se}$ , and (6)  $\text{Ge} + \alpha \rightarrow ^{73}\text{Se}$ . The targets used for the measurement were  $\text{BaSeO}_3$ ,  $\text{NaBr}$ ,  $\text{Mg}_2\text{As}_2\text{O}_7$  and metallic germanium in the form of plate made by pressing or of film made by sedimentation or evaporation onto aluminum foil. They were stacked and bombarded. The cyclotron was used for all the reactions. In the proton reactions, the FM cyclotron of the Institute for Nuclear Study, University of Tokyo, was also used for the extension of the measurement energy range from 16 MeV up to 52 MeV.

The excitation curves are shown in Figs. 1 to 5 for the targets of natural isotopic composition. Since the proton energy of this cyclotron was always 52 MeV, notable spreading of proton energy

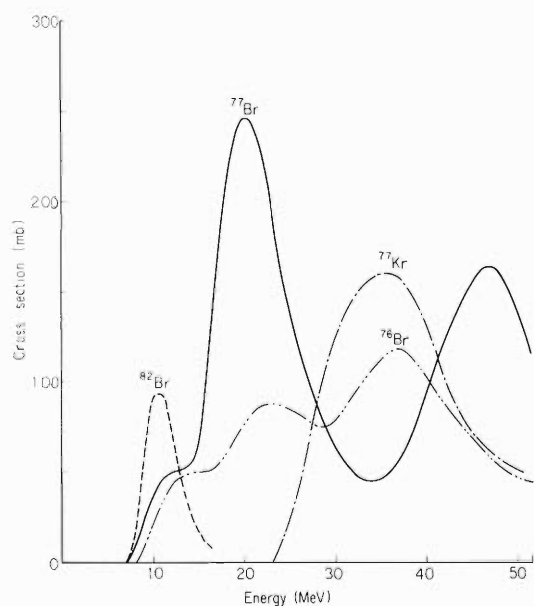


Fig. 1. Excitation curves for the reactions of  $\text{Se} + \text{p} \rightarrow ^{77}\text{Br}$ ,  $^{76}\text{Br}$ ,  $^{82}\text{Br}$ , and  $\text{Br} + \text{p} \rightarrow ^{77}\text{Kr} \rightarrow ^{77}\text{Br}$ .

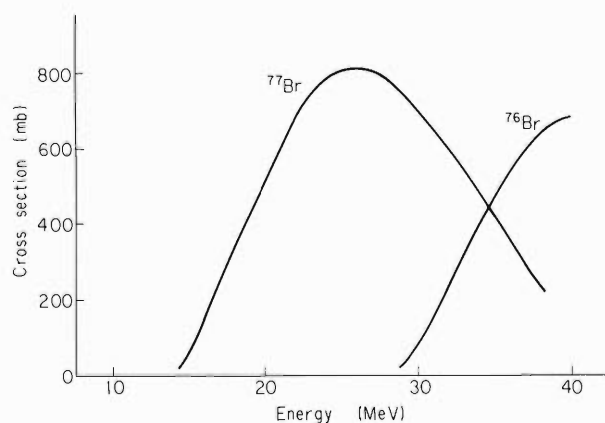


Fig. 2. Excitation curves for the reactions of  $^{75}\text{As}(\alpha, 2\text{n})^{77}\text{Br}$  and  $^{75}\text{As}(\alpha, 3\text{n})^{76}\text{Br}$ .

\* National Nakano Chest Hospital.

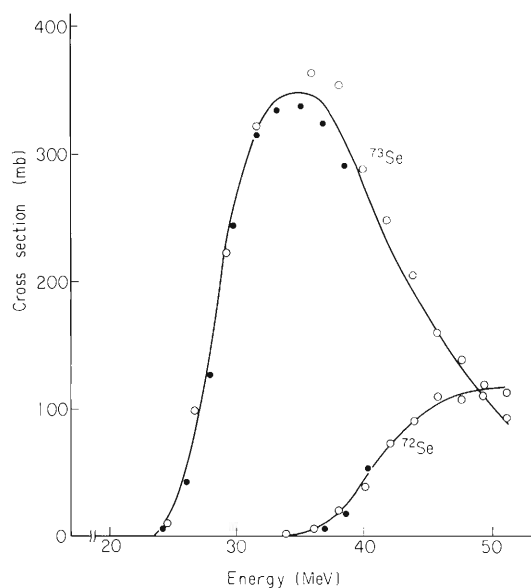


Fig. 3. Excitation curves for the reactions of  $^{75}\text{As}(p, 3n)^{73}\text{Se}$  and  $^{75}\text{As}(p, 4n)^{72}\text{Se}$ .

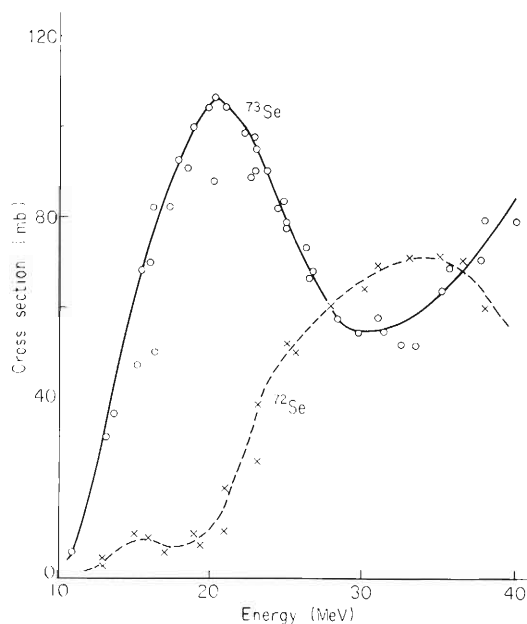


Fig. 4. Excitation curves for the reactions of  $\text{Ge} + {}^3\text{He} \rightarrow {}^{73}\text{Se}, {}^{72}\text{Se}$ .

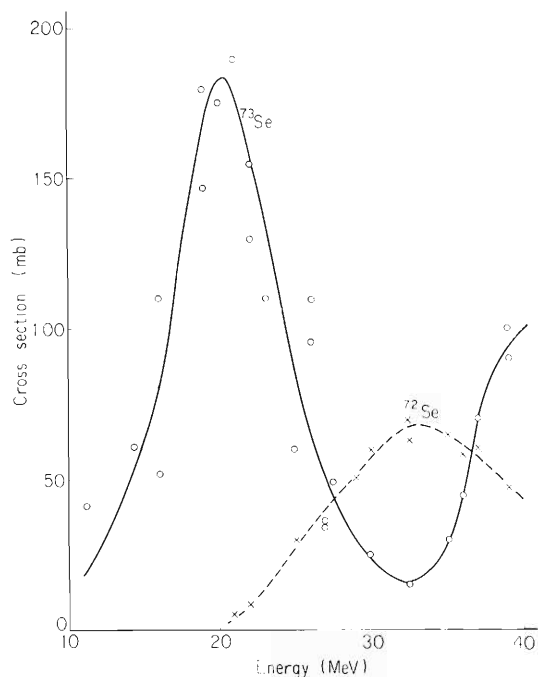


Fig. 5. Excitation curves for the reactions of  $\text{Ge} + \alpha \rightarrow {}^{73}\text{Se}, {}^{72}\text{Se}$ .

took place inevitably when it degraded down to 30 MeV or less in the stack. Hence, the excitation curves for Reactions 1 and 4 involve some uncertainty in the energy region between 16 MeV and about 30 MeV. We intend to examine the curves in this energy region by the use of another machine.

Target substances of arsenic and selenium convenient for isotopic production were looked for, together with methods of chemical separation of the product nuclides. As the arsenic target, AlAs and fused cake of  $\text{NaAsO}_2 - \text{Na}_2\text{B}_4\text{O}_7$  have been found useful in addition to  $\text{As}_2\text{O}_3$ . For selenium, fused cakes of  $\text{SeO}_2 - \text{NaOH}$  and  $\text{SeO}_2 - \text{NaOH} - \text{Na}_2\text{B}_4\text{O}_7$  have been regarded as convenient.

Procedures have been set up for the chemical separation of  $^{77}\text{Br}$  and  $^{73}\text{Se}$  from AlAs target. Chemical purity of carrier-free  $^{77}\text{Br}$  distilled from a sulphuric acid solution of arsenic targets was examined by neutron activation analysis. Successive treatment of the distillate with iron powder and  $\text{BaCO}_3$  has proved to be effective for the removal of trace arsenic. The product  $^{77}\text{Br}$  in carrier-free and salt-free state is utilized for the tracer study of bromine in rain water as well as for organic labelling.

Solvent extraction of red selenium has been found suitable for the separation of  $^{73}\text{Se}$ , when the addition of a small amount (e.g.,  $60\ \mu\text{g}$ ) of carrier is permissible. The product  $^{73}\text{Se}$  has been used for the biosynthesis of selenomethionine- $^{73}\text{Se}$ . Carrier-free separation of  $^{73}\text{Se}$  from arsenic targets is now under study. Coprecipitation of  $^{73}\text{Se}$  with elementary tellurium will offer a good procedure, the  $^{73}\text{Se}$  and tellurium being separated by ion exchange.

Chemical behaviour of carbon-halogen bonds of radio-halogen derivatives of cholesterol and phenylalanine in animal body has been studied in collaboration with the National Institute of Radiological Sciences. Doubly labelled compounds have profitably been made use of. Although interesting phenomena have been observed, some further time will be needed before we can present our results with confidence.

10-2. Biosynthesis of Selenomethionine-<sup>73</sup>Se

K. Ogawa,\* K. Taki, T. Nozaki, and M. Okano

Selenomethionine-<sup>75</sup>Se is widely used in nuclear medicine for diagnostic visualization of pancreas by scintigraphy,<sup>1)</sup> though the biological half-life of <sup>75</sup>Se is so long as to give noticeable internal radiation exposure to the patient. The replacement of selenomethionine-<sup>75</sup>Se by selenomethionine-<sup>73</sup>Se is thus desired, <sup>73</sup>Se being a positron emitter of 7.1 h half-life. This nuclide will become more useful with progressive development of the positron emitter localization technique. Hence, a convenient method should be sought for rapid synthesis of selenomethionine-<sup>73</sup>Se in a state suitable for intravenous injection. We reported previously the preparation of this compound starting from the <sup>3</sup>He bombardment of germanium.<sup>2)</sup>

We have continued the study of the biosynthesis of selenomethionine-<sup>73</sup>Se using the proton bombardment of arsenic. The yield of <sup>73</sup>Se for the <sup>75</sup>As (p, 3n) <sup>73</sup>Se reaction is described separately in the present volume of this report.

Aluminium arsenide (AlAs) and arsenous oxide (As<sub>2</sub>O<sub>3</sub>) were used as the target (1.4 g/cm<sup>2</sup> thickness). They were bombarded by protons from the synchro-cyclotron of the Institute for Nuclear Study, University of Tokyo, through aluminium plates for the degradation of the proton energy from its initial value of 52 MeV to 43 MeV.

The bombarded AlAs target (about 4 g) was transferred into a 500 ml flask containing H<sub>2</sub>SeO<sub>3</sub> (0.1 mg) as carrier and water (10 ml). The flask was equipped with a reflux condenser and warmed. Then HCl-HNO<sub>3</sub> (1:3, 10 ml) was added in small portions to the flask, and the warming continued until the beginning of NO<sub>2</sub> evolution. After the solution was left to cool, insoluble particles suspending in it was removed by centrifugation and millipore filtration. As for the As<sub>2</sub>O<sub>3</sub> target, it was simply dissolved in dil. HCl. Selenium-73 in the solution was then precipitated as red selenium by reduction with H<sub>2</sub>NNH<sub>2</sub>·HCl (20% solution, 3 ml) under heating for 5 to 10 min. After cooling to room temperature, the selenium was extracted into CS<sub>2</sub> and the extract washed with water. By evaporation of the solvent, the <sup>73</sup>Se was obtained as red selenium in satisfying radiochemical purity. The separation time was about 2.5 h, and the yield about 70%.

The red selenium was dissolved in HNO<sub>3</sub>, and the excess acid removed by evaporation under reduced pressure. The residue was dissolved in water, and the pH of the resultant solution adjusted to 7 with NaOH. This solution, as described in our previous report,<sup>2)</sup> was added to the fermented liquor on which TO-1 strain had been grown for 10 h, and the strain further cultivated for 6 h. The strain was then harvested by centrifugation, and its protein fraction hydrolyzed by being kept with 6 N HCl in a sealed tube at 120°C for 5 h. About 80% of the <sup>73</sup>Se was found in the hydrolysate.

Radio-selenium compounds in the hydrolysate was then separated by starch column chromatography with the solvent of 1:2:1 mixture of n-butanol, n-propanol and 0.1 N HCl. The effluent was collected (0.1 ml/min elution rate) in 0.5 ml portions by an automatic fraction collector. The selenomethionine fraction was identified by activity measurement and by paper

\* Department of Hygiene, Kitazato University.

chromatography on Toyo Filter Paper No. 51 with the solvent of 3:1:1 mixture of n-butanol, acetic acid and water. Authentic selenomethionine prepared by chemical synthesis<sup>3)</sup> was used for the paper-chromatographical identification of the selenomethionine-<sup>73</sup>Se ( $R_f = 0.55$ ).

The time required for the preparation was about 20 h after the end of the bombardment, and 32.3  $\mu$ Ci of selenomethionine-<sup>73</sup>Se was obtained from 2.3 mCi of <sup>73</sup>Se separated from the arsenic target.

#### References

- 1) M. Brau: *Biochem. Biophys. Acta*, 49, 389 (1961).
- 2) T. Nozaki, S. Ambe, Y. Itoh, M. Iwamoto, T. Karasawa, M. Okano, K. Fukushi, T. Irie, T. Hara, and K. Taki: *IPCR Cyclotron Progr. Rep.*, 10, 120 (1976).
- 3) D. L. Klayman and T. S. Griffin: *J. Amer. Chem. Soc.*, 95, 197 (1973); G. Z. Dansky: *Arkiv Kemi*, 9, 550 (1962).

## 10-3. Separation of Carrier-free Radioactive Krypton

M. Aratani and T. Nozaki

We have undertaken some experiments to find out a simple and efficient way of separating carrier-free radioactive krypton in a form convenient for practical use and fundamental study. For trapping the krypton with this intention, glass beads were thought to be preferable to any other strong adsorbents. The radionuclides,  $^{77}\text{Kr}^*$  and  $^{79}\text{Kr}$ , were produced by the reactions,  $^{79}\text{Br}(\text{p}, 3\text{n})^{77}\text{Kr}$  and  $^{79}\text{Br}(\text{p}, \text{n})^{79}\text{Kr}$ , respectively, the target being NaBr powder and pellet.

## Separation system 1:

A cylindrical brass vessel with 50  $\mu\text{m}$  stainless steel foil window in the central part was made and used in all the following steps: i) charged particle bombardment of the powder target under water cooling of the vessel bottom; ii) dissolution of the bombarded powder by the addition of water; iii) removal of the radioactive krypton from the solution by helium bubbling. The radioactive krypton was carried by the helium, passed through NaOH- $\text{Na}_2\text{SO}_3$  to be made free from radiobromines, byproducts of the reactions, and then trapped on glass beads at liq.  $\text{N}_2$  temperature.

## Separation system 2:

The same vessel was also used for the pellet target. The bombarded pellet was put in the vessel, and treated similarly as above.

## Separation system 3:

A box-type vessel with demountable stainless steel windows on both sides was made for the bombardment to optimal amount of target material. Radioactive krypton evolving from the target in the course of bombardment was transferred from the vessel with a helium gas stream and was trapped on the glass beads at liq.  $\text{N}_2$  temperature. After the bombardment a small amount of water was introduced into the vessel. The resultant solution was then transferred into a gas-washing vessel with a sintered glass inlet, by being pushed with helium gas. The krypton in the solution was expelled with helium bubbles of small diameters formed at the sintered glass, and was trapped similarly.

The three systems above were of open types. Though they had the advantage of simplicity, some of disadvantages were observed. For example, the radioactivity of the trapped krypton gradually decreased after its maximum, indicating inherent difficulty in getting krypton quantitatively. A separation system of closed type was also developed.

## Separation system 4:

The separation system of closed type is illustrated in Fig. 1. The following three parts were connected with stopcocks, abbreviated as SC, (1, 2, 3 and 4 in Fig. 1) between them: (A) an empty gas-washing vessel with sintered glass inlet at room temperature, (B) an evacuated NaOH- $\text{Na}_2\text{SO}_3$  trap kept at dry ice temperature, and (C) an evacuated glass-beads trap kept at liq.  $\text{N}_2$  temperature. A bombarded pellet was put in (A), which was evacuated by an aspirator pump

\* This was produced by using F. M. Cyclotron of Institute for Nuclear Study, The University of Tokyo.

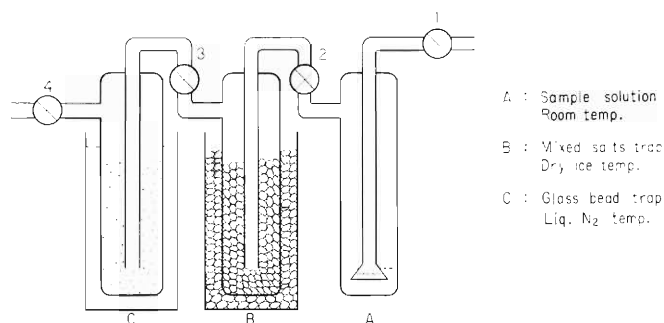


Fig. 1. The closed type system for separation of carrier-free radioactive krypton.

through SC 1. Then, it was shut off. Thus, the entire system was made closed. With an injector, a minimal amount of water was introduced up to the level slightly higher than the sintered glass inlet of (A). After the pellet was dissolved, SC 2 was opened. Due to the differences of pressure and temperature between the vessel and the trap, the radioactive krypton in the solution was carried away with small bubbles formed automatically at the sintered glass, and was trapped on the NaOH-Na<sub>2</sub>SO<sub>3</sub> cooled to the dry ice temperature. After SC 2 was shut off, SC 3 was opened. Thus, the radioactive krypton was moved to and trapped on the glass beads.

Distribution of the radioactive krypton in three vessels after the separation is shown in Table 1. Collection efficiency in case of the closed system is seen to amount to nearly 100%. In the practical separation, care should be taken to maintain the contents of the traps at the desired temperatures, especially in the closed system. It is concluded that simple and efficient separation of radioactive krypton can be carried out by a glass-beads trap at liq. N<sub>2</sub> temperature in open or closed type.

Table 1. The distribution of the radioactive krypton after separation.

He bubble diameter	Type	NaBr soln. (%)	NaOH-Na <sub>2</sub> SO <sub>3</sub> (%)	Glass beads (%)
4 mm	O*	42.6	—	57.4***
8 mm	O	64.3	7.9	27.8
30-20 μm	O	5.9	10.4	>83.7
30-20 μm	O	15.0	14.7	70.3
—	C**	1.5	2.1	96.4****

\* open,           \*\* closed

\*\*\* <sup>77</sup>Kr,       \*\*\*\* <sup>79</sup>Kr

## 11. RADIATION MONITORING

## 11-1. Routine Monitoring

K. Igarashi, I. Sakamoto, and I. Usuba

Results of routine radiation monitoring carried out on the cyclotron from April 1976 to March 1977 are described.

No remarkable change in leakage radiation and residual activities was observed during this period.

## (1) Surface and air contamination

The surface contamination has been kept below  $10^{-6}$   $\mu\text{Ci}/\text{cm}^2$  on the floor of cyclotron room and the underground passage, and below  $10^{-7}$   $\mu\text{Ci}/\text{cm}^2$  in the experimental areas, hot laboratory and chemical laboratories. The contamination was wiped off twice a year, and after each decontamination, the higher level contamination could be reduced below  $10^{-7}$   $\mu\text{Ci}/\text{cm}^2$ .

When the accelerating chamber was opened, slight contamination of the air in the cyclotron room was observed. The value of radioactivity concentration ( $\beta$ - $\gamma$ ) was  $10^{-13}$   $\mu\text{Ci}/\text{cm}^3$ .

Tritium still remained in the accelerating chamber since the last triton acceleration in December 1970. The tritium concentration of the air in the chamber was still of the order of  $10^{-4}$ – $10^{-5}$   $\mu\text{Ci}/\text{cm}^3$ .<sup>1)</sup> As the air in the chamber is purged completely before overhauling, air contamination was not found in the cyclotron room.

Table 1. Annual exposure dose received by the cyclotron workers from April 1976 to March 1977.

Workers	Number of persons			Collective dose (man-mrem)
	Dose undetectable	10–100 (mrem)	>100 (mrem)	
Operators		3	4	1030
Nuclear physicists	15	7	1	380
Accelerator physicists	2	5		140
Physicists in other fields	6	4		130
Nuclear chemists		2	2	500
Radiation chemists	3			
Biological chemists	4			
Health physicist	1			
			Total	2180

Average annual dose per person: 36.9 mrem.

Maximum individual annual dose: 270 mrem.

(2) Drainage

The radioactive concentration of the drain water from the cyclotron building was found to be of the order of  $10^{-7}$   $\mu\text{Ci}/\text{cm}^3$ . The total quantity of activities in the aqueous release in this period was about 3  $\mu\text{Ci}$ , which decreased by about one-eighteenth compared with that of the last year.

(3) Personnel monitoring

The external exposure dose received during the present period, by all cyclotron workers to whom the  $\gamma$ -ray and, to some of them also, the neutron film badge are provided, is shown in Table 1. The collective  $\gamma$ -ray dose to all workers was 2180 man-mrem, while those due to thermal and fast neutron exposures were too small to be detected.

The dose to the cyclotron workers increased by about 7% compared with that of the last year. In this period the dose to the cyclotron operators was 1030 man-mrem, which was 47.2% of the dose of cyclotron workers.

Reference

- 1) S. Fujita and I. Sakamoto: IPCR Cyclotron Progr. Rep., 9, 108 (1975).

## 11-2. Leakage Radiation Measurement at the Underground Passage

I. Sakamoto

Leakage radiation during operation of the cyclotron at the underground passage of the cyclotron building was measured. Leakage dose received during the present period by the  $\gamma$ -neutron film badges which are left at the underground passage, is shown in Table. 1. The ratio of  $\gamma$  dose to thermal neutron dose was 3.0.

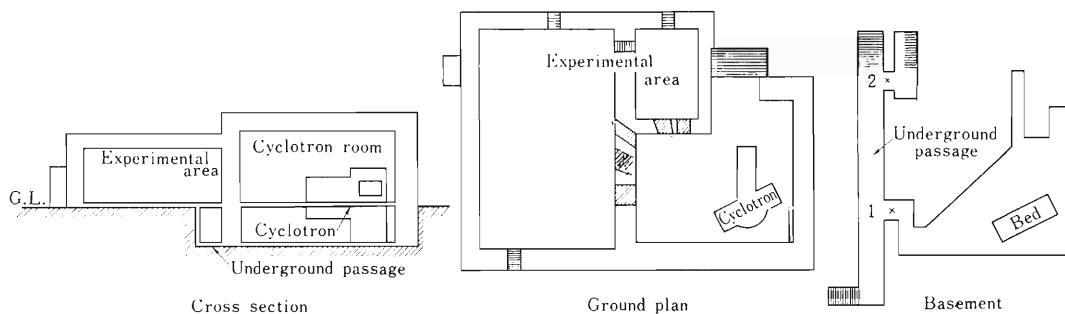
Among the dose at the point No. 1 measured every month, the maximum dose of 1690 mrem was observed in September, which was 44.6% of the total dose in this period. In this month, the machine time allotted for deuteron acceleration was 91 h, which was 34.0% of total scheduled beam time in this period.

Fast neutron dose was measured with another film badge at the point No. 1 in July 1977. In this case, the values of fast neutron dose,  $\gamma$  dose and thermal neutron dose were 20 mrem, 770 mrem and 290 mrem, respectively. It is shown that fast neutron dose was small compared with  $\gamma$ -ray and thermal neutron dose at the underground passage.

Table 1. Leakage radiation dose (in mrem) at the underground passage from April 1976 to March 1977

Radiation	Point of observation*	
	1	2
$\gamma$ -ray (mrem)	2840	180
Thermal neutron (mrem)	950	60
Total (mrem)	3790	240

\* See the figure shown below.



## 12. HEAVY ION LINEAR ACCELERATOR PROJECT

### 12-1. Status of the Constructional Work

M. Odera

Installation of the high voltage ion source terminal and the first resonator was completed in December 1976. Vacuum pressure of  $3 \times 10^{-7}$  Torr was obtained for the resonator in January 1977. The 500 kV unit was tested to its full voltage in March. However, humidity from the concrete wall of the injector room was still high and the leakage current as high as  $300 \mu\text{A}$  was observed at times. Electric dehumidifiers were installed and the state is improving.

The first high power amplifier and its power supply were installed in April. Several minor modifications were found necessary during the low power tests and took a couple of months. A power feeder to the resonator was fabricated and installed in September.

The contract for construction of cooling system was made. The part for cooling of the ion source on the high voltage terminal was completed at the end of October and will be used tentatively for cooling of the first resonator and the radiofrequency amplifier for a year until the whole system is installed.

Fabrication of the remaining five resonators are progressing in the factory of the contractor. Acceptance test of No. 2 cavity was also completed at the end of October. All the cavities will be set in the accelerator vault by the end of March, 1978.

## 12-2. The Proto-type Buncher

M. Odera, I. Takeshita, and F. Yoshida

A single frequency bunching system was investigated and a proto-type resonator was fabricated and tested. In the variable frequency linac scheme of our machine, the accelerating frequency is adjusted according to the charge to mass ratio of ions so that the flight length of the ions in one period of the radiofrequency remains the same regardless of the ions under acceleration. This makes calculation of the buncher parameters simple by normalizing time in unit of the period of radiofrequency and length in unit of the length of the drift tube cell of the buncher.

The resonant frequency of the buncher must be adjustable easily for the full range of frequency required, by a method as simple as possible, otherwise, the buncher system adds complication to the operation of the accelerator. As such a method we chose that of capacity tuning. Figure 1 shows cross section of the proto-type cavity. A vacuum variable capacitor connected to the center electrode of the buncher can adjust frequency in the required wide range. The method of tuning has been found simple and it permits fine adjustment. The capacitor which has the maximum capacity of 250 pF and the maximum voltage rating of 30 kV is selected for the present design.

Position of the buncher is chosen 3m upstream from the first gap of the first accelerating resonator. Relatively low voltage less than 3 kV is expected to be sufficient for the center electrode of the buncher in that configuration. Therefore, there is ample margin for the vacuum capacitor rating. Power consumption was also found small and was less than 200 W at most.

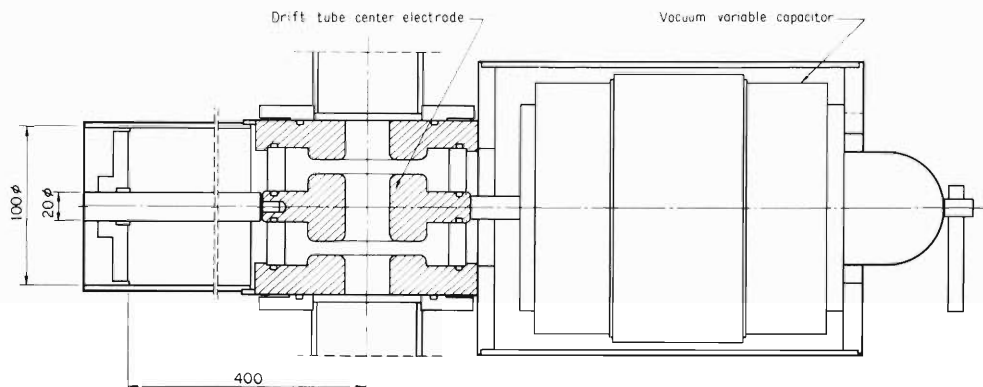


Fig. 1. Cross section of the proto-type buncher.

12-3. A Lay-out Plan of the Beam Diagnostic Elements

M. Odera

Figure 1 shows schematically a lay-out of the beam diagnostic elements. Abbreviations are explained at the lower part of the figure. Ions extracted from the ion source IS are focused by an electrostatic lens ESL. A slit Sl. 1 selects certain charge states and defines source profile of the beam. The beam intensity can be measured by a beam stopper BS. 1 which can be plunged into the beam path by a pneumatic device. After passing through the accelerating column, direction and centering of the beam with respect to the acceleration axis are adjusted by a pair of the steering magnets St. 1 and St. 2. The probe container box PC. 1 can house several types of diagnostic probes according to kind of measurement desired. Then a quadrupole doublet DQ. 1 focuses beam onto Sl. 2 and the state of dispersion of the beam is investigated by a profile monitor PM. 1 in front of Sl. 3. A mass analysing magnet D. 1 can single-out any isotope if desired. D. 2 inflects the beam into the buncher. Performance of the buncher can be measured by plunging into the beam path a bunch pick-up probe in PC. 2 in front of the valve V. 3. Baffles Baf. 1-4 define the cross section of the beam allowed to enter each cavity. Emittance variation along the beam line can be checked by inserting emittance probes EM 1~8 into a suitable probe container among PC. 1~8. Roles of any other diagnostic elements in the Fig. 1 may be understood in the same way.

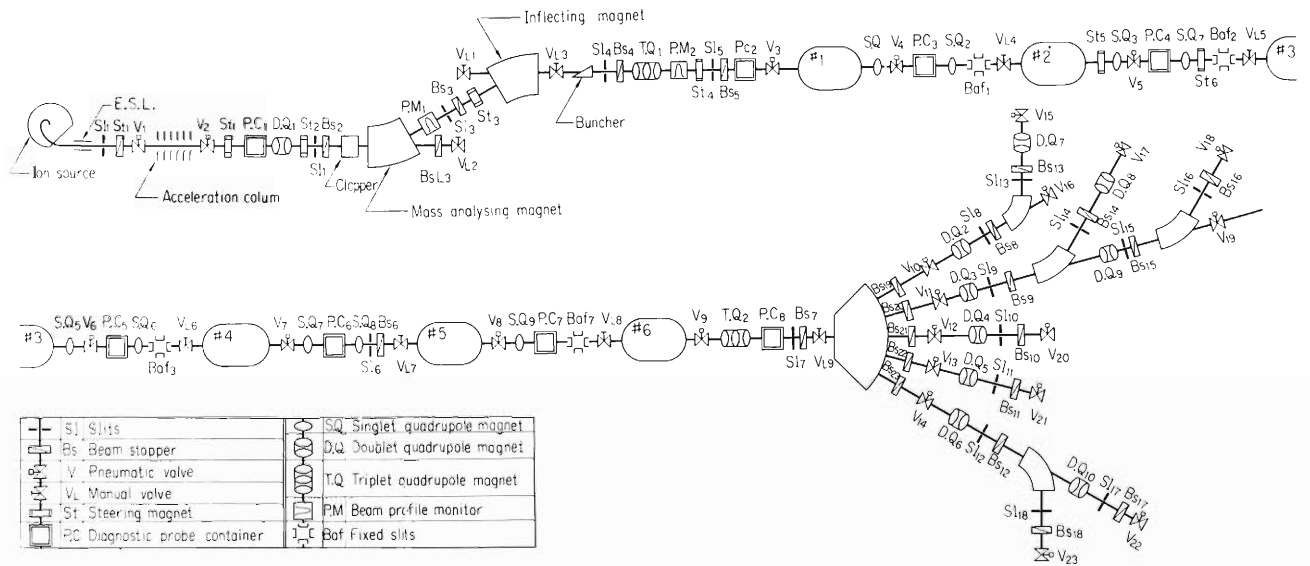


Fig. 1. Arrangement of the beam diagnostic and handling elements along the beam transport line.

## 12-4. Orbit Analysis of the Beam after Charge Stripping

M. Odera and F. Yoshida

Though the linac has been designed so as to be able to function without charge stripping it is interesting to investigate effects of the charge change on the beam dynamics through the linac. If it is possible to increase charge of the ions by that process without causing much complication to the operation, it is very desirable in view of saving of power consumption of the linac system. The radiofrequency power loss is inversely proportional to the square of charge of the ion, when the energy to be gained is fixed.

The most probable charge states of Xe-8+ and Ne-5+ when stripped between the fourth and the fifth resonators are 24 and 9 respectively. Figure 1 shows variations of emittance of beam after passing through the next cavity and acceptance of the later part of the linac according to the charge states when the parameters of the machine are chosen to give best result for the ions having the most probable charge states. A large portion of the xenon beam is found to be able to pass through all the later sections in spite of a large difference existing in charge states. For the

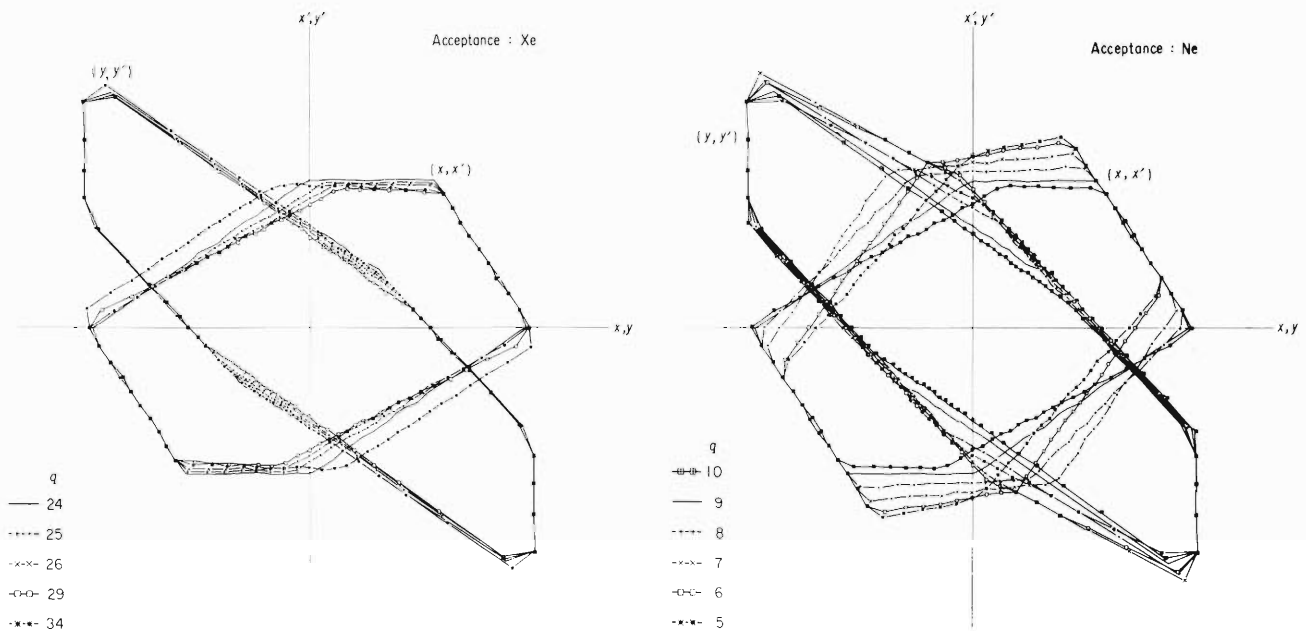


Fig. 1. (a) and (b): variations of acceptance of the beam of #5 cavity according to charge states. Stripping is made at the entrance of the cavity. Number of charge  $q$  is as follows:

Xe: —  $q = 24$ , + — +  $q = 25$ , X — X  $q = 26$ ,  
 $\square$  —  $\square$   $q = 29$ , \* — \*  $q = 34$ ;  
 Ne: —  $q = 9$ , + — +  $q = 8$ , X — X  $q = 7$ ,  
 $\square$  —  $\square$   $q = 6$ , \* — \*  $q = 5$ ,  $\boxplus$  —  $\boxplus$   $q = 10$

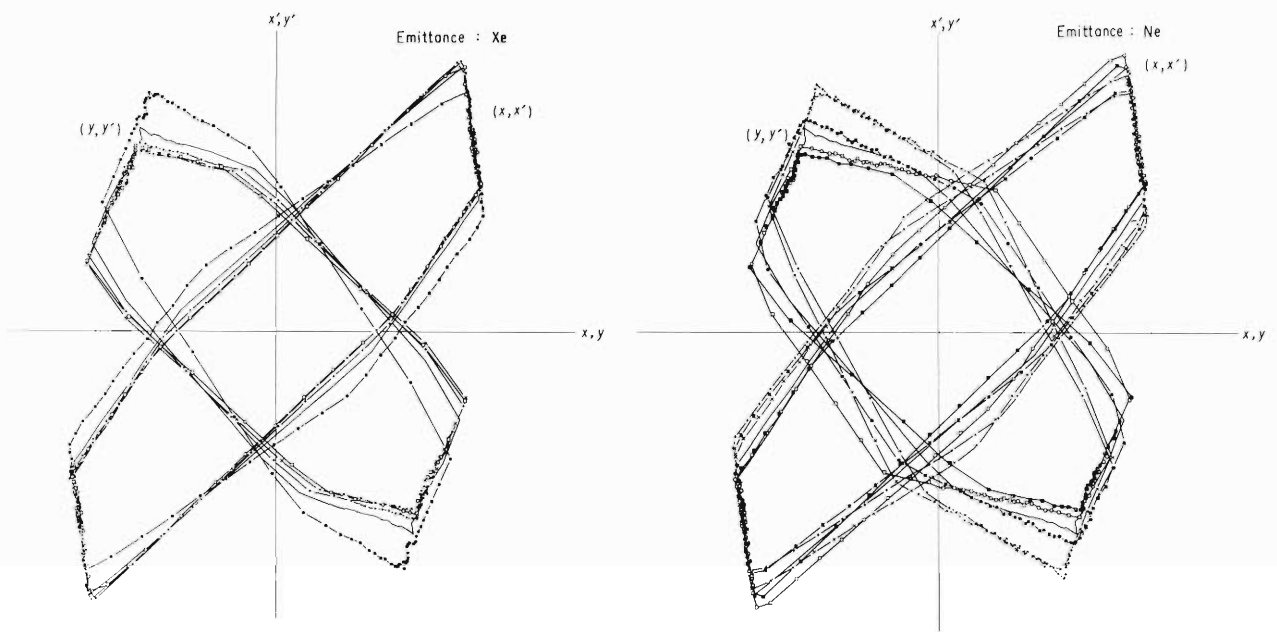


Fig. 1. (c) and (d): variations of emittance of the stripped beam after the #5 cavity. Other parameters are the same with those of (a) and (b).

neon beams, transmission is somewhat worse. However, substantial portion of particles of various charge states seems to go through later sections in this case too. So discrimination of the charge states by difference in emittance and acceptance seems difficult. It will cause some difficulties in the beam diagnosis.

## 12-5. Test Facility for Heavy Ion Source

I. Kohno, A. Shimamura, and T. Tonuma

The linac is designed to be able to accelerate ions whose mass to charge ratios are between 4 and 24. For the production of these ions we adopted a hot cathode PIG type ion source similar to the heavy ion source<sup>1)</sup> of the cyclotron. A test facility was equipped to study the production of multiply-charged ions of all elements and the formation of ion beam extracted from the ion source.

Figure 1 shows the experimental arrangement. Ions of different charges were extracted radially and separated by a magnetic field which at the same time maintains the arc plasma of the ion source. The selected ions were deflected by about 120 degrees in the field of the source magnet and they passed through a magnetic shield into an emittance measurement apparatus.

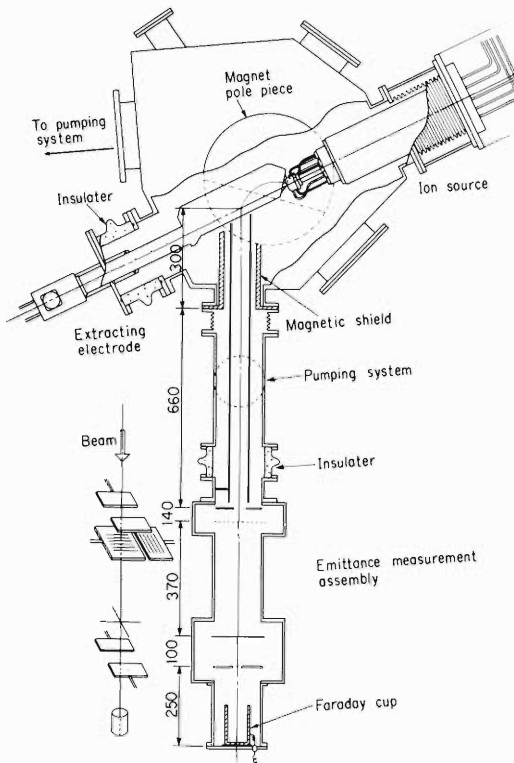


Fig. 1. Test facility for PIG source.

The radius of beam trajectory in the source magnet was decided to be 13 cm to extract all ions with mass to charge ratios between 4 and 24. Therefore, the required maximum field strength of the source magnet was 7 kG and the electric voltage of up to 35 kV was needed for ion extraction. As the hot cathode PIG ion source, which was already described,<sup>2)</sup> was 14 cm high, the gap width of the magnet was decided to be 15 cm and the beam extraction system is supplied with a negative high potential.

Furthermore, the magnetic shield was installed to reduce the magnetic fringing field resulting from the rather large gap width of the magnet. Figure 2 shows the magnetic field distribution with and without the magnetic shield. It is found that the magnetic fringing field is reduced by the use of the magnetic shield.

At present we are studying the characteristics of the PIG type ion source with this test facility.

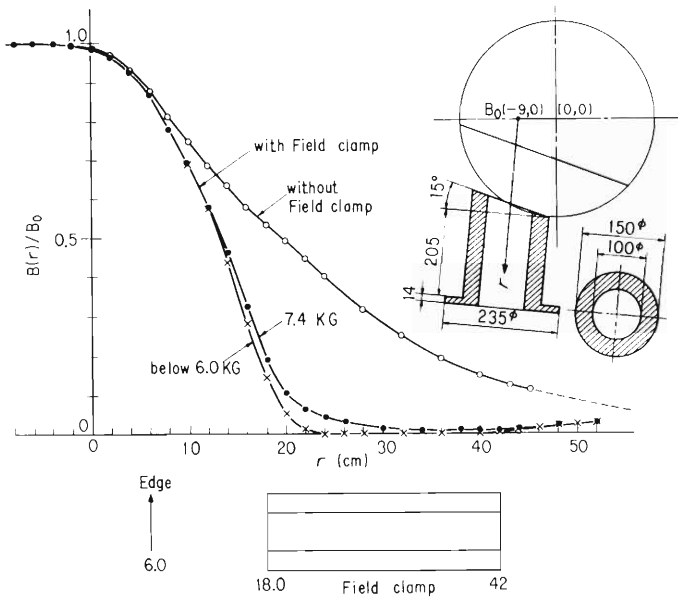


Fig. 2. Effect of the magnetic shield (field clamp) on the magnetic field.

## References

- 1) Y. Miyazawa, I. Kohno, T. Tonuma, and A. Shimamura: IEEE Trans. Nucl. Sci., NS-19, No. 2, 105 (1972).
- 2) K. Ikegami and I. Takeshita: IPCR Cyclotron Progr. Rep., 10, 147 (1976).

## 13. LIST OF PUBLICATIONS

- 1) M. Ichimura, M. Igarashi, S. Landwne, C. H. Dasso, B. S. Wilsson, R. A. Broglis, and A. Winther: "On Solving Coupled Equations for Scattering Problems under the Many Channel and Short Wave Length Conditions of Heavy Ion Collisions", *Phys. Lett.*, 67B, 129 (1977).
- 2) T. Inamura, M. Ishihara, T. Fukuda, T. Shimoda, and K. Hiruta: "Gamma-Rays from an Incomplete Fusion Reaction Induced by 95 MeV  $^{14}\text{N}$ ", *Phys. Lett.*, 68B, 51 (1977).
- 3) K. Sugimoto, N. Takahashi, A. Mizobuchi, Y. Nojiri, T. Minamisono, M. Ishihara, K. Tanaka, and H. Kamitsubo: "Spin Polarization of  $^{12}\text{B}$  in the Heavy-Ion Reaction  $^{100}\text{Mo}(^{14}\text{N}, ^{12}\text{B})^{102}\text{Ru}$ ", *Phys. Rev. Lett.*, 39, 323 (1977).
- 4) F. G. Resmini, F. Soga, and H. Kamitsubo: "Possibility of Quasimolecular Bands in  $^{28}\text{Si}$ ", *Phys. Rev.*, C15, 2241 (1977).
- 5) F. Kearns, G. Varley, G. D. Dracoulis, T. Inamura, J. C. Lisle, and J. C. Willmott: "Lifetimes of High Spin Rotational States", *Nucl. Phys.*, A278, 109 (1977).
- 6) N. Bendjaballah, B. Delaunay, J. Delaunay, and T. Nomura: "High-Spin States in  $^{57}\text{Co}$ ", *Nucl. Phys.*, A280, 228 (1977).
- 7) N. Bendjaballah, J. Delaunay, A. Jaffrin, T. Nomura, and K. Ogawa: "The Level Structure of  $^{56}\text{Fe}$ ", *Nucl. Phys.*, A284, 513 (1977).
- 8) S. Cavallaro, J. Delaunay, R. Ballini, T. Nomura, N. Bendjaballah, and C. Tosello: "High-Spin States in  $^{58}\text{Fe}$ -Ground-State and Quasi  $\gamma$  Bands-", *Nucl. Phys.*, A293, 125 (1977).
- 9) I. Kohno, K. Katori, T. Mikumo, T. Motobayashi, S. Nakajima, M. Yoshie, and H. Kamitsubo: "Single-and Multi-Nucleon Transfer Reactions Induced by  $^{14}\text{N}$  and  $^{12}\text{C}$  on fb-Shell Nuclei", *J. Phys. Soc. Japan*, 42, 1 (1977).
- 10) K. Koyama, N. Nakanishi, S. Takeda, S. Yamada, H. Sakaguchi, M. Nakamura, S. Takeuchi, and H. Ohnuma: " $(^3\text{He}, d)$  Stripping to Bound and Unbound States in  $^{29}\text{P}$ ", *J. Phys. Soc. Japan*, 43, 755 (1977).
- 11) S. Yamaji, K. H. Ziegenhain, H. J. Fink, W. Greiner, and W. Scheid: "The Mass Transfer in the Collision  $^{238}\text{U} - ^{238}\text{U}$ ", *J. Phys.*, 3, 1283 (1977).
- 12) T. Nomura, N. Bendjaballah, and J. Delaunay: "Unusually Strong Difference in the Side-Feeding to the  $6^+$  Doublets of  $^{56}\text{Fe}$  Populated in Heavy-Ion Compound Reactions", *Nucl. Instr. Methods*, 146, 310 (1977).
- 13) Y. Horikawa, T. Hoshino, and A. Arima: "Core Polarization Effects on the Coulomb Form Factor", *Nucl. Phys.*, A278, 297 (1977).
- 14) T. Hoshino: "Attempts to Extend the Thomas-Fermi Approximation", *Genshikaku Kenkyu*, 22, 64 (1977).
- 15) S. Motonaga, T. Fujisawa, H. Kamitsubo, and F. G. Resmini: "Polarized Ion Source for SF-Cyclotron", *Genshikaku Kenkyu*, (in Japanese), 22, 93 (1977).
- 16) H. Nakajima, S. Kohara, T. Kageyama, and I. Kohno: "Production of C, N, O, and Ne Ions by Pulsed Ion Source and Acceleration of These Ions in the Cyclotron", *Reports I. P. C. R.*, (in Japanese), 53, 132 (1977).
- 17) Y. Awaya, M. Akiba, T. Katou, H. Kumagai, Y. Tendow, K. Izumo, T. Takahashi, A. Hashizume, M. Okano, and T. Hamada: "The  $K\alpha$  and  $K\beta$  X-Ray Spectra of Al, Ti, Cr, Fe, and Ni Induced by 84 MeV Nitrogen Ions", *Phys. Lett.*, 61A, 111 (1977).

- 18) T. Hayashi, K. Takayama, T. Yanagimachi, and S. Kobayashi: "Variation of Response between the Top and Bottom Surface of Plastic Films", *Ionizing Radiation*, Japan Soc. Appl. Phys., (in Japanese), 4, No.3, 22 (1977).
- 19) T. Doke, T. Hayashi, K. Ito, T. Yanagimachi, K. Hisano, K. Nagata, and M. Miyajima: "Observation of the Tracks of Heavy Primary Cosmic Rays by Plastic and X-Ray Films", *Bull. Inst. Space and Aeronautical Sci., Univ. of Tokyo*, 13, 875 (1977).
- 20) H. Tawara, Y. Awaya, Y. Tendow, T. Katou, M. Akiba, and T. Tonuma: "The Innershell Ionization of Ar K-shell Electrons by High Energy Carbon Ions", *Studies of Atomic Collisions and Related Topics in Japan (Progr. Report)*, No.3, p. 56 (1977).
- 21) Y. Awaya, T. Hamada, M. Okano, A. Hashizume, T. Takahashi, K. Izumo, Y. Tendow, H. Kumagai, T. Katou, and M. Akiba: "K X-Rays of Al, Ti, Cr, Fe, and Ni Induced by Nitrogen Ions", *Studies of Atomic Collisions and Related Topics in Japan (Progr. Report)*, No.3, p. 57 (1977).
- 22) H. Kumagai, Y. Awaya, Y. Tendow, T. Katou, and M. Akiba: "A Step Scan Controll and a Data Accumulating System of an On-line Bragg Crystal Spectrometer", *Reports I. P. C. R.*, (in Japanese), 53, 153 (1977).
- 23) T. Watanabe, H. Tawara, and Y. Awaya: "By Using Heavy Ions as Projectile", *Butsuri*, (in Japanese), 32, 306 (1977).
- 24) T. Takahashi: "Spatial Distribution of Ionization Energy Deposited about the Path of a Heavy Ion — Application to Target Theory", *Tech. Rep. Res. React. Inst., Kyoto Univ.*, (in Japanese).
- 25) E. Yagi, A. Koyama, H. Sakairi, and R. R. Hasiguti: "Defect Structures of Slightly Reduced Semiconducting Rutile as Observed by the Channelling Method", *Rad. Effec. in Semiconduc. 1976*, The Inst. of Phys., London, p.485 (1977).
- 26) E. Yagi, A. Koyama, H. Sakairi, and R. R. Hasiguti: "Investigation of Ti Interstitials in Slightly Reduced Rutile (TiO<sub>2</sub>) by Means of Channeling Method", *J. Phys. Soc. Japan*, 42, 939 (1977).
- 27) H. Sakairi, E. Yagi, A. Koyama, T. Karasawa, and R. R. Hasiguti: "Atomic Displacement in Copper Irradiated with Protons,  $\alpha$ -Particles and Carbon Ions from a Cyclotron", *J. Phys. Soc. Japan*, 43, 999 (1977).
- 28) K. Matsumoto, T. Kataoka, M. Terasawa, M. Shimada, S. Nakahigashi, H. Sakairi, and E. Yagi: "Embrittlement of Austenitic Stainless Steel Irradiated with  $\alpha$ -Particles", *J. Nucl. Materials*, 67, 97 (1977).
- 29) A. Koyama: "Contribution of Directly Excited Electrons to the Secondary Electron Emission from Al by High Energy Proton or  $\alpha$ -Particle Bombardment", *Japan. J. appl. Phys.*, 16, 431 (1977).
- 30) N. Shiotani, T. Okada, H. Sekizawa, S. Wakoh, and Y. Kubo: "Angular Correlation of Positron Annihilation Radiation in Chromium and Molybdenum", *J. Phys. Soc. Japan*, 43, 1229 (1977).
- 31) T. Mizoguchi, S. von Molnar, G. S. Cargill III, T. Kudo, N. Shiotani, and H. Sekizawa: "Structure and Physical Properties of an Amorphous Cu<sub>57</sub>Zr<sub>43</sub> Alloy, Amorphous Magnetism II", Ed. by R. A. Levy and R. Hasegawa, p.513, Plenum Press (1977).
- 32) T. Nozaki, K. Fukushi, and T. Irie: "Some Radiohalogen Derivatives of Cholesterol", *J. Labelled Comp.*, 13, 226 (1977).

- 33) Y. Harata, M. Matsui, and M. Imamura: "Radiation-Induced Chain Isomerization of cis-2-Butene in Benzene Solution", Chem. Lett., 1977, 199.
- 34) S. Kitayama and A. Matsuyama: "Separation of DNA-Dependent DNA Polymerase Activities in Micrococcus radiodurans", Biochim. Biophys. Acta, 475, 23 (1977).
- 35) S. Kitayama, K. Shiratori, F. Yatagai, and A. Matsuyama: "Enhanced Lethal Effect of Various Agents on M. radiodurans by Postincubation at Nonpermissive Temperature", Agr. Biol. Chem., 41, 2297 (1977).
- 36) F. Yatagai and A. Matsuyama: "LET-Dependent Radiosensitivity of Escherichia coli K-12 rec and uvr Mutants", Radiat. Res., 71, 259 (1977).

(Papers presented at meetings)

- 1) T. Inamura: "A Comment on Calculations of Multiple Coulomb Excitations with the Winther-De Boer Code", The IPCR Symp. on Coul. Excit. of Atom. Nucl. and the Related Problems, Wako, Jan. (1977).
- 2) T. Inamura: "Coulomb Excitation with Projectile Energies Exceeding the Coulomb Barrier", The IPCR Symp. on Coul. Excit. of Atom. Nucl. and the Related Problems, Wako, Jan. (1977).
- 3) A. Hashizume: "Coulomb Excitation of High Spin States of Deformed Nuclei", The IPCR Symp. on Coul. Excit. of Atom. Nucl. and the Related Problems, Wako, Jan. (1977).
- 4) T. Motobayashi: "Alpha-Transfer Reactions between Light Nuclei", Symp. on Light and Heavy Ion Reactions, Osaka, Jan. (1977).
- 5) T. Takahashi: "Ionization Efficiency in Condensed Phases", Symp. on the Heavy Ion Irrad. Effect on Biological Material, Oiso, Jan. (1977).
- 6) A. Hashizume: "High Spin States in Even Cadmium Isotopes", The IPCR Symp. on High Spin States, Wako, Feb. (1977).
- 7) E. Yagi, A. Koyama, H. Sakairi, M. Iwaki, and R. R. Hasiguti: "Ni-Ion Irradiation of Al", Heavy Ion Symp., Toyonaka, Feb. (1977).
- 8) I. Kohno: "Multiply-Charged Heavy Ion Source", Symp. on Ion Sources and Application Technol., Tokyo, Feb. (1977).
- 9) I. Kohno, A. Shimamura, and T. Tonuma: "A Penning Multiply-Charged Ion Source for The IPCR Cyclotron and Linac", Symp. on Ion Sources and Application Technol. Tokyo, Feb. (1977).
- 10) T. Doke, T. Hayashi, K. Ito, T. Yanagimachi, S. Kobayashi, K. Hisano, K. Nagata, and M. Miyajima: "Observation of Relativistic Primary Cosmic Ray Particles with  $Z > 26$ ", Primary Cosmic Ray Symp., Tanashi, Tokyo, Mar. (1977).
- 11) T. Fujisawa, S. Motonaga, and H. Kamitsubo: "Acceleration of Polarized Proton on the INS-Cyclotron", Spring Divisional Meeting of Phys. Soc. of Japan, Saga, Apr. (1977).
- 12) K. Hiruta: "Gamma-rays from Incomplete Fusion Reactions Induced by Heavy Ions", Spring Divisional Meeting of Phys. Soc. of Japan, Saga, Apr. (1977).
- 13) Y. Toba, H. Sakaguchi, N. Nakanishi, A. Goto, F. Ohtani, and N. Kishida: "Blocking Effects in the Core-Excitation of  $^{29}\text{Si}$  and  $^{89}\text{Y}$ ", Spring Divisional Meeting of Phys. Soc. of Japan, Saga, Apr. (1977).
- 14) T. Shimoda, M. Ishihara, H. Kamitsubo, T. Motobayashi, and T. Fukuda: "Measurement of Particle-Particle Correlation in Heavy Ion Reaction (II)", Spring Divisional Meeting of Phys. Soc. of Japan, Saga, Apr. (1977).
- 15) H. Amakawa and K. I. Kubo: "Incident Energy Dependence of the (p, t) Reactions", Spring Divisional Meeting of Phys. Soc. of Japan, Saga, Apr. (1977).
- 16) T. Hoshino: "Attempts to Extend the Thomas-Fermi Approximation", Spring Divisional Meeting of Phys. Soc. of Japan, Saga, Apr. (1977).
- 17) M. Odera: "Fabrication of the Drift Tubes of the RILAC", Spring Divisional Meeting of Phys. Soc. of Japan, Saga, Apr. (1977).
- 18) T. Doke, T. Hayashi, K. Ito, T. Yanagimachi, S. Kobayashi, K. Hisano, K. Nagata, and M. Miyajima: "Observation of the Flux of Relativistic Primary Cosmic Ray Particles with  $Z > 26$ ", Spring Divisional Meeting of Phys. Soc. of Japan, Saga, Apr. (1977).

- 19) T. Takahashi, Y. Awaya, K. Izumo, T. Tonuma, A. Hashizume, S. Uchiyama, and T. Doke: "Electronic Stopping Power of Several MeV/amu C- and He-ions", Spring Divisional Meeting of Phys. Soc. of Japan, Yamaguchi, Apr. (1977).
- 20) H. Sekizawa, K. Asai, T. Okada, and N. Shiotani: "Perturbed Angular Correlation of Gamma-Rays Emitted from Cd in NiFe<sub>2</sub>O<sub>4</sub>", Spring Divisional Meeting of Phys. Soc. of Japan, Yamaguchi, Apr. (1977).
- 21) Y. Awaya, K. Katou, H. Kumagai, T. Tonuma, Y. Tendow, K. Izumo, T. Takahashi, A. Hashizume, M. Okano, and T. Hamada: "Ti K X-Rays Induced by Heavy Ion Bombardment", Spring Divisional Meeting of Phys. Soc. of Japan, Yamaguchi, Apr. (1977).
- 22) M. Uda, K. Maeda, Y. Awaya, M. Kobayashi, Y. Sasa, H. Kumagai, and T. Tonuma: "Bonding Effect in Characteristic X-Rays Induced by Heavy Ions", Spring Divisional Meeting of Phys. Soc. of Japan, Yamaguchi, Apr. (1977).
- 23) S. Kitayama and A. Matsuyama: "DNA Polymerase of *M. radiodurans*. I. Purification and Properties", Ann. Meet. of the Agr. Chem. Soc. of Japan, Yokohama, Apr. (1977).
- 24) T. Inamura: "Gamma-Rays from an Incomplete Fusion Reaction Induced by 95 MeV <sup>14</sup>N", Symp. on Highly Excited States, Osaka, Apr. (1977).
- 25) Y. Harata, M. Matsui, and M. Imamura: "Radiation-Induced Chain Isomerization of cis-2-Butene in Benzene Solution", 36th Ann. Meet. of the Chem. Soc. of Japan, Osaka, Apr. (1977).
- 26) B. Imanishi: "Coupled Channel Analysis of the <sup>12</sup>C + <sup>13</sup>C Resonances with the Core-Exchange Model", Intern. Conf. on the Resonances in Heavy Ion Reactions, Hvar, Yugoslavia, May-June (1977).
- 27) O. Tanimura and B. Imanishi: "Folding Model Study of Fusion Cross Section and Resonance in <sup>12</sup>C + <sup>12</sup>C Scattering", Intern. Conf. on the Resonances in Heavy Ion Reactions, Hvar, Yugoslavia, May-June (1977).
- 28) T. Motobayashi, T. Ooi, S. Nakajima, and I. Kohno: "α-Transfer Reactions Induced by Heavy Ions to Excite the Ground State Band of <sup>20</sup>Ne", Intern. Conf. on Phys. of Light and Medium Nucl., Florence, June (1977).
- 29) J. Delaunay and T. Nomura: "A Possible Low Lying δ Band in <sup>58</sup>Ni", Intern. Conf. on Phys. of Light and Medium Nucl., Florence, June (1977).
- 30) Y. Awaya, T. Katou, H. Kumagai, T. Tonuma, Y. Tendow, K. Izumo, T. Takahashi, A. Hashizume, M. Okano, and T. Hamada: "The Dependence of Multiple Inner-Shell Ionization on the Projectile Energies and on Target Elements by Nitrogen-Ion Bombardment at the Energy above 4 MeV/amu", 10th Intern. Conf. on the Phys. of Elec. and Atomic Collisions, Paris, July (1977).
- 31) M. Uda, K. Maeda, Y. Awaya, M. Kobayashi, Y. Sasa, H. Kumagai, and T. Tonuma: "Bonding Effect in X-Ray Spectra Induced by 84 MeV N<sup>4+</sup> Ions", 10th Intern. Conf. on the Phys. of Elec. and Atomic Collisions, Paris, July (1977).
- 32) T. Hoshino, K. Yazaki, and T. Yukawa: "Canonical Quantization from the Time-Dependent Hartree-Fock Theory in the Lipkin Model", Intern. Conf. on Nucl. Struct., Tokyo, Sept. (1977) [Contributed Papers, p. 122].
- 33) J. Delaunay and T. Nomura: "Systematics of High-Spin States in Even Fe Isotopes", Intern. Conf. on Nucl. Struct., Tokyo, Sept. (1977), [ibid., p. 264].
- 34) A. Hashizume, T. Katou, Y. Tendow, and H. Kumagai: "Excited States in <sup>104</sup>Cd via the (<sup>3</sup>He, 3n) Reaction", Intern. Conf. on Nucl. Struct., Tokyo, Sept. (1977), [ibid., p. 335].

- 35) A. Hashizume, T. Katou, Y. Tendow, and H. Kumagai: "High Spin States in  $^{162}\text{Yb}$ ,  $^{164}\text{Yb}$  and  $^{166}\text{Yb}$ ", Intern. Conf. on Nucl. Struct., Tokyo, Sept. (1977), [ibid., p. 406].
- 36) Y. Toba, H. Sakaguchi, N. Nakanishi, A. Goto, F. Ohtani, and N. Kishida: "Blocking Effects in the Core-Excitation of  $^{29}\text{Si}$ ", Intern. Conf. on Nucl. Struct., Tokyo, Sept. (1977), [ibid., p. 494].
- 37) M. Igarashi and M. Ichimura: "A New Method for Solving Coupled Equations for Scattering Problems", Intern. Conf. on Nucl. Struct., Tokyo, Sept. (1977), [ibid., p. 503].
- 38) Y. Suzuki, T. Ando, and B. Imanishi: "Coupled Channels Analysis of  $\alpha + ^{12}\text{C}$  Scattering with Orthogonality Constraint", Intern. Conf. on Nucl. Struct., Tokyo Sept. (1977), [ibid., p. 515].
- 39) M. Kawai, B. Imanishi, and M. Ichimura: "Energy Dependence of Channel Coupling Effects in (d, p) Reactions", Intern. Conf. on Nucl. Struct., Tokyo, Sept. (1977), [ibid., p. 526].
- 40) T. Hasegawa, T. Fujisawa, S. Motonaga, N. Ueda, T. Wada, Y. Toba, and N. Kishida: "Measurement of Analyzing Power for  $^{12}\text{C}(\bar{p}, d)^{11}\text{C}$  Reaction at 27.4 MeV", Intern. Conf. on Nucl. Struct., Tokyo, Sept. (1977), [ibid., p. 539].
- 41) K. Koyama, N. Nakanishi, and H. Ohnuma: " $(^3\text{He}, d)$  Stripping to Unbound States in Light Nuclei", Intern. Conf. on Nucl. Struct., Tokyo, Sept. (1977), [ibid., p. 546].
- 42) N. Matsuoka, A. Shimizu, K. Hosono, T. Saito, M. Kondo, N. Nakanishi, Y. Toba, A. Goto, and F. Ohtani: " $(^3\text{He}, ^3\text{He}_0)$  and  $(^3\text{He}, d)$  Reactions on  $^{54}\text{Fe}$  and  $^{58,60}\text{Ni}$  of 90 MeV", Intern. Conf. on Nucl. Struct., Tokyo, Sept. (1977), [ibid., p. 549].
- 43) N. Matsuoka, A. Shimizu, K. Hosono, T. Saito, M. Kondo, N. Nakanishi, Y. Toba, A. Goto, and F. Ohtani: "Continuous Proton and Deuteron Spectra Emitted in  $^3\text{He}$  Induced Reactions", Intern. Conf. on Nucl. Struct., Tokyo, Sept. (1977), [ibid., p. 574].
- 44) B. Imanishi, O. Tanimura, and H. Ohnishi: Repeated Neutron Transfer in the Elastic and Inelastic Scattering of  $^{16}\text{O}$  on  $^{17}\text{O}$ ", Intern. Conf. on Nucl. Struct., Tokyo, Sept. (1977), [ibid., p. 588].
- 45) T. Motobayashi: "A Modified Brink's Semi-classical Theory for Heavy-Ion Induced Transfer Reactions", Intern. Conf. on Nucl. Struct., Tokyo, Sept. (1977), [ibid., p. 615].
- 46) T. Motobayashi, I. Kohno, T. Ooi, and S. Nakajima: " $\alpha$ -Transfer Reactions between Light Nuclei", Intern. Conf. on Nucl. Struct., Tokyo, Sept. (1977), [ibid., p. 628].
- 47) F. Soga, J. Shimizu, N. Takahashi, K. Takimoto, R. Wada, T. Fujisawa, T. Wada, and H. Kamitsubo: "Study of the Quasimolecular Resonance by the  $^{24}\text{Mg}(\alpha, ^{12}\text{C})^{16}\text{O}$  Reaction", Intern. Conf. on Nucl. Struct., Tokyo, Sept. (1977), [ibid., p. 650].
- 48) T. Motobayashi, S. M. Lee, T. Ooi, T. Numao, T. Fukuda, T. Shimoda, H. Utsunomiya, M. Yanokura, M. Ishihara, and I. Kohno: "Fusion Reaction in  $^{12}\text{C} + ^{14}\text{N}$  and  $^{16}\text{O} + ^{10}\text{B}$  Systems", Intern. Conf. on Nucl. Struct., Tokyo, Sept. (1977), [ibid., p. 662].
- 49) T. Nomura, J. Delaunay, C. Tosello, and N. Bendjaballah: "Test of the Evaporation Model in Heavy-Ion Fusion Reactions", Intern. Conf. on Nucl. Struct., Tokyo, Sept. (1977), [ibid., p. 666].
- 50) T. Fukuda, M. Ishihara, T. Inamura, T. Numao, T. Shimoda, and T. Nomura: "Complete Fusion Cross Section Measurement by Beam Attenuation Method", Intern. Conf. on Nucl. Struct., Tokyo, Sept. (1977), [ibid., p. 667].
- 51) S. Yamaji, K. H. Ziegenhain, H. J. Fink, W. Greiner, and W. Scheid: "The Mass Transfer in the Collision  $^{238}\text{U} - ^{238}\text{U}$ ", Intern. Conf. on Nucl. Struct., Tokyo, Sept. (1977), [ibid., p. 670].
- 52) A. Iwamoto, K. Harada, K. Sato, S. Yamaji, and S. Yoshida: "Description of Heavy-Ion Reaction and Fission with Linear Response Theory", Intern. Conf. on Nucl. Struct., Tokyo, Sept. (1977), [ibid., p. 680].

- 53) T. Shimoda, M. Ishihara, H. Kamitsubo, T. Motobayashi, and T. Fukuda: "Three Body Process Associated with  $\alpha$  Particle Emission in the Reaction of  $^{14}\text{N} + ^{93}\text{Nb}$ ", Intern. Conf. on Nucl. Struct., Tokyo, Sept. (1977), [ibid., p. 703].
- 54) T. Inamura, K. Hiruta, T. Fukuda, T. Shimoda, and M. Ishihara: "Emission of Fast  $\alpha$ -Particles and a Peripheral Heavy-Ion Reaction", Intern. Conf. on Nucl. Struct., Tokyo, Sept. (1977), [ibid., p. 735].
- 55) T. Nomura, H. Utsunomiya, T. Motobayashi, and T. Inamura: "Preequilibrium  $\alpha$ -Particle Emission from  $^{209}\text{Bi} + ^{14}\text{N}$  Reactions", Intern. Conf. on Nucl. Struct., Tokyo, Sept. (1977), [ibid., p. 736].
- 56) M. Ichimura: "Exchange Magnetic Moment Associated with a Two-body Spin-orbit Interaction", Intern. Conf. on Nucl. Struct., Tokyo, Sept. (1977), [ibid., p. 819].
- 57) A. Koyama: "Theory of the Secondary Electron Emission from Al by High Energy Proton or  $\alpha$ -Particle Bombardment", 7th Intern. Conf. on Atomic Collisions in Solids, Moscow, Sept. (1977).
- 58) K. Hiruta: "Measurement of Fast  $\alpha$ -Particles in Coincidence with  $\gamma$ -Rays Detected by Ge(Li) and the Angular Momentum Window for the Reaction", Intern. Symp. on Macroscopic Features of Heavy Ion Collisions and the Pre-Equilibrium Process, Hakone, Sept. (1977).
- 59) T. Shimoda: " $\alpha$ -Light Product Correlation in the  $^{14}\text{N} + ^{93}\text{Nb}$  Reaction and the Excitation of Light Fragments", Intern. Symp. on Macroscopic Features of Heavy Ion Collisions and the Pre-Equilibrium Process, Hakone, Sept. (1977).
- 60) T. Nomura: "Preequilibrium  $\alpha$ -Particle Emission from  $^{209}\text{Bi} + ^{14}\text{N}$  Reactions Statistical Analysis of Energy Spectra and Nuclear Temperature of a Composite System", Intern. Symp. on Macroscopic Features of Heavy Ion Collision and the Pre-Equilibrium Process, Hakone, Sept. (1977).
- 61) T. Shimoda, M. Ishihara, H. Kamitsubo, T. Motobayashi, and T. Fukuda: "Measurement of Particle-Particle Correlation in Heavy Ion Reaction (III)", Ann. Meeting of Phys. Soc. of Japan, Tokyo, Oct. (1977).
- 62) S. Motonaga, N. Nakanishi, K. Ogiwara, and H. Kamitsubo: "Design Study of Separate Sector Cyclotron for Heavy Ion", Ann. Meeting of Phys. Soc. of Japan, Tokyo, Oct. (1977).
- 63) K. Hiruta, T. Inamura, S. Ise, M. Ishihara, T. Shimoda, and T. Nomura: "Fast  $\alpha$ -Particle Emission Process in Heavy Ion Reactions", Ann. Meeting of Phys. Soc. of Japan, Tokyo, Oct. (1977).
- 64) N. Kishida, N. Nakanishi, Y. Toba, and H. Ohnuma: "The (d, p) Reaction at  $E_d = 24$  MeV I:  $^{54}\text{Fe}(d, p)^{55}\text{Fe}$ ", Ann. Meeting of Phys. Soc. of Japan, Tokyo, Oct. (1977).
- 65) Y. Tendow, T. Katou, H. Kumagai, and A. Hashizume: "High Spin States in  $^{166}\text{Yb}$ ", Ann. Meeting of Phys. Soc. of Japan, Tokyo, Oct. (1977).
- 66) A. Hashizume, T. Tendow, T. Katou, and H. Kumagai: "High Spin States in  $^{162}\text{Yb}$ ", Ann. Meeting of Phys. Soc. of Japan, Tokyo, Oct. (1976).
- 67) T. Nomura, H. Utsunomiya, T. Motobayashi, T. Inamura, and M. Yanokura: "Pre-Equilibrium  $\alpha$ -Particle Emission from  $^{209}\text{Bi} + ^{14}\text{N}$  Reactions", Ann. Meeting of Phys. Soc. of Japan, Tokyo, Oct. (1977).
- 68) S. Uchiyama, T. Takahashi, Y. Awaya, K. Izumo, T. Tonuma, A. Hashizume, and T. Doke: "Electronic Stopping Power of 5 MeV/amu C- and He-ions", Ann. Meeting of Phys. Soc. of Japan, Tokyo, Oct. (1977).
- 69) I. Kohno, A. Shimamura, T. Tonuma, and I. Takeshita: "Heavy Ion Source for the Linac (1)", Ann. Meeting of Phys. Soc. of Japan, Tokyo Oct. (1977).

- 70) M. Odera: "Status of the RILAC", Ann. Meeting of Phys. Soc. of Japan, Tokyo, Oct. (1977).
- 71) T. Doke, T. Hayashi, T. Yanagimachi, and S. Kobayashi: "Calibration for the Identification of Relativistic Heavy Charged Particles in Plastic Films", Ann. Meeting of Phys. Soc. of Japan, Tokyo, Oct. (1977).
- 72) K. Kimura and M. Imamura: "Excitons in Alkali-Halide Single Crystals Studied by Pulsed Heavy-Ion Beams", 20th Conf. Rad. Chem., Sapporo, Oct. (1977).
- 73) S. Kitayama and A. Matsuyama: "DNA Polymerase of M. radiodurans. III. DNA Polymerases in Postincubated Cells or Radiosensitive Mutants", 20th Ann. Meet. of the Jap. Rad. Res. Soc., Sendai, Oct. (1977).
- 74) Y. Hattori, F. Yatagai, and A. Matsuyama: "Inactivation of Ribonuclease A by Cyclotron Beams", 20th Ann. Meet. of Jap. Rad. Res. Soc., Sendai, Oct. (1977).
- 75) F. Yatagai, S. Kitayama, Y. Kimura, K. Nozawa, and A. Matsuyama: "Induction of Mutations in Bacteriophage  $\phi$ X 174 by Radiations", 20th Ann. Meeting of the Jap. Rad. Res. Soc., Sendai, Oct. (1977).
- 76) M. Yanokura, H. Nakahara, and K. Miyano: "Decay of  $^{211}\text{At}$ ,  $^{211}\text{Po}$ , and  $^{207}\text{Bi}$ ", 22th Meeting of Radiochem., Kanazawa, Oct. (1977).
- 77) T. Nozaki, M. Iwamoto, and Y. Itoh: "Comparison of Various Methods for the Production of  $^{77}\text{Br}$ ", 21th Discussion Meet. of Radiochem., Tatsunokuchi, Oct. (1977).
- 78) T. Nozaki, Y. Itoh, and K. Ogawa: "Comparison of Various Methods for the Production of  $^{73}\text{Se}$ ", 21th Discussion Meet. of Radiochem., Tatsunokuchi, Oct. (1977).
- 79) T. Nozaki and M. Iwamoto: "Activation Analysis of Oxygen on High-purity Silicon Surface", 21th Discussion Meet. of Radiochem., Tatsunokuchi, Oct. (1977).
- 80) Y. Itoh, M. Aratani, and T. Nozaki: "Charge Spectra of  $^{198}\text{Hg}^{n+}$  Produced from the  $\text{B}^-$  Decay of  $^{198}\text{Au}$ ", 21th Discussion Meet. of Radiochem., Tatsunokuchi, Oct. (1977).
- 81) H. Shinno, H. Shiraishi, R. Watanabe, H. Kamitsubo, I. Kohno, and T. Shikata: "Effects of Irradiation Temperature and Prestrain on the Helium Embrittlement of SUS 316 Stainless steel", 81th Meeting of Japan Inst. of Metals, Hiroshima, Oct. (1977).
- 82) S. Kitayama, S. Miyai, and A. Matsuyama: "Exonuclease Activity Associated with DNA Polymerase of M. radiodurans", 50th Ann. Meet. of Jap. Biochem. Soc., Tokyo, Oct. (1977).
- 83) Y. Awaya: "Studies of Heavy-Ion Excited X Rays in I. P. C. R. ", 3rd Hakone Symp. on the Elec. Struct. and Collision Process of Heavy Ions, Hakone, Nov. (1977).
- 84) T. Doke, T. Hayashi, K. Ito, T. Yanagimachi, S. Kobayashi, K. Nagata, and M. Miyajima: "On the Observation of Heavy Primary Cosmic Rays", Primary Cosmic Ray W. G. Symposium, Tanashi, Tokyo, Nov. (1977).
- 85) Y. Awaya: "X Rays Induced by Heavy Ions", Symp. on the Solid State Phys. by Using Heavy Ions, Tokai, Dec. (1977).
- 86) S. Motonaga: "Design Study of Linac-Injected Separate Sector Cyclotron", Meeting on the Next Project of Accelerator, Osaka, Dec. (1977).

## 14. LIST OF PERSONNEL

## Members of the Board

DOE Toshihiko	土手敏彦 (Chairman)	HAMADA Tatsuji	浜田達二
KAMITSUBO Hiromichi	上坪宏道	KOHNO Isao	河野功
NAKANE Ryohei	中根良平	NOZAKI Tadashi	野崎正
ODERA Masatoshi	小寺正俊		

## Users Committee

HAMADA Tatsuji	浜田達二 (Chairman)	IMAMURA Masashi	今村昌
KAMITSUBO Hiromichi	上坪宏道	KOHNO Isao	河野功
MATSUYAMA Akira	松山晃	NOZAKI Tadashi	野崎正
ODERA Masatoshi	小寺正俊	SAKAIRI Hideo	坂入英雄
SEKIZAWA Hisashi	関沢尚		

## Operation and Machine Maintenance Group

FUJITA Shin	藤田新	IKEGAMI Kumio	池上九三男
KAGEYAMA Tadashi	影山正	KOHARA Shigeo	小原重夫
KOHNO Isao	河野功	NAKAJIMA Hisao	中嶋尚雄
OGIWARA Kiyoshi	荻原清	TAKEBE Hideki	武部英樹

## Scientific and Engineering Personnel

## Cyclotron Laboratory

AMAKAWA Hirota	天川博隆	FUJISAWA Takashi	藤沢高志
FUJITA Jiro	藤田二郎	INAMURA Takashi	稲村卓
ISHIHARA Masayasu	石原正泰	KAMITSUBO Hiromichi	上坪宏道
KARASAWA Takashi	唐沢孝	KOHNO Isao	河野功
MOTOBAYASHI Tohru	本林透	MOTONAGA Shoshichi	元永昭七
NAKAJIMA Shunji	中島諄二	NAKANISHI Noriyoshi	中西紀喜
NOMURA Toru	野村亨	SHIKATA Takashi	四方隆史
WADA Takeshi	和田雄	YAMAJI Shuhei	山路修平

## (Visitors)

HIRUTA Kotaro	蛭田幸太郎	(Dept. Phys., Tokyo Gakugei Univ.)
ICHIMURA Munetake	市村宗武	(Inst. Phys., College General Education, Univ. of Tokyo)
IGARASHI Masamichi	五十嵐正道	(Tokyo Medical College)
IMANISHI Bunryu	今西文竜	(Inst. Nucl. Study, Univ. of Tokyo)
KAMMURI Tetsuo	冠哲夫	(Dept. Phys., Osaka Univ.)
KATORI Kenji	鹿取謙二	(Inst. Phys., Tsukuba Univ.)
KAWAI Mitsuji	河合光路	(Dept. Phys., Kyushu Univ.)
KOIKE Masahiro	小池正宏	(Inst. Nucl. Study, Univ. of Tokyo)
LEE S. M.	李相茂	(Centrum de Recherche Nucl. Strasbourg)
MIKUMO Takashi	三雲昂	(Inst. Phys., Tsukuba Univ.)
MORINAGA Haruhiko	森永晴彦	(Dept. Phys., München Tech. Univ.)

NOJIRI Yoichi 野尻洋一 (Lab. Nucl. Study, Osaka Univ.)  
 OHNUMA Hajime 大沼甫 (Dept. Phys., Tokyo Inst. Technol.)  
 SHIMIZU Jun 清水純 (Inst. Nucl. Study, Univ. of Tokyo)  
 SHINNO Hitoshi 新野仁 (Nat. Res. for Metals)  
 SHIRAIISHI Haruki 白石春樹 (Nat. Res. for Metals)  
 SOGA Fuminori 曾我文宣 (Inst. Nucl. Study, Univ. of Tokyo)  
 TAKAHASHI Noriaki 高橋憲明 (Lab. Nucl. Study, Osaka Univ.)  
 TAKAHASHI Noriyuki 高橋令幸 (Dept. Phys., Univ. of Tokyo)  
 TAKEMASA Tadashi 武政尹士 (Dept. Phys., Saga Univ.)  
 TAKIMOTO Kiyohiko 滝本清彦 (Dept. Phys., Kyoto Univ.)  
 UDAGAWA Takeshi 宇田川猛 (Dept. Phys., Texas Univ.)  
 WADA Ryoichi 和田良一 (Dept. Phys., Kyoto Univ.)  
 YOSHIDA Hiroshi 吉田弘 (Dept. Phys. Tokyo Inst. Technol.)

(Students)

HASHIMOTO Naoki 橋本直樹 (Dept. Phys., Tokyo Inst. Technol.)  
 ISE Sugao 伊勢須賀雄 (Dept. Phys., Tokyo Gakugei Univ.)  
 KISHIDA Norio 岸田則生 (Dept. Phys., Tokyo Inst. Technol.)  
 MIAKE Yasuo 三明康郎 (Lab. Nucl. Study, Osaka Univ.)  
 NORO Tetsuo 野呂哲夫 (Dept. Phys., Kyoto Univ.)  
 OOI Takao 大井孝雄 (Inst. Phys., Tsukuba Univ.)  
 SATO Kenichi 佐藤憲一 (Dept. Phys., Tohoku Univ.)  
 SHIMODA Tadashi 下田正 (Dept. Phys., Kyoto Univ.)  
 TANAKA Koichiro 田中耕一郎 (Dept. Phys., Univ. of Tokyo)  
 TOBA Yoshiyuki 外羽吉幸 (Dept. Phys., Kyoto Univ.)  
 UTSUNOMIYA Hiroaki 宇都宮弘章 (Dept. Phys., Kyoto Univ.)  
 YANOKURA Minoru 矢野倉実 (Dept. Chem., Tokyo Metropolitan Univ.)

#### Linac Laboratory

CHIBA Yoshiaki 千葉好明	HEMMI Masatake 逸見政武
HOSHINO Tohru 星野亨	INOUE Toshihiko 井上敏彦
KAMBARA Tadashi 神原正	MIYAZAWA Yoshitoshi 宮沢佳敏
ODERA Masatoshi 小寺正俊	SHIMAMURA Akira 島村旻
TAKESHITA Isao 竹下勇夫	TONUMA Tadao 戸沼正雄
YOKOYAMA Ichiro 横山一郎	YOSHIDA Fusako 吉田房子

(Visitor)

TAKEDA Shigeru 竹田繁 (Nat. Lab. High Energy Phys.)

#### Radiation Laboratory

AWAYA Yohko 粟屋容子	HAMADA Tatsuji 浜田達二
HASHIZUME Akira 橋爪朗	IZUMO Koichi 出雲光一
KATOU Takeo 加藤武雄	KONNO Satoshi 金野智
KUMAGAI Hidekazu 熊谷秀和	OKANO Masaharu 岡野真治
TAKAHASHI Tan 高橋旦	TENDOW Yoshihiko 天道芳彦

(Visitors)

DOKE Tadayoshi 道家忠義 (Sci. and Eng. Res. Lab., Waseda Univ.)  
 FUJIOKA Manabu 藤岡学 (Dept. Phys., Tohoku Univ.)

HAYASHIBE Shogo 林部昭吾 (Dept. Phys., Tohoku Univ.)  
 IIO Masahiro 飯尾正宏 (Tokyo Metropol. Geriatric Hosp.)  
 NAGAHARA Teruaki 永原照明 (Inst. Atomic Energy, Rikkyo Univ.)  
 SUZUKI Kazuaki 鈴木一明 (Japan Anal. Chem. Res. Inst.)  
 TAWARA Hiroyuki 俵博之 (Dept. Nucl. Eng., Kyushu Univ.)

(Student)

UCHIYAMA Sadayuki 内山貞幸 (Sci. and Eng. Res. Lab., Waseda Univ.)

#### Metal Physics Laboratory

KOYAMA Akio 小山昭雄 SAKAIRI Hideo 坂入英雄  
 SHIOTANI Nobuhiro 塩谷亘弘 YAGI Eiichi 八木栄一

(Visitors)

HASIGUTI R. Rukiti 橋口隆吉 (Faculty of Eng., Univ. of Tokyo)  
 NAGAI Ryo 永井亮 (Dept. Metallurgy and Materials Sci. Faculty Eng., Univ.  
 of Tokyo)  
 TANIGAWA Shoichiro 谷川庄一郎 (Dept. Metallurgy and Materials Sci. Faculty Eng.,  
 Univ. of Tokyo)

(Student)

HINODE Kenji 日野出憲治 (Dept. Metallurgy and Materials Sci. Faculty Eng., Univ.  
 of Tokyo)

#### Magnetic Materials Laboratory

ASAI Kichizo 浅井吉蔵 OKADA Takuya 岡田卓也  
 SAKAI Nobuhiko 坂井信彦 SEKIZAWA Hisashi 関沢尚

(Visitor)

MIZOGUCHI Tadashi 溝口正 (Dept. Phys., Gakushuin Univ.)

#### Ceramics Laboratory

KOBAYASHI Masayoshi 小林雅義 MAEDA Kuniko 前田邦子  
 SASA Yoshihiko 佐々嘉彦 UDA Masayuki 宇田応之

#### Nuclear Analytical Chemistry Laboratory

AMBE Fumitoshi 安部文敏 AMBE Shizuko 安部静子  
 ARATANI Michi 荒谷美智 ITO Yoshiko 伊東芳子  
 IWAMOTO Masako 岩本正子 NOZAKI Tadashi 野崎正  
 TERAJ Yoshiro 寺井善郎

(Visitors)

FUKUSHI Kiyoshi 福士清 (Nat. Inst. of Radiological Sci.)  
 HARA Toshihiko 原敏彦 (Nat. Nakano Chest Hosp.)  
 IRIE Toshiaki 入江俊章 (Nat. Inst. of Radiological Sci.)  
 KASIDA Yoshihiko 榎田義彦 (Nat. Inst. of Radiological Sci.)  
 TAKI Ko 滝幸 (Dept. of Hygen., Kitazato Univ.)

## Radiation Chemistry Laboratory

IMAMURA Masashi 今村 昌  
KIRA Akira 吉良 爽

KIMURA Kazuie 木村 一宇

(Visitor)

MATSUI Masao 松井正夫 (Dept. of Pharmacy, Hokuriku Univ.)

(Student)

HARATA Yasuo 原田康雄

## Radiobiology Laboratory

HATTORI Yukihiro 服部行彦  
KITAYAMA Shigeru 北山 滋  
YATAGAI Fumio 谷田具文夫

KANEKO Ichiro 金子一郎

MATSUYAMA Akira 松山 晃

(Visitors)

OKADA Shigefumi 岡田重文 (Faculty of Medicine, Univ. of Tokyo)

SASAKI Masao 佐々木正夫 (Dept. Cytogenetic, Medical Res. Inst., Tokyo Medical and Dental Univ.)

SAWADA Shozo 澤田昭三 (Res. Inst. Nucl. Medicine and Biology, Hiroshima Univ.)

## Safety Control Affairs Office

HAMADA Tatsuji 浜田達二  
SAKAMOTO Ichiro 坂本一郎

IGARASHI Kazui 五十嵐一茂  
USUBA Isao 薄葉 勲

## 15. LIST OF OUTSIDE USERS AND THEIR THEMES

(Jan. – Dec. 1977)

- |   |  |
|---|--|
| 1) T. Furuta, K. Fukai, T. Otomo, and<br>H. Kamizuka<br>“Study of Effect of Helium Bubbles on<br>the Mechanical Behavior of Stainless Steel”                              | Japan Atomic Energy Research Inst.   |
| 2) M. Shimada, K. Une, M. Terasawa, and<br>K. Kohashi<br>“Cyclotron Irradiation for Study of FBR<br>Material Embrittlement”   | Toshiba R. and D. Center   |
| 3) A. Hishinuma, K. Fukai, and T. Furuta<br>“Simulation Test on Neutron<br>Irradiation Damage of Stainless Steel<br>for Fast Breeder Reactors by $\alpha$<br>Bombardment” | Japan Atomic Energy Research Inst.   |
| 4) H. Nakahara, K. Miyano,* M. Yanokura,<br>M. Watanabe, and Y. Nakamura<br>“Study of the $^{55}\text{Mn} + \alpha$ Reaction”   | Faculty of Science, Tokyo Metropolitan Univ.<br>*Faculty of Science, Niigata Univ. |
| 5) H. Nakahara, M. Watanabe,<br>H. Muramatsu, M. Yanokura,<br>Y. Nakamura, and Y. Nagame<br>“Study of the $^{55}\text{Mn} + ^3\text{He}$ Reaction”                        | Faculty of Science, Tokyo Metropolitan Univ.                                       |
| 6) N. Nagashima<br>“Determination of C in Si by<br>Activation Analysis”   | Semiconductor Department, Hitachi, Ltd.  |
| 7) K. Komura and N. Yanase<br>“Measurement of Excitation Function<br>for the $\text{U} + ^3\text{He}$ Reaction”   | Faculty of Science, Kanazawa Univ.   |
| 8) Y. Honma and K. Kurata<br>“Production of $^{48}\text{V}$ , $^{48}\text{Cr}$ , $^{51}\text{Cr}$ , $^{81}\text{Rb}$ ,<br>and $^{82\text{m}}\text{Rb}$ ”                  | Kyoritsu College of Pharmacy   |

- 9) K. Hata  
“Production of  $^{237}\text{Pu}$ ”  
Japan Atomic Energy Research Inst.
- 10) K. Yuita  
“Production of  $^{43}\text{K}$ ”  
National Inst. of Agricultural Sciences
- 11) H. Nakahara, N. Watanabe, and  
Y. Nakamura  
“Production of  $^{57}\text{Cr}$  by the  $^{55}\text{Mn}(\alpha, xn)$   
Reaction”  
Faculty of Science, Tokyo Metropolitan  
Univ.
- 12) K. Usami and K. Mukai  
“Surface Analysis by Charged Particle  
Activation”  
Hitachi R. and D. Center
- 13) H. Nakahara, K. Muramatsu,  
M. Watanabe, and Y. Nakamura  
“Study of the Natural  $\text{Cd} + ^3\text{He}$   
Reaction”  
Faculty of Science, Tokyo Metropolitan  
Univ.

## AUTHOR INDEX

- AMAKAWA Hirotaka 天川博隆 20
- ARATANI Michi 荒谷美智 119, 139
- ASAI Kichizo 浅井吉蔵 106
- AWAYA Yohko 粟屋容子 85, 89, 91, 93  
96, 99
- DOKE Tadayoshi 道家忠義 82, 89
- DOYAMA Masao 堂山昌男 109, 111
- EJIRI Hiroyasu 江尻宏泰 77
- FUJISAWA Takashi 藤沢高志 8, 18, 34
- FUJITA Shin 藤田新 2
- FUKUDA Tomokazu 福田共和 54, 56
- FUKUSHI Kiyoshi 福士清 134
- GOTO Akira 後藤彰 22
- HAMADA Tatsuji 浜田達二 89, 91, 93
- HARA Toshihiko 原敏彦 134
- HARADA Kichinosuke 原田吉之助 48
- HASEGAWA Takeo 長谷川武夫 8, 18, 22  
69, 72, 74
- HASHIZUME Akira 橋爪朗 77, 85, 89,  
91, 93
- HASIGUTI R. Ryukiti 橋口隆吉 102, 104
- HATTORI Yukihiro 服部行彦 130
- HAYASHI Takayoshi 林孝義 82
- HINODE Kenji 日野出憲治 109, 111
- HIRUTA Kotaro 蛭田幸太郎 58, 67
- HOSHINO Tohru 星野亨 51
- ICHIMURA Munetake 市村宗武 31
- IGARASHI Kazui 五十嵐一茂 141
- IKEGAMI Kumio 池上九三男 2
- IMAMURA Masashi 今村昌 122, 124
- IMANISHI Bunryu 今西文龍 31, 36
- IMAZATO Jun 今里純 66
- INAMURA Takashi 稲村卓 58, 63, 67
- IRIE Toshiaki 人江俊章 134
- ISE Sugao 伊勢須賀雄 58, 67
- ISHIHARA Masayasu 石原正泰 43, 54, 56,  
58, 66, 67
- ITOH Yoshiko 伊東芳子 119, 134
- IWAMOTO Akira 岩本昭 48, 134
- IWAMOTO Masako 岩本正子 116
- IZUMO Koichi 出雲光一 89, 91, 93
- KAGEYAMA Tadashi 影山正 2, 6
- KAMBARA Tadashi 神原正 96  
8, 10, 13, 18
- KAMITSUBO Hiromichi 上坪宏道 34, 43, 54, 56,  
114
- KAMMURI Tetsuo 冠哲夫 25
- KANEKO Ichiro 金子一郎 132
- KARASAWA Takashi 唐沢孝 15, 134
- KATOU Takeo 加藤武雄 69, 72, 74, 85, 91, 93
- KAWAI Mitsuji 河合光路 31
- KIMURA Kazuie 木村一宇 122
- KIRA Akira 吉良爽 124
- KISHIDA Norio 岸田則生 22, 28

- KITAYAMA Shigeru 北山 滋 126, 128
- KOBAYASHI Masayoshi 小林雅義 99
- KOHARA Shigeo 小原重夫 2, 6
- KOHNO Isao 河野 功 2, 39, 40, 82, 87, 96  
114, 149
- KOYAMA Akio 小山昭雄 102, 104
- KUMAGAI Hidekazu 熊谷秀和 69, 72, 74, 85  
89, 91, 93, 96,  
99
- LEE S. M. 李 相茂 39
- MAEDA Kuniko 前田邦子 99
- MATSUI Masao 松井正夫 124
- MATSUYAMA Akira 松山 晃 126, 128, 130,  
132
- MIAKE Yasuo 三明康郎 43
- MINAMISONO Tadanori 南園忠則 43
- MIYANO Kazumasa 宮野和政 79
- MIZOBUCHI Akira 溝淵 明 43
- MORI Akihiko 森 昭彦 20
- MORINAGA Haruhiko 森永晴彦 66
- MOTOBAYASHI Tohru 本林 透 39, 40, 54  
56, 63, 87
- MOTONAGA Shoshichi 元永昭七 8, 10, 13  
18
- NAGAI Ryo 永井 亮 111
- NAKAHARA Hiromichi 中原弘道 79, 87
- NAKAJIMA Hisao 中嶋尚雄 2, 6
- NAKAJIMA Shunji 中島諄二 40
- NAKAMURA Masanobu 中村正信 18
- NAKANISHI Noriyoshi 中西紀喜 10, 13, 22,  
28
- NAKAYAMA Shintaro 中山信太郎 77
- NOJIRI Yoichi 野尻洋一 43
- NOMURA Toru 野村 亨 58, 60, 63, 66, 67, 81
- NOZAKI Tadashi 野崎 正 116, 119, 134, 137,  
139
- ODERA Masatoshi 小寺正俊 144, 145, 146, 147
- OGAWA Koji 小川幸次 137
- OGIWARA Kiyoshi 荻原 清 2, 4, 10
- OHNUMA Hajime 大沼 甫 28
- OHTANI Fumihiko 大谷文彦 22
- OKADA Shigefumi 岡田重文 132
- OKADA Takuya 岡田卓也 106
- OKANO Masaharu 岡野真治 91, 93, 137
- OOI Takao 大井孝雄 40
- SAKAGUCHI Harutaka 坂口治隆 22
- SAKAI Nobuhiko 坂井信彦 106
- SAKAIRI Hideo 坂入英雄 102, 104
- SAKAMOTO Ichiro 坂本一郎 141, 143
- SASA Yoshihiko 佐々義彦 99
- SASAKI Masao 佐々木正夫 132
- SATO Kenichi 佐藤憲一 48
- SAWADA Shozo 沢田昭三 132
- SEKIZAWA Hisashi 関沢 尚 106
- SHIBATA Tokushi 柴田徳志 77
- SHIKATA Takashi 四方隆史 114

- SHIMAMURA Akira 島村 旻 149
- SHIMIZU Jun 清水 純 34
- SHIMODA Tadashi 下田 正 39, 54, 56, 58, 67
- SHINNO Hitoshi 新野 仁 114
- SHIOTANI Nobuhiro 塩谷 亘弘 106, 109, 111
- SHIRAISHI Haruki 白石 春樹 114
- SOGA Fuminori 曾我 文宣 18, 34
- SUGIMOTO Kenzo 杉本 健三 43
- TAKAHASHI Noriaki 高橋 憲明 43
- TAKAHASHI Noriyuki 高橋 令幸 34
- TAKAHASHI Tan 高橋 旦 89, 91, 93
- TAKEBE Hideki 武部 英樹 2, 4
- TAKEMASA Tadashi 武政 尹士 45
- TAKESHITA Isao 竹下 勇夫 145
- TAKI Ko 滝 幸 137
- TAKIMOTO Kiyohiko 滝本 清彦 34
- TANAKA Koichiro 田中 耕一郎 43
- TANIGAWA Shoichiro 谷川 庄一郎 109, 111
- TENDOW Yoshihiko 天道 芳彦 69, 72, 74, 85, 91, 93
- TOBA Yoshiyuki 外羽 吉幸 8, 18, 22, 28
- TONUMA Tadao 戸沼 正雄 89, 91, 93, 96, 99, 149
- UCHIYAMA Sadayuki 内山 貞幸 89
- UDA Masayuki 宇田 応之 99
- UEDA Nozomi 上田 望 8, 18
- USUBA Isao 薄葉 勲 141
- UTSUNOMIYA Hiroaki 宇都宮 弘章 39, 60, 63
- WADA Ryoichi 和田 良一 34
- WADA Takeshi 和田 雄 8, 18, 34
- WATANABE Ryoji 渡辺 亮治 114
- YAGI Eiichi 八木 栄一 102, 104, 106
- YAMADA Satoru 山田 聡 8
- YAMAJI Shuhei 山路 修平 48
- YAMAKOSHI Kazuo 山越 和雄 87
- YANAGIMACHI Tomoki 柳町 朋樹 82
- YANOKURA Minoru 矢野 倉 実 39, 63, 66, 79, 87
- YASUE Masaharu 安江 正治 18, 22
- YATAGAI Fumio 谷田 具文夫 126, 128, 130, 132
- YAZAKI Koichi 矢崎 紘一 20, 51
- YOKOYAMA Ichiro 横山 一郎 10
- YOSHIDA Fusako 吉田 房子 10, 13, 145, 147
- YOSHIDA Hiroshi 吉田 弘 45
- YOSHIDA Shiro 吉田 思郎 48
- YUKAWA Tetsuyuki 湯川 哲之 51

## **IPCR Cyclotron Progress Report**

理化学研究所サイクロトン年次報告 第11巻(1977)

---

印刷 昭和53年(1978)3月25日

発行 昭和53年(1978)3月30日

発行者 理化学研究所

代表者 福 井 伸 二

〒351 埼玉県和光市広沢2番1号

電話(0484)62-1111

編集者 理化学研究所サイクロトン利用者委員会

印刷所 丸 星 印 刷 株 式 会 社

〒130 東京都墨田区亀沢1丁目3番3号

---

定価 3,000円

理化学研究所

埼玉県 和光市 広沢